COBAMIDE BIOSYNTHESIS IS ANCHORED TO THE MEMBRANE

by

VICTORIA LEIGH JETER

(Under the Direction of Jorge C. Escalante-Semerena)

ABSTRACT

Cobamides (Cbas) are complex, cobalt-containing cyclic tetrapyrroles belonging to a family of cofactors called 'the pigments of life.' Complete synthesis of Cbas is restricted to bacteria and archaea, yet it is an essential cofactor for cells in all domains of life. Cbas are structurally unique from cofactors like hemes, chlorophylls and coenzyme F_{430} by their upper and lower ligands. Adenosylcobalamin (AdoCbl), the coenzymic form, is characterized by an upper 5'-deoxyadenosine moiety (Ado) and a 5,6-dimethylbenzimidazole (DMB) lower ligand. Prokaryotes utilize two distinct pathways for corrin ring synthesis: anaerobic or aerobic. These pathways converge at the synthesis and attachment of the lower ligand, a pathway referred to as Nucleotide Loop Assembly (NLA). NLA is characterized by two branches: i) the attachment of an aminopropanol-phosphate linker (CbiB EC 6.3.1.10) to and activation of the corrin ring (CobU EC 2.7.7.62/ EC 2.7.1.156) and ii) the activation of the nucleotide base (CobT EC 2.4.2.21). Cobamide 5'-phosphate synthase (CobS EC 2.7.8.26) joins these two pathways by condensing the activated corrin ring and nucleotide base substrates to form adenosylcobamide-phosphate (AdoCba-P). The final step of the pathway

is catalyzed by CobC (EC 3.1.3.73) which dephosphorylates AboCba-P to form AdoCba.

There are numerous homologous enzymes in bacteria and archaea responsible for carrying out the steps of NLA. Here we present a structural and functional characterization of *Mj*CobT, an archaeal CobT homolog from hyperthermophile *Methanocaldococcus jannaschii*. Phylogenetic analysis of *Mj*CobT uncovered the presence of homologous base activating enzymes in cyanobacterial genomes, a group of organisms previously thought to lack CobT. In addition to our work on archaeal base activation, we sought to expand our understanding of CobS.

CobS is a polytopic integral membrane protein in all Cba producing organisms. This membrane conservation raises a number of questions about the significance of membrane-associated Cba biosynthesis. We developed a protocol for overproduction, purification and reconstitution of CobS into liposomes which led to the functional characterization of this enzyme. Additionally, we identified the physiological challenges excess CobS poses on the cell. Collectively, this work allowed us to begin unraveling the multi-protein complex of NLA enzymes, identifying CobS interactions with CobU, CobT and CobC.

INDEX WORDS: Adenosylcobalamin, Cobamide, B_{12}, Archaea, Bacteria, membrane, *Salmonella*, *Methanocaldococcus*

COBAMIDE BIOSYNTHESIS IS ANCHORED TO THE MEMBRANE

by

VICTORIA LEIGH JETER

BS, University of Florida, 2012

A Dissertation Submitted to the Graduate Faculty of The University of Georgia in Partial Fulfillment of the Requirements for the Degree

DOCTOR OF PHILOSOPHY

ATHENS, GEORGIA

2020

COBAMIDE BIOSYNTHESIS IS ANCHORED TO THE MEMBRANE

by

VICTORIA LEIGH JETER

Major Professor:	Jorge C. Escalante-Semerena
Committee:	Timothy Hoover Janet Westpheling Vincent Starai

Electronic Version Approved:

Ron Walcott
Dean of the Graduate School
The University of Georgia
December 2020

ACKNOWLEDGEMENTS

I would like to first like to thank the members of the Escalante lab, past and present, for your role in my growth as a scientist. I have had the privilege of working with so many driven, intelligent individuals who have mentored me along the way. My time with you all will be fondly remembered.

I am so grateful for my family and their support. My parents have always been supportive and helped to remind me why I started this journey whenever I doubted myself. Their unconditional love and encouragement made this Ph.D. possible. I am so appreciative of the opportunities made available to me because of them. Love you, Mom and Dad. I am also blessed to have the most loving and supportive in-laws. Thank you for all the Disney trips to get a break from the lab and the family board game nights. I feel so lucky to have you all in my life. Love you, Janice, Bob, Bobby, Stephanie and Brad.

A special acknowledgement goes to my fiancé Stephen Garza who has been an endlessly supportive, patient, and loving partner throughout this entire process. The coffee deliveries and dog visits to helped me through numerous rough days in lab. I am so thankful Athens has brought us together. Now that my Ph.D is done we can finally get married.

TABLE OF CONTENTS

Page

LIST OF TABLES

Page

LIST OF FIGURES

Page

CHAPTER 1

INTRODUCTION AND LITERATURE REVIEW

OVERVIEW OF COBAMIDES

Cobamides (Cba) are cobalt-containing, cyclic tetrapyrroles that belong to a class of molecules commonly referred to as 'the pigments of life.' Other metal-containing tetrapyrroles like chlorophylls, factor F_{430}, and hemes belong to this group of compounds (1, 2). Cobamides are structurally complex and unique in that they have an upper and lower ligand coordinated to the cyclic tetrapyrrole or corrin ring. The upper axial ligand (Cob) can be a 5'-deoxyadenosine (AdoCba), methyl (MeCba), hydroxyl (OHCba), or cyano (CNCba). The lower axial ligand (Coa) can accommodate a number of different compounds and is a source major source of diversity amongst cobamide producers (3-5). Benzimidazoles, purines, and phenols are found as naturally occurring lower ligand bases. Cobalamin (Cbl, vitamin-B_{12}) is characterized by a 5,6-dimethylbenzimidazole (DMB) lower nucleotide base and the coenzymic form (AdoCbl, co-B_{12}) has a 5'-deoxyadenosine upper ligand. The structure of AdoCbl is shown in Figure 1.1. Organisms capable of synthesizing Cbas have dedicated a considerable amount of genetic information (~30 genes) to carrying out this process.

Cbas are essential to cells from all domains of life, yet *de novo* synthesis is carried out by few archaea and bacteria. Bioinformatic analysis suggests 85% of

bacteria have a Cba-dependent enzyme while only 37% are capable of synthesizing biologically active molecules (6, 7). Cbas have been shown to be important small molecule modulators in community dynamics (8, 9). Myriad cellular processes involve Cbas including methanogenesis (10), acetogenesis (4, 11, 12), methionine synthesis (13, 14), reductive dehalogenation (15-20), ribonucleotide metabolism (21-26), and ethanolamine (27-31), 1,2-propanediol (32-36), short chain fatty acid, glutamate, and anaerobic glycerol catabolism (32, 37-42). In addition to these roles, studies have also identified Cba-dependent photoreceptors responsible for regulating carotenoid biosynthesis in *Myxococcus xanthus* and *Rhodobacter capsulatus* (43-45). A relatively new class of cba-dependent radical SAM methyltransferase have been implicated in processes like antimicrobial production and bacteriochlorophyll synthesis (46). In some Eukaryotes, methionine synthase (MetH) and methylmalonyl-CoA mutase (MCM) are Cbl-dependent enzymes (47, 48, 21). In the coenzymic form, AdoCbl is used for radical chemistry required for deaminations, dehydrations, reductive dehalogenations, and intramolecular rearrangements (21,49). In methyltransferase reactions, MeCbl serves as a co-substrate (48).

COBAMIDE BIOSYNTHESIS IN *S. TYPHIMURIUM*

Salmonella enterica eneterica serovar Typhimurium LT2 (henceforth *S.* Typhimurium) is an ideal organism for the study of AdoCba biosynthesis. Advantages to using *S*. Typhimurium as a model organism include well-defined genetic systems, rapid growth in minimal medium and multiple cobamide-

dependent enzymes that allow for phenotypic evaluation. Cobalamin-dependence in *S*. Typhimurium is found in ethanolamine and 1,2-propanediol utilization pathways as well as the synthesis of methionine. Ethanolamine ammonia lyase (EutBC, EC 4.3.1.7) and 1,2-propanediol dehydratase (PduCD, EC 4.2.1.28) are Cbl-dependent enzymes necessary for the catabolism of ethanolamine and 1,2-propanediol, respectively (50-56). Catabolism of these carbon sources requires high concentrations of Cbl (57). Methionine synthesis in *S*. Typhimurium can be performed by MetE (EC 2.1.1.14), a Cba-independent enzyme or MetH (EC 2.1.1.13), a Cba-dependent enzyme that uses homocysteine and methyl-tetrahydrofolate to generate methionine (58-60). Methionine synthesis by MetH requires low concentrations of Cba (61). The difference in Cba demand amongst these Cba-dependent enzymes provides a powerful tool to assess Cba-related phenotypes in *S*. Typhimurium.

De novo synthesis of the corrin ring only occurs under anaerobic conditions in *S.* Typhimurium (6, 62). The late steps or nucleotide loop assembly (NLA), responsible for activation and attachment of the lower ligand, can be assessed in aerobic conditions. In addition to *de novo* synthesis, *S*. Typhimurium can transport and salvage incomplete Cbas like cobinamide (Cbi) and cobyric acid (Cby) in aerobic and anaerobic conditions (63). These features allow for the implementation of genetic and biochemical techniques to solve the complexities of Cba biosynthesis in this organism. Utilizing these tools, the enzymes involved in the late steps of Cba biosynthesis in *S*. Typhimurium have been elucidated (64-75). In addition to identifying the components of Cba biosynthesis in *S.* Typhimurium, this

organism has been extensively used to determine the enzymatic functions of AdoCba biosynthetic genes from other bacteria and archaea (76-82).

DE NOVO SYNTHESIS

Corrin Synthesis. The early steps of de novo Cba biosynthesis are responsible for generating the corrin component. There are two major routes for corrin synthesis that are utilized independently in various Cba producers: the anaerobic and aerobic routes. (83). The anaerobic pathway is not strictly anaerobic, however there are a number of oxygen-sensitive intermediates thus this pathway proceeds more efficiently in the absence of oxygen (84). The aerobic pathway requires oxygen. Timing of cobalt insertion relative to ring contraction is a defining difference between these two pathways. The anaerobic pathway is defined by early insertion of cobalt (85-89). In the aerobic pathway, cobalt is inserted after ring contraction or late (90).

Genes of the aerobic pathway for corrin synthesis have the *cob* prefix for their role in cobalamin synthesis (91, 92). In the anaerobic pathway, genes have both *Cbi* and *Cob* prefixes: Cbi for their role in cobinamide synthesis and Cob for the synthesis of cobalamin from cobinamide (74, 93-95). The anaerobic pathway is found in many bacteria and archaea, while the aerobic pathway is predominantly found in a-proteobacteria. *S*. Typhimurium has the best characterized anaerobic pathway, though it is found in various bacteria and archaea as well (64-75). The aerobic pathway is predominantly found in a-proteobacteria and best characterized in *Rhodobacter capsulatus* (96-102) and *Pseudomonas denitrificans*

(103-115). Though these two pathways have significantly different intermediates due to the cobalt insertion, there are a number of homologous enzymes. The differences in cobalt insertion are exemplified by cobaltochelases and ring contraction enzymes. In the aerobic pathway, cobaltochelases CobS, CobT, and CobN (115) are responsible for cobalt insertion and CobZ and CobG (100, 116) for ring contraction. The anaerobic pathway cobaltochelases are CbiK and CbiX or CysG (88, 85, 117) and CbiH for ring contraction (118). Figure 1.2 shows the aerobic and anaerobic pathways of corrin synthesis.

Upper ligand attachment. Prior to entering the late steps or nucleotide loop assembly pathway, the corrinoid must be adenosylated (119). ATP:Co(I)rrinoid adenosyltrasnferases (ACATs) are responsible for catalyzing the formation of an organometallic bond between the 5'deoxyadenosyl ligand and the upper axial cobalt of the corrin ring (120-122). In general, the adenosylation reaction requires reduction from Co^{3+} to Co^{2+} and from Co^{2+} to Co^{1+}. In *S.* Typhimurium, the first reduction from Co^{3+} to Co^{2+} occurs non-enzymatically by dihydroflavins (123). The reduction from Co^{2+} to Co^{1+} is facilitated by ACATs by binding five-coordinate Co^{2+}-cobamide and displacing the lower ligand to yield four-coordinate Co^{2+}-cobamide. The change to four-coordinate Co^{2+}-cobamide raises the redox potential allowing for reduction by dihydroflavins (124, 125). The reduced Co^{1+}-cobamide performs a nucleophilic attack on the 5'C of ATP yielding an adenosylated cobamide and phosphate by-product. The adenosylated product can continue to the nucleotide loop assembly pathway in the case of AdoCbi or AdoCby acid.

ACATs are a family of enzymes with broad diversity and divided into three types: CobA , PduO, and EutT (EC 2.5.1.17). In *S*. Typhimurium, CobA is the housekeeping ACAT responsible for adenosylating *de novo* synthesized corrinoids and salvaged incomplete corrinoids before proceeding to the late steps (68, 119, 126). The Cba-dependent 1,2-propanediol and ethanolamine utilization pathways each have dedicated adenosyltransferases: PduO and EutT respectively. The utilization of each of these carbon sources occurs in metabolosome microcompartments to sequester reactive aldehyde intermediates (127, 128). EutT-type ACATs can be further divided into Class I and Class II. Class I EutT-type ACATs, like *S*. Typhimurium EutT, contain a metal-binding motif and require Fe^{2+} for activity (129, 130). Class II EutT-type ACATs, like EutT from *Listeria monocytogenes*, lack the metal-binding motif found in class I and do not require a metal for function (131).

Nucleotide Loop Assembly. The late steps of Cba biosynthesis are characterized by two distinct pathways that converge to form a complete cobamide (Figure 1.3). One pathway activates the corrin ring while the other activates the nucleotide base. Prior to activation of the corrin ring, an aminopropanol linker is synthesized that will form the connection between the corrin ring and nucleotide base. In *S*. Typhimurium and other organisms with anaerobic *de novo* synthesis pathways, the aminopropanol-phosphate linker is formed from L-threonine by PduX (EC 2.7.1.177) and CobD (EC 4.1.1.81) (64, 65, 132, 133). PduX phosphorylates L-threonine to yield L-threonine-phosphate (64) before CobD, a

PLP-dependent decarboxylase, converts L-threonine-phosphate to aminopropanol-phosphate (65). In other organisms that employ aerobic *de novo* synthesis, non-homologous enzymes BluE and CobD perform the two-step conversion of L-threonine to aminopropanol-phosphate (134). Archaea differ from bacteria by substituting the two-step process with a bifunctional CobD (135). Some Cba producers, like *Sulfurospirillum multivorans*, use a CobD homolog to generate an ethanolamine phosphate linker from L-serine in place of aminopropanol-phosphate to yield nor-Cba (136, 137).

The integral membrane protein CbiB (EC 6.3.1.10) is responsible for taking adenosylcobyric acid from *de novo* synthesis and attaching the aminopropanol-phosphate (ethanolamine-phosphate in some cases) linker generating adenosylcobinamide-phosphate (AdoCbi-P) intermediate. (70, 138). AdoCbi-P is then guanylylated by the bifunctional NTP:AdoCbl kinase/GTP:AdoCbi-P guanylyltransferase CobU (EC 2.7.1.156) in *S*. Typhimurium or CobP in *P. denitrificans* yielding the activated corrin ring adenosylcobinamide-GDP (AdoCbi-GDP) (69, 111, 139, 140). CobY is responsible for performing the AdoCbi-P guanylyltransferase (EC 3.1.3.73) activity in archaea, however it lacks the kinase activity (76, 141-144). In the conversion of AdoCbi-P to AdoCbi-GDP, CobU self-guanylylates a histidine residue generating a CobU-GMP intermediate resulting in a significant conformational change (69, 145). CobU is only able to act on adenosylated corrinoids, limiting nucleotide loop attachment to intermediates with nucleoside upper ligands (119, 140, 146).

Nucleotide base activation is characterized by the unique generation of an a-*N*-glycosidic bond between ribose and a base. A number of different benzimidazole, purine, and phenolic bases can be activated and attached to generate diverse Cbas (Figure 1.4). Cobalamin contains DMB as the lower nucleotide base. DMB synthesis has been characterized in multiple organisms. In *R. sphaeroides* and *S. meliloti*, BluB catalyzes the one-step oxidation of flavin mononucleotide to DMB under aerobic conditions (79, 147). In *E. limosum*, a five-enzyme pathway generates DMB from 5'-aminoimidazole ribotide (AIR) (148). Though *S*. Typhimurium can synthesize DMB *de novo*, the pathway has yet to be characterized (149, 150). *S*. Typhimurium can generate cobalamin in a microaerophilic environment, but under the anoxic conditions necessary for *de novo* Cba synthesis, *S*. Typhimurium incorporates adenine forming pseudocobalamin (psCbl). In *S*. Typhimurium, DMB is activated by attaching the ribosyl-5'-phosphate from nicotinate mononucleotide yielding α-ribazole-phosphate (α-RP). This reaction is catalyzed by CobT (EC 2.7.8.26) the NaMN:DMB phosphoribosyltransferase (72, 151). In archaea and cyanobacteria, a CobT homolog performs the same activity (82). Bacterial and archaeal CobTs have been shown to activate a broad range benzimidazole and purine substrates, contributing to the diversity of complete Cbas (82, 152). In *Sporomusa ovata*, the heterodimer ArsAB catalyzes the ribosyltransfer reaction (153). Notably, ArsAB is capable of activating phenolic bases such as phenol and p-cresol in addition to benzimidazoles and purines (153). Some firmicutes utilize an alternative pathway to generate α-RP and rely on environmental a-ribazole (α-R). Membrane

transporter CblT imports exogenous α-R from the environment followed by phosphorylation to a-RP by kinase CblS (150, 81).

The penultimate step in Cba biosynthesis is catalyzed by cobamide 5'-phosphate synthase which condenses the activated corrin ring AdoCbi-GDP and base α-RP to yield Cba 5'-phosphate. The cobamide 5'-phosphate synthase is called CobS (EC 2.7.8.26) in *S*. Typhimurium and CobV in *P. denitrificans* (71, 154). A phosphodiester bond is formed when the 3' hydroxyl of the α-ribotide displaces the GMP moiety of the activated corrin ring producing Cba-phosphate. CobS is an integral membrane protein in all Cba-producers, bacteria and archaea alike. Membrane topology was determined using a series of LacZ and PhoA fusions (154, 68). Overproduction of this protein is challenging, resulting in an increase of phage shock protein A (PspA) which is often indicative of membrane stress (154). Work done on CobV, the CobS homolog of *P. denitrificans*, showed cobamide synthase activity was isolated with a high molecular weight complex (107). Other proteins from this complex were not identified, but the evidence of a potential multi-enzyme complex involved in Cba biosynthesis at the cell membrane is compelling.

In bacteria, CobC catalyzes the final step of the Cba biosynthetic pathway by dephosphorylating AdoCba-P to AdoCba (71, 66). In archaea, Cba-phosphate is dephosphorylated by a non-orthologous CobC homolog CobZ or the bifunctional CbiS (77, 78). The mechanism of action has not yet been reported for this phosphatase. The conservation of membrane association of both CbiB and CobS raises the question of membrane significance in the late steps of Cba biosynthesis.

TRANSPORT AND SALVAGING

As previously mentioned, a limited number of prokaryotes can synthesize complete Cbas de novo, but the requirement for Cbas is found amongst prokaryotes and eukaryotes. (93). Organisms lacking *de novo* synthetic pathways rely on importing exogenous Cbas. Figure 1.5. shows the well characterized prokaryotic cobamide transport systems of Gram-negative bacteria. Corrinoids are transported across the outer membrane of Gram-negative bacteria by TonB-dependent BtuB (155). BtuF binds the imported corrinoid in the periplasm and delivers it to the inner membrane ABC-transporter BtuCD where the corrinoid is then transported across the inner membrane to the cytoplasm (156-159). BtuM of *Thiobacillus denitrificans* serves as an alternative to BtuCDF, transporting Cbl and Cbi across the inner membrane (160). Another alternative to the Btu transport system has been characterized in Gram-positive *Lactobacillus delbruekii.* Cbl and Cbi are transported to the cytoplasm by an energy coupling factor-type ABC transporter CbrT (161).

Several organisms lacking complete *de novo* Cba biosynthetic pathways have enzymes for the salvaging and remodeling of incomplete corrinoids to meet the cell's Cba requirements (142, 162, 163). Exogenous Cbi can be adenosylated upon uptake to generate AdoCbi which can be modified and activated by the bifunctional CobU/CobP in bacteria (111, 69). Other organisms like *R. sphaeroides* and *M. mazei* use amidohydrolase CbiZ to generate AdoCby (138, 162-164). In archaea, a bifunctional amidohydrolase/phosphatase CbiS has been identified, yet

the physiological role of this fusion has yet to be elucidated (78). The products of these remodeling systems can then enter the late steps of Cba biosynthesis (70).

DISSERTATION OUTLINE

A longstanding question in the field surrounds the physiological role of associating Cba biosynthesis with the cell membrane. Given the biosynthetic effort undertaken by the cell to generate Cba *de novo*, it is reasonable to question if localization of late step enzymes to the membrane facilitates efficient flux of intermediates through the pathway. Cobamide synthase is one of two highly conserved integral membrane proteins in Cba biosynthesis. Little is known about CobS and the conservation of membrane-association and physiological implications of this are areas of particular interest. This dissertation expands on our understanding of this enzyme through functional analyses and by exploring interactions with the cell membrane and other enzymes of the nucleotide loop assembly pathway.

This dissertation covers multiple facets of the nucleotide loop assembly pathway, with a focus on the penultimate step performed by cobamide synthase. Chapter 2 will discuss the identification of a new class of phosphoribosyltransferase found in methanogens and cyanobacteria. Chapter 3 will discuss structural studies on the archaeal phosphoriboslytranferase we identified in Chapter 2. Methods for the overproduction, purification and reconstitution of CobS in a lipid bilayer were developed to probe the significance of membrane-associated NLA and drove the majority of the work presented in

Chapters 4, 5 and 6. Chapter 4 will discuss the characterization of cobamide synthase from *S*. Typhimurium. Chapter 5 will discuss the physiological challenges imposed on the cell by excess cobamide synthase. Chapter 6 will discuss the identification of the multienzyme complex responsible for catalyzing the late steps of Cba biosynthesis at the cell membrane. Chapter 7 summarizes the contributions of this work.

REFERENCES

1. Battersby, A.R., et al., *Biosynthesis of the pigments of life: formation of the macrocycle.* Nature, 1980. **285**: p. 17-21.
2. Battersby, A.R., *Tetrapyrroles: the pigments of life.* Nat. Prod. Rep., 2000. **17**: p. 507-526.
3. Renz, P., *Biosynthesis of the 5,6-dimethylbenzimidazole moiety of cobalamin and of other bases found in natural corrinoids*, in *Chemistry and Biochemistry of B12.*, R. Banerjee, Editor. 1999, John Wiley & Sons, Inc.: New York. p. 557-575.
4. Stupperich, E., H.J. Eisinger, and B. Kräutler, *Diversity of corrinoids in acetogenic bacteria. p-Cresolylcobamide from Sporomusa ovata, 5-methoxy-6-methylbenzimidazolylcobamide from Clostridium formicoaceticum and vitamin B12 from Acetobacterium woodii.* Eur. J. Biochem., 1988. **172**: p. 459-464.
5. Allen, R.H. and S.P. Stabler, *Identification and quantitation of cobalamin and cobalamin analogues in human feces.* Am. J. Clin. Nutr., 2008. **87**: p. 1324-1335.
6. Rodionov, D.A., et al., *Comparative genomics of the vitamin B_{12} metabolism and regulation in prokaryotes.* J. Biol. Chem., 2003. **278**: p. 41148-41159.

7. Shelton, A.N., et al., *Uneven distribution of cobamide biosynthesis and dependence in bacteria predicted by comparative genomics.* ISME J, 2019. **13**(3): p. 789-804.
8. Croft, M.T., et al., *Algae acquire vitamin B12 through a symbiotic relationship with bacteria.* Nature, 2005. **438**: p. 90-93.
9. Degnan, P.H., M.E. Taga, and A.L. Goodman, *Vitamin B12 as a modulator of gut microbial ecology.* Cell Metab., 2014. **20**: p. 769-778.
10. Stadtman, T.C. and B.A. Blaylock, *Role of B12 compounds in methane formation.* Fed. Proc., 1966. **25**: p. 1657-1661.
11. Stupperich, E., H.J. Eisinger, and S.P. Albracht, *Evidence for a super-reduced cobamide as the major corrinoid fraction in vivo and a histidine residue as a cobalt ligand of the p-cresolyl cobamide in the acetogenic bacterium Sporomusa ovata.* Eur. J. Biochem., 1990. **193**: p. 105-109.
12. Stupperich, E. and H.J. Eisinger, *Biosynthesis of para-cresolyl cobamide in Sporomusa ovata.* Arch. Microbiol., 1989. **151**: p. 372-377.
13. Weissbach, H. and R. Taylor, *Role of vitamin B12 in methionine synthesis.* Fed Proc, 1966. **25**(6): p. 1649-56.
14. Taylor, R.R., *B12-dependent methionine synthesis*, in *B12*, D. Dolphin, Editor. 1982, John Wiley & Sons: New York. p. 307-356.
15. Yan, J., et al., *Guided cobalamin biosynthesis supports Dehalococcoides mccartyi reductive dechlorination activity.* Philos. Trans. R. Soc. Lond. B Biol. Sci., 2013. **368**: p. 20120320.
16. Bommer, M., et al., *Structural basis for organohalide respiration.* Science, 2014. **346**: p. 455-458.

17. Reinhold, A., et al., *Impact of vitamin B12 on formation of the tetrachloroethene reductive dehalogenase in Desulfitobacterium hafniense strain Y51.* Appl. Environ. Microbiol., 2012. **78**: p. 8025-8032.

18. Smith, M.H. and S.L. Woods, *Regiospecificity of chlorophenol reductive dechlorination by vitamin B12s.* Appl. Environ. Microbiol., 1994. **60**: p. 4111-4115.

19. Wohlfarth, G. and G. Diekert, *Reductive dehalogenases.*, in *Chemistry and Biochemistry of B12.*, R. Banerjee, Editor. 1999, John Wiley & Sons, Inc.: New York. p. 871-893.

20. Kräutler, B., et al., *The cofactor of tetrachloroethene reductive dehalogenase of Dehalospirillum multivorans is Norpseudo-B12, a new type of natural corrinoid.* Helvetica Chimica Acta, 2003. **86**: p. 3698-3716.

21. Banerjee, R., *Radical carbon skeleton rearrangements: catalysis by coenzyme B12-dependent mutases.* Chem. Rev., 2003. **103**: p. 2083-2094.

22. Blakley, R.L., *Cobalamin-dependent ribonucleotide reductases*, in *B12*, D. Dolphin, Editor. 1982, John Wiley & Sons: New York. p. 381-418.

23. Booker, S., et al., *Coenzyme B12-dependent ribonucleotide reductase: evidence for the participation of five cysteine residues in ribonucleotide reduction.* Biochemistry, 1994. **33**: p. 12676-12685.

24. Jordan, A., et al., *B12-dependent ribonucleotide reductases from deeply rooted eubacteria are structurally related to the aerobic enzyme from Escherichia coli.* Proc. Natl. Acad. Sci. USA, 1997. **94**: p. 13487-13492.

25. Jordan, A. and P. Reichard, *Ribonucleotide reductases.* Ann. Rev. Biochem., 1998. **67**: p. 71-98.

26. Fontecave, M. and E. Mulliez, *Ribonucleotide Reductases*, in *Chemistry and Biochemistry of B12*, R. Banerjee, Editor. 1999, John Wiley & Sons, Inc.: New York. p. 731-756.

27. Babior, B.M., *The mechanism of action of ethanolamine ammonia-lyase, a B12-dependent enzyme. VII. The mechanism of hydrogen transfer.* J Biol Chem, 1970. **245**(22): p. 6125-33.

28. Chang, G.W. and J.T. Chang, *Evidence for the B12-dependent enzyme ethanolamine deaminase in Salmonella.* Nature, 1975. **254**: p. 150-151.

29. Blackwell, C.M. and J.M. Turner, *Microbial metabolism of amino alcohols. Formation of coenzyme B12-dependent ethanolamine ammonia-lyase and its concerted induction in Escherichia coli.* Biochem. J., 1978. **176**: p. 751-757.

30. Babior, B.M., *Ethanolamine ammonia-lyase*, in *B12*, D. Dolphin, Editor. 1982, John Wiley & Sons: New York. p. 263-288.

31. Roof, D.M. and J.R. Roth, *Ethanolamine utilization in Salmonella typhimurium.* J. Bacteriol., 1988. **170**: p. 3855-3863.

32. Toraya, T., et al., *Coenzyme B12-dependent diol dehydratase: regulation of apoenzyme synthesis in Klebsiella pneumoniae (Aerobacter aerogenes) ATCC 8724.* J Bacteriol, 1978. **135**(2): p. 726-9.

33. Poznanskaja, A.A., et al., *Coenzyme B12-dependent diol dehydrase: purification subunit heterogeneity, and reversible association.* Arch. Biochem. Biophys., 1979. **194**: p. 379-386.

34. Toraya, T., S. Honda, and S. Fukui, *Fermentation of 1,2-propanediol and 1,2-ethanediol by some genera of enterobacteriaceae involving coenzyme-B12-dependent diol dehydratase.* J. Bacteriol., 1979. **139**: p. 39-47.

35. Rondon, M.R. and J.C. Escalante-Semerena, *The poc locus is required for 1,2-propanediol-dependent transcription of the cobalamin biosynthetic (cob) and*

propanediol utilization (pdu) genes of Salmonella typhimurium. J. Bacteriol., 1992. **174**: p. 2267-2272.

36. Bobik, T.A., M. Ailion, and J.R. Roth, *A single regulatory gene integrates control of vitamin B12 synthesis and propanediol degradation.* J Bacteriol, 1992. **174**(7): p. 2253-66.

37. Rétey, J., *Methylmalonyl-CoA mutase*, in *B12*, D. Dolphin, Editor. 1982, John Wiley & Sons: New York. p. 357-380.

38. Halpern, J., *Mechanisms of coenzyme B_{12}-dependent rearrangements.* Science, 1985. **227**: p. 869-875.

39. Mancia, F., et al., *How coenzyme B12 radicals are generated: the crystal structure of methylmalonyl-coenzyme A mutase at 2Å resolution.* Structure, 1996. **4**: p. 339-350.

40. Toraya, T., et al., *Studies on the mechanism of the adenosylcobalamin-dependent diol dehydrase reaction by the use of analogs of the coenzyme.* J Biol Chem, 1977. **252**: p. 963-970.

41. Reitzer, R., et al., *Glutamate mutase from Clostridium cochlearium: the structure of a coenzyme B12-dependent enzyme provides new mechanistic insights.* Structure Fold Des., 1999. **7**: p. 891-902.

42. Ohmori, H., et al., *Correlation between the level of vitamin-B12-dependent methionine synthetase and intracellular concentration of vitamin B12 in some bacteria.* Eur. J. Biochem., 1974. **47**: p. 207-218.

43. Perez-Marin, M.C., et al., *Vitamin B12 partners the CarH repressor to downregulate a photoinducible promoter in Myxococcus xanthus.* Mol. Microbiol., 2008. **67**: p. 804-819.

44. Diez, A.I., et al., *Analytical ultracentrifugation studies of oligomerization and DNA-binding of TtCarH, a Thermus thermophilus coenzyme B12-based photosensory regulator.* Eur. Biophys. J., 2013. **42**: p. 463-476.

45. Vermeulen, A.J. and C.E. Bauer, *Members of the PpaA/AerR antirepressor family bind Cobalamin.* J. Bacteriol., 2015. **197**: p. 2694-2703.

46. Bridwell-Rabb, J., et al., *A B12-dependent radical SAM enzyme involved in oxetanocin A biosynthesis.* Nature, 2017. **544**: p. 322-326.

47. Banerjee, R. and S.W. Ragsdale, *The many faces of vitamin B12: catalysis by cobalamin-dependent enzymes.* Annu. Rev. Biochem., 2003. **72**: p. 209-247.

48. Banerjee, R.V. and R.G. Matthews, *Cobalamin-dependent methionine synthase.* FASEB J, 1990. **4**: p. 1450-1459.

49. Ludwig, M.L. and R.G. Matthews, *Structure-based perspectives on B12-dependent enzymes.* Annu. Rev. Biochem., 1997. **66**: p. 269-313.

50. Faust, L.R., et al., *Cloning, sequencing, and expression of the genes encoding the adenosylcobalamin-dependent ethanolamine ammonia-lyase of Salmonella typhimurium.* J. Biol. Chem., 1990. **265**: p. 12462-12466.

51. Stojiljkovic, I., A.J. Baumler, and F. Heffron, *Ethanolamine utilization in Salmonella typhimurium: nucleotide sequence, protein expression, and mutational analysis of the cchA cchB eutE eutJ eutG eutH gene cluster.* J. Bacteriol., 1995. **177**: p. 1357-1366.

52. Kofoid, E., et al., *The 17-gene ethanolamine (eut) operon of Salmonella typhimurium encodes five homologues of carboxysome shell proteins.* J. Bacteriol., 1999. **181**: p. 5317-5329.

53. Roof, D.M. and J.R. Roth, *Functions required for vitamin B12-dependent ethanolamine utilization in Salmonella typhimurium.* J. Bacteriol., 1989. **171**: p. 3316-3323.

54. Bobik, T.A., et al., *Propanediol utilization genes (pdu) of Salmonella typhimurium: three genes for the propanediol dehydratase.* J. Bacteriol., 1997. **179**: p. 6633-6639.

55. Toraya, T., et al., *A reactivating factor for coenzyme B12-dependent diol dehydratase.* Biofactors, 2000. **11**(1-2): p. 105-107.

56. Jeter, R.M., *Cobalamin-dependent 1,2-propanediol utilization by Salmonella typhimurium.* J. Gen. Microbiol., 1990. **136**: p. 887-896.

57. Bradbeer, C., *The clostridial fermentation of choline and ethanolamine. II. Requirement for a cobamide coenzyme by an ethanolamine deaminase.* J. Biol. Chem., 1965. **240**: p. 4675-4681.

58. Peariso, K., et al., *Characterization of the zinc sites in cobalamin-independent and cobalamin-dependent methionine synthase using zinc and selenium X-ray absorption spectroscopy.* Biochemistry, 2001. **40**: p. 987-993.

59. Gonzalez, J.C., et al., *Comparison of cobalamin-independent and cobalamin-dependent methionine synthases from Escherichia coli: two solutions to the same chemical problem.* Biochemistry, 1992. **31**: p. 6045-6056.

60. Hondorp, E.R. and R.G. Matthews, *Oxidative stress inactivates cobalamin-independent methionine synthase (MetE) in Escherichia coli.* PLoS Biol., 2004. **2**: p. e336.

61. Bradbeer, C., *Cobalamin transport in microorganisms.*, in *B12*, D. Dolphin, Editor. 1982, John Wiley & Sons: New York. p. 31-56.

62. Escalante-Semerena, J.C. and M.J. Warren, *Biosynthesis and use of cobalamin (B_{12})*, in *EcoSal - Escherichia coli and Salmonella: cellular and molecular biology*, A. Böck, et al., Editors. 2008, ASM Press: Washington, D. C.

63. Escalante-Semerena, J.C., *Conversion of cobinamide into adenosylcobamide in bacteria and archaea.* J. Bacteriol., 2007. **189**: p. 4555-4560.

64. Fan, C. and T.A. Bobik, *The PDUX enzyme of Salmonella enterica is an L-threonine kinase used for coenzyme B_{12} synthesis.* J. Biol. Chem., 2008. **283**: p. 11322-11329.

65. Brushaber, K.R., G.A. O'Toole, and J.C. Escalante-Semerena, *CobD, a novel enzyme with L-threonine-O-3-phosphate decarboxylase activity, is responsible for the synthesis of (R)-1-amino-2-propanol O-2-phosphate, a proposed new intermediate in cobalamin biosynthesis in Salmonella typhimurium LT2.* J. Biol. Chem., 1998. **273**: p. 2684-2691.

66. O'Toole, G.A., J.R. Trzebiatowski, and J.C. Escalante-Semerena, *The cobC gene of Salmonella typhimurium codes for a novel phosphatase involved in the assembly of the nucleotide loop of cobalamin.* J. Biol. Chem., 1994. **269**: p. 26503-26511.

67. Anderson, P.J., et al., *One pathway can incorporate either adenine or dimethylbenzimidazole as an alpha-axial ligand of B_{12} cofactors in Salmonella enterica.* J. Bacteriol., 2008. **190**: p. 1160-1171.

68. Maggio-Hall, L.A. and J.C. Escalante-Semerena, *In vitro synthesis of the nucleotide loop of cobalamin by Salmonella typhimurium enzymes.* Proc. Natl. Acad. Sci. U S A, 1999. **96**: p. 11798-11803.

69. O'Toole, G.A. and J.C. Escalante-Semerena, *Purification and characterization of the bifunctional CobU enzyme of Salmonella typhimurium LT2. Evidence for a CobU-GMP intermediate.* J. Biol. Chem., 1995. **270**: p. 23560-23569.

70. Zayas, C.L., K. Claas, and J.C. Escalante-Semerena, *The CbiB protein of Salmonella enterica is an integral membrane protein involved in the last step of the de novo corrin ring biosynthetic pathway.* J. Bacteriol., 2007. **189**: p. 7697-7708.

71. Zayas, C.L. and J.C. Escalante-Semerena, *Reassessment of the late steps of coenzyme B_{12} synthesis in Salmonella enterica: Evidence that dephosphorylation of adenosylcobalamin-5'-phosphate by the CobC phosphatase is the last step of the pathway.* J. Bacteriol., 2007. **189**: p. 2210-2218.

72. Trzebiatowski, J.R., G.A. O'Toole, and J.C. Escalante-Semerena, *The cobT gene of Salmonella typhimurium encodes the NaMN: 5,6-dimethylbenzimidazole phosphoribosyltransferase responsible for the synthesis of N^1-(5-phospho-alpha-D-ribosyl)-5,6-dimethylbenzimidazole, an intermediate in the synthesis of the nucleotide loop of cobalamin.* J. Bacteriol., 1994. **176**: p. 3568-3575.

73. Escalante-Semerena, J.C. and J.R. Roth, *Regulation of cobalamin biosynthetic operons in Salmonella typhimurium.* J. Bacteriol., 1987. **169**: p. 2251-2258.

74. Jeter, R., et al., *Synthesis and use of vitamin B12*, in *Escherichia coli and Salmonella tyhpimurium : cellular and molecular biology*, F.C. Neidhardt, et al., Editors. 1987, Am. Soc. Microbiol.: Washington, D. C. p. 551-556.

75. Raux, E., et al., *Salmonella typhimurium cobalamin (vitamin B_{12}) biosynthetic genes: functional studies in S. typhimurium and Escherichia coli.* J. Bacteriol., 1996. **178**: p. 753-t67.

76. Otte, M.M. and J.C. Escalante-Semerena, *Biochemical characterization of the GTP:adenosylcobinamide-phosphate guanylyltransferase (CobY) enzyme of the hyperthermophilic archaeon Methanocaldococcus jannaschii.* Biochemistry, 2009. **48**: p. 5882-5889.

77. Zayas, C.L., J.D. Woodson, and J.C. Escalante-Semerena, *The cobZ gene of Methanosarcina mazei Gö1 encodes the nonorthologous replacement of the α-ribazole-5'-phosphate phosphatase (CobC) enzyme of Salmonella enterica.* J. Bacteriol., 2006. **188**: p. 2740-2743.

78. Woodson, J.D. and J.C. Escalante-Semerena, *The cbiS gene of the archaeon Methanopyrus kandleri AV19 encodes a bifunctional enzyme with adenosylcobinamide amidohydrolase and alpha-ribazole-phosphate phosphatase activities.* J. Bacteriol., 2006. **188**: p. 4227-4235.

79. Gray, M.J. and J.C. Escalante-Semerena, *Single-enzyme conversion of $FMNH_2$ to 5,6-dimethylbenzimidazole, the lower ligand of B_{12}.* Proc. Natl. Acad. Sci. U S A, 2007. **104**: p. 2921-2926.

80. Woodson, J.D. and J.C. Escalante-Semerena, *CbiZ, an amidohydrolase enzyme required for salvaging the coenzyme B_{12} precursor cobinamide in archaea.* Proc. Natl. Acad. Sci. USA, 2004. **101**: p. 3591-3596.

81. Gray, M.J. and J.C. Escalante-Semerena, *A new pathway for the synthesis of alpha-ribazole-phosphate in Listeria innocua.* Mol. Microbiol., 2010. **77**: p. 1429-1438.

82. Jeter, V.L., et al., *A new class of phosphoribosyltransferases involved in cobamide biosynthesis is found in methanogenic archaea and cyanobacteria.* Biochemistry, 2019. **58**: p. 951-964.

83. Raux, E., H.L. Schubert, and M.J. Warren, *Biosynthesis of cobalamin (vitamin B12): a bacterial conundrum.* Cell. Mol. Life Sci., 2000. **57**: p. 1880-1893.

84. Moore, S.J., et al., *Elucidation of the anaerobic pathway for the corrin component of cobalamin (vitamin B12).* Proc. Natl. Acad. Sci. U S A, 2013. **110**: p. 14906-14911.

85. Beck, R., et al., *CbiX: a novel metal-binding protein involved in sirohaem biosynthesis in Bacillus megaterium.* Biochem. Soc.Trans., 1997. **25**: p. 77S.

86. Leech, H.K., et al., *Characterization of the cobaltochelatase CbiXL: evidence for a 4Fe-4S center housed within an MXCXXC motif.* J. Biol. Chem., 2003. **278**: p. 41900-4197.

87. Müller, G., et al., *Timing of cobalt insertion in vitamin B12 biosynthesis.* J. Amer. Chem. Soc., 1991. **113**: p. 9893-9895.

88. Raux, E., et al., *A role for Salmonella typhimurium cbiK in cobalamin (vitamin B12) and siroheme biosynthesis.* J. Bacteriol., 1997. **179**: p. 3202-3212.

89. Romao, C.V., et al., *Evolution in a family of chelatases facilitated by the introduction of active site asymmetry and protein oligomerization.* Proc. Natl. Acad. Sci. U S A, 2011. **108**: p. 97-102.

90. Debussche, L., et al., *Purification and characterization of cobyrinic acid a,c-diamide synthase from Pseudomonas denitrificans.* J. Bacteriol., 1990. **172**: p. 6239-6244.

91. Blanche, F., et al., *Vitamin-B12 - How the problem of its biosynthesis was solved.* Angewand. Chem. Intern. Ed., 1995. **34**: p. 383-411.

92. Battersby, A.R., *How nature builds the pigments of life: the conquest of vitamin B_{12}.* Science, 1994. **264**: p. 1551-1557.

93. Roth, J.R., J.G. Lawrence, and T.A. Bobik, *Cobalamin (coenzyme B12): synthesis and biological significance.* Annu. Rev. Microbiol., 1996. **50**: p. 137-181.

94. Escalante-Semerena, J.C., M.G. Johnson, and J.R. Roth, *The CobII and CobIII regions of the cobalamin (vitamin B12) biosynthetic operon of Salmonella typhimurium.* J Bacteriol, 1992. **174**: p. 24-29.

95. Roth, J.R., et al., *Characterization of the cobalamin (vitamin B_{12}) biosynthetic genes of Salmonella typhimurium.* J. Bacteriol., 1993. **175**: p. 3303-3316.

96. Pollich, M. and G. Klug, *Identification and sequence analysis of genes involved in late steps of cobalamin (vitamin B12) synthesis in Rhodobacter capsulatus.* J. Bacteriol., 1995. **177**: p. 4481-4487.

97. Pollich, M., C. Wersig, and G. Klug, *The bluF gene of Rhodobacter capsulatus is involved in conversion of cobinamide to cobalamin (vitamin B_{12}).* J. Bacteriol., 1996. **178**: p. 7308-7310.

98. Vlcek, C., et al., *Sequence of a 189-kb segment of the chromosome of Rhodobacter capsulatus SB1003.* Proc Natl Acad Sci U S A, 1997. **94**: p. 9384-9388.

99. McGoldrick, H., et al., *Cobalamin (vitamin B12) biosynthesis in Rhodobacter capsulatus.* Biochem. Soc. Trans., 2002. **30**: p. 646-648.

100. McGoldrick, H.M., et al., *Identification and characterization of a novel vitamin B12 (cobalamin) biosynthetic enzyme (CobZ) from Rhodobacter capsulatus, containing flavin, heme, and Fe-S cofactors.* J. Biol. Chem., 2005. **280**: p. 1086-1094.

101. Heldt, D., et al., *Aerobic synthesis of vitamin B12: ring contraction and cobalt chelation.* Biochem. Soc. Trans., 2005. **33**: p. 815-819.

102. Campbell, G.R., et al., *Sinorhizobium meliloti bluB is necessary for production of 5,6-dimethylbenzimidazole, the lower ligand of B12.* Proc. Natl. Acad. Sci. U S A, 2006. **103**: p. 4634-4369.

103. Blanche, F., et al., *Purification and characterization of S-adenosyl-L-methionine: uroporphyrinogen III methyltransferase from Pseudomonas denitrificans.* J. Bacteriol., 1989. **171**: p. 4222-4231.

104. Cameron, B., et al., *Cloning and analysis of genes involved in coenzyme B12 biosynthesis in Pseudomonas denitrificans.* J. Bacteriol., 1989. **171**: p. 547-557.

105. Thibaut, D., et al., *Assay and purification of S-adenosyl-L-methionine:precorrin-2 methyltransferase from Pseudomonas denitrificans.* J. Bacteriol., 1990. **172**: p. 6245-6251.

106. Crouzet, J., et al., *Genetic and sequence analysis of an 8.7-kilobase Pseudomonas denitrificans fragment carrying eight genes involved in transformation of precorrin-2 to cobyrinic acid.* J. Bacteriol., 1990. **172**: p. 5980-5990.

107. Cameron, B., et al., *Genetic analysis, nucleotide sequence, and products of two Pseudomonas denitrificans cob genes encoding nicotinate-nucleotide: dimethylbenzimidazole phosphoribosyltransferase and cobalamin (5'-phosphate) synthase.* J. Bacteriol., 1991. **173**: p. 6066-6073.

108. Blanche, F., et al., *Biosynthesis of vitamin B12: stepwise amidation of carboxyl groups b, d, e, and g of cobyrinic acid a,c-diamide is catalyzed by one enzyme in Pseudomonas denitrificans.* J. Bacteriol., 1991. **173**: p. 6046-6051.

109. Crouzet, J., et al., *Nucleotide sequence and genetic analysis of a 13.1-kilobase-pair Pseudomonas denitrificans DNA fragment containing five cob genes and identification of structural genes encoding Cob(I)alamin adenosyltransferase, cobyric acid synthase, and bifunctional cobinamide kinase-cobinamide phosphate guanylyltransferase.* J. Bacteriol., 1991. **173**: p. 6074-6087.

110. Debussche, L., et al., *Purification and partial characterization of cob(I)alamin adenosyltransferase from Pseudomonas denitrificans.* J. Bacteriol., 1991. **173**: p. 6300-6302.

111. Blanche, F., et al., *A bifunctional protein from Pseudomonas denitrificans carries cobinamide kinase and cobinamide phosphate guanylyltransferase activities.* J. Bacteriol., 1991. **173**: p. 6052-6057.

112. Blanche, F., et al., *Biosynthesis of vitamin B_{12} in Pseudomonas denitrificans: the biosynthetic sequence from precorrin-6y to precorrin-8x is catalyzed by the cobL gene product.* J. Bacteriol., 1992. **174**: p. 1050-1052.

113. Blanche, F., et al., *Purification and characterization of Cob(II)yrinic acid a,c-diamide reductase from Pseudomonas denitrificans.* J. Bacteriol., 1992. **174**: p. 7452-7454.

114. Blanche, F., et al., *Precorrin-6x reductase from Pseudomonas denitrificans: purification and characterization of the enzyme and identification of the structural gene.* J. Bacteriol., 1992. **174**: p. 1036-1042.

115. Debussche, L., et al., *Assay, purification, and characterization of cobaltochelatase, a unique complex enzyme catalyzing cobalt insertion in hydrogenobyrinic acid a,c-diamide during coenzyme B_{12} biosynthesis in Pseudomonas denitrificans.* J. Bacteriol., 1992. **174**: p. 7445-7451.

116. Scott, A.I., et al., *Biosynthesis of vitamin B_{12}. Discovery of the enzymes for oxidative ring contraction and insertion of the fourth methyl group.* FEBS Lett., 1993. **331**: p. 105-108.

117. Fazzio, T.G. and J.R. Roth, *Evidence that the CysG protein catalyzes the first reaction specific to B12 synthesis in Salmonella typhimurium, insertion of cobalt.* J. Bacteriol., 1996. **178**: p. 6952-6959.

118. Moore, S.J., et al., *Characterization of the enzyme CbiH60 involved in anaerobic ring contraction of the cobalamin (vitamin B12) biosynthetic pathway.* J. Biol. Chem., 2012. **288**: p. 297-305.

119. Escalante-Semerena, J.C., S.J. Suh, and J.R. Roth, *cobA function is required for both de novo cobalamin biosynthesis and assimilation of exogenous corrinoids in Salmonella typhimurium.* J. Bacteriol., 1990. **172**: p. 273-280.

120. Lundqvist, J., et al., *The AAA(+) motor complex of subunits CobS and CobT of cobaltochelatase visualized by single particle electron microscopy.* J. Struct. Biol., 2009. **167**: p. 227-234.

121. Johnson, C.L., et al., *Functional genomic, biochemical, and genetic characterization of the Salmonella pduO gene, an ATP:cob(I)alamin adenosyltransferase gene.* J. Bacteriol., 2001. **183**: p. 1577-1584.

122. Buan, N.R., S.J. Suh, and J.C. Escalante-Semerena, *The eutT gene of Salmonella enterica encodes an oxygen-labile, metal-containing ATP:corrinoid adenosyltransferase enzyme.* J. Bacteriol., 2004. **186**: p. 5708-5714.

123. Fonseca, M.V. and J.C. Escalante-Semerena, *Reduction of cob(III)alamin to cob(II)alamin in Salmonella enterica Serovar Typhimurium LT2.* J. Bacteriol., 2000. **182**: p. 4304-4309.

124. Stich, T.A., et al., *Spectroscopic evidence for the formation of a four-coordinate Co(2+)cobalamin species upon binding to the human ATP:Cobalamin adenosyltransferase.* J. Am. Chem. Soc., 2005. **127**: p. 7660-7661.

125. Pallares, I.G., et al., *Spectroscopic studies of the Salmonella enterica adenosyltransferase enzyme SeCobA: Molecular-level insight into the mechanism of substrate cob(II)alamin activation.* Biochemistry, 2014. **53**: p. 7969-7982.

126. Moore, T.C., et al., *Structural insights into the mechanism of four-coordinate cob(II)alamin formation in the active site of the Salmonella enterica ATP:co(I)rrinoid adenosyltransferase (CobA) enzyme: Critical role of residues Phe91 and Trp93.* Biochemistry, 2012. **51**: p. 9647-9657.

127. Havemann, G.D. and T.A. Bobik, *Protein content of polyhedral organelles involved in coenzyme B12-dependent degradation of 1,2-propanediol in Salmonella enterica serovar Typhimurium LT2.* J. Bacteriol., 2003. **185**: p. 5086-5095.

128. Sampson, E.M. and T.A. Bobik, *Microcompartments for B_{12}-dependent 1,2-propanediol degradation provide protection from DNA and cellular damage by a reactive metabolic intermediate.* J. Bacteriol., 2008. **190**: p. 2966-2971.

129. Pallares, I.G., et al., *Spectroscopic studies of the EutT adenosyltransferase from Salmonella enterica: Mechanism of four-coordinate Co(II)Cbl formation.* J. Am. Chem. Soc., 2016. **138**: p. 3694-3704.

130. Pallares, I.G., et al., *Spectroscopic studies of the EutT adenosyltransferase from Salmonella enterica: Evidence of a tetrahedrally coordinated divalent transition metal cofactor with cysteine ligation.* Biochemistry, 2017. **56**: p. 364-375.

131. Costa, F.G. and J.C. Escalante-Semerena, *A new class of EutT ATP:Co(I)rrinoid adenosyltransferases found in Listeria monocytogenes and other Firmicutes does not require a metal Ion for activity.* Biochemistry, 2018. **57**(34): p. 5076-5087.

132. Cheong, C.G., J.C. Escalante-Semerena, and I. Rayment, *Structural studies of the L-threonine-O-3-phosphate decarboxylase (CobD) enzyme from Salmonella enterica: the apo, substrate, and product-aldimine complexes.* Biochemistry, 2002. **41**: p. 9079-9089.

133. Cheong, C.G., et al., *Three-dimensional structure of the L-threonine-O-3-phosphate decarboxylase (CobD) enzyme from Salmonella enterica.* Biochemistry, 2002. **41**: p. 4798-4808.

134. Tavares, N.K., C.M. VanDrisse, and J.C. Escalante-Semerena, *Rhodobacterales use a unique L-threonine kinase for the assembly of the nucleotide loop of coenzyme B12.* Mol. Microbiol., 2018. **110**: p. 239-261.

135. Tavares, N.K., C.L. Zayas, and J.C. Escalante-Semerena, *The Methanosarcina mazei MM2060 gene encodes a bifunctional kinase/decarboxylase enzyme involved in cobamide biosynthesis.* Biochemistry, 2018. **57**(30): p. 4478-4495.

136. Keller, S., et al., *The SMUL_1544 gene product governs norcobamide biosynthesis in the tetrachloroethene-respiring bacterium Sulfurospirillum multivorans.* J. Bacteriol., 2016. **198**: p. 2236-2243.

137. Keller, S., et al., *Exogenous 5,6-dimethylbenzimidazole caused production of a non-functional tetrachloroethene reductive dehalogenase in Sulfurospirillum multivorans.* Environ. Microbiol., 2013. **16**: p. 3361-3369.

138. Woodson, J.D., C.L. Zayas, and J.C. Escalante-Semerena, *A new pathway for salvaging the coenzyme B_{12} precursor cobinamide in archaea requires cobinamide-phosphate synthase (CbiB) enzyme activity.* J. Bacteriol., 2003. **185**: p. 7193-7201.

139. Ronzio, R.A. and H.A. Barker, *Enzymic synthesis of guanosine diphosphate cobinamide by extracts of propionic acid bacteria.* Biochemistry, 1967. **6**: p. 2344-2354.

140. O'Toole, G.A. and J.C. Escalante-Semerena, *cobU-dependent assimilation of nonadenosylated cobinamide in cobA mutants of Salmonella typhimurium.* J. Bacteriol., 1993. **175**: p. 6328-6336.

141. Woodson, J.D., et al., *The cobY gene of the archaeon Halobacterium sp. strain NRC-1 is required for de novo cobamide synthesis.* J Bacteriol, 2003. **185**: p. 311-316.

142. Thomas, M.G. and J.C. Escalante-Semerena, *Identification of an alternative nucleoside triphosphate: 5'- deoxyadenosylcobinamide phosphate nucleotidyltransferase in Methanobacterium thermoautotrophicum ΔH.* J. Bacteriol., 2000. **182**: p. 4227-4233.

143. Newmister, S.A., et al., *Structure and mutational analysis of the archaeal GTP:AdoCbi-P guanylyltransferase (CobY) from Methanocaldococcus jannaschii:*

Insights into GTP binding and dimerization. Biochemistry, 2011. **50**: p. 5301-5313.

144. Singarapu, K.K., et al., *Solution structural studies of GTP:Adenosylcobinamide-phosphate guanylyltransferase (CobY) from Methanocaldococcus jannaschii.* PLoS One, 2015. **10**: p. e0141297.

145. Thompson, T.B., et al., *Three-dimensional structure of adenosylcobinamide kinase/adenosylcobinamide phosphate guanylyltransferase (CobU) complexed with GMP: evidence for a substrate-induced transferase active site.* Biochemistry, 1999. **38**: p. 12995-3005.

146. Glusker, J.P., *X-Ray Crystallography of B12 and Cobaloximes.*, in *B12*, D. Dolphin, Editor. 1982, John Wiley & Sons: New York. p. 23-106.

147. Taga, M.E., et al., *BluB cannibalizes flavin to form the lower ligand of vitamin B12.* Nature, 2007. **446**: p. 449-453.

148. Hazra, A.B., et al., *Anaerobic biosynthesis of the lower ligand of vitamin B12.* Proc. Natl. Acad. Sci. U S A, 2015. **112**: p. 10792-10797.

149. Johnson, M.G. and J.C. Escalante-Semerena, *Identification of 5,6-dimethylbenzimidazole as the Coα ligand of the cobamide synthesized by Salmonella typhimurium. Nutritional characterization of mutants defective in biosynthesis of the imidazole ring.* J. Biol. Chem., 1992. **267**(19): p. 13302-13305.

150. Mattes, T.A. and J.C. Escalante-Semerena, *Salmonella enterica synthesizes 5,6-dimethylbenzimidazolyl-(DMB)-alpha-riboside. Why some Firmicutes do not require the canonical DMB activation system to synthesize adenosylcobalamin.* Mol. Microbiol., 2017. **103**: p. 269-281.

151. Cheong, C.G., J.C. Escalante-Semerena, and I. Rayment, *The three-dimensional structures of nicotinate mononucleotide:5,6- dimethylbenzimidazole*

phosphoribosyltransferase (CobT) from Salmonella typhimurium complexed with 5,6-dimethybenzimidazole and its reaction products determined to 1.9Å resolution. Biochemistry, 1999. **38**: p. 16125-16135.

152. Cheong, C.G., J.C. Escalante-Semerena, and I. Rayment, *Structural investigation of the biosynthesis of alternative lower ligands for cobamides by nicotinate mononucleotide: 5,6-dimethylbenzimidazole phosphoribosyltransferase from Salmonella enterica.* J. Biol. Chem., 2001. **276**: p. 37612-37620.

153. Chan, C.H. and J.C. Escalante-Semerena, *ArsAB, a novel enzyme from Sporomusa ovata activates phenolic bases for adenosylcobamide biosynthesis.* Mol. Microbiol., 2011. **81**: p. 952-967.

154. Maggio-Hall, L.A., K.R. Claas, and J.C. Escalante-Semerena, *The last step in coenzyme B(12) synthesis is localized to the cell membrane in bacteria and archaea.* Microbiology, 2004. **150**: p. 1385-1395.

155. Kadner, R.J. and G. McElhaney, *Outer membrane-dependent transport systems in Escherichia coli: turnover of TonB function.* J. Bacteriol., 1978. **134**: p. 1020-1029.

156. Cadieux, N., et al., *Identification of the periplasmic cobalamin-binding protein BtuF of Escherichia coli.* J. Bacteriol., 2002. **184**: p. 706-717.

157. Mireku, S.A., et al., *Conformational change of a tryptophan residue in BtuF facilitates binding and transport of cobinamide by the vitamin B12 transporter BtuCD-F.* Sci. Rep., 2017. **7**: p. 41575.

158. DeVeaux, L.C. and R.J. Kadner, *Transport of vitamin B12 in Escherichia coli: cloning of the btuCD region.* J. Bacteriol., 1985. **162**: p. 888-896.

159. Borths, E.L., et al., *In vitro functional characterization of BtuCD-F, the Escherichia coli ABC transporter for vitamin B12 uptake.* Biochemistry, 2005. **44**(49): p. 16301-16309.

160. Rempel, S., et al., *Cysteine-mediated decyanation of vitamin B12 by the predicted membrane transporter BtuM.* Nat. Commun., 2018. **9**: p. 3038.

161. Santos, J.A., et al., *Functional and structural characterization of an ECF-type ABC transporter for vitamin B12.* Elife, 2018. **7**.

162. Gray, M.J. and J.C. Escalante-Semerena, *The cobinamide amidohydrolase (cobyric acid-forming) CbiZ enzyme: a critical activity of the cobamide remodelling system of Rhodobacter sphaeroides.* Mol. Microbiol., 2009. **74**: p. 1198-1210.

163. Gray, M.J. and J.C. Escalante-Semerena, *In vivo analysis of cobinamide salvaging in Rhodobacter sphaeroides strain 2.4.1.* J. Bacteriol., 2009. **191**: p. 3842-3851.

164. Gray, M.J., N.K. Tavares, and J.C. Escalante-Semerena, *The genome of Rhodobacter sphaeroides strain 2.4.1 encodes functional cobinamide salvaging systems of archaeal and bacterial origins.* Mol. Microbiol., 2008. **70**: p. 824-836.

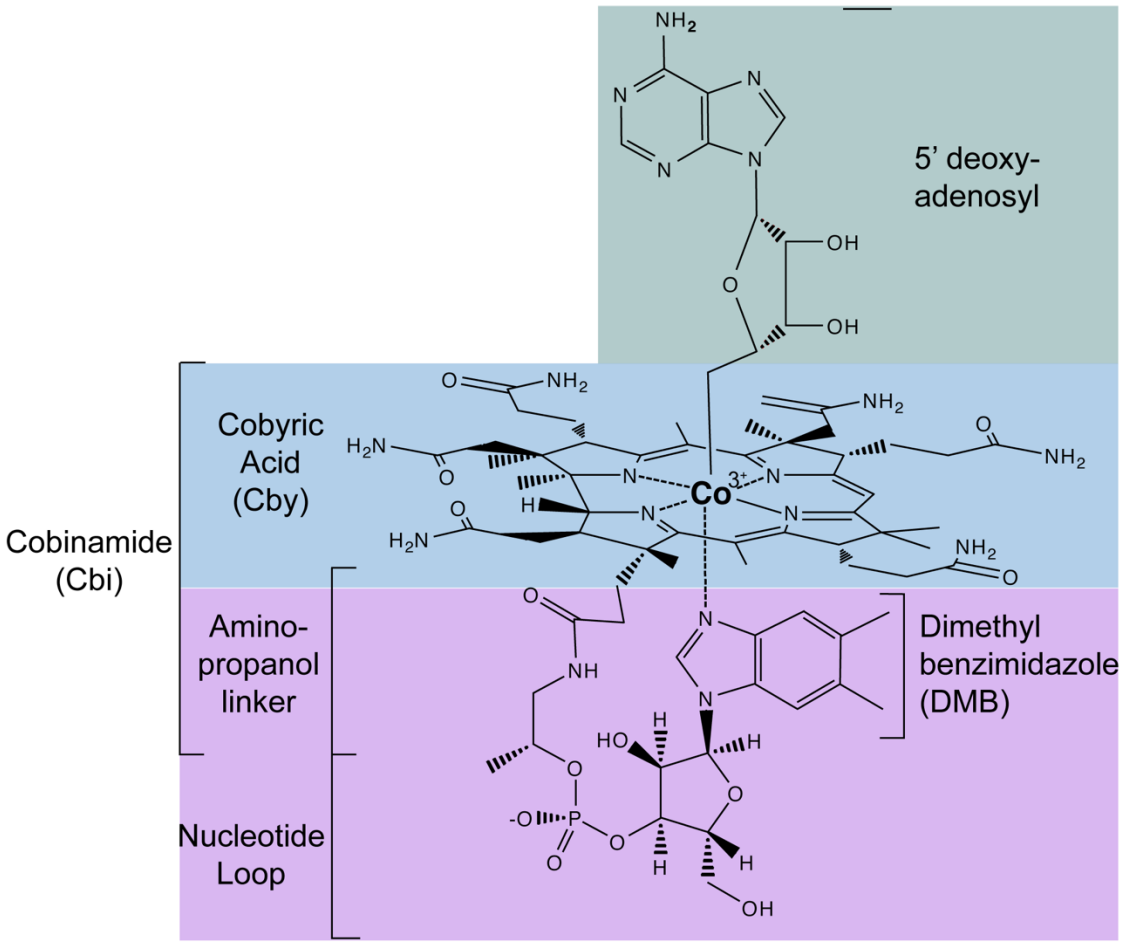

Figure 1.1 Chemical structure of adenosylcobalamin. Upper ligand in highlighted in teal, the corrin ring is highlighted in blue, and the lower ligand is highlighted in purple. Cobyric acid (Cby) is the fully amidated corrin ring. The covalent bond between 5'-deoxyadenosine and the Co ion, *i.e*, the *Cob* ligand of the ring, is critical for coenzyme function. The nucleotide loop is attached to the corrin ring by an aminopropanol linker (AP-P). The lower ligand base is 5,6-dimethylbenzimidazole (DMB).

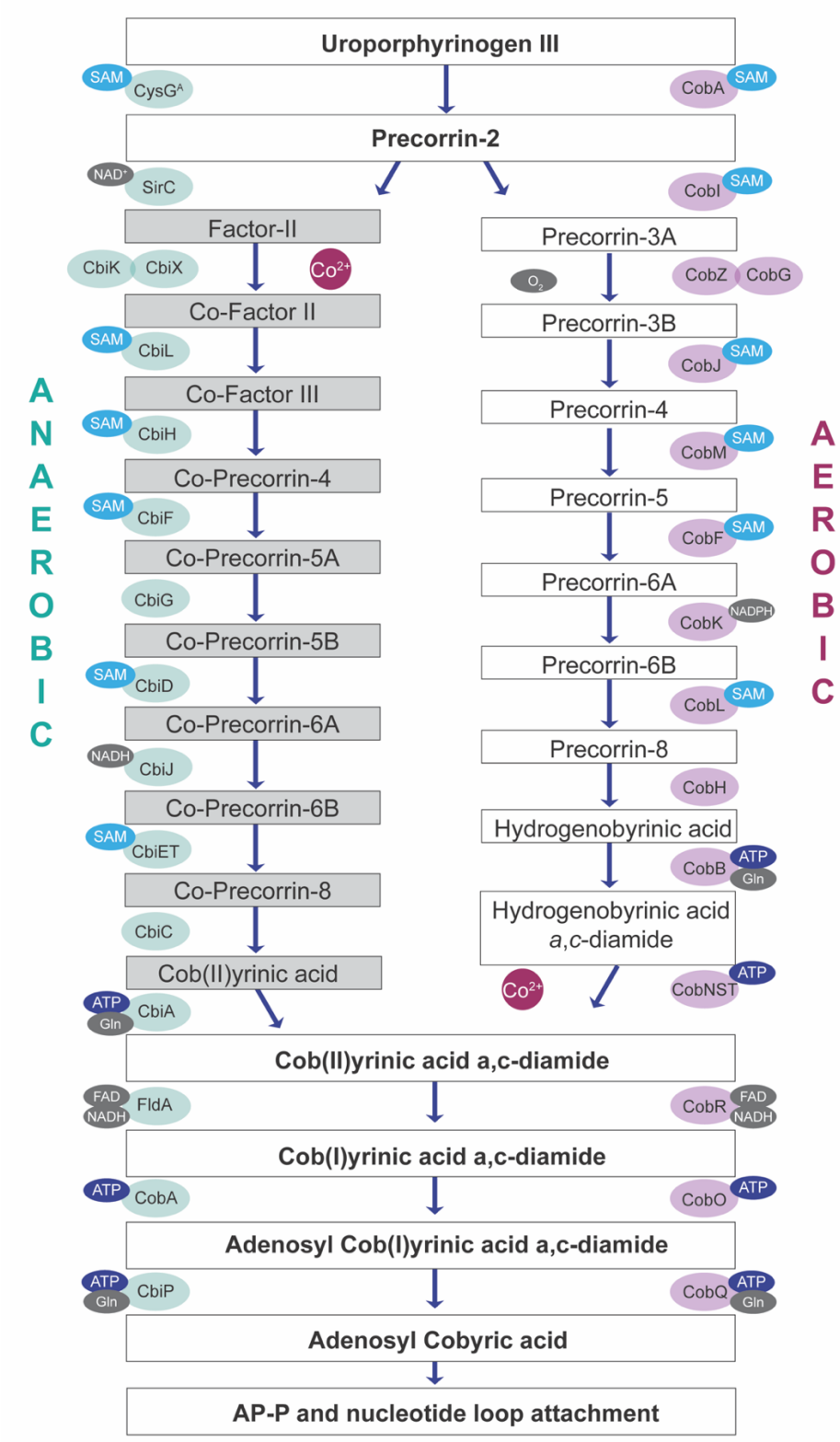

Legend on following page.

Figure 1.2. **Flow chart of the early steps of *de novo* Cba biosynthesis.** Summary of the early steps of cobamide biosynthetic pathways. Anaerobic pathway (early cobalt insertion) enzymes are shown in teal and aerobic (late cobalt insertion) pathway enzymes are shown in purple. Shared precursors, intermediates, and products are in bold.

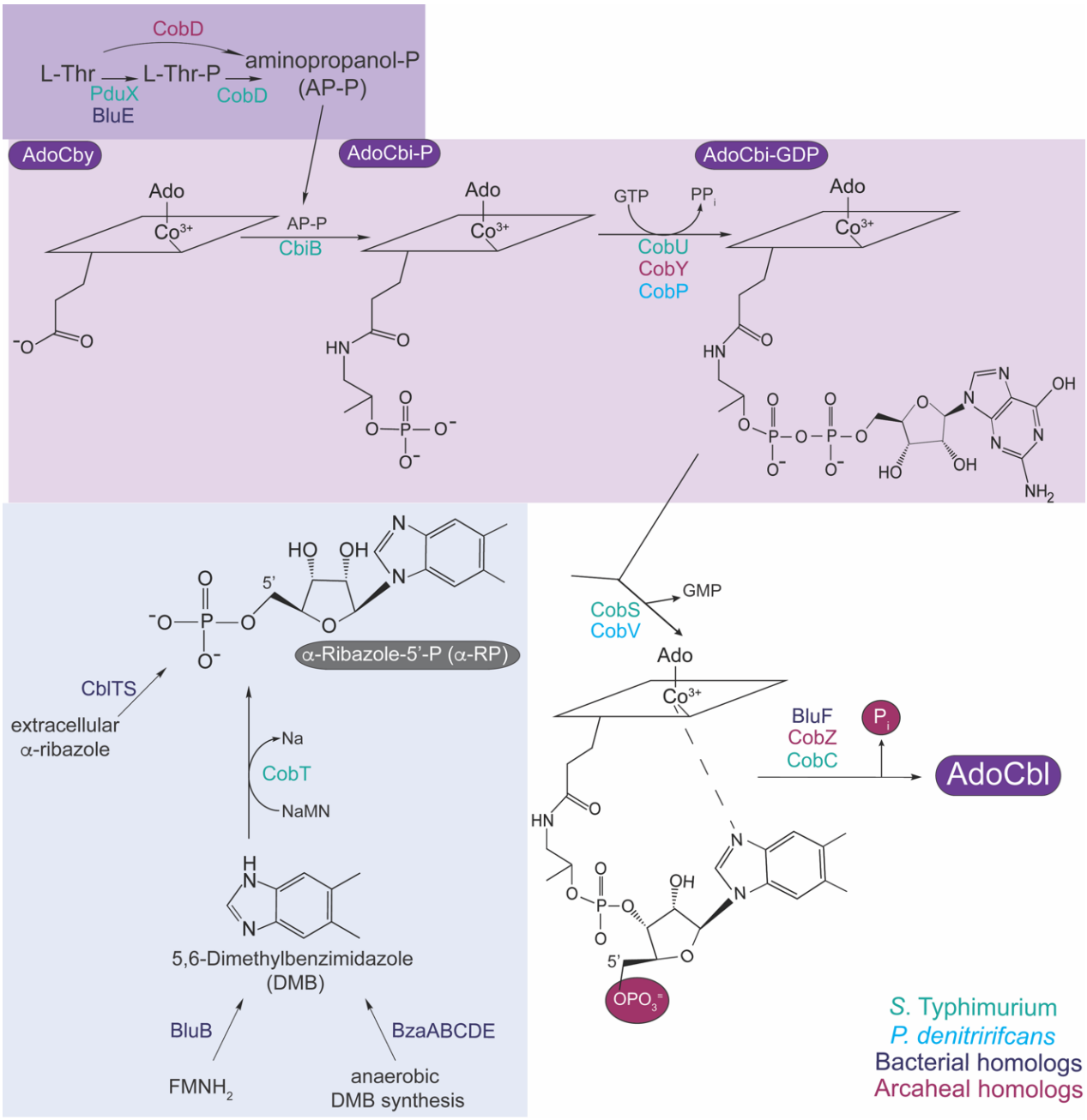

Legend on following page.

Figure 1.3. Nucleotide loop assembly pathway. The formation of adenosylcobalamin (AdoCbl) from adenosylcobyric acid is shown. AdoCby is converted to adenosylcobinamide-P (AdoCbi-P) by the addition of the aminopropanol-phosphate (AP-P) linker. Synthesis of the AP-P linker is highlighted in purple. The subsequent activation of the corrin ring is shown in maroon. Conversion of adenosylcobinamide-GDP (AdoCbi-GDP) to adenosylcobalamin-phosphate (AdoCbl-P) is achieved through attachment of the activated base α-ribazole-5'-phosphate (α-RP) to AdoCbi-GDP. Strategies of α -RP syntheses are highlighted in blue. *S.* Typhimurium enzymes are displayed in teal, other homologs are shown as follows: *Pseudomonas denitrificans* (blue), other bacterial organisms (purple), or archaeal organisms (maroon).

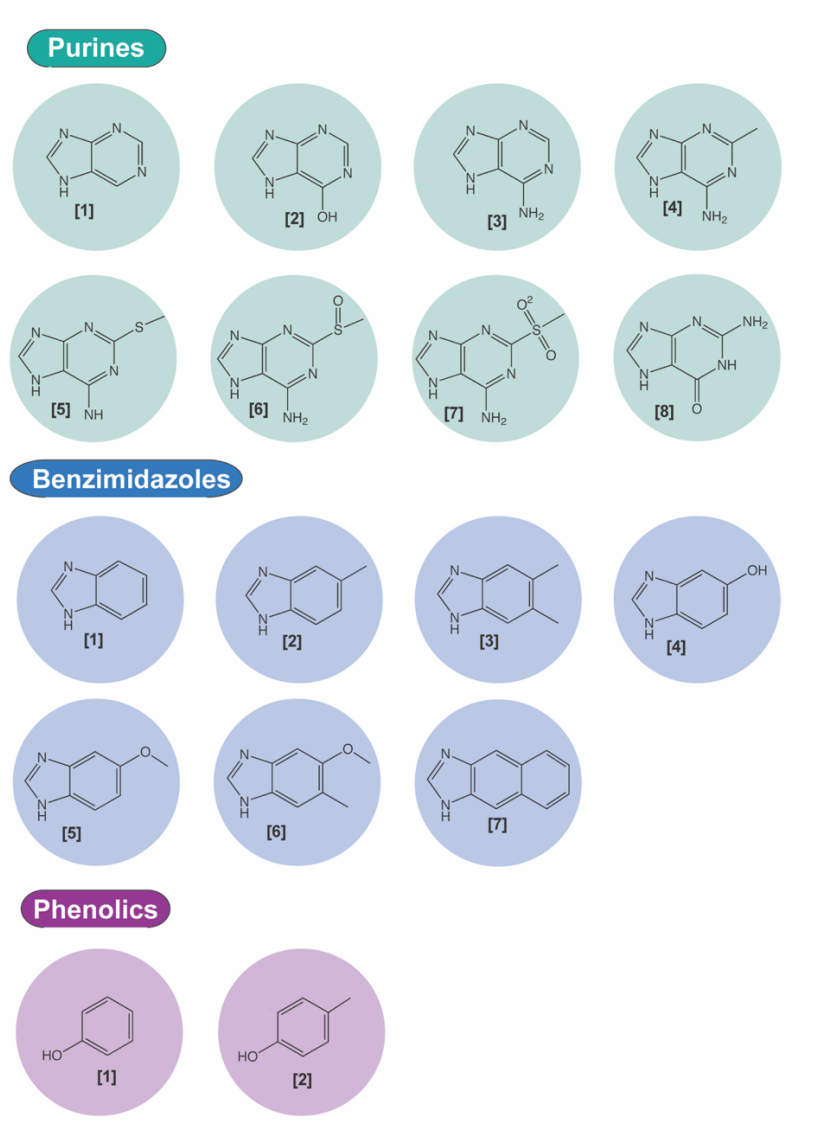

Figure 1.4. Cobamide base diversity. The lower ligand of Cbas can accommodate diverse bases. Purines and purine analogues found in Cbas: [1], purine; [2]. hypoxanthine; [3], adenine; [4], 2-methyladenine; [5], 2-methylmercaptoadenine; [6], 2-methylsulfinyladenine; [7], 2-methylsulfonyladenine; [8], guanine. Benzimidazole and its analogues: [1], benzimidazole; [2], 5-methylbenzimidazole; [3], 5,6-dimethylbenzimidazole; [4], 5-hydroxybenzimidazole; [5], 5-methoxybenzimidazole; [6], 5-methoxy-6-methylbenzimidazole; [7], naphthimidazole. Phenolics: [1], phenol; [2], *p*-cresol.

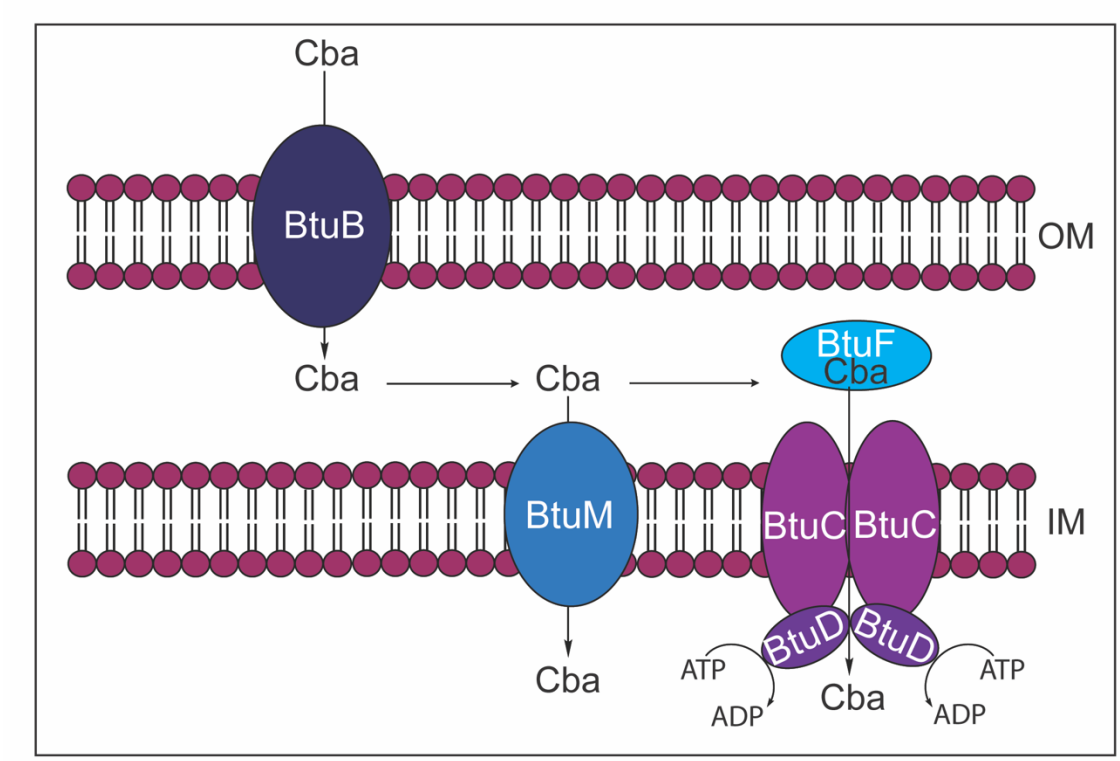

Figure 1.5. **Gram-negative cobamide transport.** Outer membrane, Ton-dependent transporter BtuB actively transports exogenous Cba or incomplete corrinoids (i.e. Cbi or Cby) into the periplasm. Two systems exist for the transport of Cbas or incomplete corrinoids from the periplasm across the inner membrane: BtuCDF or BtuM. BtuM directly transports Cbas or incomplete corrinoids to the cytoplasm. Periplasmic protein BtuF shuttles Cbas or incomplete corrinoids to the ABC-transporter BtuCD which brings Cbas into the cytoplasm.

CHAPTER 2

A NEW CLASS OF PHOSPHORIBOSYLTRANSFERASE INVOLVED IN COBAMIDE BIOSYNTHESIS IS FOUND IN METHANOGENIC ARCHAEA AND CYANOBACTERIA[1]

[1] Jeter V.L, Mattes T.A., Beattie N.R., and Escalante-Semerena J.C. 2019. *Biochemistry* 58:951-964.

Reprinted here with permission from the publisher.

ABSTRACT

Cobamides (Cbas) are coenzymes used by cells from all domains of life, but made *de novo* only by some bacteria and archaea. The last steps of the cobamide biosynthetic pathway activate the corrin ring and the lower ligand base, condense the activated intermediates, and dephosphorylate the product prior to the release of the biologically active coenzyme. In bacteria, a phosphoribosyltransferase (PRTase) enyzme activates the base into its α-mononucleotide. The enzyme from *Salmonella enterica* (*Se*CobT) has been extensively biochemically and structurally characterized. The crystal structure of the putative PRTase from the archaeum *Methanocaldococcus jannaschii* (*Mj*CobT) is known but its function has not been validated. Here we report the *in vivo* and *in vitro* characterization of *Mj*CobT. *In vivo*, *in vitro*, and phylogenetic data reported here show that *Mj*CobT belongs to a new class of NaMN-dependent PRTase. We also show that the *Synechococcus* sp. WH7803 CobT protein has PRTase activity *in vivo*. Lastly, results of isothermal titration calorimetry and analytical ultracentrifugation analysis show that the biologically active form of *Mj*CobT is a dimer, not a trimer, as suggested by its crystal structure.

INTRODUCTION

Cobamides (Cba) are cobalt-containing cyclic tetrapyrroles used by cells from all domains of life but are produced *de novo* only by some bacteria and archaea [reviewed in 1]. Cbas are involved in enzymatic carbon skeleton rearrangements, methyl-group transfers, reductive dehalogenation, and elimination reactions (2-6).

Additionally, cobamide-dependence is common amongst radical SAM enzymes. Recent work has identified a role for Cbas in gene regulation as photoreceptors (reviewed in 7).

Structurally, Cbas are characterized by a central cobalt ion equatorially coordinated by the nitrogens of the pyrrole rings. Unlike other cyclic tetrapyrroles (*e.g.,* heme, factor F_{430}, bacteriochlorophylls), most Cbas contain an upper and a lower ligand. The coenzymic form of the Cba known as cobalamin (Cbl) has a 5'-deoxyadenosyl (Ado) group as its upper ligand and 5,6-dimethylbenzimidazole (DMB) as the lower ligand (Fig. 2.1A). In addition to DMB, other purines and benzimidazole homologues can serve as the lower ligand and form a coordination bond with the central cobalt ion (8) (Fig. 2.1B,C). Some organisms (*e.g., Sporomusa ovata*) can also incorporate phenolics as bases into Cbas (Fig. 2.1D), but such bases cannot form coordination bonds with the cobalt ion of the ring.

Vitamin B_{12} (cyanocobalamin, CNCbl) is a Cba whose upper ligand is a cyano (CN) group, and its lower ligand is DMB. As shown in figure 2.1, the diversity of bases found in Cbas is broad (4, 8). For example, *Salmonella enterica* produces three Cbas with varying nucleotide bases: one with DMB (a.k.a. cobalamin, Cbl), one with adenine (a.k.a. pseudocobalamin, psCbl), and one with 2-methyladenine (a.k.a. Factor A) (9-11).

Lower ligand bases require activation to an α-ribotide prior to their incorporation into the Cba. The last steps of AdoCba biosynthetic pathways activate the corrin ring and the lower ligand base, condense the activated intermediates into an AdoCba-phosphate (AdoCba-P), and, finally, removes the phosphate to yield the

final product of the pathway (Fig. 2.3). In *Salmonella enterica*, the CobT enzyme (EC2.4.2.21), a nicotinate mononucleotide (NaMN):Base phosphoribosyltransferase (PRTase), activates the lower ligand base (Fig. 2.2). The product of this reaction is the intermediate known as α-ribazole-5'-phosphate (α-RP) (12).

Previous *in vitro* studies of *Se*CobT showed that the enzyme has a broad range of substrate specificity and can activate purine and benzimidazole analogues (Fig. 2.1) (12, 13). This lack of substrate specificity is shared by *S. enterica* CobT (*Se*CobT) homologues in other microorganisms (14). At present, we know little about the function of archaeal *Se*CobT homologues. The crystal structure of the putative apo NaMN:Base PRTase from the methanogenic archaeum *Methanocaldococcus jannaschii* (ORF MJ_RS08515) has been reported, but evidence supporting the annotated activity has not been published.

Bioinformatics analyses of the MJ_RS08515 amino acid sequence compared with that of the *Se*CobT enzyme showed limited identity (18%) and similarity (32%) (Fig. 2.3). These enzymes also differed in their oligomeric state, with the archaeal enzyme forming trimers (PDB 3L0Z), according to the structure deposited into the Research Collaboratory for Structural Bioinformatics Protein Database (RCSB PDB) (unpublished work), while the bacterial enzyme forms dimers (12) (PDB 1L4B).

We note that previous studies by other investigators suggested that cyanobacteria solely produce psCbl. Additionally, these studies showed that 121 of the 123 cyanobacterial genomes searched lacked *cobT* (15, 16). In contrast to

these findings, our bioinformatics analysis identified CobT homologues in many cyanobacterial genomes. These homologues were similar in amino acid sequence composition to MJ_RS08515.

The work reported here shows that *M. jannaschii* CobT (*Mj*CobT) belongs to a new class of base-activating PRTase enzymes. We determined that *Mj*CobT represents a new class of base-activating PRTase enzymes based on both structural and taxonomic differences from the extensively characterized *Se*CobT. In this study we used *S. enterica* as a heterologous complementation system to show that *Mj*CobT has *bona fide* NaMN:DMB PRTase activity *in vivo*. Consistent with our *in vivo* results, *Mj*CobT exhibited robust enzymatic activity *in vitro* at pH 7. We found that under the conditions used to assay *Mj*CobT activity, the *Se*CobT enzyme also displayed strong activity. This finding was of interest, because in the past we had only measured strong *Se*CobT activity at pH 10. We identify potassium phosphate (KP_i) as the ingredient of the reaction mixture needed by *Se*CobT to be active at pH 7. We also report that *MjCobT* has broad substrate specificity and high affinity for its NaMN substrate. Finally, our data support the idea that *Mj*CobT is biologically active as a dimer.

MATERIALS AND METHODS

Culture media and growth conditions

All chemicals were reagent grade and were purchased from Sigma-Aldrich unless otherwise stated. Purchased chemicals were used without further purifications. All strains used in this study were grown at 37°C in no-carbon energy (NCE) minimal

medium (17) supplemented with ribose (20 mM) as a carbon and energy source. Minimal medium was also supplemented with $MgSO_4$ (1 mM) and trace minerals (18). When used, ampicillin, kanamycin, or chloramphenicol were added at 100 μg/mL, 50 μg/mL or 25 μg/mL, respectively. For all growth experiments, two μL of overnight cultures (12-16 h old) grown in nutrient broth (NB, Difco) was used to inoculate 198 μL of minimal medium with supplements (1% inoculum, v/v). Strains were grown in triplicate in 96-well microtiter plates for growth experiments. Growth was monitored using a computer-controlled BioTek plate reader (Model Eon). Optical density at 630 nm was measured every 30 min for a total time of 24 h; the microtiter dish was shaken between measurements. Data were analyzed using GraphPad Prism v6 software. Doubling times were calculated using the exponential growth equation included with the GraphPad Prism v6 software.

Strain constructions

All strains used in in this study were derivatives of *Salmonella enterica enterica* sv Typhimurium (hereafter *S. enterica*) LT2 or *Escherichia coli* BL21. Strain genotypes are described in Table 2.2. Plasmids were introduced into *S. enterica* by electroporation (19) and into *E.coli* by heat-shock transformation (20). Deletions in *S. enterica* were constructed and resolved with pCP20 as described elsewhere (21).

Plasmid constructions

All primers used during the course of this work are described in Table 2.3. Restriction enzymes were purchased from Fermentas. BspQI restriction enzyme was purchased from New England BioLabs. *Synechococcus* sp. WH7803 cobT gene was codon optimized for expression in *E. coli* by GenScript (Fig. 2.15).

Plasmid pMjCobT1. This plasmid was constructed using the polymerase incomplete primer extension (PIPE) method (22). The *Methanocaldococcus jannaschii* wildtype allele of ORF MJ_RS08515 was amplified from *M. jannaschii* genomic DNA (a gift from W. B. Whitman, University of Georgia) using the primers Mj_1598_cobT_PIPE_f and Mj_1598_cobT_PIPE_r. Vector pBAD24 (23) was amplified using primers pBAD24-PIPE-5' and pBAD24-PIPE-3'. Amplified fragments were cut with DpnI (ThermoFisher) overnight at 37°C. Fragments were mixed in equal volumes and transformed in chemically competent *E. coli* DH5α (20). The completed plasmid contained ORF MJ_RS08515 coding sequence inserted between KpnI and SalI sites of pBAD24. The plasmid was used for complementation analyses and generation of cobamides in *S. enterica.* Plasmid pMjCobT1 is 5,601 bp long and encodes resistance to ampicillin.

Plasmid pMjCobT2. This plasmid was also constructed using the PIPE method as described above using primers Mj_1598_TEV5_PIPE_f and Mj_1598_TEV5_PIPE_r to amplify ORF MJ_RS08515 and primers pTEV5-PIPE-5' and pTEV5-PIPE-3' to amplify the pTEV5 vector (24). pMjCobT2 contained the wildtype MJ_RS08515 coding sequence inserted between NheI and

XhoI sites of pTEV5. pMjCobT2 was used for protein overproduction. The plasmid is 6,381 bp long and encodes resistance to ampicillin. Transcription of MJ_RS08515 was induced by the addition of isopropyl-β-D-1-thiogalactopyranoside (IPTG), which triggered the synthesis of T7 polymerase, the enzyme responsible for the transcription of MJ_RS08515.

Plasmid pCOBT140. The construction of this vector has been described (25). The plasmid encodes *S. enterica cobT*$^{+}$, is ~5.6 kb long and encodes ampicillin resistance.

Plasmid pMjCobT3. This plasmid encoded *Mj*CobT^{E315A} and was constructed using overlapping primers MjCobT_sdm_E315A_F and MjCobT_sdm_E315A_R with plasmid pMjCobT1 DNA as the template. Briefly, the primers indicated encoding E315A changes were used to amplify the ORF MJ_RS08515 on pMjCobT1. Amplified products were cut with DpnI (ThermoFisher) overnight at 37°C. The amplification product was then transformed in *E. coli* DH5α and its nucleotide sequence verified.

Plasmid pMjCobT4. This plasmid encoded variant *Mj*CobT$^{E150A\ E315A}$ and was constructed using overlapping primers MjCobT_sdm_E150A_F and MjCobT_sdm_E150A_R with plasmid pMjCobT3 DNA as the template. Briefly, the primers indicated encoding E150A changes were used to amplify the ORF MJ_RS08515 with the E315A change on pMjCobT3. Amplified products were cut with DpnI (ThermoFisher) overnight at 37°C. The amplification product was then transformed in *E. coli* DH5α and its nucleotide sequence verified.

Plasmid pMjCobT5. This plasmid encoded *Mj*CobT^{E150A} and was constructed using overlapping primers MjCobT_sdm_E150A_F and MjCobT_sdm_E150A_R with plasmid pMjCobT1 DNA as the template. Briefly, the primers encoding E150A changes were used to amplify the ORF MJ_RS08515 on pMjCobT1. Amplified products were cut with DpnI (ThermoFisher) overnight at 37°C. The amplification product was then transformed in *E. coli* DH5α and its nucleotide sequence verified.

Plasmid pSynCobT2. This plasmid was constructed using the BspQI high-efficiency cloning method outlined elsewhere (26) using primers SynCobT pCV1 F and SynCobT pCV1 R to amplify the codon optimized *Synechococcus* sp. WH7803 CobT (SYNWH7803_RS09275). The completed plasmid contained codon optimized SYNWH7803_RS09275 coding sequence inserted between the pair of BspQI sites of pCV1. The plasmid was used for complementation analyses in *S. enterica.* Plasmid pSynCobT2 is 5,724 bp long and encodes resistance to ampicillin.

Cobamide extraction and high-performance liquid chromatography (HPLC) analysis. Overnight culture of strain JE18114 (Δ*metE* Δ*cobT* Δ*cobB* / pMjCobT1) and strain JE18115 (Δ*metE* Δ*cobT* Δ*cobB* / pCOBT140) grown in nutrient broth (NB) supplemented with ampicillin (100 μg/mL), kanamycin (50 μg/mL), and chloramphenicol (25 μg/mL) was used to inoculate NCE minimal medium supplemented with ribose (20 mM) as a carbon and energy source. Minimal medium also contained trace minerals, magnesium sulfate (1 mM), ampicillin (100 μg/mL) arabinose (500 μM), and dicyanocobinamide [$(CN)_2$Cbi] (300 nM). Where indicated, DMB, adenine, 5-methoxybenzimidazole (5-MeO-Bza), or 5-

hydroxybenzimidazole (5-HO-Bza) was provided at a final concentration of 200 μM. Cultures (250 mL) were grown for >20 h at 37°C in an Innova 44R gyratory incubator (New Brunswick Scientific) shaking at 180 rpm. Cells were harvested by centrifugation at 4°C for 15 min at 6,000 x *g* using an Avanti J20-XPI refrigerated centrifuge (Beckman) equipped with JLA-8.1000 rotor. Pelleted cells were re-suspended in ammonium acetate buffer (100 mM, pH 4.5) containing KCN (10 mM), and stored at -20 °C. Cobamides were extracted using methods described elsewhere 27, 28. Cell suspensions were thawed on ice and subsequently incubated at 70°C with shaking at 180 rpm in an Innova 44R gyratory incubator (New Brunswick Scientific) for 2 h. After incubation, cell suspensions were centrifuged in an Avanti J-251 equipped with a JA 25.25 rotor (Beckman) at 43,000 x *g* for 40 min at 4°C. Clarified cell-free extract was filtered through a syringe filter unit (0.45 μm) and mixed with Amberlite XAD4 resin (Rohm-Haas). Cell-free extract and resin mixtures were incubated at 37°C with shaking at 180 rpm in an Innova 43 gyratory incubator (New Brunswick Scientific) for 16 h. After allowing the resin to settle, free liquid was removed, taking care not to disturb the resin. Resin was washed thrice with four bed volumes of deionized water (Millipore) allowing the resin to settle for 20 min between washes. After the final wash, two bed volumes of methanol (100%) were added to the resin and the solution incubated 16 h at room temperature. After incubation, methanol was removed from the resin, collected in a microfuge tube and subjected to vacuum centrifugation in an Eppendorf Vacufuge Plus set at 60 °C until dry. Dried pellets were re-suspended in a 1:4 ratio of buffer B [KH_2PO_4 (100 mM), KCN (10 mM), pH 8 + 50%

(v/v) acetonitrile] and buffer C [KH_2PO_4 (100 mM), KCN (10 mM), pH 6.5] in preparation for separation by HPLC. Cbas were resolved by RP-HPLC using a Shimadzu Prominence UFLC SPD-M30A equipped with a Phenomenex Syngergi 4μ hydro-RP80A 150 x 4.6 mm LC column as described (29, 30) with some modifications as outlined in (25). Cbas were detected at 367 nm and 525 nm.

Mass spectrometry of corrinoids. Corrinoids with retention times of 12, 13, and 16 min were collected, desalted using C18 SepPaks (Waters) and dried under vacuum centrifugation. The molecular mass of each corrinoid was determined by MALDI-TOF mass spectrometry at the PAMS facility of the University of Georgia.

Protein purification. Wild-type *Mj*CobT protein was overproduced from plasmid pMjCobT2 in strain JE6663 (*E. coli* C41) in 2-L cultures of Terrific Broth (31). Protein synthesis was induced by the addition of IPTG at a final concentration of 500 μM in mid-log phase cultures (OD_{600} ~0.6) growing at 37°C with shaking at 180 rpm in an Innova44 (New Brunswick Scientific) gyratory incubator. After induction, cultures were grown for 17 h at 30°C with shaking at 180 rpm. Cultures were harvested by centrifugation at 4°C for 15 min at 6,000 x *g* in an Avanti J20-XPI refrigerated centrifuge equipped with JLA-8.1000 rotor. Pelleted cells were stored at -80°C until used. Frozen cells were thawed on ice and re-suspended in Tris-HCl buffer (25 mM, pH 7.5) containing NaCl (0.5 M) and imidazole (20 mM) at a rate of 20% cell weight to buffer volume. Lysozyme (1μg/mL) and DNaseI (25μg/mL) were added to the cell suspension and incubated on ice for 10 min. Cells were lysed by cell press in a cell disruptor (Constant Systems) set at 1.72e8 Pa. Phenylmethylsulfonyl fluoride (PMSF) was added to the cell lysate at a final

concentration of 0.5 mM. The cell lysate was incubated for 30 min at 70°C to precipitate *E. coli* proteins. Cell debris and precipitated proteins were removed by centrifugation at room temperature for 30 min at 40,000 x *g* in an Avanti J-251 centrifuge (Beckman/Coulter) equipped with a JA 25.25 rotor. Clarified extract was filtered using a 0.45-μm syringe filter unit and applied to a 4-mL HisPur nickel-nitrilotriacetic acid (Ni-NTA) affinity column (ThermoFisher Scientific). The column was washed with 10 column volumes of Tris-HCl buffer (25 mM, pH 7.5) containing NaCl ((0.5 M) and imidazole (20 mM) and six column volumes of Tris-HC buffer (25 mM, pH 7.5) containing NaCl (0.5 M)) and imidazole (40 mM). H_6-*Mj*CobT was eluted with six column volumes of Tris-HCl buffer (25 mM, pH 7.5) containing NaCl (0.5 M) and imidazole (0.5 M). Fractions were collected throughout the wash and elution steps and H_6-*Mj*CobT purification was monitored by SDS-PAGE gel compared to Precision Plus Protein Standards (BioRad). Fractions containing H_6-*Mj*CobT were pooled and dialyzed against Tris-HCl buffer (25 mM, pH 7.5) containing NaCl (0.5 M) to remove imidazole. N-terminally tagged, recombinant tobacco etch virus protease (H_7-rTEV) was purified as described elsewhere (32) and mixed with H_6-*Mj*CobT at a ratio of 1:10 H_6-*Mj*CobT:H_7-rTEV. The mixture was incubated at 34°C for 3 h to remove the H_6 tag on *Mj*CobT. Cleaved *Mj*CobT was purified away from the tag and H_7-rTEV using the Ni-NTA affinity purification method outlined above and tag-less protein was dialyzed against Tris-HCl buffer (25 mM, pH 7.5) in steps with decreasing concentrations of NaCl down to 150 mM. Purified *Mj*CobT was flash frozen in liquid nitrogen and stored at -80°C until used. Protein concentration was measured using a NanoDrop 1000 spectrophotometer

(Thermo Scientific) using the molecular mass of 37600 Da and ε_{280} of 20400 M^{-1} cm^{-1} as determined by ProtParam [33].

Analytical ultracentrifugation. *Mj*CobT was dialyzed against 50 mM Na/K phosphate (pH 7.5) and 100 mM NaCl and diluted to a final concentration of 1 mg/ml. Quantification was performed on an Agilent 8453 UV/vis and used an ε_{280} of 20400 M^{-1} cm^{-1} as determined by ProtParam (33). The protein sample was loaded with the dialysis buffer to a final concentration of 1 mg/ml before being loaded into cells with 12 mm double-sector Epon centerpieces. The loaded cells were allowed to equilibrate in the rotor for 1 h at 20 °C. Sedimentation velocity data were collected at 50,000 rpm at 20 °C in an Optima XLA analytical ultracentrifuge. Data were recorded at 280 nm in radial step sizes of 0.003 cm. SEDNTERP (34) was used to calculate the partial specific volume of *Mj*CobT (0.756018 mL/g) as well as3435[3535] the density (1.0093 g/mL) and viscosity coefficient (0.010291) of the buffer. SEDFIT (35) was used to analyze the raw sedimentation data. Data were modeled as a continuous sedimentation coefficient distribution [c(s)], and were fit using the baseline, meniscus, frictional coefficient, and systematic time-invariant and radial-invariant noise. Fit data for the experiment had a root mean square deviations of (r.m.s.d) < 0.004 AU. The theoretical sedimentation coefficient (s) values were calculated from the atomic coordinates of *Mj*CobT(PDB ID 3L0Z) using HYDROPRO20 (36).

***In vitro* NaMN:DMB phosphoribosyltransferase assay.** NaMN:DMB PRTase activity was assayed as described elsewhere with minor changes to the reaction conditions detailed in each of the following sections (12). Asterisks shown

represent the following p-values: * denotes a p-value<0.05, ** denotes a p-value<0.01, *** denotes a p-value<0.001.

Specific activity measurements. To determine the specific activity of *Mj*CobT, the protein was diluted in potassium phosphate buffer (0.25 M, pH 8.0). Reaction mixtures contained phosphate buffer (0.25 M, pH 8.0), DMB (1.5 nmol), [2-^{14}C]-DMB (0.5 nmol) and *Mj*CobT (190 ng) in a final volume of 20 μL. NaMN was provided in the following amounts: 20 nmoles, 15 nmoles, 10 nmoles, and 5 nmoles. Reactions mixtures were incubated at 37°C. Samples were removed after 0, 3, 5, 10, and 15 min incubations and immediately spotted (5 μL) onto a silica gel thin-layer chromatography (TLC) plate (Whatman PE SIL G/UV). TLCs were developed for 1.5 h in a TLC chamber pre-equilibrated with a 3:2 (v/v) chloroform:methanol mobile phase. After drying in a fume hood, plates were exposed to a phosphor screen for 18 h. Distribution of radioactivity on TLC plates was visualized using a Typhoon Trio+ Variable Mode Imager (GE Life Sciences) with ImageQuant v5.2. Pixel density of TLC plates was analyzed using 1D gel analysis in TotalLab TL100 (Nonlinear Dynamics) and the resulting data were analyzed using Prism v6 (GraphPad). Each reaction was performed in triplicate.

Effect of pH on *Mj*CobT activity. Reactions were conducted as outlined above with NaMN (1 mM) and buffer (25 mM) at the following pHs: sodium malate, pH 5, sodium succinate, pH 5.5, 4- morpholineethansulfonic acid (MES) pH 6, Bis-Tris pH 6.5, imidazole pH 7, Tris-HCl, pH 7, Tris-HCl pH 8, potassium phosphate pH 8, Tris-HCl pH 9, 2-(cyclohexylamino)ethanesulfonic acid (CHES) pH 9, CHES pH

9.5, glycine pH 10, and glycine pH 10.5. Reaction mixtures were incubated for 15 min at 37°C.

Effect of ionic strength on *Mj*CobT activity. Varying concentrations of salt tested as outlined above with NaMN (1 mM) and either potassium chloride or sodium chloride at the following concentrations: 0.1, 0.2, 0.3, 0.4 and 0.5 M. Reaction mixtures were incubated for 15 min at 37 °C.

Effect of temperature on *Mj*CobT activity. *Mj*CobT activity as a function of incubation temperature was tested as outlined above with NaMN (1 mM). Reactions were incubated for 10 min at 40, 50, 70, or 80°C.

Effect of phosphate on *Mj*CobT activity. *Mj*CobT activity as a function of phosphate concentration was measured as described above with NaMN (1 mM) and phosphate at either 0.025, 0.05, 0.075, 0.1, 0.2 or 0.4 M phosphate salts adjusted to pH 7.0. Reaction mixtures were incubated for 15 min at 80°C. Equivalent reactions were prepared with sodium salts of sulfate, vanadate, selenate, or molybdate in lieu of potassium phosphate for comparison.

Determination of kinetic parameters. Pseudo-first order kinetic data were obtained at a range of NaMN concentrations (0.075 to 1 mM) with a saturating concentration of DMB (100 μM). The data were fit to the Michaelis-Menten equation to determine the K_m and maximum velocity (V_{max}):

$$v = \frac{V_{max}[S]}{K_m + [S]}$$

The turnover constant (k_{cat}) was obtained with the following equation where E represents enzyme concentration:

$$k_{cat} = \frac{V_{max}}{E}$$

Catalytic efficiency was determined by the following: k_{cat}/K_m.

Isothermal titration calorimetry. Binding assays of *Mj*CobT and NaMN substrate were performed using a Nano ITC isothermal titration calorimeter (TA instruments). *Mj*CobT was dialyzed against Tris-HCl buffer (25 mM, pH 7.5) containing NaCl (150 mM); NaMN was solubilized in the final protein dialysate. Samples were degassed for 20 min at 25°C before use. *Mj*CobT protein was present in the sample cell at 33 μM under constant stirring at 350 rpm, and NaMN was present in the injection syringe at 1 mM. Every 5 min, injections (2.4 μL) were made into the sample cell and heat released was recorded. Experiments were conducted at 25°C. Data were analyzed using NanoAnalyze software (TA instruments).

Phylogenetic analysis.

We searched for *Mj*CobT homologues using NCBI BLASTP with CobT query sequences from *M. jannaschii* (accession: WP_064496984.1), *S. enterica* (accession: NP_460961.1), *P. denitrificans* (accession: WP_015478315.1), and *B. megaterium* (accession: YP_003563500.1) 37. Query sequences were used to search cyanobacteria (taxid: 1117), thaumarchaeota (taxid: 651137), methanogens class I (taxid: 2283794), and methanogens class II (taxid: 224756). Results with a minimum 85% query coverage and e-value cutoff of $<10^{-40}$ were included in the supplementary tables. Results were screened using the NCBI conserved domain database (CDD) to confirm DMB-PRT_CobT superfamily (accession: cl11435, PSSM Id: 325029) placement 38. The percent identity and

percent positives are also provided. Results from "uncultured marine thaumarchaeotes" were omitted from the tables. The phylogenetic tree (Fig. 2.14) was constructed using SeaView software 39. CobT homologue sequences from the following organisms were used to generate a MUSCLE alignment: *M. jannaschii*, *M. thermoautotrophicus*, *S. acidocaldarius*, *P. denitrificans*, *S. enterica*, *S. ovata* (ArsAB), *Synechococcus* sp. WH7803, *G. kilaueensis*, *L. rosea*, *Anabaena* sp. PCC 7108,

Nostoc sp. PCC 7524, *Synechocystis sp.* PCC 7509, *T. erythraeum*, *L. aestuarii*, *H. rivularis*, *P. minor*, *C. watsonii*, *S. meliloti* and *M. aeruginosa*. The tree was then constructed using the PhyML algorithm (100 bootstraps) with BLOSUM 62 as the model. The tree was modified for publication using the FigTree1.4.3 program available online (http://tree.bio.ed.ac.uk/software/figtree/).

RESULTS & DISCUSSION

In vivo evidence that _M. jannaschii_ CobT (_Mj_CobT) is a functional enzyme. We used an *in vivo* approach to determine whether *Mj*CobT had NaMN:DMB phoshoribosyltransferase (PRTase) activity. For this purpose, we introduced a plasmid encoding *M. jannaschii cobT*$^{+}$ into a *S. enterica* Δ*cobT* strain to try to restore AdoCbl synthesis in the absence of *Se*CobT function. ORF MJ_RS08515 (referred to as *M. jannaschii cobT*$^{+}$) was placed under the control of an arabinose-inducible promoter in plasmid pBAD24 23 to yield pMjCobT1, which was moved into strain JE12893 (Δ*cobT1379* Δ*cobB1374*) yielding strain JE18114 (Table 2.2).

Strain JE12893 failed to grow without exogenous Cbl (Fig. 2.5, triangles), but grew when Cbl was present in the medium (Fig. 2.5, diamonds). Ectopic expression of *M. janaschii cobT*$^{+}$ allowed strain JE18114 to grow when Cbi was present in the medium (Fig. 2.5, inverted triangles). This result indicated that *Mj*CobT had *Se*CobT-like activity. Strain JE18115 (Δ*cobT* Δ*cobB* / pCOBT140) served as positive control for CobT function (Fig. 2.5, squares).

***Mj*CobT activates diverse bases to their corresponding α-ribotides.** To gain insights into the substrate specificity of *Mj*CobT, guided biosynthesis experiments were performed. For this purpose, Cbas were extracted from *S. enterica* Δ*cobT* Δ*cobB* / p*Mj*CobT (strain JE18114) after growth in culture medium supplemented with Cbi alone or Cbi plus varying bases (*i.e.,* 5,6-dimethylbenzimidazole (DMB), adenine, 5-methoxybenzimidazole, or 5-hydroxybenzimidazole). Reverse-phase, high-performance liquid chromatography (RP-HPLC) and MALDI-TOF mass spectrometry analyses of extracted Cbas showed that all the bases tested were incorporated into the final product (Fig. 2.6), indicating that *Mj*CobT activated each base to its corresponding α-ribotide. Notably, when no base was provided, *Mj*CobT activated endogenous adenine and the final product was psCbl. As a positive control, the same analyses were performed with Cbas extracted from the *S. enterica* Δ*cobT* Δ*cobB* / p*Se*CobT (strain JE18115) (data not shown).

***In vitro* optimization of conditions for *Mj*CobT NaMN:DMB PRTase activity.**

NaMN:DMB PRTase activity was measured using thin layer chromatography (TLC) and [2-^{14}C]-DMB substrate as described elsewhere (40).

Effect of pH on the reaction. To determine optimal buffer and pH for *Mj*CobT activity, activity level was assessed using multiple buffers over a range of pH (Fig. 2.7). *Mj*CobT showed greatest activity at pH 10, similar to *Se*CobT (40). Given that the internal pH of *S. enterica* is not 10, the buffer system with the highest activity within a physiologically relevant pH range was used for subsequent analyses. Subsequent experiments were performed with KP_i buffer pH 8.

Phosphate positively affects Mj*CobT activity.* Given the precedent of positive effects of phosphate on the activity of another Cba biosynthetic enzyme from a hyperthermophile (41), we varied the phosphate concentration in the reaction mixture to investigate the effect of phosphate on *Mj*CobT activity. We varied the concentration of KP_i in the reaction mixture (25-400 mM) and observed a modest increase in the amount of α-RP synthesized over a period of 15 min, from 1.0 to 1.8 nmol α-RP. To determine whether observed effect of activity was specific to phosphate, an equivalent experiment was performed with sulfate (Fig 2.8). The amount of DMB converted to α-RP by *Mj*CobT was measured after incubation of enzyme (250 nM) with substrates at 80ºC for 15 min in the presence of sulfate, phosphate or neither. In the absence of either sulfate or phosphate the enzyme converted 0.8 nmol of DMB (40% of the initial amount) to α-RP. To assess the effect of other oxyanions on the activity of *Mj*CobT compared to phosphate, an equivalent experiment was performed with sodium salts of vanadate, selenate, or

molybdate. Compared to phosphate (25 mM), none of the oxyanions tested stimulated *Mj*CobT activity, even when tested at 50 mM or 100 mM (Fig. 2.8).

Effect of ionic strength. To determine the effect of salts on the activity of *Mj*CobT, varying concentrations of sodium chloride and potassium chloride were tested (100-500 mM). Altering the ionic strength of the reaction system showed no significant change in the activity of *Mj*CobT with either salt (data not shown).

Enzyme activity as a function of temperature. We also probed the effect of temperature on the activity of *Mj*CobT. As expected for an enzyme from a hyperthermophile, the activity of *Mj*CobT increased as a function of temperature, exhibiting the highest activity (~4-fold increase from 37°C) at 80°C (data not shown).

Enzyme activity as a function of NaMN. As shown in figure 2.9A, the amount of *Mj*CobT-generated α–RP is displayed as a function of time for each concentration of NaMN tested. The specific activity of *Mj*CobT at each level of NaMN is shown in Figure 2.9B. *Mj*CobT shows NaMN:DMB PRTase activity at a physiological pH, where *Se*CobT activity was previously undetectable (40).

Effect of salting out agents. To assess the effect of crowding agents on the activity of *Mj*CobT, varying amounts of ammonium sulfate (75-750 mM) were added to the reaction, but no significant changes in activity were observed (data not shown).

Pseudo-first order kinetics analysis of *Mj*CobT

Kinetic parameters for the reaction catalyzed by *Mj*CobT were obtained with NaMN when DMB was provided at saturating levels (100μM). The rate of the reaction as

a function of NaMN concentration is shown in figure 2.10 with the corresponding summary of apparent kinetic parameters shown in the inset. Kinetic parameters of *Mj*CobT for DMB were not obtained because of the limit of product detection of the assay. The plot in figure 2.10 is missing points below 50 μM NaMN because below that concentration product formation was not detectable. Of note, the apparent K_m of *Mj*CobT for NaMN was 5-fold lower than that of *Se*CobT (42).

Biologically active *Mj*CobT is a dimer

The oligomeric state of *Mj*CobT was determined by analytical ultracentrifugation. *Mj*CobT protein used for this analysis was 99% homogenous (Fig. 2.11A). Sedimentation velocity analysis showed that 27 μM *Mj*CobT existed primarily as a 4.4 S (81.3%) species that was consistent with the expected size of a dimer (Fig. 2.11B). Examining the crystal structure with PISA identified a dimeric assembly with a reasonable buried interface (940 $Å^2$) and a favorable P-value of 0.164, which is good evidence of a specific, stable dimer interface (43) (Fig. 2.11C). The identified dimer gives a predicted sedimentation value of 4.4 S, which matches the experimentally observed species. Additional evidence supporting our identification of the dimer can be seen in the crystal structure of the distant homologue, CobT from *Pyrococcus horikoshii* (PDB 3U4G), which contains the same dimeric assembly despite a sequence identity of 37% (Fig. 2.11C). The sedimentation distribution also revealed a small amount of a 6.5 S species (12.7%), which was consistent with a predicted tetramer (6.7 S) formed from the association of two of the dimers. We believe that this species is most likely caused

by aggregation of the protein, with the 0.2 difference in S value being the result of the aggregate forming a less compact structure than the modeled tetramer. Finally, there was a minor peak representing 3.8% of the distribution at 0.75S. Based on the small size, this is likely a minor contaminant in the sample.

*Mj*CobT has a high affinity for NaMN substrate

Isothermal titration calorimetry (ITC) was used to determine the affinity of *Mj*CobT for the NaMN substrate. The calculated dissociation constant (K_d) of the *Mj*CobT/NaMN complex was 3.2 μM, indicating a high affinity for the substrate (Fig. 2.12). Given the low concentration of NaMN in the cell (44), a high affinity for NaMN would be consistent with our expectations. ITC experiments aimed at determining the K_d of *Mj*CobT for DMB were not performed due to incompatibility of the solvent used to solubilize DMB (DMSO) with the ITC instrument. The molar ratio of ~2 was consistent with two active sites per *Mj*CobT dimer.

*Mj*CobT residues E150 and E315 are necessary for function

In *Se*CobT, residues E174 and E317 are required for activity (45). To investigate whether the equivalent residues in *Mj*CobT, *i.e.,* E150 and E315 (Fig. 2.4) were needed for activity, these residues were changed to alanine and the activity of the resulting variants was assessed *in vivo*. Sweeps of DMB and adenine were added to the growth medium. The minimum concentration of base necessary to confer growth of strains expressing variant proteins were included in Table 2.1. In the presence of DMB (50 μM) the strain that synthesized variant *Mj*CobT^{E150A} had a

doubling time similar to that of the strain that synthesized wild-type *Mj*CobT (Table 2.1). The strain that synthesized variant *Mj*CobT^{E150A} failed to grow when adenine (1 mM) substituted for DMB in the medium. At present it is unclear whether the *Mj*CobT^{E150A} variant could not use adenine as substrate because it cannot bind it or because it is catalytically inactive. ITC experiments aimed
at answering the question of binding could not be performed due to incompatibility of the solvent needed to keep adenine in solution.

In contrast, the *Mj*CobT^{E315A} variant restored growth with 10-fold less DMB (5 μM) in the medium, suggesting that the E315A substitution did not negatively affect enzyme activity as much as the E150A substitution. Unlike *Mj*CobT^{E150A}, *Mj*CobT^{E315A} did support psCbl synthesis, even when the concentration of adenine in the medium was reduced to 0.5 mM (Table 2.1).

The strain that synthesized the double variant MjCobT^{E150A,E315A} failed to synthesize AdoCbl or psCbl when inoculated into medium containing DMB or adenine, suggesting that in spite of their structural differences, *Se*CobT and *Mj*CobT likely catalyze the reaction via similar mechanisms. It was previously suggested that in archaeal orthologues, an acidic residue at the position equivalent to *Se*CobT E174 might be necessary and sufficient for activity (45). This idea was based on analyses of structural alignments which showed a valine residue in place of *Se*CobT E317 in two archaeal orthologues, one of them being *Mj*CobT. Here we show that the *Mj*CobT E315 is in fact, the equivalent to *Se*CobT E317 and both acidic residues in the active site are necessary for function *in vivo*.

*Mj*CobT homologues are commonly found in methanogenic archaea

Using *Mj*CobT as a query sequence, we identified many homologues in both class I and class II methanogens (Table 2.4). Homologues identified in class I methanogens showed a high level of identity and similarity to *Mj*CobT, while class II methanogens showed a more divergent homologue. On the basis of phylogenetic analysis, *Mj*CobT is likely representative of the class of NaMN:DMB phosphoribosyltransferases found in class I methanogenic archaea.

The *cobT*$^+$ allele of the cyanobacterium *Synechococcus sp.* restores AdoCba biosynthesis in a CobT-deficient *S. enterica* strain when DMB is provided. To determine whether *Synechococcus sp.* CobT had NaMN:Base PRTase activity *in vivo*, we introduced a plasmid encoding *Synechococcus sp.* WH7803 *cobT*$^+$ into a *S. enterica* Δ*cobT* strain to attempt to restore AdoCbl synthesis in the absence of *Se*CobT function. ORF SYNWH7803_RS09275 (*i.e., Synecococcus cobT*$^+$) placed under the control of an arabinose-inducible promoter in plasmid pCV1 (26) was moved into strain JE12893 (Δ*cobT* Δ*cobB*) yielding strain JE24636 (Δ*cobT* Δ*cobB* / pSynCobT2) (Table 2.2). Strain JE12893 failed to grow without exogenous CNCbl (Fig. 2.13, inverted triangles), but grew when CNCbl was present in the medium (Fig. 2.13, diamonds). Ectopic expression of *Synechococcus sp. cobT*$^+$ allowed strain JE24636 to grow when $(CN)_2$Cbi and DMB were present in the medium. Strain JE24636 failed to grow when only $(CN)_2$Cbi was provided. This result indicated *Synechococcus sp.* CobT supported *Se*CobT-like activity *in vivo* when DMB was provided (Fig. 2.13, triangles). Previously, cyanobacterial species were

shown to solely produce psCbl. Our findings indicate *Synechococcus sp*. CobT can activate DMB, ultimately yielding AdoCbl. Strain JE18115 *(*Δ*cobT* Δ*cobB* / pCOBT140) served as positive control for CobT function (Fig. 2.13, squares).

Phylogenetic analysis suggests that CobT in cyanobacteria has an archaeal origin. Previous studies have suggested that the majority of cyanobacterial genomes lack *cobT* and that none of the sequenced *Synechococcus* genomes encode *cobT* (16). When searching for homologues using CobT from *S. enterica*, *P. denitrificans*, and *B. megaterium*, our findings were consistent with the data reported by Helliwell *et. al* (Table 2.5). With the identification of the archaeal *cobT* from *M. jannaschii*, we found numerous *cobT* homologues in the genomes of cyanobacteria, including *Synechococcus* (Table 2.6). The report by Helliwell *et. al.* showed that *Synechococcus* solely produced psCbl even when provided with DMB (1μM) to "guide" the biosynthesis of cobalamin. The sole synthesis of psCbl by *Synechococcus* may be attributed to a lack of DMB transport and may not indicate the exclusive production of psCbl. Our bioinformatics findings in combination with the complementation of Cbl-dependent growth by a *Synechococcus* CobT homologue suggest that cyanobacteria can activate DMB via the canonical NaMN:DMB phosphoribosyltransfer mechanism. These findings also suggest that cyanobacteria can produce Cbl in addition to psCbl.

Our phylogenetic analysis shows that the CobT homologues found in archaea and cyanobacteria cluster into a distinct clade separate from the homologues found in *Firmicutes* and proteobacteria (Fig 2.14). Within this clade, the majority of

the cyanobacterial CobT homologues cluster tightly within a major clade and are distinctly separate from the archaeal CobTs which form another major clade. This likely suggests that the cyanobacterial CobTs are of archaeal origin and significantly differ from the CobTs found in *Firmicutes* and Proteobacteria. This difference is likely why previous studies did not identify CobT homologues in cyanobacteria.

Previous work has implicated thaumarchaeota as major Cbl producers in marine environments (15). Previously reported genome analyses performed showed the absence of *cobT* from all thaumarchaeota and suggested that an alternative pathway for DMB activation existed in these microorganisms. Our identification of archaeal *Mj*CobT prompted the search for homologues in thaumarchaeota. We found that *cobT* is commonly found in thaumarchaeotal genomes (Table 2.7). Given the prevalence of *cobT* in thaumarchaeotal genomes and the previously reported production of cobalamin, it is likely that thaumarchaeota activate DMB using a NaMN:DMB phosphoribosyltransferase enzyme.

CONCLUDING REMARKS

This study reports a new class of NaMN:DMB phosphoribosyltransferases (CobT) enzymes involved in cobamide biosynthesis in archaea and in cyanobacteria, but not in bacteria. Structurally, there are significant differences between *Mj*CobT and *Se*CobT, most notably the absence of the small domain in *Mj*CobT which is essential in forming the active site of *Se*CobT. *Mj*CobT groups with both the CobT homologues found in archaea and cyanobacteria and this group is highly divergent

from the CobT homologs found in bacteria. *Mj*CobT sequence identity compared to *Se*CobT is too low to be detected by NCBI BLASTp. Additionally, we see a greater degree of amino acid sequence similarity between *Mj*CobT and the cyanobacterial and archaeal CobT homologues than we see compared to bacterial CobT. Given this information, we feel MjCobT represents a class of NaMN:DMB phosphoribosyltransferase that is significantly different from bacterial CobT. In addition, this work corrects information regarding the oligomeric state of the PRTase from *Methanocaldococcus jannaschii* (PDB 3L0Z), whose crystal structure suggests it is a trimer. Our data indicate that in solution, the biologically active *Mj*CobT enzyme is dimeric.

ACKNOWLEDGEMENTS

The authors have no conflict of interest to declare. This work was supported by NIH grant R37-GM040313 to J.C.E.-S.

UniProtKB Protein IDs

*Mj*CobT (UniProtKB Q58993)

*Se*CobT (UniProtKB Q05603)

*Syn*CobT (UniProtKB A5GMZ1)

REFERENCES

1. Mattes, T.A., et al., *Cobalamin Biosynthesis and Insertion*, in *Encyclopedia of Inorganic and Bioinorganic Chemistry*, R.A. Scott, Editor. 2017, John Wiley & Sons, Ltd: Chichester, UK. p. 1-24.
2. Kräutler, B., et al., *The cofactor of tetrachloroethene reductive dehalogenase of Dehalospirillum multivorans is Norpseudo-B12, a new type of natural corrinoid.* Helvetica Chimica Acta, 2003. **86**: p. 3698-3716.
3. Marsh, E.N., *Coenzyme B12 (cobalamin)-dependent enzymes.* Essays Biochem., 1999. **34**: p. 139-154.
4. Yan, J., et al., *Purinyl-cobamide is a native prosthetic group of reductive dehalogenases.* Nat. Chem. Biol., 2018. **14**: p. 8-14.
5. Jones, A.R., et al., *Probing reversible chemistry in coenzyme B12 -dependent ethanolamine ammonia lyase with kinetic isotope effects.* Chemistry, 2015. **21**: p. 8826-8831.
6. Bobik, T.A., et al., *Propanediol utilization genes (pdu) of Salmonella typhimurium: three genes for the propanediol dehydratase.* J. Bacteriol., 1997. **179**: p. 6633-6639.
7. Padmanabhan, S., et al., *A new facet of vitamin B12: Gene regulation by cobalamin-based photoreceptors.* Annu. Rev. Biochem., 2017. **86**: p. 485-514.
8. Renz, P., *Biosynthesis of the 5,6-dimethylbenzimidazole moiety of cobalamin and of other bases found in natural corrinoids*, in *Chemistry and Biochemistry of B12.*, R. Banerjee, Editor. 1999, John Wiley & Sons, Inc.: New York. p. 557-575.
9. Johnson, M.G. and J.C. Escalante-Semerena, *Identification of 5,6-dimethylbenzimidazole as the Coα ligand of the cobamide synthesized by*

Salmonella typhimurium. Nutritional characterization of mutants defective in biosynthesis of the imidazole ring. J. Biol. Chem., 1992. **267**(19): p. 13302-13305.

10. Keck, B. and P. Renz, *Salmonella typhimurium forms adenylcobamide and 2-methyladenylcobamide, but no detectable cobalamin during strictly anaerobic growth.* Arch. Microbiol., 2000. **173**: p. 76-77.
11. Anderson, P.J., et al., *One pathway can incorporate either adenine or dimethylbenzimidazole as an alpha-axial ligand of B_{12} cofactors in Salmonella enterica.* J. Bacteriol., 2008. **190**: p. 1160-1171.
12. Trzebiatowski, J.R. and J.C. Escalante-Semerena, *Purification and characterization of CobT, the nicotinate-mononucleotide:5,6-dimethylbenzimidazole phosphoribosyltransferase enzyme from Salmonella typhimurium LT2.* J. Biol. Chem., 1997. **272**: p. 17662-17667.
13. Cheong, C.G., J.C. Escalante-Semerena, and I. Rayment, *Structural investigation of the biosynthesis of alternative lower ligands for cobamides by nicotinate mononucleotide: 5,6-dimethylbenzimidazole phosphoribosyltransferase from Salmonella enterica.* J. Biol. Chem., 2001. **276**: p. 37612-37620.
14. Hazra, A.B., et al., *Analysis of substrate specificity in CobT homologs reveals widespread preference for DMB, the lower axial ligand of vitamin B(12).* Chem. Biol., 2013. **20**: p. 1275-1285.
15. Heal, K.R., et al., *Two distinct pools of B12 analogs reveal community interdependencies in the ocean.* Proc. Natl. Acad. Sci. U S A, 2017. **114**: p. 364-369.
16. Helliwell, K.E., et al., *Cyanobacteria and eukaryotic algae use different chemical variants of vitamin B12.* Curr. Biol., 2016. **26**: p. 999-1008.

17. Berkowitz, D., et al., *Procedure for identifying nonsense mutations.* J. Bacteriol., 1968. **96**: p. 215-220.

18. Balch, W.E., et al., *Methanogens: reevaluation of a unique biological group.* Microbiol. Rev., 1979. **43**: p. 260-296.

19. O'Toole, G.A., M.R. Rondon, and J.C. Escalante-Semerena, *Analysis of mutants of defective in the synthesis of the nucleotide loop of cobalamin.* J. Bacteriol., 1993. **175**: p. 3317-3326.

20. Maniatis, T., E.F. Fritsch, and J. Sambrook, *Introduction of plasmid and bacteriophage lambda into Escherichia coli*, in *Molecular cloning: a laboratory manual.*, T. Maniatis, E.F. Fritsch, and J. Sambrook, Editors. 1982, Cold Spring Harbor Laboratory: Cold Spring Harbor, New York. p. 250-251.

21. Datsenko, K.A. and B.L. Wanner, *One-step inactivation of chromosomal genes in Escherichia coli K-12 using PCR products.* Proc. Natl. Acad. Sci. USA, 2000. **97**: p. 6640-6645.

22. Klock, H.E., et al., *Combining the polymerase incomplete primer extension method for cloning and mutagenesis with microscreening to accelerate structural genomics efforts.* Prot.-Struct. Funct. Bioinformat., 2008. **71**(2): p. 982-994.

23. Guzman, L.M., et al., *Tight regulation, modulation, and high-level expression by vectors containing the arabinose PBAD promoter.* J Bacteriol, 1995. **177**(14): p. 4121-30.

24. Rocco, C.J., et al., *Construction and use of new cloning vectors for the rapid isolation of recombinant proteins from Escherichia coli.* Plasmid, 2008. **59**: p. 231-237.

25. Mattes, T.A. and J.C. Escalante-Semerena, *Salmonella enterica synthesizes 5,6-dimethylbenzimidazolyl-(DMB)-alpha-riboside. Why some Firmicutes do not*

require the canonical DMB activation system to synthesize adenosylcobalamin. Mol. Microbiol., 2017. **103**: p. 269-281.

26. VanDrisse, C.M. and J.C. Escalante-Semerena, *New high-cloning-efficiency vectors for complementation studies and recombinant protein overproduction in Escherichia coli and Salmonella enterica.* Plasmid, 2016. **86**: p. 1-6.
27. Kittaka-Katsura, H., et al., *Purification and characterization of a corrinoid compound from Chlorella tablets as an algal health food.* J. Agric. Food Chem., 2002. **50**: p. 4994-4997.
28. Keller, S., et al., *The SMUL_1544 gene product governs norcobamide biosynthesis in the tetrachloroethene-respiring bacterium Sulfurospirillum multivorans.* J. Bacteriol., 2016. **198**: p. 2236-2243.
29. Blanche, F., et al., *Identification and quantitation of corrinoid precursors of cobalamin from Pseudomonas denitrificans by high-performance liquid chromatography.* Anal. Biochem., 1990. **189**: p. 24-29.
30. Chan, C.H. and J.C. Escalante-Semerena, *ArsAB, a novel enzyme from Sporomusa ovata activates phenolic bases for adenosylcobamide biosynthesis.* Mol. Microbiol., 2011. **81**: p. 952-967.
31. Sambrook, J., E.F. Fritsch, and T. Maniatis, *Molecular Cloning: A Laboratory Manual*. Second ed. 1989, Cold Spring Harbor, N.Y.: Cold Spring Harbor Laboratory.
32. Blommel, P.G. and B.G. Fox, *A combined approach to improving large-scale production of tobacco etch virus protease.* Protein Expr. Purif., 2007. **55**: p. 53-68.
33. Gasteiger, E., et al., *ExPASy: The proteomics server for in-depth protein knowledge and analysis.* Nucleic Acids Res., 2003. **31**: p. 3784-3788.

34. Laue, T.M., B.D. Shah, and T.M. Ridgeway, *Analytical ultracentrifugation in biochemistry and polymer science.* R. Soc. Chem., 1992: p. 90-125.

35. Schuck, P., *On the analysis of protein self-association by sedimentation velocity analytical ultracentrifugation.* Anal. Biochem., 2003. **320**(1): p. 104-124.

36. Ortega, A., D. Amoros, and J. Garcia de la Torre, *Prediction of hydrodynamic and other solution properties of rigid proteins from atomic- and residue-level models.* Biophys. J., 2011. **101**(4): p. 892-898.

37. Altschul, S.F., et al., *Gapped BLAST and PSI-BLAST: a new generation of protein database search programs.* Nucleic Acids Res, 1997. **25**(17): p. 3389-402.

38. Marchler-Bauer, A., et al., *CDD: specific functional annotation with the Conserved Domain Database.* Nucleic Acids Res., 2009. **37**(Database issue): p. D205-10.

39. Gouy, M., S. Guindon, and O. Gascuel, *SeaView version 4: A multiplatform graphical user interface for sequence alignment and phylogenetic tree building.* Mol. Biol. Evol., 2010. **27**(2): p. 221-224.

40. Claas, K.R., et al., *Functional analysis of the nicotinate mononucleotide:5,6-dimethylbenzimidazole phosphoribosyltransferase (CobT) enzyme, involved in the late steps of coenzyme B_{12} biosynthesis in Salmonella enterica.* J. Bacteriol., 2010. **192**: p. 145-154.

41. Woodson, J.D. and J.C. Escalante-Semerena, *The cbiS gene of the archaeon Methanopyrus kandleri AV19 encodes a bifunctional enzyme with adenosylcobinamide amidohydrolase and alpha-ribazole-phosphate phosphatase activities.* J. Bacteriol., 2006. **188**: p. 4227-4235.

42. Maggio-Hall, L.A. and J.C. Escalante-Semerena, *Alpha-5,6-Dimethylbenzimidazole adenine dinucleotide (alpha-DAD), a putative new*

intermediate of coenzyme B12 biosynthesis in Salmonella typhimurium. Microbiology, 2003. **149**: p. 983-990.

43. Krissinel, E. and K. Henrick, *Inference of macromolecular assemblies from crystalline state.* J. Mol. Biol., 2007. **372**(3): p. 774-797.

44. Bochner, B.R. and B.N. Ames, *Complete analysis of cellular nucleotides by two-dimensional thin layer chromatography.* J. Biol. Chem., 1982. **257**: p. 9759-9769.

45. Chan, C.H., et al., *Dissecting cobamide diversity through structural and functional analyses of the base-activating CobT enzyme of Salmonella enterica.* Biochim. Biophys. Acta, 2014. **1840**: p. 464-475.

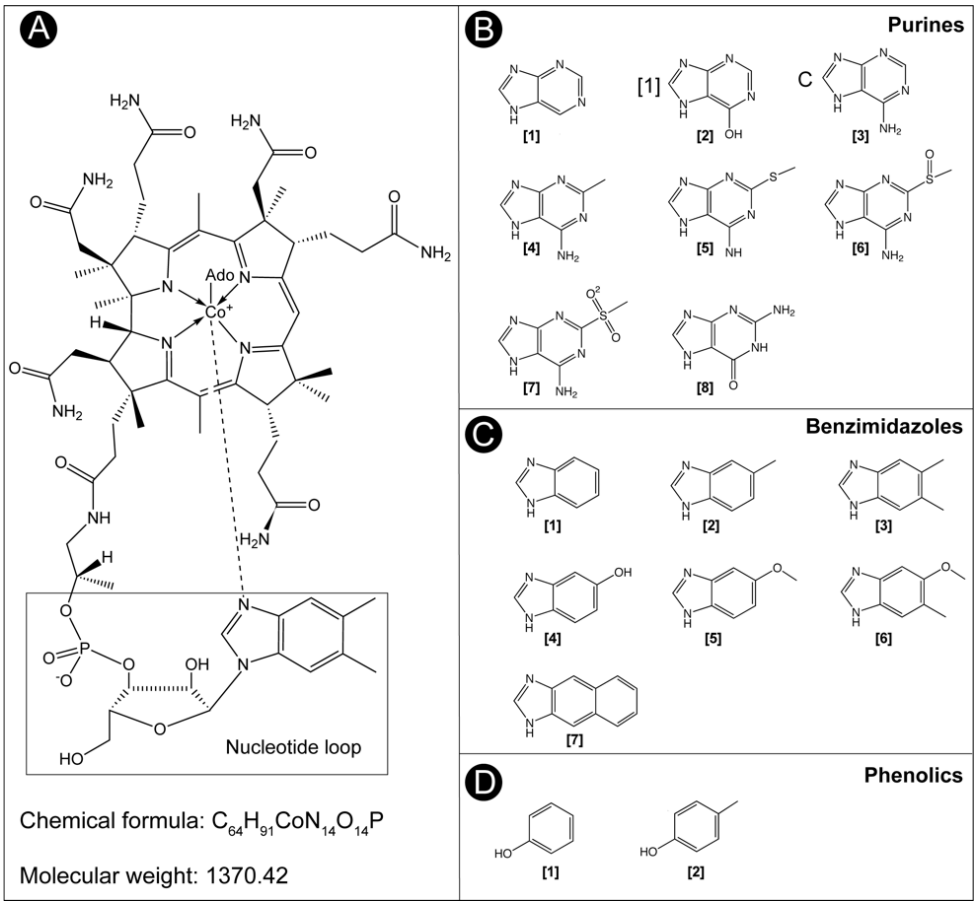

Figure 2.1. Adenosylcobamide (AdoCba) structure and nucleotide base diversity. A. The nucleotide loop is boxed. B. Purines and purine analogues found in Cbas: [1], purine; [2]. hypoxanthine; [3], adenine; [4], 2-methyladenine; [5], 2-methylmercaptoadenine; [6], 2-methylsulfinyladenine; [7], 2-methylsulfonyladenine; [8], guanine. C. Benzimidazole and its analogues: [1], benzimidazole; [2], 5-methylbenzimidazole; [3], 5,6-dimethylbenzimidazole; [4], 5-hydroxybenzimidazole; [5], 5-methoxybenzimidazole; [6], 5-methoxy-6-methylbenzimidazole; [7], naphthimidazole. D. Phenolics: [1], phenol; [2], *p*-cresol.

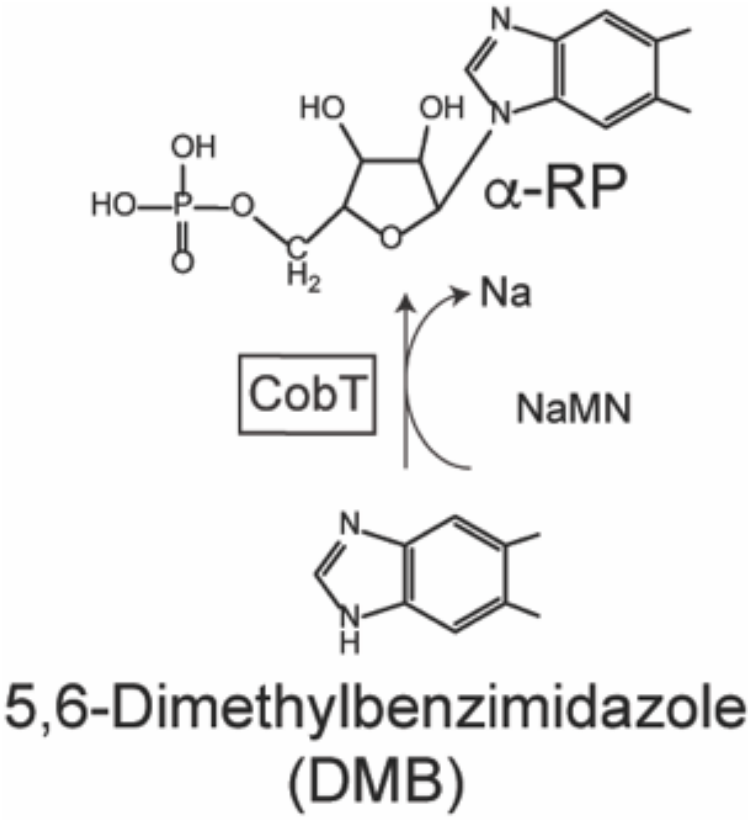

Figure 2.2. Base Activation by CobT. The activation of 5,6-dimethylbenzimidazole (DMB) to its α-ribotide by CobT PRTase is shown.

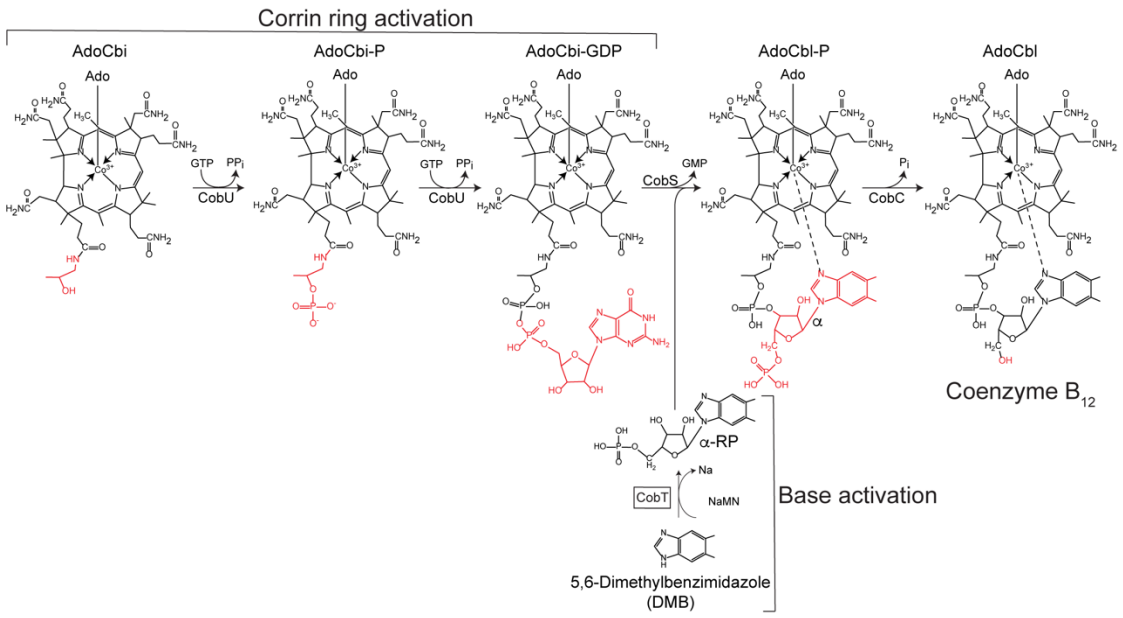

Figure 2.3. Late steps of coenzyme B_{12} biosynthesis. This figure schematizes the two branches of the nucleotide loop assembly (NLA) pathway that yields coenzyme B_{12} in *S. enterica*. This bacterium can assimilate exogenous, incomplete corrinoids such as cobinamide (Cbi) converting it to AdoCbi and activating it to AdoCbi-GDP via AdoCbi-P using the bifunctional kinase/guanylyltransferase (CobU) enzyme. The base shown in this scheme is 5,6-dimethylbenzimidazole (DMB), which is activated to its α-ribotide by the CobT PRTase (shown inside the box). Condensation of the activated intermediates followed by dephosphorylation yields biologically active coenzyme B_{12}.

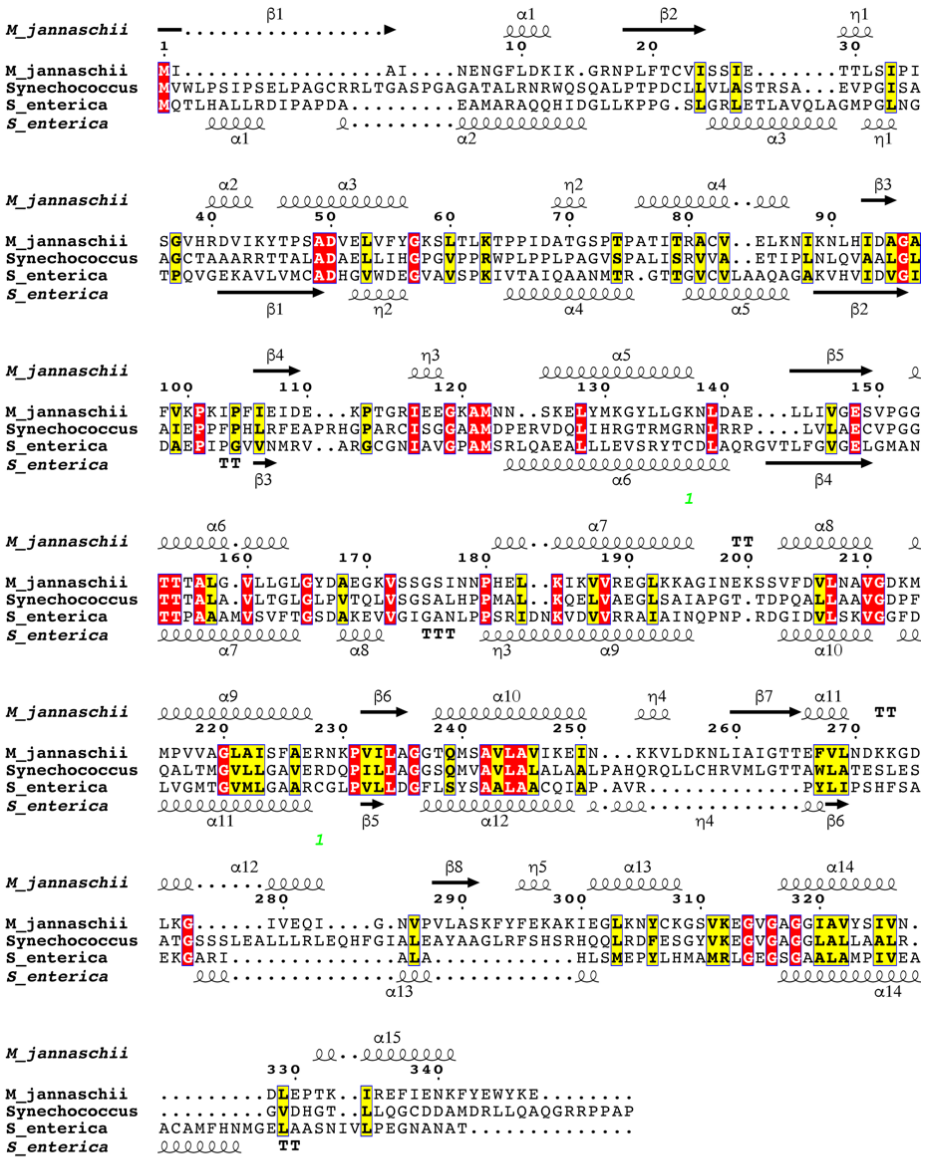

Figure 2.4. Protein sequence similarities and identities among *Mj*CobT, *Se*CobT, and *Synechococcus* CobT. The alignment was generated using Clustal Omega and visualized with ESPript 3.0 web-based program. Alpha helices and beta sheets for *Mj*CobT (PDB 3L0Z) and *Se*CobT (PDB 1L4B) obtained from the reported crystal apo structures are shown. The structure of *Synechococcus* CobT has not been reported

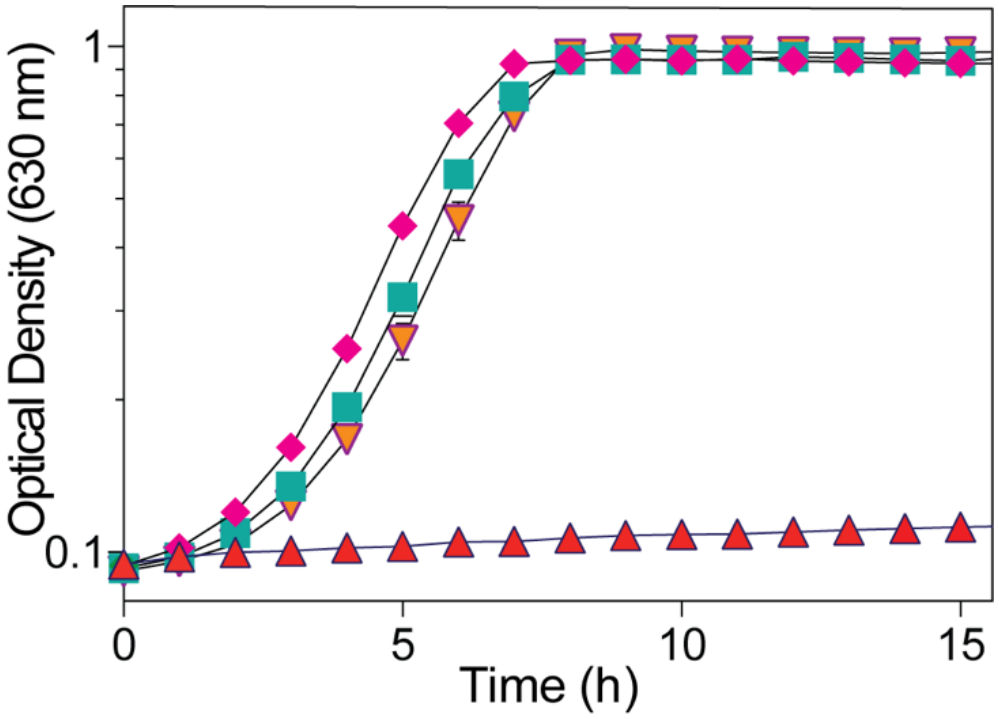

Figure 2.5. *Mj*CobT supports AdoCbl-dependent growth of *S. enterica*. Strains were grown in minimal NCE medium supplemented with ribose (20 mM) as carbon and energy source. $(CN)_2$Cbi (15 nM) was added to all cultures, except to the culture growing in the presence of CNCbl (diamonds). DMB (150 μM) was added to all cultures except for the culture to which CNCbl was added (diamonds).

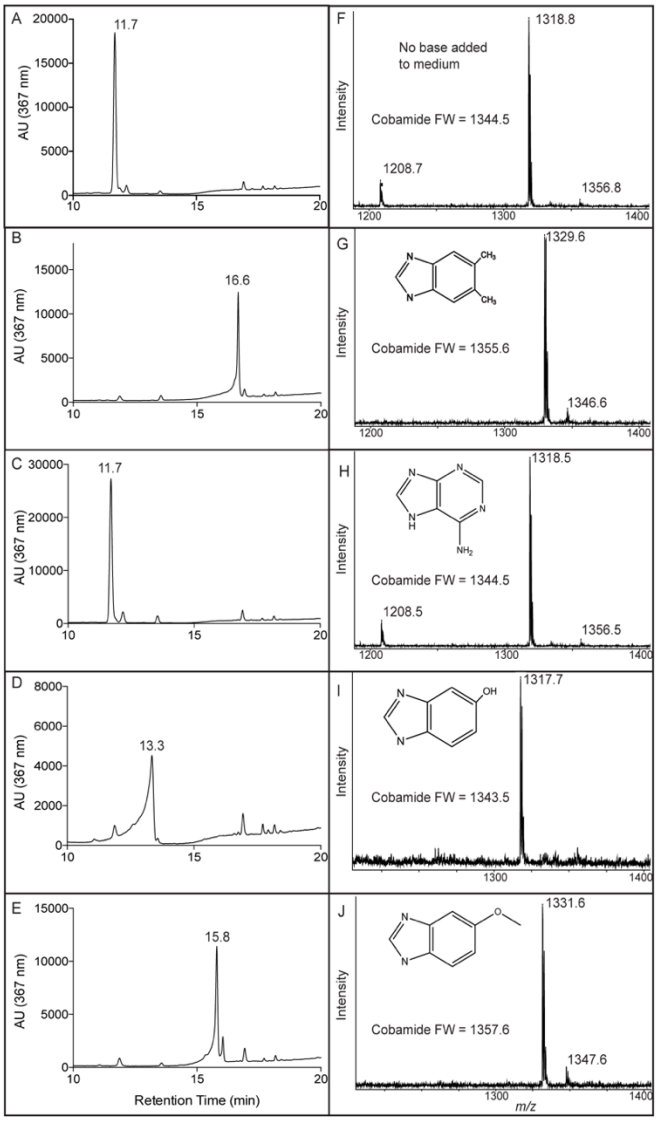

Figure 2.6. *Mj*CobT can activate different bases. The figure shows RP-HPLC tracings (panels A-E) and MALDI-TOF mass spectra (panels F-J) of α-ribotides synthesized by *Mj*CobT under conditions described under *Materials and Methods*. The substrates used were: 5,6-dimethylbenzymidazole (panels B, G), adenine (panels C, H), 5-hydroxybenzimidazole (panels D, I), and 5-methoxybenzimidazole (panels (E, J).

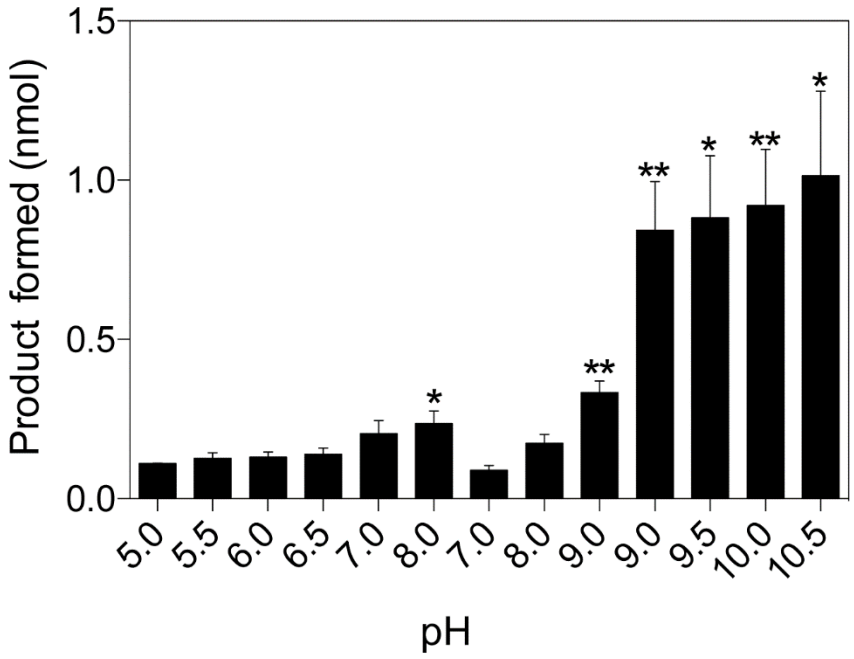

Figure 2.7. Effect of pH on *Mj*CobT activity. Conditions for the PRTase reaction are described under *Materials and Methods*. Product formation is displayed as a function of pH. Error bars represent the standard error of the mean. Asterisks represent significance determined by unpaired T test compared to pH 7. The following buffers were tested in order of appearance: sodium malate (pH 5), sodium succinate (pH 5.5), MES (pH 6), 2-[Bis(2-hydroxyethyl)amino]-2-(hydroxymethyl)propane-1,3-diol (Bis-Tris, pH 6.5), imidazole (pH 7), phosphate (pH 8), 2-amino-2-(hydroxymethyl)-1,3-propanediol chloride (Tris-HCl pH 7, 8, 9), *N*-cyclohexyl-2-aminoethanesulfonic acid (CHES pH 9, 9.5), and glycine (pH 10, 10.5).

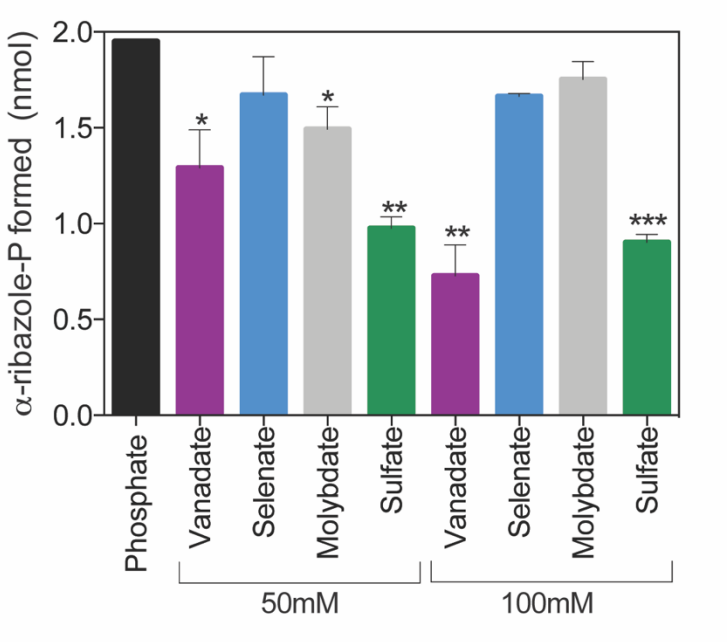

Figure 2.8. Phosphate positively affects *Mj*CobT activity, vanadate, selenate, molybdate and sulfate do not. Conditions for the PRTase reaction are described under *Materials and Methods*. Product formation is shown for each oxyanion provided at 50 mM and 100 mM compared to 25 mM phosphate. Error bars represent the standard error of the mean. Asterisks show significance determined by unpaired T test compared to phosphate condition.

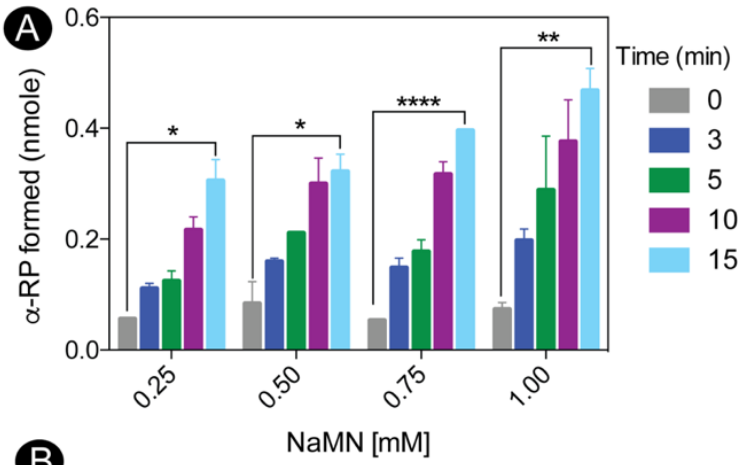

B

NaMN [mM]	Specific Activity (nmol/min/mg)
0.25	87 ± 18
0.5	95 ± 9
0.75	121 ± 7
1	132 ± 11

Figure 2.9. *Mj*CobT activates 5,6-dimethylbenzimidazole to α-ribazole-phosphate (α-RP). Conditions for the PRTase reaction are described under *Materials and Methods*. In panel A, product formation is shown as a function of time across varying NaMN concentrations. Product formation was quantified as a function of time. Error bars represent standard error of the mean. Asterisks shown significance determined by unpaired T test comparing time 0 to time 15. Panel B shows average specific activities with standard deviations for each concentration of NaMN tested.

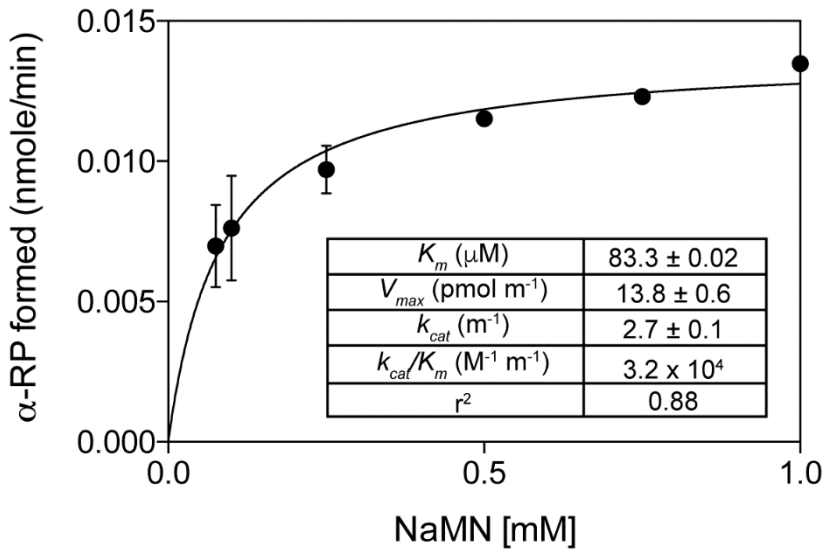

Figure 2.10. Pseudo-first order kinetics of the *Mj*CobT reaction as a function of NaMN. In all reaction mixtures DMB was present at saturating levels (100 μM). Details of the protocol used can be found under *Materials and Methods.* Apparent kinetic parameters are shown in the inset.

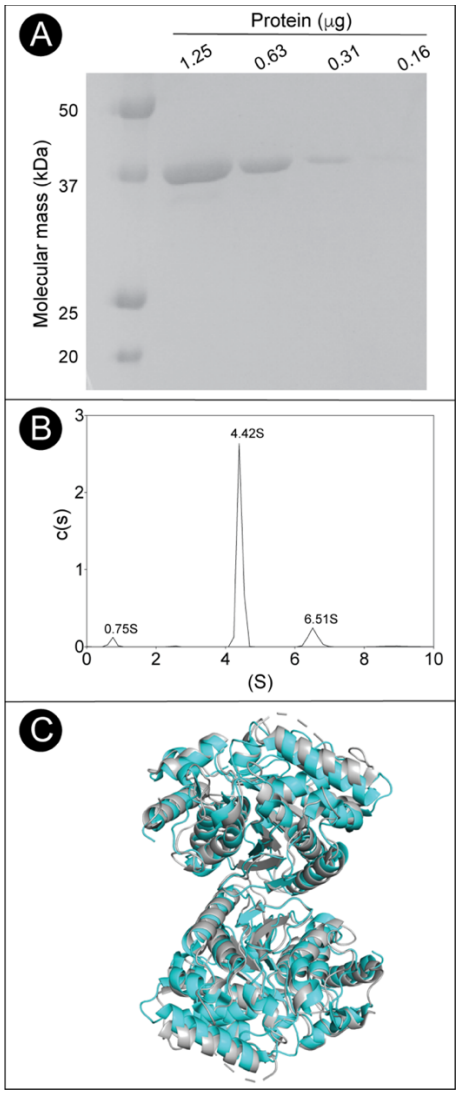

Figure 2.11. Oligomeric state and purity of *Mj*CobT. A. SDS-PAGE behavior of *Mj*CobT compared to BioRad Precision Plus Protein Standards. Based on the data shown in panel B, *Mj*CobT was estimated to be >99% homogeneous. B. Sedimentation velocity c(s) distribution of *Mj*CobT at pH7.5 showing three species at 0.75 S, 4.42 S, and 6.51 S C. Cartoon model of the *Mj*CobT dimer (cyan) identified in the crystal structure (PDB ID 3L0Z) superimposed onto the homologous CobT from *Pyrococcus horikoshii* dimer in grey (PDB ID 3U4G).

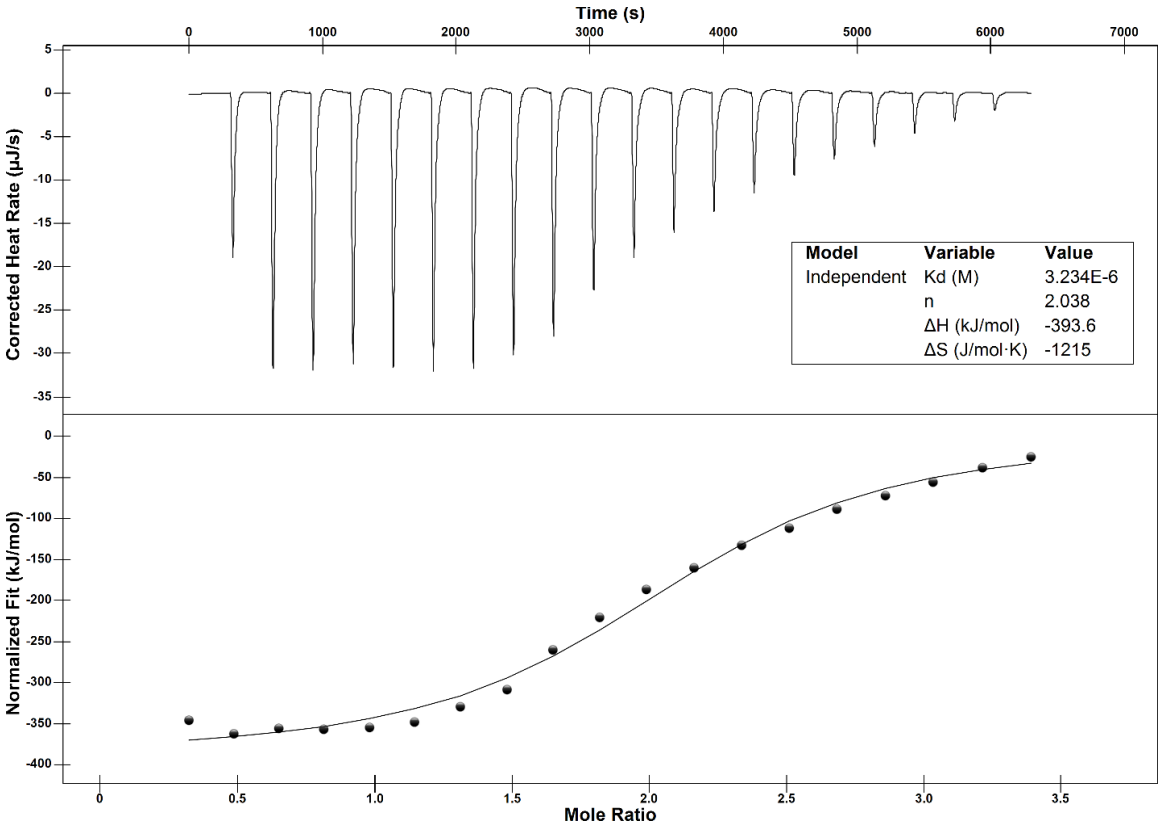

Figure 2.12. ITC analysis of NaMN binding to *Mj*CobT. Sample preparation for ITC analysis is described in detailed under *Materials and Methods*. Twenty 2.4-µL injections of 1 mM NaMN spaced every 5 min were made during the course of the experiment. The top panel shows the heat released per injection. The interaction between *Mj*CobT and NaMN is shown as enthalpy per mol of NaMN injected as a function of the molar ratio of protein to ligand (bottom panel). The binding isotherm was obtained from the integrals of the peaks. Shown in the inset are the best-fit values for the dissociation constant (K_d), stoichiometry (n), enthalpic change (ΔH), and entropic change (ΔS).

Table 2.1. Doubling times (h) of a *S. enterica cobT cobB* strain harboring plasmids encoding *Mj*CobT proteins				
Variant (plasmid)	Cbi (15 nM)	Cbi + DMB	Cbi + Ade	Cbl (100 nM)
Vector (pBAD24)	NG	NG	NG	1.2 ± 0.01[3 h lag]
***Mj*CobT^{WT} (pMjCobT1)**	1.6 ± 0.01 [3 h lag]	1.4 ± 0.01, [3 h lag] (10 nM)	1.5 ± 0.01, [3 h lag] (10 nM)	1.2 ± 0.01, [3 h lag]
***Mj*CobT^{E150A} (pMjCobT5)**	NG	2.0 ± 0.02, [3 h lag] (50 μM) 3.4 ± 0.12, [20 h lag] (1 μM)	NG (1mM)	1.5 ± 0.01, [4 h lag]
***Mj*CobT^{E315A} (pMjCobT3)**	NG	1.6 ± 0.01, [3 h lag] (5 μM) 2.0 ± 0.19[19 h lag] (50 nM)	2.2 ± 0.03, [6 h lag] (0.5 mM)	1.8 ± 0.03, [4 h lag]
***Mj*CobT$^{E150A\ E315A}$ (pMjCobT4)**	NG	NG	NG	1.9 ± 0.17, [4 h lag]

Cells were grown in NCE minimal medium supplemented with ribose (20mM) as the sole carbon and energy source. Doubling times are shown in hours with the standard error of the mean. Lag times are shown in brackets. Concentrations of added ring precursor or base are shown in parenthesis. NG, no growth; Cbi, dicyanocobinamide [$(CN)_2$Cbi]; DMB, 5,6-dimethylbenzimidazole; Cbl, cyanocobalamin (CNCbl, vitamin B_{12}); Ade, adenine

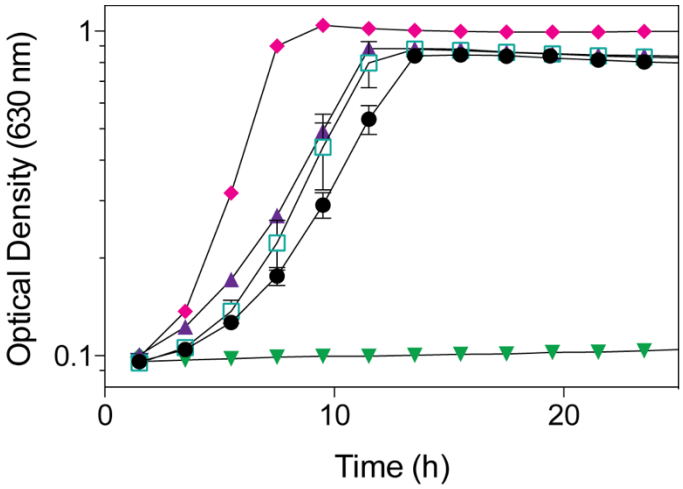

Figure 2.13. *Synechococcus* CobT supports AdoCbl-dependent growth of *S. enterica* in the absence of *cobT* and *cobB*. *S. enterica* strains were grown in minimal medium supplemented with ribose (20 mM). $(CN)_2$Cbi (15 nM) and DMB (150 μM) were added to all cultures except to the one to which CNCbl was added (diamonds). *Synechococcus* CobT (triangles) and *Se*CobT (squares) were expressed *in trans* in a Δ*cobT* Δ*cobB S. enterica* strain. A *cobT*$^+$ *cobB*$^+$ *S. enterica* strain (circles) served as positive control. A *S. enterica* strain deficient in CobT and CobB activity served as negative control (inverted triangles).

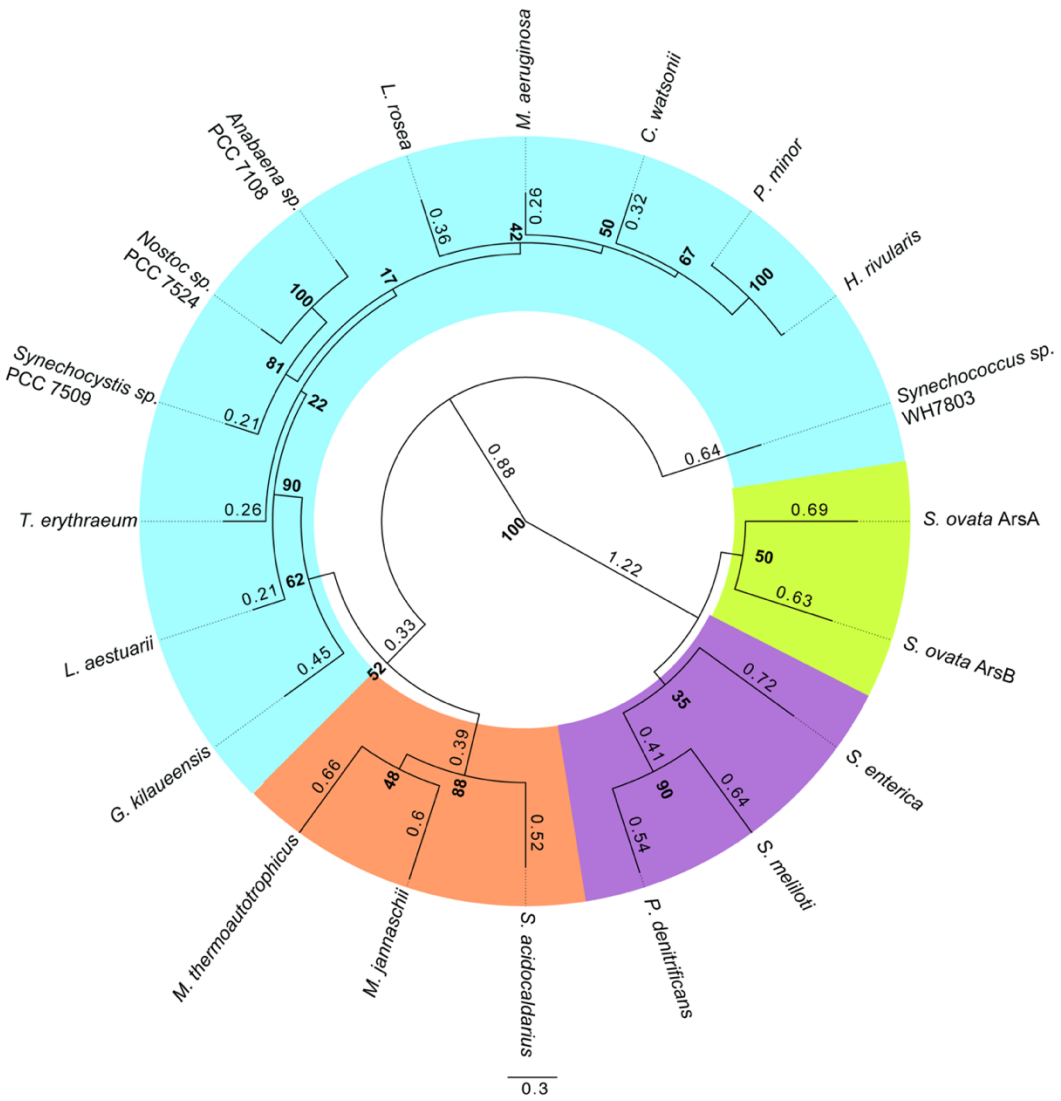

Figure 2.14. Cyanobacterial CobT homologues are of archaeal origin. Phylogenetic relationship of CobT homologues from diverse archaea and bacteria are shown. The tree was built based on a MUSCLE alignment using PhyML algorithm with BLOSUM62 model (100 bootstraps). Bootstrap values are presented in bold at the nodes and branch times are shown to 2 significant figures. Branch times below 0.2 were omitted from the tree. Organism highlighting is as follows: cyanobacteria in blue, archaea in orange, proteobacteria in purple, and firmicutes in green.

Table 2.2 Strains used in this study.		
Strains	**Genotype**	**Source**
S. enterica[1]		
JE7088	Δ*metE2702 ara-9*	Laboratory strain collection
Derivatives of JE7088		
JE11685	/ pBAD24	Laboratory strain collection
JE12872	*cobT1379*::*kan*$^+$	Laboratory strain collection
JE12893	*cobT1379*::*kan*$^+$ *cobB1374*::*cat*$^+$	Laboratory strain collection
JE17824	*cobT1379*::*kan*$^+$ / pCOBT140	Laboratory strain collection
JE18113	*cobT1379*::*kan*$^+$ / pMjCobT1	This study
JE18114	*cobT1379*::*kan*$^+$ *cobB1374*::*cat*$^+$ / pMjCobT1	This study
JE18115	*cobT1379*::*kan*$^+$ *cobB1374*::*cat*$^+$ / pCOBT140	This study
JE22263	/ pCV1	
JE24014	*cobT1379*::*kan*$^+$ *cobB1374*::*cat*$^+$ / pMjCobT3	This study
JE24016	*cobT1379*::*kan*$^+$ *cobB1374*::*cat*$^+$ / pMjCobT4	This study
JE24494	*cobT1379*::*kan*$^+$ *cobB1374*::*cat*$^+$ / pMjCobT5	This study
JE24636	*cobT1379*::*kan*$^+$ *cobB1374*::*cat*$^+$ / pSynCobT2	This study
E. coli strains		
JE21547	F$^-$ f80d *lacD*(*lacZ*)M15 Δ(lacZYA-*argF*) *U169 deoR recA1 endA1 hsdR17* (rK$^-$, mK$^+$) *phoA supE44* l- *thi1 gyrA96 relA1*	Laboratory strain collection
JE6663 C41(λDE3)	F$^-$ *ompT hsdSB (*rB$^-$ mB$^-$) *gal dcm* (λDE3)	Avidis
Plasmids		
pTEV5	Overexpression vector that fuses the *N*-terminus of the protein of interest to a H_6 tag, which can be removed by rTEV protease, *bla*+ (Ap^R)	[1]
pBAD24	complementation vector, P_{araBAD}, L-(+)-arabinose inducible promoter, *bla*+ (Ap^R)	[2]
pCOBT140	*S. enterica cobT*$^+$	[3]
pMjCobT1	MJ_RS08515 *cobT*$^+$ *bla*$^+$ (Ap^R) cloned into pBAD24	This study
pMjCobT2	MJ_RS08515 *cobT*$^+$ *bla*$^+$ (Ap^R) cloned into pTEV5	This study
pMjCobT3	MJ_RS08515 *cobT*$^+$ (CobT^{E315A}) *bla*$^+$ (Ap^R) cloned into pBAD24	This study
pMjCobT4	MJ_RS08515 *cobT*$^+$ (CobT$^{E150A\ E315A}$) *bla*$^+$ (Ap^R) cloned into pBAD24	This study
pMjCobT5	MJ_RS08515 *cobT*$^+$ (CobT^{E150A}) *bla*$^+$	This study

	(Ap^R) cloned into pBAD24	
pSynCobT2	SYNWH7803_RS09275$^+$ *bla*$^+$ (Ap^R) cloned into pCV1	This study

[1]All strains were derivatives of *Salmonella enterica enterica* sv Typhimurium LT2

Table 2.3 Primers used in this study.	
Primer Name	**Primer Sequence (5'-3')**
Mj_1598_cobT_PIPE_f	CAG GAG GAA TTC ACC ATG AGC ATA ATA GCA AT
Mj_1598_cobT_PIPE_rev	TTG CAT GCC TGC AGG TCG GCT TTA TTC TTT ATA CCA C
pBAD24-PIPE-5'	CAT GGT GAA TTC CTC CTG CTA GCC CA
pBAD24-PIPE-3'	CGA CCT GCA GGC ATG CAA GCT T
Mj_1598_TEV5_PIPE_f	AAC CTG TAT TTT CAG GGC ATG AGC ATA ATA GCA AT
Mj_1598_TEV5_PIPE_rev	AGC TCG AGA ATT CCA TGG GCT TTA TTC TTT ATA CCA C
pTEV5-PIPE-5'	CAT GGT GAA TTC CTC CTG CTA GCC CA
pTEV5-XhoI-3'	CGA CCT GCA GGC ATG CAA GCT T
MjCobT_sdm_E150A_F	GTCCCACCAGGAACACTCGCCCCAACAATTAATAATT
MjCobT_sdm_E150A_R	AATTATTAATTGTTGGGGCGAGTGTTCCTGGTGGGAC
MjCobT_sdm_E315A_F	CAGCCCCTACTCCTGCTTTTACTGAACCTTTGCA
MjCobT_sdm_E315A_R	TGCAAAGGTTCAGTAAAAGCAGGAGTAGGGGCTG
SynCobT pCV1 F	NNGCTCTTCNTTCATGGTGTGGCTGCCGAGC
SynCobT pCV1 R	NNGCTCTTCNTAATTACGGCGCCGGCGGACG

Table 2.4 Methanogen CobT homologues			
Query	***M. jannaschii* CobT Homology**		
Methanogen Class I			
Organism	**% Identity**	**% Positives**	**E-value**
Methanocaldococcus sp. FS406-22	94	97	0.0
Methanocaldococcus bathoardescens	93	97	0.0
Methanocaldococcus fervens	89	94	0.0
***Methanocaldococcus fervens* AG86**	**88**	**94**	**0.0**
Methanocaldococcus vulcanius	85	92	0.0
Methanotorris igneus	73	84	0.0
Methanocaldococcus villosus	73	86	0.0
Methanotorris formicicus	70	84	0.0
Methanothermococcus okinawensis	66	81	2e-162
Methanococcus vannielii	66	79	7e-159
Methanothermococcus thermolithotrophicus	65	78	3e-158
Methanocaldococcus infernus	69	82	3e-158
***Methanocaldococcus infernus* ME**	**69**	**82**	**5e-158**
Methanococcus maripaludis	62	78	5e-154
Methanococcus maripaludis C6	62	77	1e-150
Methanococcus maripaludis C7	61	75	1e-148
Methanococcus aeolicus	61	78	6e-148
Methanococcus voltae	58	73	2e-133
Methanothermus fervidus	48	64	5e-90
Methanothermobacter tenebrarum	43	61	1e-83
Methanogen Class II			
Organism	**% Identity**	**% Positives**	**E-value**
Methanocella arvoryzae	39	56	8e-65
Methanocella paludicola SANAE *	38	54	4e-64
Methanosarcina mazei	37	56	1e-61
Methanosarcina sp. MTP4	38	57	2e-61
Methanohalobium evestigatum	38	59	3e-61
Methanosarcina sp. Kolksee	36	57	4e-61
Methanosarcina thermophila	37	57	1e-60
Methanosarcina vacuolata	36	57	2e-60
Methanosarcina spelaei	37	56	2e-59
Methanosarcina flavescens	38	58	2e-59
Methanosalsum zhilinae	36	58	5e-59
Methanosarcina barkeri	36	56	2e-58

Methanosarcina horonobensis	37	55	2e-58
Methanosarcina lacustris	37	54	1e-57
Methanohalophilus halophilus	39	57	1e-57
Methanococcoides vulcani	37	57	8e-57
Methanosarcina siciliae	36	56	2e-56
Methanosarcina acetivorans	36	56	4e-56
Methanohalophilus mahii	38	57	4e-56
Methanocella conradii	38	54	3e-55

Results from a protein homology search using NCBI BLASTP are shown. *M. jannaschii* CobT coding sequence was used as the query protein to search for homologues in Methanogen Class I (taxid: 2283794) and Methanogen Class II (taxid:224756). The organism name is provided with the identity (%) and similarity (% positives) to the query sequence as well as the E-value. Results shown in bold typeface are annotated as nicotinate-nucleotide-dimethylbenzimidazole phosphoribosyltransferases and results with an asterisk (*) are annotated as hypothetical or putative proteins. All other hits are annotated as TIGR00303 family proteins. 20 unique results with the highest bit scores are shown for brevity. Only hits with query coverage > 85% are included in the table.

Table 2.5. Cyanobacterial CobT homologues to *S. enterica LT2* CobT, *B. megaterium* DSM 319 CobT, and *P. denitrificans* ATCC 13867 CobT			
		Homology	
Query | ***S.* Typhimurium[1] CobT**	% Identity	% Positives	E-value
Prochlorothrix hollandica PCC 9006	38	54	6e-50
Nostoc sp. 3335mG	34	50	5e-48
Query | ***B. megaterium* DSM 319 CobT**			
Prochlorothrix hollandica PCC 9006	45	61	2e-75
Nostoc sp. 3335mG	40	52	9e-60
Query | ***P. denitrificans* ATCC 13867 CobT**			
Prochlorothrix hollandica PCC 9006	72	79	2e-153
Nostoc sp. 3335mG	48	61	7e-85

Homologues from a protein homology search using NCBI BLASTP are shown. *S. enterica enterica* sv Typhimurium LT2 (*S.* Typhimurium) CobT, *Bacillus megaterium* DSM 319 CobT, and *Pseudomonas denitrificans* ATCC 13867 CobT coding sequences were used as queries to search for homologues in cyanobacteria (taxid:1117). The species name is provided with the identity (%) and similarity (% positives) to the query sequence as well as the E-value. All hits were annotated as nicotinate-nucleotide-dimethylbenzimidazole PRTase. Only hits with query coverage > 90% are included in the table.

Table 2.6 Cyanobacterial CobT homologues			
Query	***M. jannaschii* CobT Homology**		
Bacterium	**% Identity**	**% Positives**	**E-value**
Synechococcus sp. PCC 8807	39	56	3e-59
Pleurocapsa minor	40	55	1e-58
Synechococcus sp. NKBG042902	38	56	4e-58
Synechococcus sp. BDU 130192	38	56	1e-57
Synechococcus sp. PCC 73109	38	55	1e-57
Crocosphaera watsonii	40	54	4e-57
Synechococcus sp. NIES-970	38	56	4e-57
Synechococcus sp. PCC 7117	38	56	5e-57
Roseofilum reptotaenium AO1-A	36	56	2e-56
Synechococcus sp. PCC 7003	37	57	3e-56
Geminocystis sp. NIES-3708	38	55	8e-56
Gloeobacter kilaueensis	34	56	3e-55
Microcystis aeruginosa	39	56	6e-55
Phormidesmis priestleyi	38	55	1e-54
Leptolyngbya frigida	37	54	1e-54
Trichodesmium erythraeum	35	56	2e-54
Lyngbya aestuarii	35	53	2e-54
Limnothrix rosea	36	54	3e-54
Cyanothece sp. PCC 7424	39	54	3e-54
Limnoraphis robusta CS-951	36	54	4e-54
Hydrococcus rivularis	39	53	7e-54
Limnoraphis robusta	36	54	8e-54
Lyngbya sp. PCC8106	34	56	1e-53
Microcystis sp. 0824	39	56	1e-53
Leptolyngbya sp. PCC 7376	35	55	2e-53
Merismopedia glauca	37	52	3e-53
***Pseudanabaena* sp. ABRG5-3**	**37**	**55**	**5e-53**
Leptolyngbya sp. '*hensonii*'	36	53	5e-53
Microcystis sp. MC19	39	55	5e-53
Cyanothece sp. CCY0110	37	53	6e-53
Cyanothece sp. BG0011	38	53	1e-52
Micorcystis sp. T1-4	39	55	1e-52
Synechocystis sp. PCC 7509	37	53	1e-52
Nostoc sp. PCC7524	37	52	5e-52
Chamaesiphon minutus	34	53	6e-52
Planktothricoides sp. SR001	34	51	9e-52
Phormidium ambiguum	36	53	1e-51
Rivularia sp. PCC 7116	34	51	1e-51
Dactylococcopis salina	37	53	2e-51

***Microcystis panniformis* FACHB-1757**	**39**	**55**	**2e-51**
Chroococcidiopsis cubana	36	53	2e-51
Euhalothece sp. KZN 001	37	53	2e-51
Anabaena sp. PCC 7108	36	50	3e-51
Chroococcidiopsis thermalis	36	53	3e-51
Calothrix sp. 336/3	37	53	3e-51
Chroococcidiopsis sp. CCALA 051	36	53	3e-51
Aphanothece hegewaldii	36	53	4e-51
***Cyanobacterium* sp. HL-69**	**36**	**52**	**5e-51**
Nodosilinea nodulosa	36	53	6e-51
Cyanbacterium TDX16	36	53	7e-51
Phormidium tenue	37	55	1e-50
Cyanothece sp. PCC 8802	39	52	1e-50
Leptolyngbya sp. NIES-3755	38	54	1e-50
Oscillatoriales cyanobacterium JSC-12	37	53	1e-50
Microcystis aeruginosa PCC 9443	37	54	1e-50
Hydrocoleum sp. CS-953	35	52	1e-50
Stanieria sp. NIES-3757	36	53	2e-50
Desertifilum sp. IPPAS B-1220	34	54	2e-50
**Nostoc* sp. HK-01	36	53	3e-50
Pleurocapsa sp. PCC 7319	34	52	3e-50
Leptolyngbya sp. NIES-2104	39	55	3e-50
Leptolyngbya ohadii	36	52	4e-50
Calothrix elsteri	35	53	4e-50
Aliterella atlantica	37	52	5e-50
Anabaenopsis circularis	37	52	5e-50

Results from a protein homology search using NCBI BLASTP are shown. *M. jannaschii* CobT coding sequence was used as the query protein to search for homologues in cyanobacteria (taxid:1117). The species name is provided with the identity (%) and similarity (% positives) to the query sequence as well as the E-value. Homologues shown in bold typeface are annotated as nicotinate-nucleotide-dimethylbenzimidazole phosphoribosyltransferases and homologues with an asterisk (*) are annotated as hypothetical proteins. All other proteins are

annotated as TIGR00303 family proteins. Only homologues with query coverage >90% are included in the table.

Table 2.7 Thaumarchaeota CobT homologues			
Query	***M. jannaschii* CobT Homology**		
Organism	**% Identity**	**% Positives**	**E-value**
Candidatus Nitrososphaera evergladensis SR1	42	60	5e-74
Candidatus Nitrososphaera gargensis Ga9.2 *	42	58	6e-73
Candidatus Nitrosocaldus islandicus	39	58	2e-69
Candidatus Nitrosocaldus cavascurensis	**39**	**58**	**2e-69**
Candidatus Nitrocosmicus oleophilus *	39	58	3e-69
Candidatus Nitrosoarchaeum sp. *	40	60	1e-65
Thaumarchaeota archaeon CSP1-1 *	39	59	3e-64
Thaumarchaeota archaeon SCGC AC-337_F14	39	58	7e-64
Nitrosopumilales archaeon	39	57	3e-63
Nitrosoarchaeum koreense	39	58	6e-63
Candidatus Nitrosotenius chungbukensis	38	59	5e-62
***Nitrosopumilus* sp. PRT-SC01**	**37**	**58**	**1e-61**
Candidatus Nitrosopumilus salaria	37	57	2e-61
Candidatus Nitrosopumilus salaria BD31 *	37	57	3e-61
Candidatus Nitrosoarchaeum limnia	39	59	3e-61
Candidatus Nitrosopumilus adriaticus	39	58	4e-61
Candidatus Nitrosopumilus piranensis *	39	59	1e-60
Candidatus Nitrosoarchaeum limnia SFB1 *	39	59	3e-60
Thaumarchaeota archaeon N4	34	56	3e-59
Nitrosopumilus maritimus SCM1	38	58	2e-58
Candidatus Nitrosopumilus sp. NM25	35	57	2e-58
Candidatus Nitrosotenius aquarius	34	56	8e-57
Candidatus Nitrosomarinus sp.	37	56	2e-56
Nitrosopumilus sp. Nsub	37	56	1e-55
Candidatus Nitrosotenius cloacae	35	57	2e-55
Candidatus Nitrosomarinus Catalina	37	56	9e-55
Candidatus Nitrosopelagicus sp.	38	54	7e-53
Candidatus Nitrosopelagicus brevis	35	52	2e-50

Results from a protein homology search using NCBI BLASTP are shown. *M. jannaschii* CobT coding sequence was used as the query protein to search for homologues in Thaumarchaeota (taxid: 651137). The organism name is provided with the identity (%) and similarity (% positives) to the query sequence as well as the E-value. Results shown in bold typeface are annotated as nicotinate-nucleotide-dimethylbenzimidazole phosphoribosyltransferases and results with an asterisk (*) are annotated as hypothetical or putative proteins. All other hits are annotated as TIGR00303 family proteins. Only hits with query coverage > 90% are included in the table. Results from organisms listed as “uncultured marine thaumarchaeote” were omitted from the table.

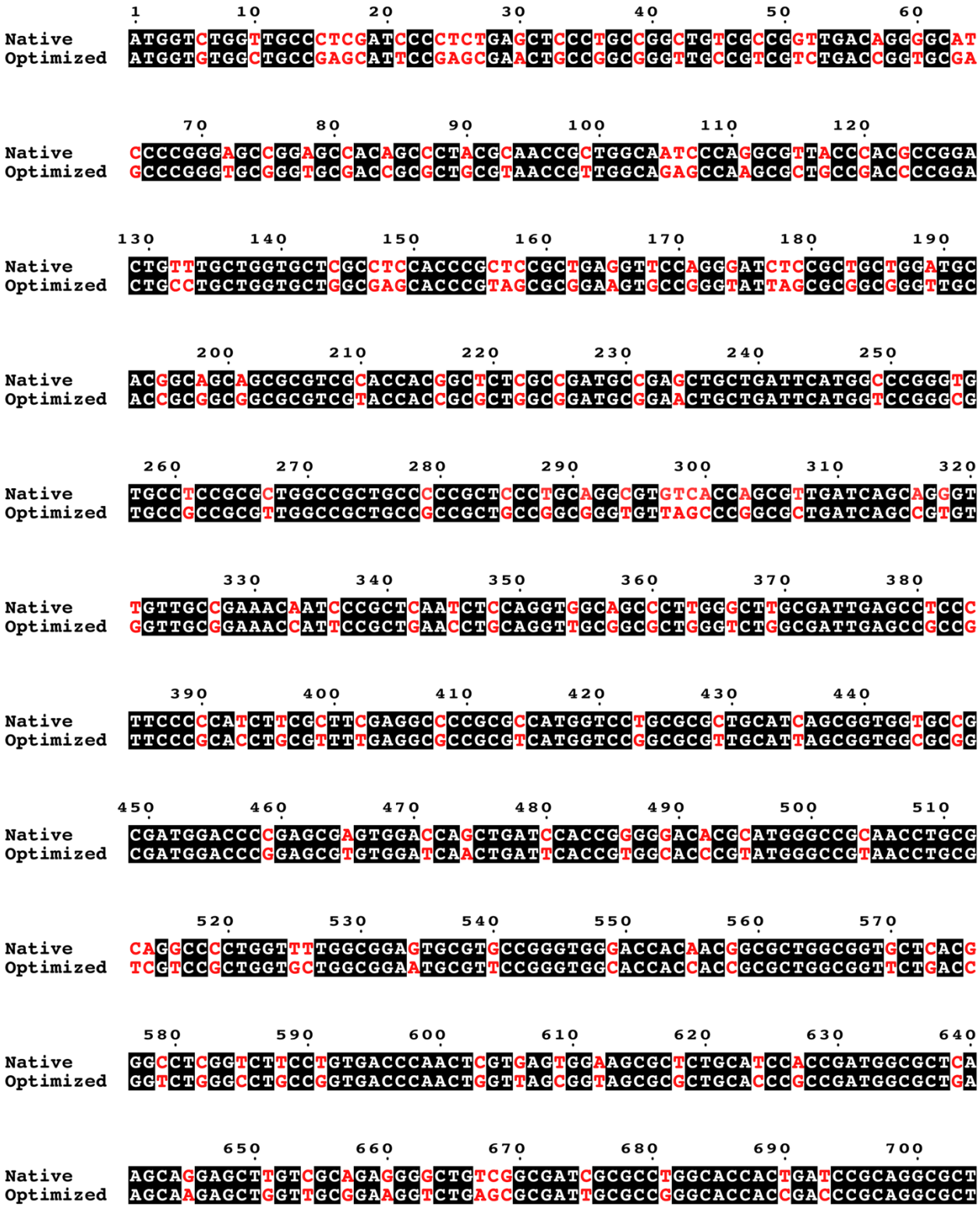
1 10 20 30 40 50 60
Native ATGGTCTGGTTGCCCTCGATCCCCTCTGAGCTCCCTGCCGGCTGTCGCCGGTTGACAGGGCAT
Optimized ATGGTGTGGCTGCCGAGCATTCCGAGCGAACTGCCGGCGGGTTGCCGTCGTCTGACCGGTGCGA
70 80 90 100 110 120
Native CCCCGGGAGCCGGAGCCACAGCCCTACGCAACCGCTGGCAATCCCAGGCGTTACCCACGCCGGA
Optimized GCCCGGGTGCGGGTGCGACCGCGCTGCGTAACCGTTGGCAGAGCCAAGCGCTGCCGACCCCGGA
130 140 150 160 170 180 190
Native CTGTTTGCTGGTGCTCGCCTCCACCCGCTCCGCTGAGGTTCCAGGGATCTCCGCTGCTGGATGC
Optimized CTGCCTGCTGGTGCTGGCGAGCACCCGTAGCGCGGAAGTGCCGGGTATTAGCGCGGCGGGTTGC
200 210 220 230 240 250
Native ACGGCAGCAGCGCGCGTCGCACCACGGCTCTCGCCGATGCCGAGCTGCTGATTCATGGCCCGGGTG
Optimized ACCGCGGCGGCGCGCGTCGTACCACCGCGCTGGCGGATGCGGAACTGCTGATTCATGGTCCGGGCG
260 270 280 290 300 310 320
Native TGCCTCCGCGCTGGCCGCTGCCCCCGCTCCCTGCAGGCGTGTCACCAGCGTTGATCAGCAGGGT
Optimized TGCCGCCGCGTTGGCCGCTGCCGCCGCTGCCGGCGGGTGTTAGCCCGGCGCTGATCAGCCGTGT
330 340 350 360 370 380
Native TGTTGCCGAAACAATCCCGCTCAATCTCCAGGTGGCAGCCCTTGGGCTTGCGATTGAGCCTCCC
Optimized GGTTGCGGAAACCATTCCGCTGAACCTGCAGGTTGCGGCGCTGGGTCTGGCGATTGAGCCGCCG
390 400 410 420 430 440
Native TTCCCCCATCTTCGCTTCGAGGCCCCGCGCCATGGTCCTGCGCGCTGCATCAGCGGTGGTGCCG
Optimized TTCCCGCACCTGCGTTTTGAGGCGCCGCGTCATGGTCCGGCGCGTTGCATTAGCGGTGGCCGCGG
450 460 470 480 490 500 510
Native CGATGGACCCCGAGCGAGTGGACCAGCTGATCCACCGGGGGACACGCCATGGGCCGCAACCTGCG
Optimized CGATGGACCCGGAGCGTGTGGATCAACTGATTCACCGTGGCACCCGTATGGGCCGTAACCTGCG
520 530 540 550 560 570
Native CAGGCCCCTGGTTTTGGCGGAGTGCGTGCCGGGTGGGACCACAACGGCGCTGGCGGTGCTCACG
Optimized TCGTCCGCTGGTGCTGGCGGAATGCGTTCCGGGTGGCACCACCACCGCGCTGGCGGTTCTGACC
580 590 600 610 620 630 640
Native GGCCTCGGTCTTCCTGTGACCCAACTCGTGAGTGGAAGCGCTCTGCATCCACCGATGGCGCTCA
Optimized GGTCTGGGCCTGCCGGTGACCCAACTGGTTAGCGGTAGCGCGCTGCACCCGCCGATGGCGCTGA
650 660 670 680 690 700
Native AGCAGGAGCTTGTCGCAGAGGGGCTGTCGGCGATCGCGCCTGGCACCACTGATCCGCAGGCGCT
Optimized AGCAAGAGCTGGTTGCGGAAGGTCTGAGCGCGATTGCGCCGGGCACCACCGACCCGCAGGCGCT

Figure 2.15. Nucleotide differences between the native nucleotide sequence of *Synechococcus sp.* WH7803 *cobT* and the nucleotide sequence optimized for expression in *E. coli*. Changes made for optimal expression in *E. coli* are shown in red bold typeface.

REFERENCES

1. Rocco, C. J., Dennison, K. L., Klenchin, V. A., Rayment, I., and Escalante-Semerena, J. C. (2008) Construction and use of new cloning vectors for the rapid isolation of recombinant proteins from *Escherichia coli*, *Plasmid 59*, 231-237.

2. Guzman, L. M., Belin, D., Carson, M. J., and Beckwith, J. (1995) Tight regulation, modulation, and high-level expression by vectors containing the arabinose PBAD promoter, *J. Bacteriol. 177*, 4121-4130.

3. Mattes, T. A., and Escalante-Semerena, J. C. (2017) *Salmonella enterica* synthesizes 5,6-dimethylbenzimidazolyl-(DMB)-alpha-riboside. Why some Firmicutes do not require the canonical DMB activation system to synthesize adenosylcobalamin, *Mol. Microbiol. 103*, 269-281.

CHAPTER 3

STRUCTURAL STUDIES OF A PHOSPHORIBOSYLTRANSFERASE INVOLVED IN COBAMIDE BIOSYNTHESIS IN METHANOGENIC ARCHAEA[2]

[2]Jeter V.L., Schwarzwalder A.H., Rayment I., and Escalante-Semerena J.C. To be submitted to *Protein Science*.

ABSTRACT

Cobamides (Cbas) are complex, cobalt-containing cyclic tetrapyrroles used by organisms from all domains of life. Despite the prevalence of Cba-dependent cellular processes, *de novo* synthesis is limited to some bacteria and archaea. The late steps of Cba biosynthesis require the activation of the corrin ring and nucleotide base before condensation of the activated substrates to form a complete Cba. Activation of the lower nucleotide ligand is catalyzed by the NaMN:DMB phosphoribosyltransferase (PRTase) CobT. Bacterial CobT homologs have been extensively characterized, yet little is known about archaeal base activating enzymes. A structure of the CobT homolog from *Methanocaldococcus jannaschii* was previously solved (3L0Z), yet the information disagreed with recently published functional characterization. Corrected structural data of *Mj*CobT is reported here, including structures with the nicotinate mononucleotide (NaMN) substrate and α-ribazole-5'-phosphate (α-RP).

INTRODUCTION

Cobamides (Cbas) are cobalt-containing cyclic tetrapyyroles belonging to a family of cofactors called 'the pigments of life.' Chlorophylls, hemes, and coenzyme F_{430} are other metal-containing cofactors that make up this family of biologically important compounds (1). *De novo* Cba biosynthesis is restricted to bacteria and archaea, yet Cba-dependent enzymes are found in cells from all domains of life (2). The prevalence of Cba-dependence has implicated Cbas an important compound in communities of organisms (3-5). The complex structure of Cbas is utilized in a diverse array of chemical reactions including enzyme catalyzed carbon

skeleton rearrangements, methyl-group transfers and reductive dehalogenation. Additionally, Cbas have been shown to act as photoreceptors in the regulation of carotenoid biosynthesis (reviewed in 6).

Cbas are structurally unique from other metal-containing cofactors in that they possess upper (CoB) and lower (CoA) axial ligands (Fig 3.1.) Cobalamin (or B_{12}) is defined by a 5,6-dimethylbenzimidazole (DMB) lower ligand nucleobase. Adenosylcobalamin (AdoCbl), the coenzymic form, is characterized by an upper 5'-deoxyadenosyl moiety which participates in radical chemistry reactions. The lower nucleobase is a source of diversity among Cba structures, incorporating purines, benzimidazoles, and in some cases phenolics (7, 8) .

De novo synthesis of Cbas can be divided into early and late steps. The early steps are responsible for constructing the corrin ring, while the late steps are responsible for activating and attaching the corrin ring and nucleotide base. The late steps are often referred to as the Nucleotide Loop assembly (NLA) pathway. In *S. enterica*, the nicotinate mononucleotide (NaMN):base phosphoribosyltransferase (*Se*CobT EC 2.4.2.21) catalyzes the activation of nucleotide bases by synthesizing α-riboside monophosphates (α-ribotides) (Fig. 3.2) (9). In the case of AdoCbl biosynthesis, *Se*CobT generates α-ribazole-5'-phosphate from DMB. *In vitro*, *Se*CobT exhibits broad substrate specificity and has been shown to act on a diverse range of purine and benzimidazole analogs (9,10). One of the defining features of base activation by *Se*CobT is the generation of a unique α-*N*-glycosidic linkage between C1 of ribose and N1 of imidazole. Numerous structures of *Se*CobT have been solved, proposing a general base

catalysis mechanism using a conserved glutamate (10-12). This work was expanded upon by demonstrating the role of two conserved glutamate residues in *Se*CobT activity and positioning of the base substrate (13). Collectively, these studies have defined the *Se*CobT active site (10-13).

Though *Se*CobT has been extensively characterized, there is little known about the function of archaeal homologs. A structure of *Methanocaldococcus jannaschii* CobT (*Mj*CobT) (PDB 3L0Z) was previously deposited without any functional characterization. Previous work has confirmed NaMN:Base phosphoribosyltransferase (PRTase) activity and further characterized the archaeal CobT homolog from *M. jannaschii* (*Mj*CobT) (14). The work reported here expands on the functional analysis presented in Jeter et al. by providing a structural context for the functional analyses. Crystal structures of *Mj*CobT without ligands (apo) and in complex with NaMN substrate with the α-ribazole-5'-phosphate and α-adenosyl-5'-phosphate products have been determined to a 2.2, 2.3, and 1.4 Å resolution, respectively. We confirmed the published findings that biologically active *Mj*CobT is, in fact, a dimer, which disagrees with the previously published structure. Additionally, we show significant differences in the dimeric interface compared to that of *Se*CobT. Though the overall protein fold is comparable between *Se*CobT and *Mj*CobT, we see a striking difference in the residue composition and location within the active site.

RESULTS AND DISCUSSION

Three structures of *Mj*CobT are reported here. First an apo structure that includes no ligands in its active site, second a complex of *Mj*CobT with nicotinic acid mononucleotide (NaMN) and nicotinic acid with α-ribazole 5′- phosphate (α-RP), and third *Mj*CobT in complex with α-adenosyl 5′- phosphate and nicotinic acid. These structures were determined to 2.2, 2.3, and 1.4 Å, respectively. Each of these structures provide unique insights into the assembly, ligand binding, specificity, and active site determinants of *Mj*CobT as described below. None of the structures described here contain a free base, although they were present in all crystallization experiments. This is true for the apo structure, which contains no ligands in the active site.

MjCobT oligomerization state

Previous structural studies of apo *Mj*CobT suggested that the enzyme might assemble as a trimer since this arrangement was observed in the crystal lattice (RCSB accession number 3L0Z). In contrast, isothermal titration calorimetry and analytical ultracentrifugation analysis show that the biologically active form of the enzyme is a dimer in solution (14). All of the structures reported here are consistent with a dimeric assembly and hence are in agreement with the biophysical studies. A ribbon representation of the apo dimer described here is shown in Figure 3.3A. The supposition that MjCobT was a trimer arose because the protein crystallized with three protomers per asymmetric unit arranged with three-fold symmetry. However, the presence of a crystallographic two-fold generates a molecule with

P32 symmetry in which the dimers assemble with the same relationship seen in the structures reported here. Indeed, the rms difference between dimers in the earlier and current apo structure is 0.86Å for 662 structurally equivalent residues (15). The dimeric packing arrangement present in the original structure (3L0Z) was described earlier in the paper by Jeter *et al* (14) and is confirmed here. The total buried surface area per protomer for this dimer is 945 $Å^2$ where 70% of this is hydrophobic. Interestingly, the total buried surface area for the trimer seen in the original structure (3L0Z) is only 515 $Å^2$ per subunit, which is significantly less that observed in the biological dimeric assembly.

The mode of dimerization observed in *Mj*CobT is markedly different from that seen in *Se*CobT. As opposed to *Mj*CobT, *Se*CobT forms a tight dimer with an extensive interface (Figure 3.3B). In this case, the buried surface area is 1720 $Å^2$ per protomer. As can be seen the components that constitute the interfaces are unrelated and lie on approximately opposite sides of each isoform. This has implications for the active site, since the binding pocket for the base in *Se*CobT is formed by components of both polypeptide chains whereas in *Mj*CobT the ligand binding sites are formed from a single polypeptide chain, as described below.

Structure of MjCobT bound to α-ribazole 5'- phosphate and NaMN

*Mj*CobT was crystallized in the presence of DMB at pH 7.0 and gave a crystal lattice that contained two protein subunits per asymmetric units. These crystals were soaked in 1 mM NaMN and a nucleotide base overnight prior to freezing. During that time the enzyme catalyzed a transferase reaction. The

contents of the two active sites are different. One subunit contains NaMN, whereas the second includes α-RP and nicotinic acid. This provides an opportunity to observe substrate and product in the same crystal lattice. The polypeptide chain for both subunits extends continuously from Met 1 to Tyr 348 except for a short break between Pro 68 and Gly 73. The two subunits are very similar as measured by an rms difference of 0.253 Å for 334 equivalent α-carbon atoms.

A superposition of the active site that contains α-RP and nicotinic acid on that which carries NaMN is shown in Figure 3.4A. This reveals the extent of the substrate binding pocket. The protein fold consists of an eight-stranded mostly parallel β-sheet with connecting α-helices on both sides where the substrate binding pocket is built from the connecting loops and resides at the end of the *C*-terminal end of β-strands. It is a compact globular protein in which the active site encloses the substrates and products. Access to the active site is most likely provided by movement of the outermost loops as indicated by a comparison of the apo structure with the polypeptide chain that carries α-RP shown in Figure 3.4B. Superposition of these two structures shows that significant changes occur in the loops extending from Ile 37 to Ile 45, 293 to 314, and Pro 333 to Tyr 348, such that the active site of the apo structure is open to solvent in contrast to that of the complex with either NaMN or α-RP and nicotinic acid. The rms difference between these two structures is 0.94Å for 329 equivalent residues, indicating the significant conformational changes that occur when substrates bind. Strikingly, residues Lys 173 to Asn 181 that were disordered in the apo structure became ordered upon ligand binding and contribute to the distal component of the binding pocket for the

nitrogenous base. Altogether, the movement of the surface loops serves to close the active site on substrate binding.

The electron density for NaMN and α-RP and nicotinic acid is unequivocal, although the occupancy of α-RP is somewhat less than 1.0 (Fig. 3.5). NaMN lies at the base of the active site for chain A where there are extensive hydrogen bonding interactions with the phosphoryl moiety, and specific interactions with the ribose 2' and 3'-oxygens and the carboxylate group of NaMN (Fig. 3.5A). The phosphoryl oxygens participate in hydrogen bonds to the amide hydrogen and Oγ of Thr 156, the Oγ of Ser 38 and amide hydrogen of Gly 154, and the amide hydrogen Gly 177. The carboxylate of NaMN is coordinated to the amide hydrogen and Oε of Gln 241 and the amide hydrogen of Thr 240. The ribose O3' of NaMN is coordinated to the amide hydrogen of Val 152 . The C1' of the ribose faces out into a cavity that lies closer to the surface loops than NaMN. This cavity forms the binding pocket for the nitrogenous base as revealed by the complex of α-RP and nicotinic acid observed associated with chain B (Fig. 3.5B).

The coordination of the ribose, phosphate, and nicotinic acid moieties in the active site that complexed α-RP is very similar to what was observed for NaMN. However, there are additional hydrogen bonds between O2' of the ribose and Oγ1 and Oγ2 of Glu 250. The binding site for DMB is formed primarily by hydrophobic components of three surface loops that extend from Val 40 – Thr48, Pro 68 – Pro 77, and Gly 311 – Val 313. There is a hydrogen bond between an imidazole nitrogen of DMB and Oγ of Asp 52 that fulfills the hydrogen bonding potential of the benzimidazole ring (Fig. 3.5B). As noted earlier, there is a disordered section

in the polypeptide chain that extends from Ile 69 to Thr 72. This short section of polypeptide chain lies at the distal end of the nitrogenous base and is disordered and cannot be modelled in either active site in the complex with NaMN and α-RP and nicotinic acid, although it is ordered in the presence of the adenine α-ribotide and in the apo structure. The position of the nitrogenous base in α-RP suggests that NaMN binds first in the active site, though this can only be confirmed by detailed kinetic studies.

Accommodation of alternative nitrogenous bases

The structure of the complex between adenine α-ribotide was determined to 1.4 Å resolution. This structure was determined in order to understand the broad specificity of *Mj*CobT (14) As noted earlier, the reaction product was prepared *in situ* by soaking the crystals in NaMN and adenine. In this case, the crystals were highly ordered and the position of the adenine α-ribotide is unequivocal (Fig. 3.6A). The overall position of the adenine α-ribotide is exceedingly similar to that α-RP so that the primary question is how the enzyme can accommodate nitrogenous bases that differ in both the composition of the aromatic ring and its side chain substitutions (Fig. 3.6B). Superposition of the two structures demonstrates that this is accomplished in this instance by conformational changes in the polypeptide chain between Ile 69 – Thr 74. As noted above, this section is ordered with adenine α-ribotide and disordered with α-RP. A change in the conformation of this loop, when α-RP is bound, is necessary because the two methyl groups in DMB overlap

with the ordered loop seen in the complex with α-ribotide. It is conceivable that the disordered section allows for varied substrate specificity which is a hallmark of CobT.

The remainder of the side chains that interface the nitrogenous bases adopt essentially the same conformation (Fig. 3.6B). An adenine specific interaction arises between the carbonyl oxygen of Gly 177 and the amino group of adenine, but this does not alter the conformation of the active site. Interestingly, there are no polar interactions between the pyrimidine ring nitrogen N1 and N3 of the purine, which instead lie at van der Waals distance from the surrounding components of the binding pocket. Note again, the additional hydrogen bonds between O2' of the ribose and Oγ1 and Oγ2 of Glu 250 relative to the complex with NaMN, suggesting that this is a feature of the ribotide product complex.

Comparison with SeCobT

The overall protein fold of *Mj*CobT is fundamentally the same as that of *Se*CobT where the rms difference between 248 equivalent α-carbon atoms is 2.2 Å. There is also a well-established equivalency in their enzymatic function, specificity and evolutionary relationship (14). As such, it would be anticipated that the active site residues would be found at equivalent locations in their sequences. However, close examination of the active sites reveals a major difference in the identity and position in the sequence of the active site base. In *Se*CobT, the active site base is Glu 317. This functional group is required since the imidazole moiety of the aromatic base will carry a single proton on one of the ring nitrogen atoms at

pH of ~7. The first pKa of benzimidazole is 5.4 whereas the second pKa is ~11.5. It is the latter pKa that is important in the chemical mechanism (Fig. 3.3). In *Mj*CobT the structurally equivalent amino acid is Val 317, where the side chains of Glu and Val 317 adopt similar positions. Instead Asp 52 is the base in *Mj*CobT. The use of an alternative base is possible because the benzimidazole ring in *Mj*CobT is rotated approximately 30° relative to that observed in *Se*CobT. This places the protonated nitrogen opposite the side chain of Asp 52.

CONCLUDING REMARKS

This study reports the corrected structure of *Mj*CobT, the only archaeal CobT to be functionally characterized. Additionally, structures containing both substrate and product in the active site were dissected. This work elucidated the structural differences between *Mj*CobT and the extensively characterized *Se*CobT. The overall protein folds of these two enzymes are similar, yet the specifics of active site construction and dimer interactions are unique. The conservation of active sites that can accommodate a broad range of substrates indicate a strong selection for maintaining the ability to synthesize diverse Cbas in drastically different environments.

MATERIALS AND METHODS

Cloning of the gene encoding MjCobT

*Mj*CobT was cloned into vector backbone pTEV5 as previously reported (14).

Protein expression and purification

The plasmid carrying *MjCobT* was used to transform BL21-CodonPlus *E. coli* cells (Agilent Technologies). Cultures were grown in LB medium with kanamycin (50 mg/L) and chloramphenicol (50 mg/L) until an optical density of A_{600} = 0.8 was reached. Cells were chilled on ice before inducing protein expression by addition of 1 mM isopropyl β-D-1-thiogalactopyranoside for a 24 hr growth at 16˚C. The cells were harvested by centrifugation at 4˚C, washed in a buffer containing 20mM Hepes pH 7.6 and 100mM NaCl, and centrifuged again before storing at -80˚C until used.

All protein purifications were carried out at 4 °C. In preparation for purification, cells were lysed by sonication on ice in lysis buffer (25 mM Tris-HCl pH 8.0, 50 mM NaCl, 20 mM imidazole) with lysozyme (1ug/mL), DNaseI (25ug/mL), and phenylmethylsulfonyl fluoride 0.5 mM added to the cells. The lysate was incubated at 80˚C for 30 min to precipitate native *E. coli* proteins before clarification at 40,000 x g at 21˚C for 30 min in an Optima LE-80K Ultracentrifuge (Beckman) using a Ti-45 rotor (Beckman/Coulter) that was pre-cooled 4°C prior to use. Clarified lysate was loaded over a 5mL Ni-NTA column, washed with ten column volumes (CV) of wash buffer (25 mM Tris-HCl pH 8.0, 500 mM NaCl, 20 mM imidazole) and six CV of a second wash buffer with imidazole increased to 40 mM, before eluting with six CV of 25 mM Tris-HCl pH 8.0, 500 mM NaCl, and 500 mM imidazole. Recombinant tobacco etch virus protease (rTEV protease was purified as described elsewhere16) was mixed with eluted *Mj*CobT to cleave the 6-His tag, and was allowed to react overnight at 21˚C in a buffer containing 25 mM

Tris-HCl pH 8.0 and 500 mM NaCl. After confirming cleavage by SDS-PAGE, the protein was passed over a Ni-NTA column to separate the rTEV protease from purified *Mj*CobT. Purified *Mj*CobT was then dialyzed into a 25 mM Tris-HCl pH 8.0, 250mM NaCl buffer overnight at 21˚C. Before crystallization, *Mj*CobT was concentrated to 13.3 mg/mL by centrifugation at 4,000 x g in a 30K molecular weight cut-off Amicon Ultra Centrifugal Filter, and flash-frozen as 30 µL droplets in liquid nitrogen for storage at -80˚C.

Crystallization

The purified *Mj*CobT (13.3 mg/mL) was screened for crystal growth at both room temperature and 4˚C across a 144-condition hanging drop, sparse-matrix screen developed by the Rayment Laboratory. The enzyme was examined for crystal growth in its apo-state, or in the presence of substrates. Drops were seeded after 24 hours to incite crystal growth. All crystals were obtained at room temperature. X-ray diffraction quality crystals were transferred to a cryogenic solution containing 20% glycerol or ethylene glycol and supplemented with additional substrates to enhance ligand binding within the crystal matrix. Crystals were allowed to soak in these conditions overnight before flash freezing for storage before data collection.

Apo crystals were obtained in 100 mM 2-(*N*-morpholino)ethanesulfonic acid (MES)/acetate buffer pH 5.5 with 8.4% polyethylene glycol (PEG) 8K and 1 mM 5-hydroxybenzimidazole (5-OH) added to the protein before screening. X-ray diffraction quality crystals were then soaked in a solution containing 20% ethylene

glycol, 100 mM (MES)/acetate buffer pH 5.5, 16% PEG 4K, and 5 mM 5,6-dimethylbenzimidazole (DMB), though neither of the substrates (5-OH and DMB) were present in the crystal lattice.

Crystals of *Mj*CobT in complex with nicotinic acid mononucleotide (NaMN) and nicotinic acid with α-ribazole 5′- phosphate were obtained in a condition containing 100 mM MES/acetate buffer pH 5.5 and 25% PEG 1.5K, with 1 mM DMB and 25mM Na/K-PO_4 pH 7.0 added to the protein. Crystals were soaked in a 20% ethylene glycol, 100 MES/acetate buffer pH 5.5, 16% PEG 4K, 1mM nicotinic acid mononucleotide (NaMN) solution overnight prior to freezing.

Crystals of *Mj*CobT in complex with adenine α-ribotide and nicotinic acid were grown in a condition containing 100mM 4-(2-Hydroxyethyl)-1-piperazinepropanesulfonic acid (HEPPS) pH 8.5 and 22% PEG 8K with both 1 mM adenine and 50 mM Na/K-PO_4 pH 7 added to the protein. Before freezing, crystals were soaked for 30 minutes in 20% ethylene glycol, HEPPS pH 8.5, 22% PEG 8K, and 25 mM Na/K-PO_4 with substrates 1 mM NaMN and 1 mM adenine. The same substrates (adenine α-ribotide and nicotinic acid) were captured in the crystal lattice by similar means after soaking I crystals in a solution containing 30% PEG 8K instead of 20% ethylene glycol and 20% PEG 8K.

X-Ray data collection and processing

X-ray data were collected at the Advanced Photon Source and processed with XDS,({Kabsch, 2010 #2209}) HKL-2000,(17) or HKL-3000 (18). Structures were determined by molecular replacement with the Phenix (19) software package

with the coordinates of the apo *Mj*CobT (RCSB accession number 3L0Z) as the search model. Model building and refinement were completed with Phenix,(19) CCP4, and COOT ({Emsley, 2010 #2184}). Model and refinement statistics are compiled in Table 3.I.

X-ray coordinates have been deposited in the Research Collaboratory or Structural Bioinformatics, Rutgers University, New Brunswick NJ (accession nos. 6PT8, 6PU6, and 6PTF)

ACKNOWLEDGEMENTS

We thank Michael Andreas for helpful discussions. This work was supported by National Institutes of Health Grant R35-GM130399 to J.C.E.-S. Use of the Structural Biology ID19 and BM19 beamlines, Argonne National Laboratory Advanced Photon Source was supported by the U.S. Department of Energy, Office of Energy Research, under Contract No. W-31-109-ENG-38.

REFERENCES

1. Battersby, A.R., *Tetrapyrroles: the pigments of life.* Nat. Prod. Rep., 2000. **17**: p. 507-526.
2. Roth, J.R., J.G. Lawrence, and T.A. Bobik, *Cobalamin (coenzyme B12): synthesis and biological significance.* Annu. Rev. Microbiol., 1996. **50**: p. 137-181.
3. Croft, M.T., et al., *Algae acquire vitamin B12 through a symbiotic relationship with bacteria.* Nature, 2005. **438**: p. 90-93.

4. Degnan, P.H., M.E. Taga, and A.L. Goodman, *Vitamin B12 as a modulator of gut microbial ecology.* Cell Metab., 2014. **20**: p. 769-778.
5. Degnan, P.H., et al., *Human gut microbes use multiple transporters to distinguish vitamin B12 analogs and compete in the gut.* Cell Host Microbe, 2014. **15**: p. 47-57.
6. Padmanabhan, S., et al., *A new facet of vitamin B12: Gene regulation by cobalamin-based photoreceptors.* Annu. Rev. Biochem., 2017. **86**: p. 485-514.
7. Renz, P., *Biosynthesis of the 5,6-dimethylbenzimidazole moiety of cobalamin and of other bases found in natural corrinoids*, in *Chemistry and Biochemistry of B12.*, R. Banerjee, Editor. 1999, John Wiley & Sons, Inc.: New York. p. 557-575.
8. Stupperich, E., H.J. Eisinger, and B. Kräutler, *Diversity of corrinoids in acetogenic bacteria. p-Cresolylcobamide from Sporomusa ovata, 5-methoxy-6-methylbenzimidazolylcobamide from Clostridium formicoaceticum and vitamin B12 from Acetobacterium woodii.* Eur. J. Biochem., 1988. **172**: p. 459-464.
9. Trzebiatowski, J.R. and J.C. Escalante-Semerena, *Purification and characterization of CobT, the nicotinate-mononucleotide:5,6-dimethylbenzimidazole phosphoribosyltransferase enzyme from Salmonella typhimurium LT2.* J. Biol. Chem., 1997. **272**: p. 17662-17667.
10. Cheong, C.G., J.C. Escalante-Semerena, and I. Rayment, *Structural investigation of the biosynthesis of alternative lower ligands for cobamides by nicotinate mononucleotide: 5,6-dimethylbenzimidazole phosphoribosyltransferase from Salmonella enterica.* J. Biol. Chem., 2001. **276**: p. 37612-37620.
11. Cheong, C.G., J.C. Escalante-Semerena, and I. Rayment, *Capture of a labile substrate by expulsion of water molecules from the active site of nicotinate*

mononucleotide:5,6-dimethylbenzimidazole phosphoribosyltransferase (CobT) from Salmonella enterica. J. Biol. Chem., 2002. **277**(43): p. 41120-41127.

12. Cheong, C.G., J.C. Escalante-Semerena, and I. Rayment, *The three-dimensional structures of nicotinate mononucleotide:5,6- dimethylbenzimidazole phosphoribosyltransferase (CobT) from Salmonella typhimurium complexed with 5,6-dimethybenzimidazole and its reaction products determined to 1.9Å resolution.* Biochemistry, 1999. **38**: p. 16125-16135.
13. Chan, C.H., et al., *Dissecting cobamide diversity through structural and functional analyses of the base-activating CobT enzyme of Salmonella enterica.* Biochim. Biophys. Acta, 2014. **1840**: p. 464-475.
14. Jeter, V.L., et al., *A new class of phosphoribosyltransferases involved in cobamide biosynthesis is found in methanogenic archaea and cyanobacteria.* Biochemistry, 2019. **58**: p. 951-964.
15. Krissinel, E. and K. Henrick, *Secondary-structure matching (SSM), a new tool for fast protein structure alignment in three dimensions.* Acta Crystalogr. Sec. D Biol. Crystalogr., 2004. **D60**: p. 2256-2268.
16. Blommel, P.G., et al., *Enhanced bacterial protein expression during auto-induction obtained by alteration of lac repressor dosage and medium composition.* Biotechnol. Prog., 2007. **23**: p. 585-598.
17. Otwinowski, Z. and W. Minor, *Processing of X-ray diffraction data collected in oscillation mode.* Methods in Enzymology, 1997. **276**: p. 307-326.
18. Minor, W., et al., *HKL-3000: the integration of data reduction and structure solution--from diffraction images to an initial model in minutes.* Acta Crystallogr. D. Biol. Crystallogr., 2006. **62**: p. 859-866.

19. Adams, P.D., et al., *PHENIX: a comprehensive Python-based system for macromolecular structure solution.* Acta Crystallogr. D Biol. Crystallogr., 2010. **66**: p. 213-221.

Table 3.I. *X-Ray Data Collection and Model Refinement Statistics*

	apo	NAMN and α-RP+nicotinic acid	adenine α-ribotide + nicotinic acid
X-ray source	**19ID**	**19ID**	**19ID**
Space Group	$P4_12_12$	$P2_1$	$P2_1$
Subunits per asymmetric unit	1	2	2
Cell dimensions (Å,°)	56.1, 56.1, 243.7	47.9, 139.09, 54.490 β= 111.67	46.4, 138.6, 51.2 β= 108.32
Resolution limits (Å)	37.7 - 2.15 (2.23 - 2.15)[a]	40.93-2.293 (2.375-2.293)	48.56-1.40 (1.45-1.40)
Number of independent reflections	22116 (2113)	28757 (2758)	118692 (11857)
Completeness (%)	99.6 (98.6)	97.39 (92.79)	98.9 (99.0)
Redundancy	24.9 (25.0)	6.9 (6.9)	
avg I/avg σ(I)	28.4 (2.8)	15.50 (2.53)	
R_{merge} (%)[b]	0.2327		
[c]*R*-factor (overall)/no. reflections			
R-factor (working)/no. reflections	0.230/22069	0.218/28677	0.184/118682
R-factor (free)no. reflections	0.268/1992	0.210/1433	0.205/5933
number of protein atoms	2593	4386	5264
average B values			
protein atoms ($Å^2$)	63.6	65.9	16.1

ligand (Å^2)	58.47	68.9	12.1
weighted RMS deviations from ideality			
bond lengths (Å)	0.008	0.014	0.015
bond angles (º)	1.01	1.62	1.89
planar groups (Å)	0.006		
Ramachandran regions (%)[d]			
most favored	93.2	92.27	97.5
additionally allowed	5.9	7.43	2.3
generously allowed	0.9	0.29	0.3

[a]Statistics for the highest resolution bin.

[a]Statistics for the highest resolution bin.

[b]R_{sym} = ($\sum$|I - $\overline{I}$ |/ $\sum$ I) x 100.

[c]*R*-factor = ($\Sigma|F_o - F_c| / \Sigma|F_o|$) where F_o is the observed structure-factor amplitude and F_c is the calculated structure-factor amplitude.

[d]Distribution of Ramachandran angles according to PROCHECK [24].

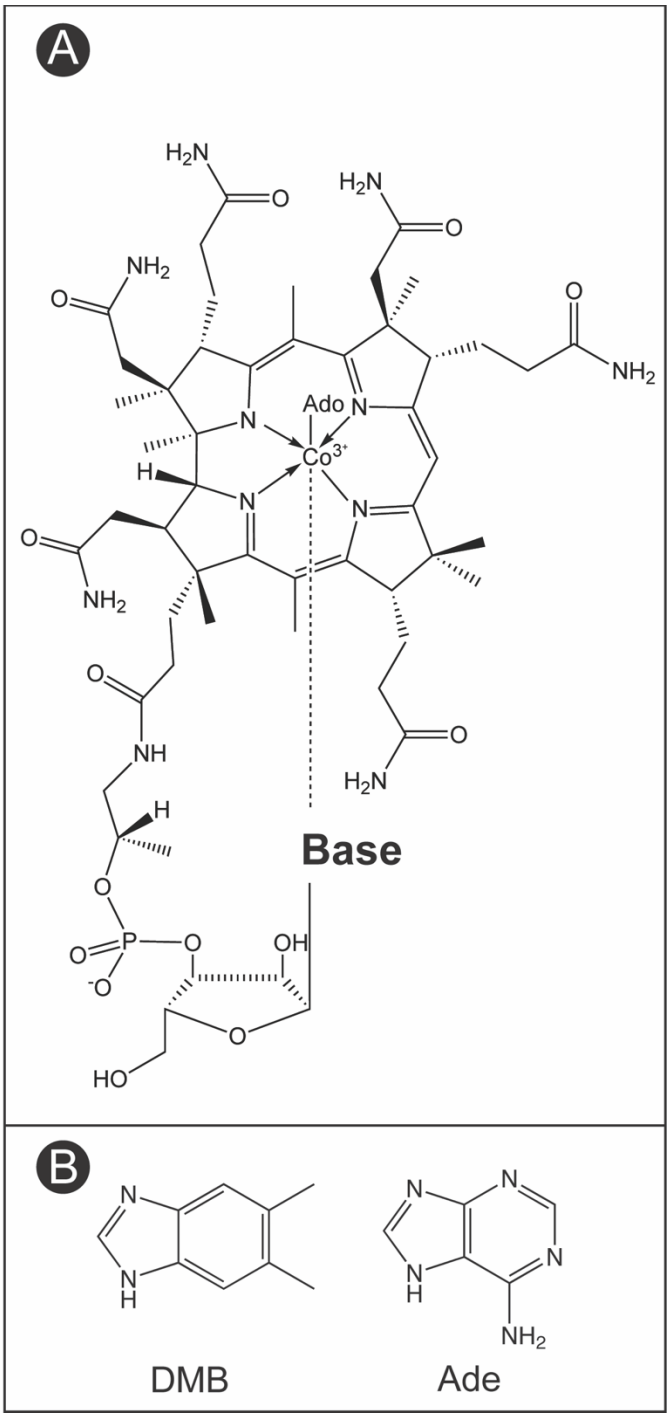

Figure 3.1. Structure of adenosylcobalamin. A. Chemical structure of adenosylcobalamin. The location of the lower nucleotide base is denoted by Base. B. Lower nucleotide bases 5,6-dimethylbenzimidazole (DMB) and adenine (Ade) identified in the active site of *Mj*CobT.

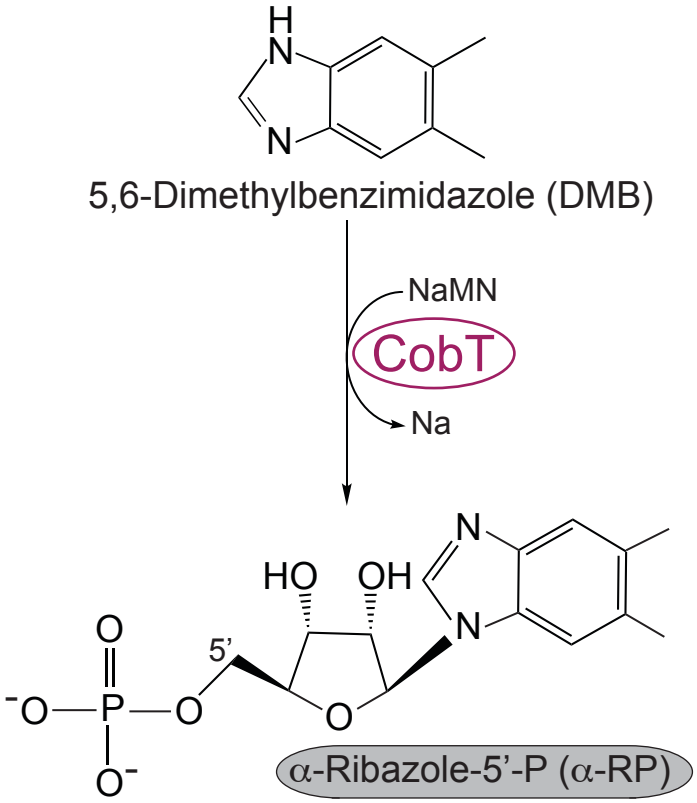

Figure 3.2. Nucleotide base activation by CobT.

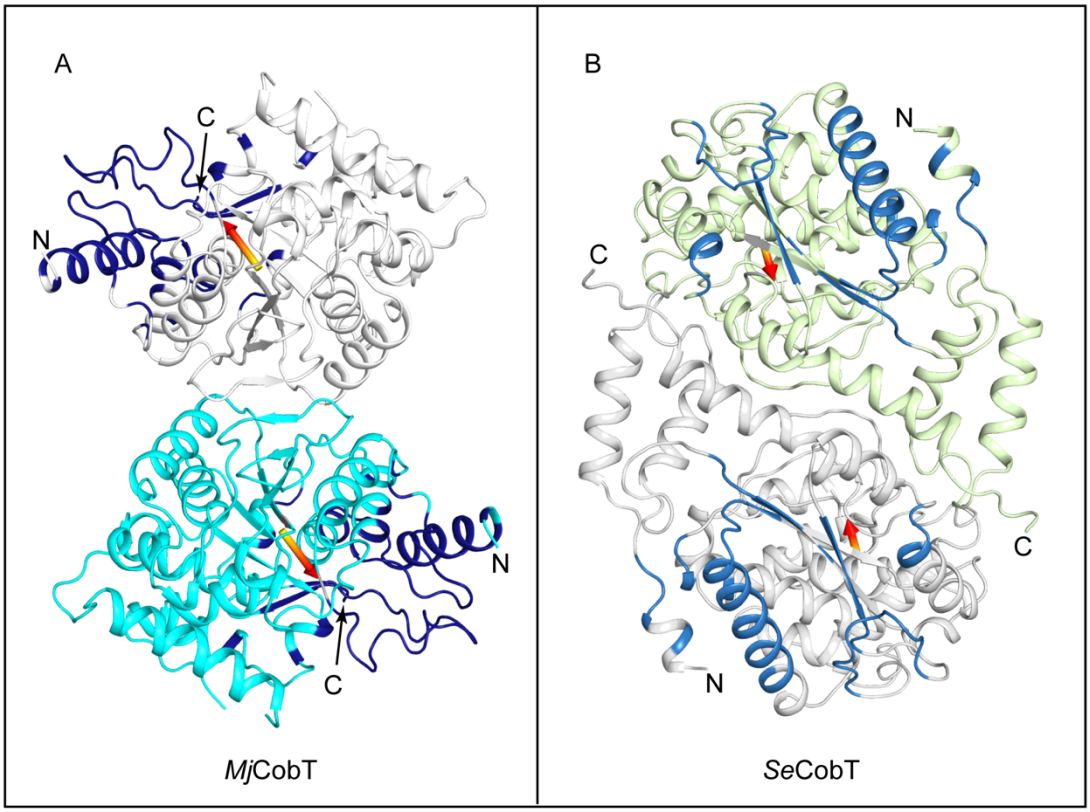

Figure 3.3. Comparison of the quaternary structures of *Mj*CobT and *Se*CobT. The orientation of *Mj*CobT in its dimer relative to that seen in *Se*CobT (1L4B)[25] is completely different as indicated by the arrows that depict a similar vector in each monomer. (A) shows the quaternary of apo-*Mj*CobT. The equivalent residues that form the dimer interface in SeCobT are depicted in dark blue. Conversely, the residues in *Se*CobT that correspond to the interface in *Mj*CobT are depicted in cyan in (B). This dramatic difference in assembly follows the rms differences between *Mj*CobT and *Se*CobT which are 2.2 Å for 248 equivalent alpha-carbon atoms. This reveals that the enzymes contain a similar fold but differ in their exterior loops.

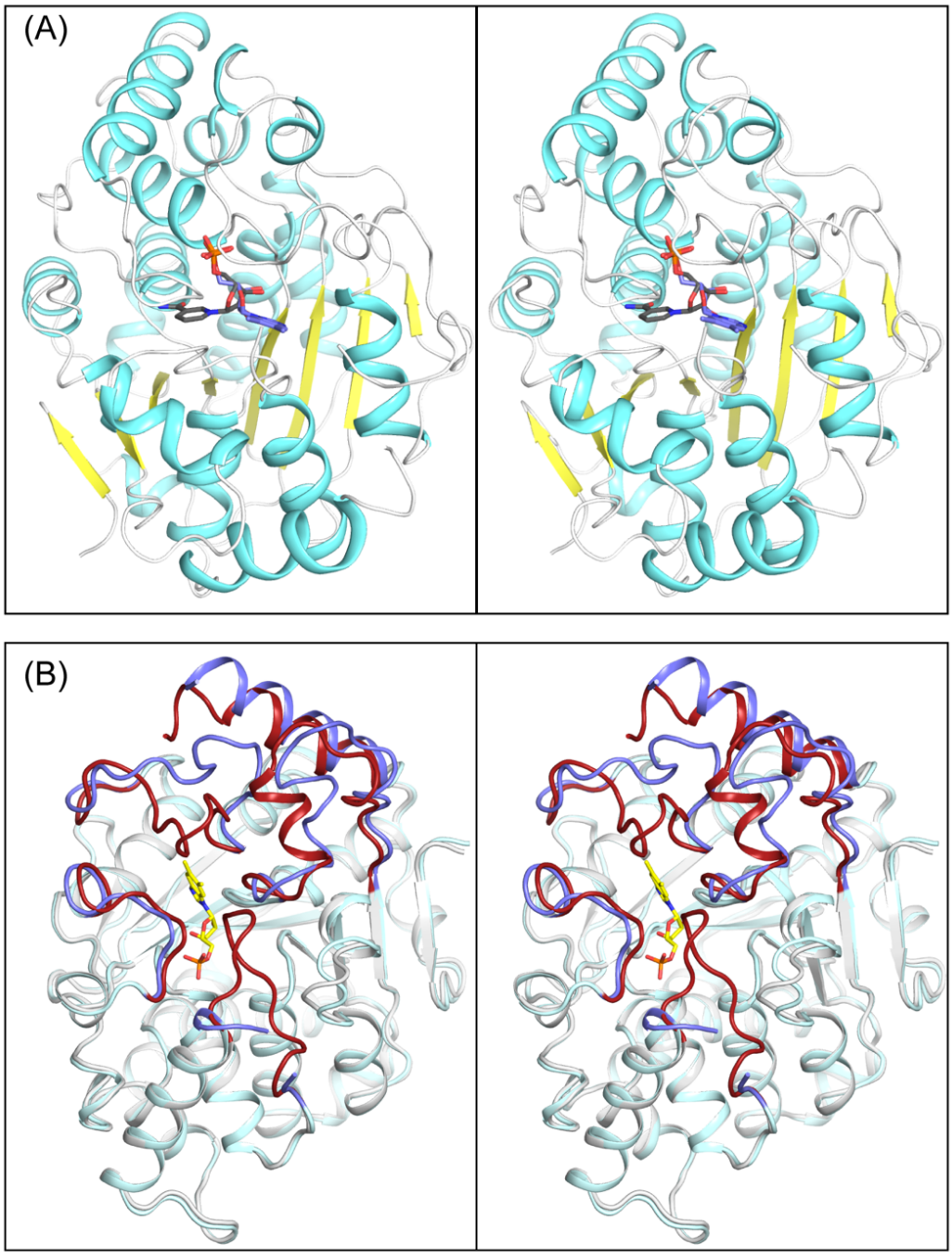

Legend on following page.

Figure 3.4 Location of the active site in MjCobT and the conformational changes that occur on ligand binding. (A) shows a superposition of NaMN and α-RP and nicotinic acid from crystalline complex of substrate and products and reveals the entirety of the active site located at the C-terminal ends of the β-sheet. B) shows a comparison between the apo-structure and subunit B that contains α-RP and nicotinic acid. The loops that show significant change between the apo *Mj*CobT and the complex with α-RP and nicotinic acid are depicted in blue and dark red respectively. This reveals that the active site is open to solvent in the apo structure, but is enclosed when product is bound. These changes in tertiary structure are associated primarily with those regions of the protein that constitute the binding site for the nitrogenous base.

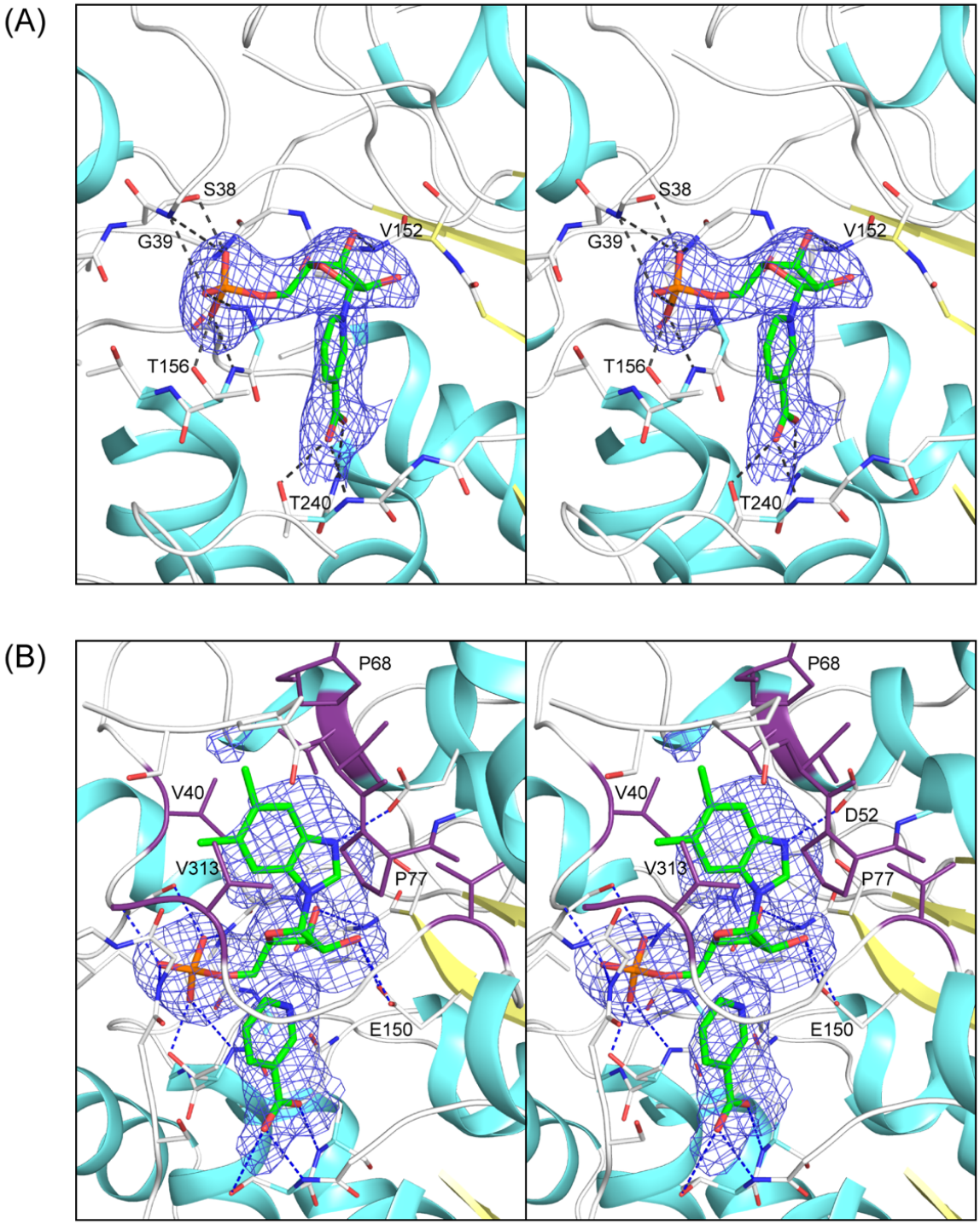

Legend on following page.

Figure 3.5. Electron density for NaMN and α-RP and nicotinic acid and their hydrogen bonding interactions. Shown in stereo in (A) and (B) are the observed electron densities for NaMN and α-RP and nicotinic acid respectively. The omit maps were calculated with coefficients of the form $F_o - F_c$ where F_o and F_c were the native and calculated structure factor amplitudes, respectively. The map was contoured at 2.5σ. (A) shows the extensive hydrogen bonding interactions of the nicotinamide ring, ribose sugar, and phosphate moiety. The same interactions are observed for the moiety in the active site that carries α-RP and nicotinic acid, together with the interactions with DMB. (B) shows the side chains that surround the nitrogenous base which are mostly hydrophobic, however there is a hydrogen bond between N3 of DMB and Oγ of Asp 52.

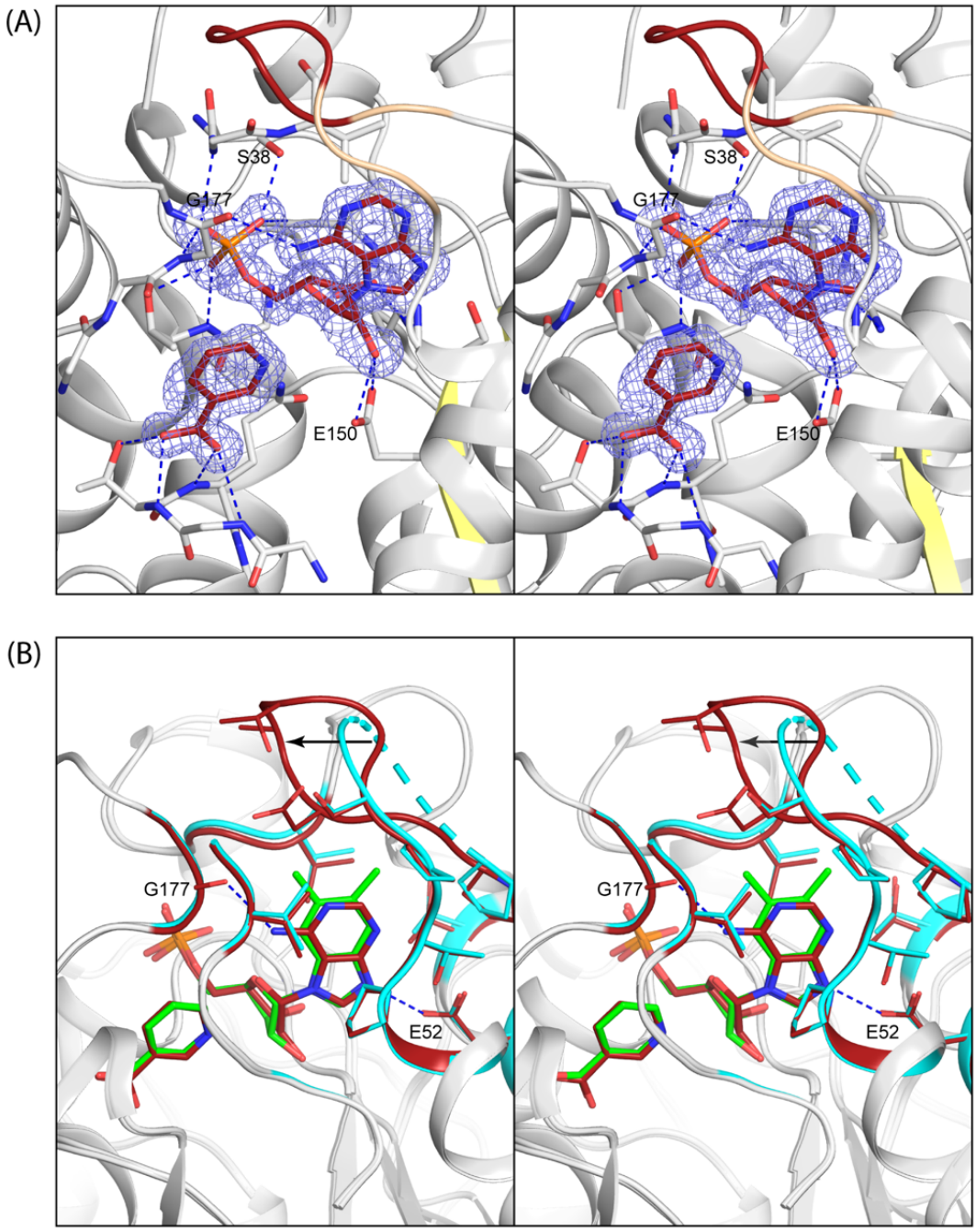

Legend on following page.

Figure 3.6 Electron density and model for the adenine ribotide and its similarity to α-RP. Shown in stereo in (A) are the observed electron density for adenine ribotide and nicotinic acid. It also shows the base specific interaction between the carbonyl oxygen of Gly 177 and the amino group of adenine. Note again that there are additional hydrogen bonds between O2' of the ribose and Oγ1 and Oγ2 of Glu 250 relative to the complex with NaMN. (B) shows the close similarity in the mode of binding of adenine ribotide and α-RP. The major difference is ordering of the loop between Ile 69 – Thr 72 such that it encloses the purine ring.

CHAPTER 4

INSIGHTS INTO THE RELATIONSHIP BETWEEN COBAMIDE SYNTHASE AND THE CELL MEMBRANE[3]

[3]Jeter V.L., and Escalante-Semerena J.C. Submitted October 2020 to *mBio*.

ABSTRACT

Cobamides are cobalt-containing cyclic tetrapyrroles used by cells from all domains of life, but only produced *de novo* by some bacteria and archaea. The 'late steps' of the adenosylcobamide biosynthetic pathway are responsible for assembly of the nucleotide loop and are required during *de novo* synthesis and precursor salvaging. These steps are characterized by activation of the corrin ring and lower ligand base, condensation of the activated precursors to adenosylcobamide-phosphate, and removal of the phosphate yielding a complete adenosylcobamide molecule. The condensation of the activated corrin ring and lower ligand base is performed by an integral membrane protein cobamide (5' phosphate) synthase (CobS) and represents an important convergence of two pathways necessary for nucleotide loop assembly. Interestingly, membrane association of this penultimate step is conserved among all cobamide producers, yet the physiological relevance of this association is not known. Here we present the purification and biochemical characterization of the CobS enzyme of the enterobacterium *Salmonella enterica enterica* serovar Typhimurium strain LT2, investigate its association with liposomes, and quantify the effect of the lipid bilayer on its enzymatic activity and substrate affinity. We report a purification scheme that yields pure CobS protein, allowing *in vitro* functional analysis. Additionally, we report a method for liposome reconstitution of CobS, allowing for physiologically relevant studies of this inner membrane protein in a phospholipid bilayer. *In vitro* and *in vivo* data reported here expand our understanding of CobS and the implications of membrane associated adenosylcobamide biosynthesis.

IMPORTANCE

Salmonella is a human pathogen of worldwide importance, and coenzyme B_{12} is critical for the pathogenic lifestyle of this bacterium. We report insights into the dramatic effect that a phospholipid bilayer has on the activity of a B_{12} biosynthetic enzyme. Previously, we proposed that the late steps of B_{12} biosynthesis are catalyzed by a multi-enzyme complex anchored to the cell membrane by two B_{12} biosynthetic enzymes, and that the alluded complex is present in every B_{12}-producing bacterium and archaeum sequenced to date. An improved method for the isolation of the enzyme that catalyzes the penultimate step of the pathway allowed us to perform *in vivo* and *in vitro* studies that advanced our understanding of the functionality of the enzyme in the context of the lipid bilayer,and sets the foundation for the functional-structural analysis of the aforementioned multienzyme complex.

KEYWORDS. B_{12} biosynthesis, cobamide 5'-phosphate synthase (CobS) enzyme, nucleotide loop assembly, liposome-enhanced CobS activity, vitamin metabolism, membrane-associated metabolism

INTRODUCTION

Cobamides (Cbas) are complex cobalt-containing, cyclic tetrapyrroles that belong to the family of cofactors known as 'the pigments of life', which includes chlorophylls, coenzyme F_{430}, and hemes (1, 2). To date, only some archaea and

bacteria are known to make Cbas *de novo*, and although cells from all domains of life may require Cbas to survive, higher plants are not known to make or use Cbas in their metabolisms (3). Notably, some microalgae, use different forms of Cbas (4-6).

Cbas are involved in diverse reactions, including reductive dehalogenation, elimination reactions, enzymatic carbon-skeleton rearrangements, radical SAM-catalyzed carbon skeleton rearrangements, and methyl-group transfers (7). Recently, Cbas were shown to serve as a light sensor associated with a transcription factor used to regulate gene expression (8).

Cbas are structurally unique among cyclic tetrapyrroles in that they have upper and lower axial ligands. Cobalamin (Cbl) is the cobamide whose structure includes a 5,6-dimethylbenzimidazole (DMB) nucleobase (Fig. 4.1). The coenzyme form of Cbl is adenosylcobalamin (AdoCbl), which contains a 5'-deoxyadenosine (Ado) as the upper axial ligand. The lower axial ligand is a source of structural diversity among Cbas in that a number of purine and benzimidazole analogues, as well as *p*-cresol and phenol can serve as the nucleobase (9-11).

Some organisms synthesize AdoCbl *de novo*, yet others rely on salvaging incomplete corrinoids such as cobinamide (Cbi) or cobyric acid (Cby). *Salmonella enterica enterica* sv Typhimurium strain LT2 (henceforth *S.* Typhimurium) synthesizes AdoCbl *de novo* under anoxic conditions, but this bacterium can synthesize AdoCba under normoxic conditions if incomplete corrinoids such as Cbi or Cby are present in the environment (12, 13).

The late steps of AboCbl biosynthesis, often referred to as Nucleotide Loop Assembly (NLA) pathway, are responsible for attaching the lower ligand to the corrin ring. In *S.* Typhimurium, the NLA pathway is comprised of two branches: i) ring activation, and ii) base activation (Fig. 4.2). Ring activation starts with the attachment of 1-amino-propanol phosphate (AP-P) to adenosyl-Cby (AdoCby) to yield adenosylcobinamide-phosphate (AdoCbi-P). This reaction is catalyzed by the AdoCbi-P synthase (CbiB, EC 6.3.1.10) enzyme (14). AdoCbiP is further activated by guanylylation to yield AdoCbi-GDP, a catalyzed by the guanylyltransferase activity of the bifunctional enzyme CobU (NTP:AdoCbi kinase EC 2.7.7.62; GTP:AdoCbi-P guanylyltransferase, EC 2.7.1.156) (15-17); AdoCbi-GDP is the activated form of the ring. In this bacterium, nucleobase activation is catalyzed by the phosphorybosyltransferase (PRTase) activity of CobT (EC 2.4.2.21). In this reaction, CobT transfers the phosphoribosyl moiety of nicotinate mononucleotide (NaMN) to 5,6-dimethylbenzimidazole (DMB) via an inversion-of-configuration displacement that yields α-ribazole-phosphate (α–RP) releasing nicotinic acid (18-22); α-RP is the activated form of the DMB nucleobase. The two active intermediates are the substrates of the cobamide 5'-P synthase (henceforth cobamide synthase) CobS (EC 2.7.8.26), which condenses AdoCbi-GDP and α-RP to generate adenosylcobalamin 5'-phosphate (henceforth AdoCbl-P) (23, 24). In the final step, AdoCbl-P is dephosphorylated by the CobC enzyme (EC 3.1.3.73) to yield AdoCbl (25, 26). CobS is a polytopic inner membrane protein that catalyzes the penultimate step of AdoCbl biosynthesis pathway (Fig. 4.3) (23), and its cellular location is conserved amongst all known Cba producers. Here we

report: i) a new and improved protocol for the isolation of the *S.* Typhimurium CobS enzyme that yields 96% homogenous protein; ii) the reconstitution of purified CobS protein into liposomes to investigate the effect of the lipid bilayer on CobS function, iii) *in vitro* substrate binding analysis, and iv) *in vivo* variant analysis identifying residues and motifs essential to cobamide synthase function.

RESULTS & DISCUSSION

Improved protocol for the isolation of the cobamide 5'-P (CobS) synthase of *S.* Typhimurium. The purification of CobS has been problematic (24), with some improvement in yield and purity accomplished over time (23, 26). However, none of those protocols yielded the quality and quantity of protein needed to perform detailed *in vitro* analysis of the function of this key enzyme of the AdoCbl biosynthesis pathway. The new method for the purification of the *S.* Typhimurium cobamide synthase (CobS) enzyme described herein yields protein at 96% homogeneity (Fig. 4.4), with a yield of 0.5 mg of protein / g of wet cells.

The activity of cobamide synthase increases dramatically when it is inserted into a lipid bilayer. To study the function of CobS in a more physiologically relevant context, we inserted CobS protein into liposomes. The protocol for generating CobS-containing proteoliposomes is detailed in the Supplemental Material under the *Materials & Methods* section.

The presence of CobS in the phospholipid bilayer of liposomes was confirmed by probing with α-CobS antibodies (Fig. 4.5A), and by means of a bioassay that

quantified the amount of product the CobS reaction generated *in vitro* (Fig. 4.5B). To quantify the effect of lipids on CobS function we used the newly implemented continuous spectrophotometric assay described under *Materials & Methods.* Using the alluded method, we measured a striking difference in specific activity between CobS and CobS embedded into liposomes. That is, the specific activity of CobS was >20-fold lower than that of CobS embedded into liposomes (0.11 *vs* 2.26 μmol AdoCbl-P min^{-1} mg^{-1} of protein, respectively) (Fig. 4.6A). Confirmation of reaction products was determined by RP-HPLC, using authentic CNCba 5'-P as the positive control (Fig. 4.6B). Clearly, a lipid environment substantially increased CobS function.

The protocol used for the generation of CobS proteoliposomes yields near-monodisperse proteoliposomes. To quantify the functionality of CobS in the proteoliposome, we needed to ensure that the population of proteoliposomes was near homogenous. To assess homogeneity, we used dynamic light scattering (DLS) to determine the ideal protein to lipid ratio and survey the variance and hydrodynamic properties of CobS-containing proteoliposome populations (Fig. 4.7). In Fig. 4.7A, the intensity of distribution of particle sizes is shown for empty liposomes (red), CobS-containing proteoliposomes generated with protein to lipid molar ratio of 1:1000 (orange), and CobS-containing proteoliposomes generated with protein to lipid molar ratio of 1:500 (green). Intensity distribution is a sensitive measure of aggregation and here we see the most consistent distribution of particle size in the CobS-containing proteoliposomes generated using a 1:1000

protein:lipid ratio. Panel B displays the percent particle number distribution of particle size of the same samples. Again, we observed that CobS-containing proteoliposomes generated with protein to lipid ratio of 1:1000 showed the least variance in particle size. Panel C shows the second-order values determined by dynamic light scattering. Here we saw that the protein to lipid ratio of 1:1000 yielded a population of proteoliposomes with more consistent Z-average, polydispersity index (PdI) and size. Given the low PdI, lower Z-average, and smaller standard deviation of particle size we concluded that our population of CobS-containing proteoliposomes generated with a protein to lipid ratio of 1:1000 was near monodisperse.

CobS orientation in liposomes. When generating proteoliposomes, we considered the two possible orientations in which CobS could orient in the lipid bilayer: Firstly, The *N* terminus of CobS could be located outside the lumen of the proteoliposome, or alternatively, the *N* terminus of CobS could be found inside the lumen of the proteoliposome (Fig. 4.8A). To assess the orientation of the population of CobS-containing proteoliposomes, we performed proteolytic digests using proteinase K (PK).

Figure 4.8B shows results of western blot experiments probing with polyclonal rabbit α-CobS antibodies generated against loop 2; lane 1 served to control for molecular mass (kDa). CobS-containing proteoliposomes not treated with PK showed one band at ~26 kDa (lane 2). Similarly, purified, lipid-free CobS that was not treated with PK showed one major band at ~26 kDa (lane 7). In addition to the

major population of full-length CobS, we saw a small population of degradation below 20 kDa (lane 7). CobS-containing proteoliposomes and lipid-free CobS digested with PK yielded multiple fragments below ~26kDa (lanes 3, 8, respectively). CobS-containing proteoliposomes incubated with Triton X-100 (0.1% and 0.5%, v/v) before PK digestion showed an increase in the intensity of low molecular mass fragments compared to PK-digested, CobS-containing proteoliposomes not treated with Triton X-100 (lanes 4, 5). We posited that incubation of proteoliposomes with detergent would disrupt the structure of the proteoliposome, making the cytoplasmic and periplasmic loops of the protein susceptible to digestion by PK. When the protease inhibitor PMSF was introduced, we saw complete inhibition of PK digestion of CobS-containing proteoliposomes (lane 6). The digestion pattern observed in the liposomes treated with PK was similar to the one observed with digested liposomes after detergent incubation, an observation that supported the conclusion that loop 2 was exposed, favoring the orientation where the *N*-terminus was located outside the lumen of the proteoliposome.

In addition to digestion with PK, we digested loop 2 with trypsin and chymotrypsin (C.trypsin) (Fig. 4.8C). As before, lane 1 served to control for molecular mass (kDa). The undigested CobS-containing liposomes showed a single band ~26 kDa (lane 2). When digested with trypsin, we observed an additional fragment below 20 kDa alone with the full-length CobS at ~26 kDa (lane 3). When incubated with Triton X-100, an increase in intensity below 20 kDa was also evident (lane 4). CobS digested with trypsin yielded three fragments below 20 kDa suggesting that

reconstitution in the lipid bilayer protected CobS from multiple trypsin cleavage sites (lane 5). Chymotrypsin digestion of CobS-containing proteoliposomes generated four major fragments: one ~20 kDa and the remaining three fragments were smaller (lane 6). When incubated with Triton X-100, we observed a decrease in intensity of the band ~20 kDa (lane 7). Digestion of purified CobS yielded additional fragments compared to CobS proteoliposomes, again suggesting occlusion (lane 8). Results of limited proteolysis were consistent with CobS being inserted into the liposome bilayer as shown in Fig. 4.8A, orientation 1.

Affinity of CobS for its nucleotide substrate in the lipid bilayer. In addition to determining the effect of a lipid environment on CobS activity, we investigated the effect of the same environment on substrate binding. Affinity for the α–RP substrate was determined by DRaCALA using radiolabelled α–RP ligand incubated with DHPC-solubilized CobS or CobS-containing proteoliposomes (Fig. 4.9). Using this approach, we calculated a dissociation constant (K_d) of the CobS / α–RP complex was 1.71 μM, indicating a high affinity for the nucleotide substrate (Panel A). The K_d of the CobS-containing proteoliposome/α–RP complex was calculated to be 0.58 μM, a 3-fold decrease in K_d compared to DHPC-solubilized CobS (Panel B). The higher affinity of liposome-embedded CobS for α–RP substrate was consistent with our expectations given the reported low intracellular concentration of the NaMN substrate of the CobT phosphoribosyltransferase that synthesizes α–RP (27). Due to the poor capillary behavior of AdoCbi-GDP on nitrocellulose, binding kinetics for this substrate were not obtained.

Nucleotide substrate binding induces a CobS conformational change. To assess the effect of substrate binding on CobS structure, CobS protein was subjected to limited trypsin proteolysis after incubation with α–RP and AdoCbi-GDP. Changes in protein structure were analyzed by tricine-SDS-PAGE (Fig. 4.10A) followed by MALDI-TOF mass spectrometry analysis (Fig.4.10B). Preincubation with AdoCbi-GDP did not provide protection from proteolysis by trypsin. As shown in Fig. 4.10A, preincubation with α–RP resulted in the retention of full-length CobS protein and a prominent ~24 kDa band over the course of a 30-min digestion. CobS protein in the absence of α–RP was readily digested. MALDI-TOF mass spectrometry analysis of the ~24 kDa peptide identified peptides from Leu^{4} to Lys^{175} (Fig. 4.10B). These data suggest a significant conformational change occurs upon α–RP binding.

***In vivo* assessment of single-amino acid variant CobS proteins.** Of interest to us were the conserved amino acid sequence motifs within cytoplasmic loops 2 and 6 (Fig. 4.3) of CobS proteins (Fig. 4.11, red highlights); for complete sequences of CobS proteins see Fig. 4.14. Given the high degree of conservation and putative cytoplasmic localization, we hypothesized that these residues might be relevant to substrate interactions or catalysis. To investigate the roles of these motifs, site-directed mutagenesis of *cobS* cloned under the control of an L-(+)-arabinose inducible promoter was performed to generate alleles that would encode single-amino acid CobS variants. Newly constructed vectors were transformed into *S.* Typhimurium strain JE8248 (*metE205 ara-9* Δ*cobS1313*) to assess CobS function

in vivo. We assessed the growth of strains that synthesized CobS variants under Cba-dependent conditions (Table 4.1; Fig. 4.15-Fig. 4.17). All strains tested carried a null allele of the Cba-independent methionine synthase (MetE) enzyme, hence demanding that the last step of methionine synthesis was performed by the Cba-dependent methionine synthase (MetH) enzyme. In addition, the strains carried a chromosomal deletion of *cobS,* making the strain ideal for the assessment of the function of CobS variants *in vivo*.

As shown in figures 4.3 and 4.11, within the first transmembrane domain (TM1) of CobS lies a conserved glycine residue at position 45. When a glutamate substitution was introduced at position 45, the resulting $CobS^{G45E}$ variant failed to synthesize enough product to support cell growth, despite the presence of Cbi and DMB precursors in the medium (Table 4.1; Fig. 4.15-Fig. 4.17 solid, green squares). This growth defect was overcome by the addition of cobalamin, indicating that G45 was critical for CobS function. Glycines, especially repeats as seen here, are often important for proper helix packing in the membrane. It is likely the glutamate substitution at this location interrupted the packing of TM1.

Cytoplasmic loop 2. We noted that cytoplasmic loop 2 of all cobamide producers contains a motif flanked by conserved residues H80 and D89, with two more conserved aspartyl residues at positions 82 and 86 (^{80}HxDxxxDxxD^{89}) (Fig. 4.11). To probe the relevance of this motif to CobS function we performed an alanine scan at the conserved residues within this motif. Under the conditions tested, alanine substitutions at D82, D86 and D89 resulted in abrogation of growth in

medium supplemented with Cbi and DMB (Table 4.1; D82A Fig. 4.15-Fig. 4.17 solid, grey diamonds; D86A Fig.S4-Fig.S6 solid, orange triangles; D89A Fig.S4-Fig.S6 grey asterisks). In each of these strains, growth was restored when cobalamin was provided. Notably, the $CobS^{H80A}$ variant was unable to synthesize enough AdoCbl-P to support growth of the test strain when a low concentration of Cbi (0.5nM) was added to the medium. However, the $CobS^{H80A}$ variant supported growth when Cbi and DMB were present in the culture medium (Table 4.1, Fig. 4.15 open, black squares). When the concentration of Cbi in the medium was increased to 1 nM, the strain that synthesized the $CobS^{H80A}$ variant grew, albeit at a slower rate relative to $CobS^{WT}$-synthesizing strains (Table 4.1; Fig. 4.16A open, black squares). Increasing Cbi to 1.5 nM resulted in a growth rate comparable to a strain that synthesized $CobS^{WT}$ (Table 4.1; Fig. 4.17A open, black squares).

At the end of loop 2, we noted an additional region of conservation between residues 98 and 106 (Fig. 4.11). When alanine was substituted for methionine at position 104, growth was observed in medium supplemented in medium containing both Cbi and DMB, but not low Cbi (0.5 nM and 1.0 nM) alone (Table 4.1; Fig. 4.15A, Fig. 4.16A solid, black circles). Increasing Cbi to 1.5 nM resulted in a growth rate comparable to a strain synthesizing $CobS^{WT}$ (Table 4.1; Fig. 4.17A solid, black circles). When lysine was substituted for arginine at position 105, no significant changes in growth were observed (Table 4.1; Fig. 4.15A, Fig. S5A, Fig. S6A open, orange diamonds). Interestingly, strains synthesizing both $CobS^{R108K}$ and $CobS^{R108E}$ exhibited a slight decrease in growth rate compared to strains synthesizing $CobS^{WT}$ on low Cbi (0.5 nM) (Table 4.1; R108K Fig. 4.15A open,

green triangles; R108E Fig. 4.15A open, upside-down, grey triangles). When DMB was provided, the slight defect in growth rate was no longer observed (Table 4.1; R108K Fig. 4.15B open, green triangles; R108E Fig. 4.15B open, upside-down, grey triangles). Given the marginal effect on growth when substituting a negatively charged residue at position 108, it is likely this position is not directly involved in binding the nucleotide substrate. The cessation of growth seen with changes to aspartyl residues in this motif may suggest an inability to interact with the activated corrin ring substrate, AdoCbi-GDP. Collectively, these results suggest that the change to a hydrophobic side may hinder AdoCbi-GDP binding, and the presence of α-RP (a hydrophobic molecule, generated from the DMB provided) helps correct the problem. In addition to these results, data obtained through DRaCALA and limited trypsin proteolysis suggest α-RP binds first. The conformational change upon α-RP binding may increase affinity for AdoCbi-GDP.

Cytoplasmic loop 4. We also investigated the variable cytoplasmic loop 4. Strains that synthesized both $CobS^{L168V}$ and $CobS^{R164K}$ exhibited a decreased growth rate under low Cbi conditions (0.5nM) compared to a strain synthesizing $CobS^{WT}$ (Table 4.1; L168V Fig. 4.15C closed, brown diamonds; R164K Fig.S4C closed, orange triangles). This defect was ameliorated upon the addition of DMB, suggesting slight modifications in residue side chain at these locations could be overcome by binding the nucleotide substrate α-RP (Table 4.1; Fig. 4.15D). Interestingly, under low Cbi conditions (0.5nM), a strain synthesizing $CobS^{R159K}$ exhibited a faster growth rate than a strain synthesizing $CobS^{WT}$ (Table 4.1; Fig. 4.15C closed, green

squares). Residue R159 lies near the interface of the cytoplasm and inner membrane. It is possible the change to lysine at this location increases affinity for the nucleotide substrate, conferring a growth advantage of strains synthesizing $CobS^{R159K}$ to wild-type CobS.

Cytoplasmic loop 6. Cytoplasmic loop 6 contains a region of highly conserved residues from 225 to 232 with a motif of $^{225}GxxGDxxG^{232}$ observed amongst all cobamide producers (Fig. 4.11); noteworthy are two additional conserved residues within the motif, namely G228 and D229. Strains that synthesized $CobS^{G225}$ exhibited growth on low Cbi (0.5 nM), but with a severe decrease in growth rate and increase in lag compared to strains synthesizing $CobS^{WT}$ (Table 4.1; Fig. 4.15E closed, orange triangles). In the presence of DMB, growth was restored to a rate and lag comparable to a strain synthesizing $CobS^{WT}$ (Table 4.1; Fig. 4.15F closed, orange triangles). Strains that synthesized $CobS^{G232A}$ failed to synthesize sufficient cobamide to support growth in in medium supplemented with low Cbi (0.5nM) only (Table 4.1; Fig. 4.15E closed, brown diamonds), but growth was restored in medium containing Cbi and DMB (Table 4.1; Fig. 4.15F closed, brown diamonds). A strain that synthesized $CobS^{D229A}$ did not grow when Cbi and DMB are provided, but growth was restored with exogenous cobalamin (Table 4.1; Fig. 4.15EF, Fig. 4.16EF, Fig. 4.17EF closed, green squares). Given the observed phenotypes, the role of residue D229 appears to be more critical to CobS function than those of other conserved residues within this motif.

CONCLUDING REMARKS.

As mentioned above, CobS is predicted to be an integral membrane protein in all cobamide producers, suggesting that a strong positive selection for the use of the cell membrane in the synthesis of cobamides has been maintained throughout evolution. Our results clearly show the impact of the lipid bilayer of liposomes on cobamide synthase activity. We speculate that in an intact cell, where the entire complex is assembled, the impact of the cell membrane on cobamide synthesis is optimized and the effect of the functionality of the enzymes in the complex must be more dramatic. Our data show that CobS embedded in liposomes exhibits a >10-fold higher affinity for its nucleotide substrate, and that binding of the nucleotide substrate to the CobS enzyme results in a significant conformational change that likely drives interactions with the corrin ring substrate. The results of our initial mutational analysis have identified side chains of residues that when altered, the enzyme activity sharply decreases and, in some instances, it is lost. Although we do not why these changes affect CobS activity, this new knowledge will inform future work on how the enzymes in the complex interact and what residues are critical for their activities. Ongoing work will provide further insights into the role of CobS in the assembly of the alluded multienzyme complex.

ACKNOWLEDGEMENTS

We gratefully acknowledge Dr. Kun Yao, Ph.D. of the UGA Integrated Bioscience and Nanotechnology Cleanroom for assistance with the dynamic light scattering experiments. This work was supported by USPHS grant from the National

Institutes of Health (R35-130399 to J.C.E.-S.). The funders had no role in the design, data collection and interpretation, or the decision to submit the work for publication. The authors have no conflict of interest to declare.

J.C.E.-S. conceived the project. V.L.J. performed the experiments. J.C.E.-S. and V.L.J. designed experiments, analyzed data and wrote the manuscript.

REFERENCES

1. Battersby AR. 2000. Tetrapyrroles: the pigments of life. Nat Prod Rep 17:507-526.
2. Bryant DA, Hunter CN, Warren MJ. 2020. Biosynthesis of the modified tetrapyrroles-the pigments of life. J Biol Chem 295:6888-6925.
3. Escalante-Semerena JC, Warren MJ. 2008. Biosynthesis and use of cobalamin (B_{12}). *In* Böck A, Curtiss III R, Kaper JB, Karp PD, Neidhardt FC, Nyström T, Slauch JM, Squires CL (ed), *EcoSal - Escherichia coli* and *Salmonella*: cellular and molecular biology. ASM Press, Washington, D. C.
4. Croft MT, Lawrence AD, Raux-Deery E, Warren MJ, Smith AG. 2005. Algae acquire vitamin B12 through a symbiotic relationship with bacteria. Nature 438:90-93.
5. Croft MT, Warren MJ, Smith AG. 2006. Algae need their vitamins. Eukaryot Cell 5:1175-1183.
6. Helliwell KE, Lawrence AD, Holzer A, Kudahl UJ, Sasso S, Krautler B, Scanlan DJ, Warren MJ, Smith AG. 2016. Cyanobacteria and eukaryotic algae use different chemical variants of vitamin B12. Curr Biol 26:999-1008.

7. Bridwell-Rabb J, Drennan CL. 2017. Vitamin B12 in the spotlight again. Curr Opin Chem Biol 37:63-70.

8. Padmanabhan S, Jost M, Drennan CL, Elias-Arnanz M. 2017. A new facet of vitamin B12: Gene regulation by cobalamin-based photoreceptors. Annu Rev Biochem 86:485-514.

9. Chan CH, Escalante-Semerena JC. 2011. ArsAB, a novel enzyme from *Sporomusa ovata* activates phenolic bases for adenosylcobamide biosynthesis. Mol Microbiol 81:952-967.

10. Keller S, Treder A, SH VR, Escalante-Semerena JC, Schubert T. 2016. The SMUL_1544 gene product governs norcobamide biosynthesis in the tetrachloroethene-respiring bacterium *Sulfurospirillum multivorans*. J Bacteriol 198:2236-2243.

11. Yan J, Bi M, Bourdon AK, Farmer AT, Wang PH, Molenda O, Quaile AT, Jiang N, Yang Y, Yin Y, Simsir B, Campagna SR, Edwards EA, Loffler FE. 2018. Purinyl-cobamide is a native prosthetic group of reductive dehalogenases. Nat Chem Biol 14:8-14.

12. Jeter RM, Olivera BM, Roth JR. 1984. *Salmonella typhimurium* synthesizes cobalamin (vitamin B12) de novo under anaerobic growth conditions. J Bacteriol 159:206-213.

13. Woodson JD, Escalante-Semerena JC. 2004. CbiZ, an amidohydrolase enzyme required for salvaging the coenzyme B_{12} precursor cobinamide in archaea. Proc Natl Acad Sci USA 101:3591-3596.

14. Zayas CL, Claas K, Escalante-Semerena JC. 2007. The CbiB protein of *Salmonella enterica* is an integral membrane protein involved in the last step of the de novo corrin ring biosynthetic pathway. J Bacteriol 189:7697-7708.

15. O'Toole GA, Escalante-Semerena JC. 1995. Purification and characterization of the bifunctional CobU enzyme of *Salmonella typhimurium* LT2. Evidence for a CobU-GMP intermediate. J Biol Chem 270:23560-23569.

16. Thomas MG, Thompson TB, Rayment I, Escalante-Semerena JC. 2000. Analysis of the adenosylcobinamide kinase/adenosylcobinamide-phosphate guanylyltransferase (CobU) enzyme of Salmonella typhimurium LT2. Identification of residue His-46 as the site of guanylylation. J Biol Chem 275:27576-27586.

17. Thompson TB, Thomas MG, Escalante-Semerena JC, Rayment I. 1999. Three-dimensional structure of adenosylcobinamide kinase/adenosylcobinamide phosphate guanylyltransferase (CobU) complexed with GMP: evidence for a substrate-induced transferase active site. Biochemistry 38:12995-3005.

18. Trzebiatowski JR, Escalante-Semerena JC. 1997. Purification and characterization of CobT, the nicotinate-mononucleotide:5,6-dimethylbenzimidazole phosphoribosyltransferase enzyme from *Salmonella typhimurium* LT2. J Biol Chem 272:17662-17667.

19. Trzebiatowski JR, O'Toole GA, Escalante-Semerena JC. 1994. The *cobT* gene of *Salmonella typhimurium* encodes the NaMN: 5,6-dimethylbenzimidazole phosphoribosyltransferase responsible for the synthesis of N^1-(5-phospho-alpha-D-ribosyl)-5,6-dimethylbenzimidazole, an intermediate in the synthesis of the nucleotide loop of cobalamin. J Bacteriol 176:3568-3575.

20. Cheong CG, Escalante-Semerena JC, Rayment I. 1999. The three-dimensional structures of nicotinate mononucleotide:5,6-dimethylbenzimidazole phosphoribosyltransferase (CobT) from *Salmonella typhimurium* complexed with 5,6-dimethybenzimidazole and its reaction products determined to 1.9Å resolution. Biochemistry 38:16125-16135.

21. Claas KR, Parrish JR, Maggio-Hall LA, Escalante-Semerena JC. 2010. Functional analysis of the nicotinate mononucleotide:5,6-dimethylbenzimidazole phosphoribosyltransferase (CobT) enzyme, involved in the late steps of coenzyme B_{12} biosynthesis in *Salmonella enterica*. J Bacteriol 192:145-154.

22. Chan CH, Newmister SA, Talyor K, Claas KR, Rayment I, Escalante-Semerena JC. 2014. Dissecting cobamide diversity through structural and functional analyses of the base-activating CobT enzyme of *Salmonella enterica*. Biochim Biophys Acta 1840:464-475.

23. Maggio-Hall LA, Claas KR, Escalante-Semerena JC. 2004. The last step in coenzyme B(12) synthesis is localized to the cell membrane in bacteria and archaea. Microbiology 150:1385-1395.

24. Maggio-Hall LA, Escalante-Semerena JC. 1999. In vitro synthesis of the nucleotide loop of cobalamin by *Salmonella typhimurium* enzymes. Proc Natl Acad Sci U S A 96:11798-11803.

25. O'Toole GA, Trzebiatowski JR, Escalante-Semerena JC. 1994. The *cobC* gene of *Salmonella typhimurium* codes for a novel phosphatase involved in the assembly of the nucleotide loop of cobalamin. J Biol Chem 269:26503-26511.

26. Zayas CL, Escalante-Semerena JC. 2007. Reassessment of the late steps of coenzyme B_{12} synthesis in *Salmonella enterica*: Evidence that dephosphorylation of adenosylcobalamin-5'-phosphate by the CobC phosphatase is the last step of the pathway. J Bacteriol 189:2210-2218.

27. Bochner BR, Ames BN. 1982. Complete analysis of cellular nucleotides by two-dimensional thin layer chromatography. J Biol Chem 257:9759-9769.

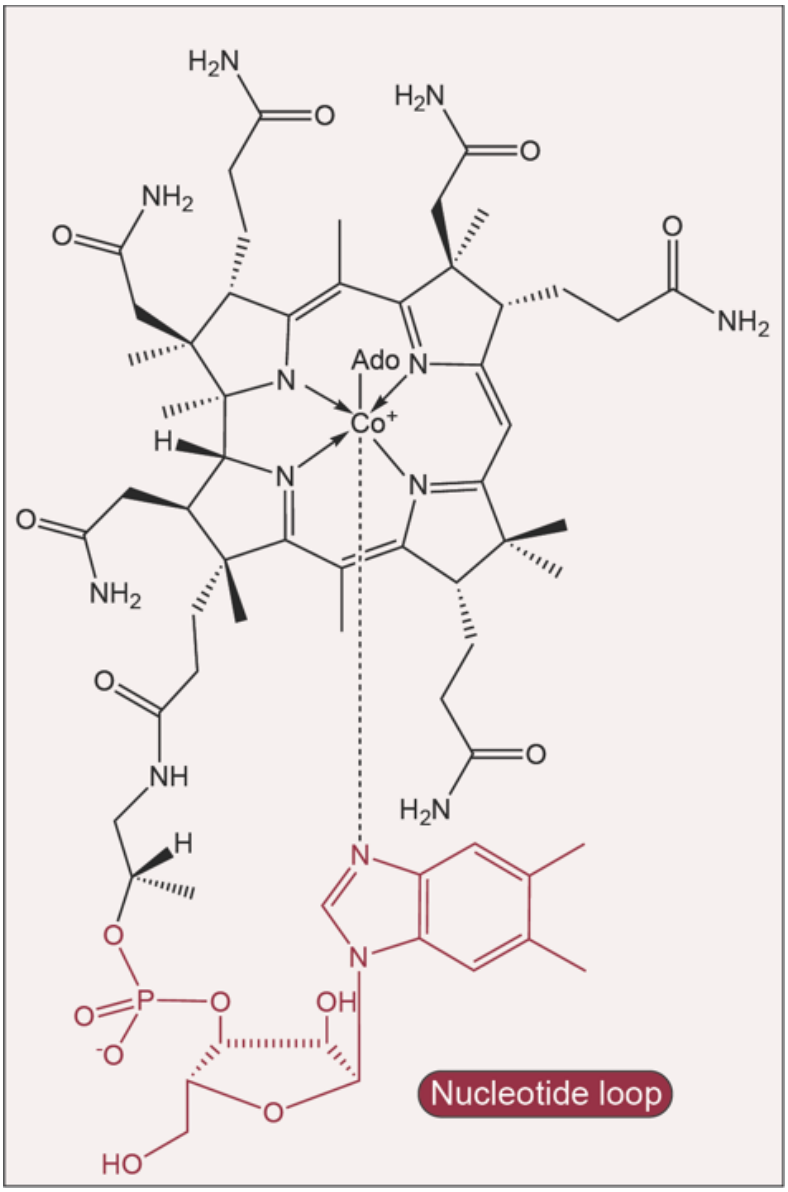

Figure 4.1. Chemical structure of adenosyl-cobalamin (AdoCbl, coenzyme B_{12}

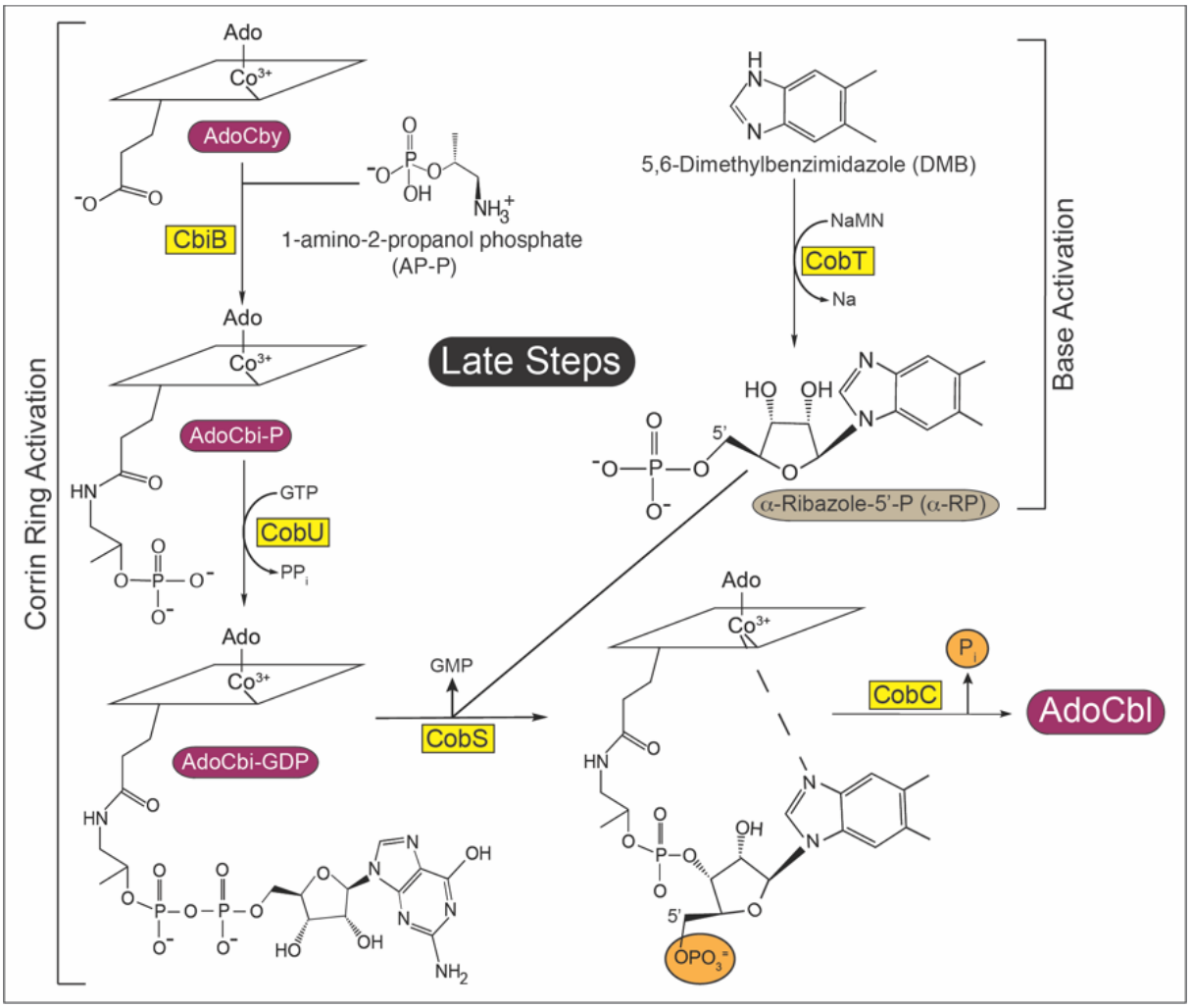

Figure 4.2. Late steps of Ado-cobamide (AdoCba) biosynthesis in *S.* Typhimurium. AdoCbi (cyclic tetrapyrrole ring) is activated to AdoCbi-GDP by CobU and DMB (nucleobase) is activated to α-RP by CobT. Cobamide synthase (CobS, in bold) catalyzes the penultimate step of cobamide biosynthesis, condensing AdoCbi-GDP and α-RP to yield AdoCbl-P. In the final step, CobC removes the phosphate yielding AdoCbl.

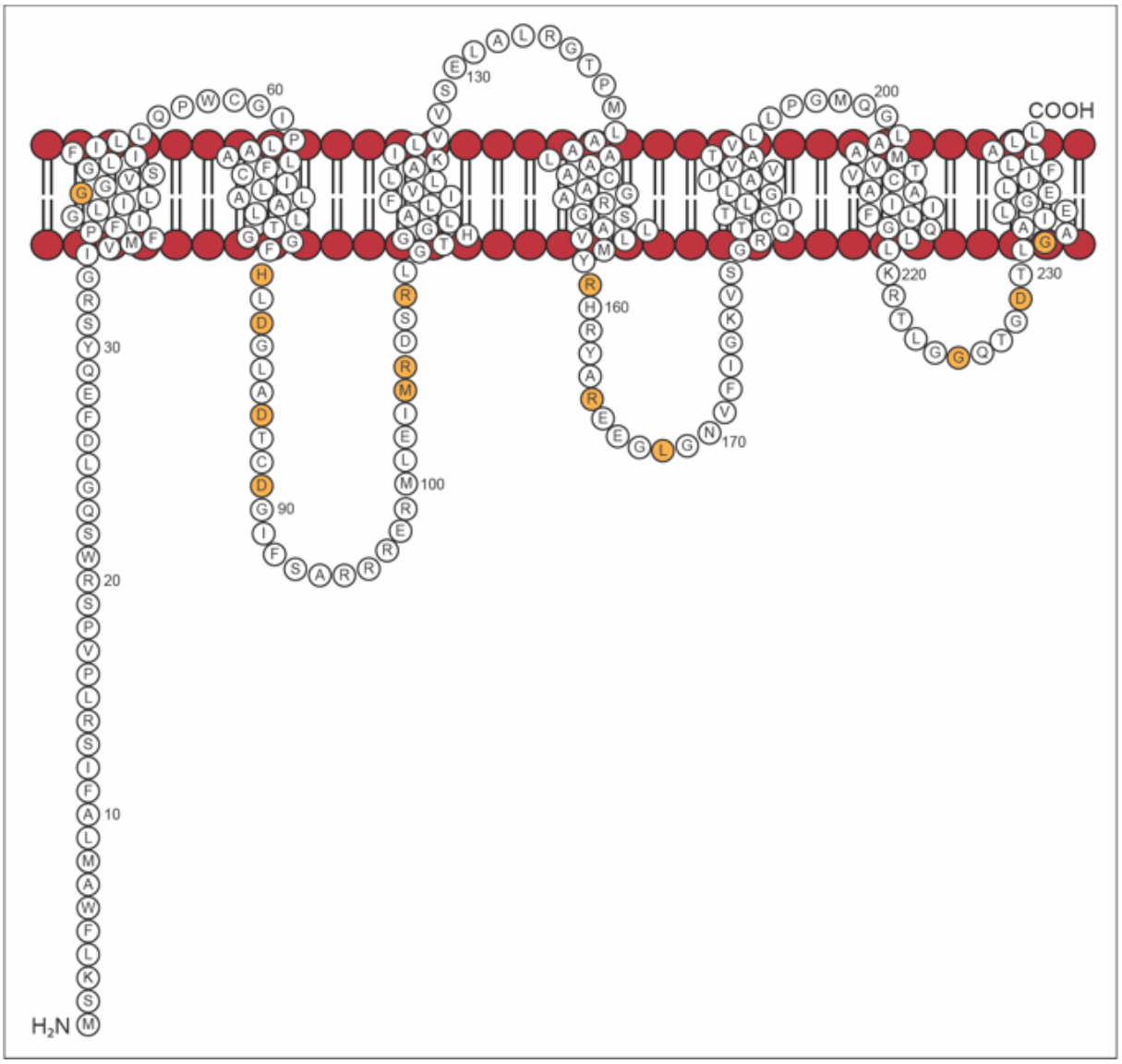

Figure 4.3. Model of CobS membrane topology. The topology of CobS was previously studied using a series of alkaline phosphatase and β-galactosidase fusions (23). Residues targeted for *in vivo* analysis of variant proteins are indicated in orange.

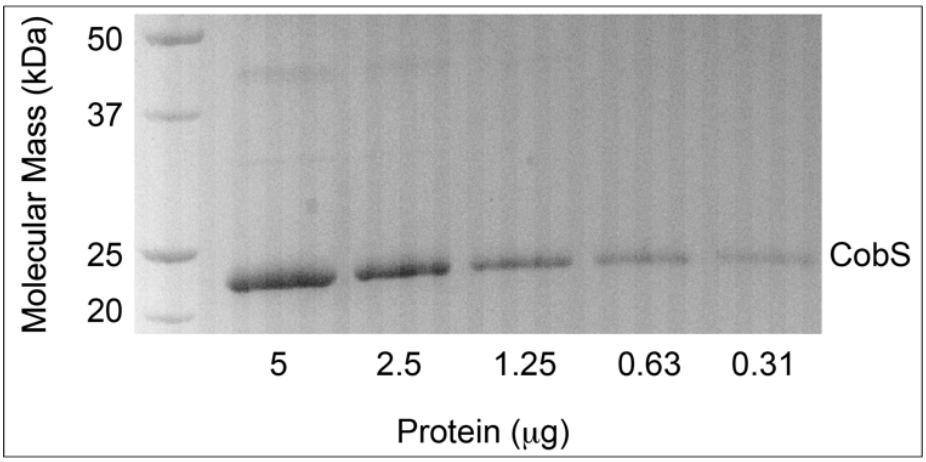

Figure 4.4. Assessment of CobS purity. SDS-PAGE behavior of lipid-free CobS compared to Bio-Rad Precision Plus Protein standards. CobS was estimated to be 96% homogenous based on the data shown.

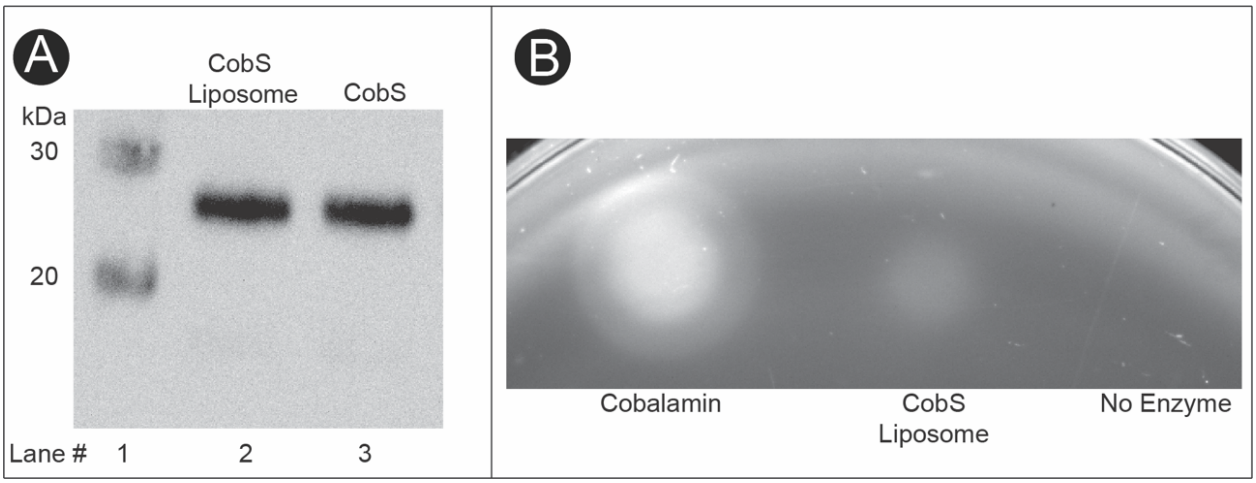

Fig. 4.5. CobS retains activity after insertion into liposomes. A. Western blot analysis of liposome flotation assay. Purified CobS protein is provided as a control. B. Bioassay of CobS function reconstituted in liposomes. Cyanocobalamin provided as a control.

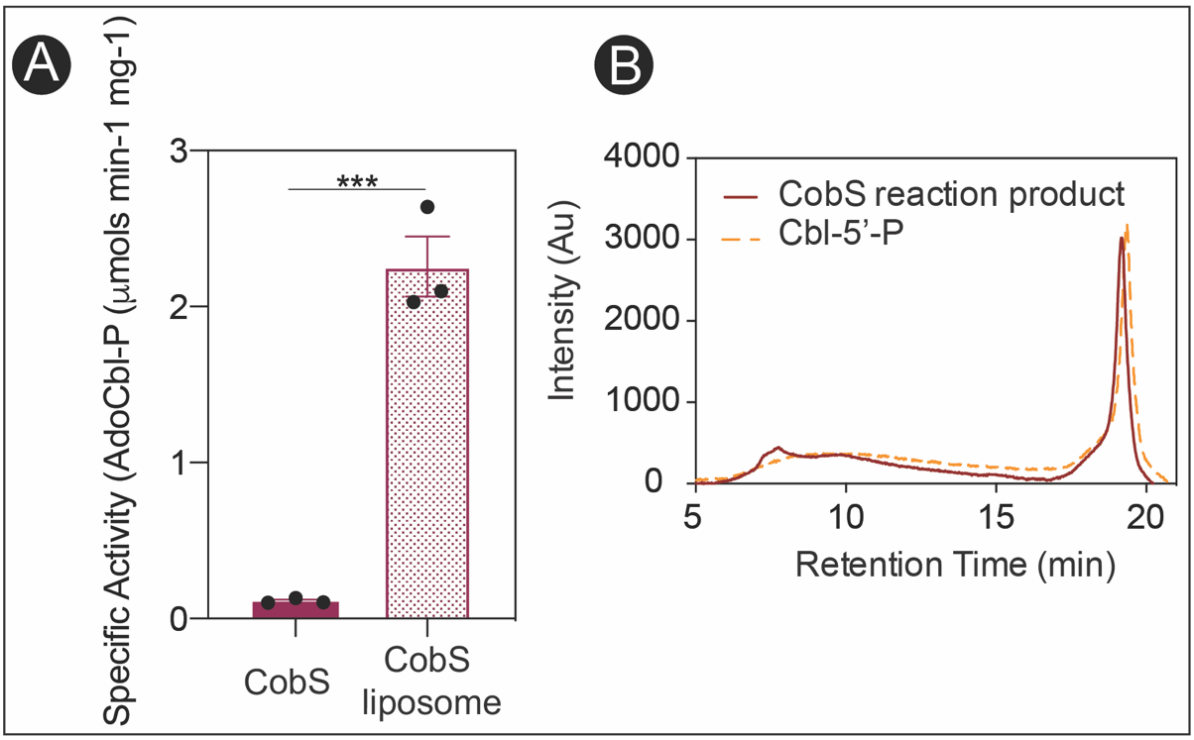

Figure 4.6. CobS activity substantially increases in liposomes. A. The specific activities (μmol AdoCbl-P min^{-1} mg^{-1}) of purified CobS and CobS-containing liposomes were determined using a continuous spectrophotometric assay. Error bars represent standard error of the mean (SEM) of technical triplicates. Asterisks represent significance as determined by unpaired student's *t*-test, *** represents a $p<0.0005$. B. HPLC separations of the reaction product from CobS assay (solid, red line) and cobamide-phosphate (dashed, orange line) are shown.

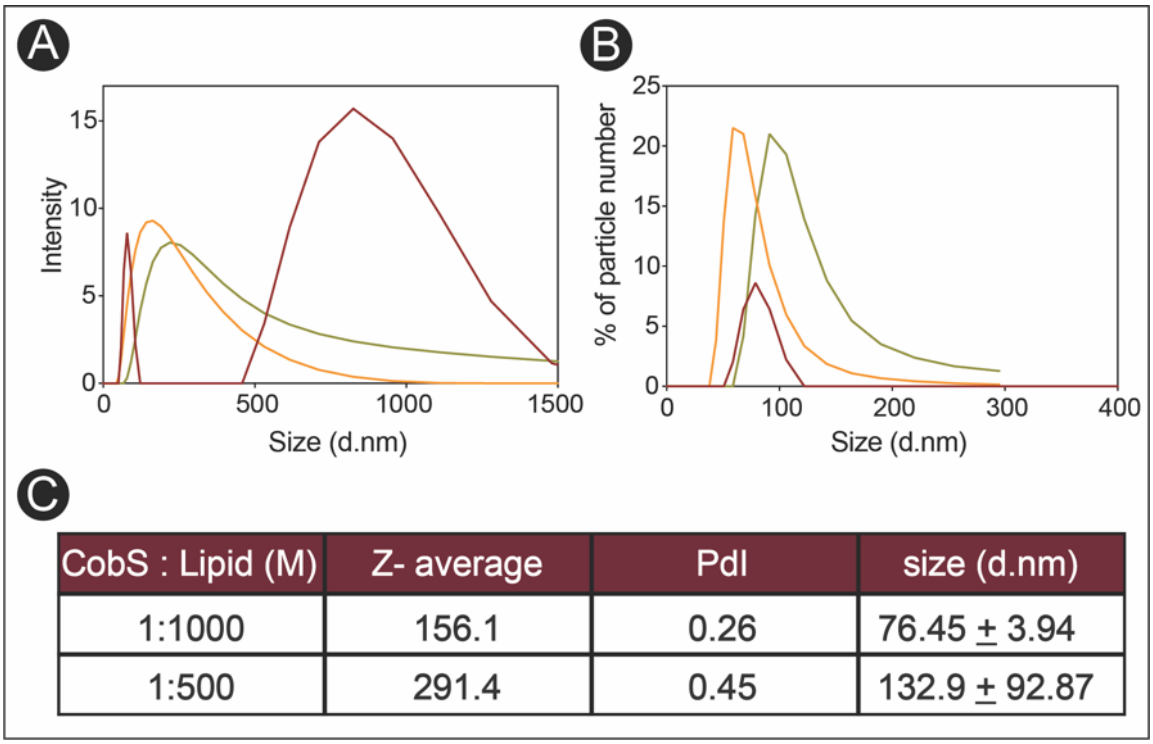

CobS : Lipid (M)	Z- average	PdI	size (d.nm)
1:1000	156.1	0.26	76.45 ± 3.94
1:500	291.4	0.45	132.9 ± 92.87

Figure 4.7. Characteristics of CobS proteoliposome populations. CobS proteoliposome populations were analyzed by dynamic light scattering using a Malvern Zetasizer. Intensity (panel A) and percent of particle number (panel B, C) measurements over a range of sizes (diameter; nm) are shown for CobS proteoliposomes (1:1000 lipid ratio, orange; 1:500 lipid ratio, green) and empty liposomes (red). Panel D displays the Z-average, polydispersity index (PdI) and average size (diameter in nanometers, (d, nm) of both CobS to lipid molar ratios tested.

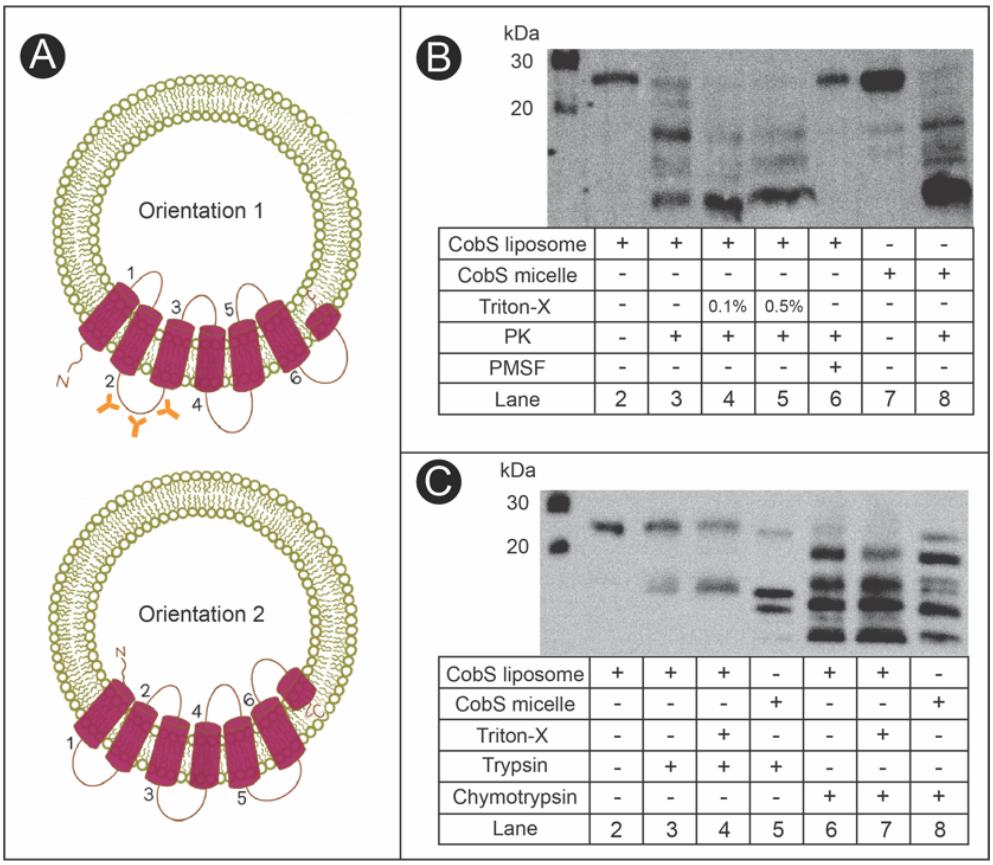

CobS liposome	+	+	+	+	+	-	-
CobS micelle	-	-	-	-	-	+	+
Triton-X	-	-	0.1%	0.5%	-	-	-
PK	-	+	+	+	+	-	+
PMSF	-	-	-	-	+	-	-
Lane	2	3	4	5	6	7	8

CobS liposome	+	+	+	-	+	+	-
CobS micelle	-	-	-	+	-	-	+
Triton-X	-	-	+	-	-	+	-
Trypsin	-	+	+	+	-	-	-
Chymotrypsin	-	-	-	-	+	+	+
Lane	2	3	4	5	6	7	8

Figure 4.8. Determination of CobS orientation in liposomes by proteolysis. A. Illustration of the two possible CobS orientations in the lipid bilayer of the liposome. Orientations 1, 2 illustrate the possible orientations of CobS once inserted into liposomes. α-CobS antibodies used in subsequent proteolysis experiments are shown in orange along the region of CobS used to elicit the aforementioned polyclonal rabbit antibodies, *i.e.,* cytoplasmic loop number two. B. Proteolytic cleavage of CobS proteoliposome population by proteinase K (PK). Protease inhibitor PMSF was used as a control. C. Proteolytic cleavage of CobS proteoliposome population by trypsin and chymotrypsin. Purified CobS was used as a control. Triton X-100 detergent was added at 0.1% or 0.5% (v/v) to disrupt the liposome and release CobS.

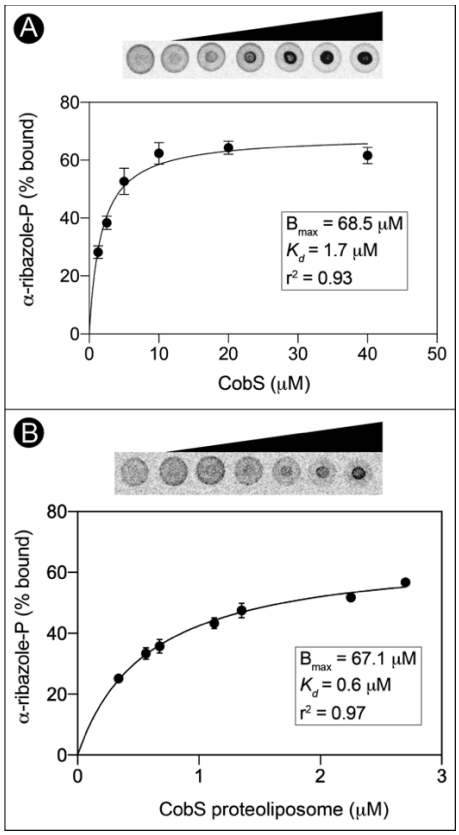

Figure 4.9. Determination of the K_d of CobS for α-RP in proteoliposomes. A. Increasing concentrations of purified CobS protein were incubated with [^{14}C]α-RP (4.2 μM). Reactions were spotted onto a nitrocellulose membrane and label distribution was visualized by phosphor imaging. Fraction of bound ligand was determined by differential radial capillary action of ligand assay (DRaCALA). Reactions were performed in biological and technical triplicate. Error bars represent standard error of the mean for technical triplicates. The dissociation constant (K_d) was determined by nonlinear regression (GraphPad Prism v8). B. Increasing concentrations of CobS-containing proteoliposomes were incubated with [^{14}C]α-RP (420 nM). Dissociation constant was determined as described above.

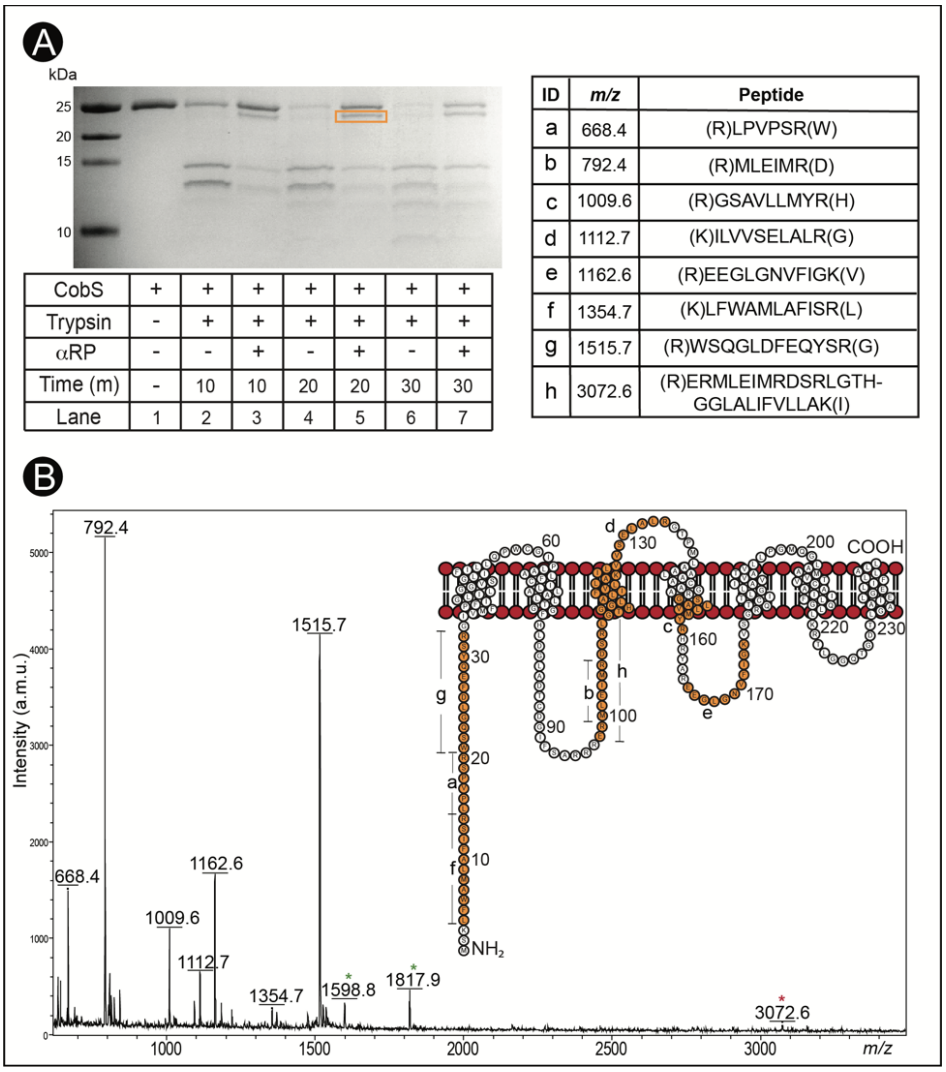

Figure 4.10. α-RP binding induces CobS conformational change. A. Tricine-SDS PAGE behavior of limited trypsin proteolysis of CobS and CobS preincubated with α -RP is shown. B. MALDI-TOF analysis of the ~24kDa peptide generated from limited trypsin proteolysis on CobS preincubated with α -RP. Peaks are labelled with the corresponding mass and identified peptide fragment. Green asterisks indicated peaks that were not assigned. Red asterisk indicates a modification to the peptide sequence. Orange residues in the CobS topology inset correspond to fragments identified by MALDI-TOF analysis.

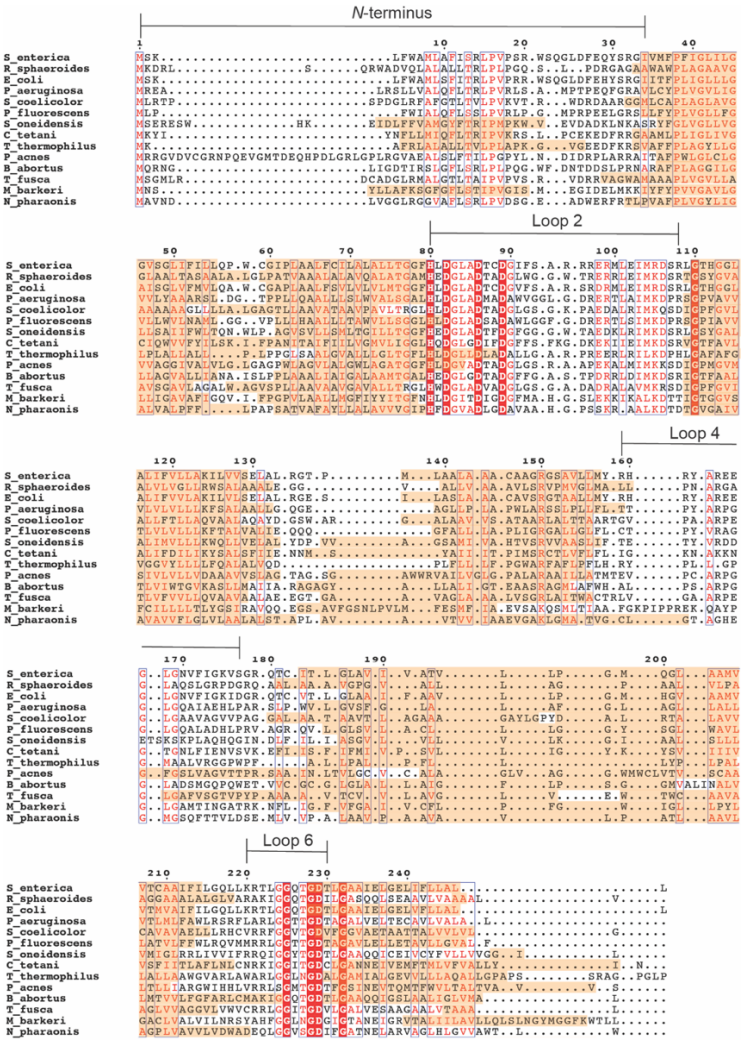

Figure 4.11. Conservation of membrane association among bacterial and archaeal cobamide synthases. The alignment was generated using T-COFFEE multiple sequence alignment server (PSI/TM-Coffee) and visualized with ESPript 3.0 web-based application. Transmembrane domains predicted by PSI/TM-COFFEE are highlighted with orange. Cytoplasmic loops *of S. enterica* CobS are labelled. Red highlight indicates amino acid residues conserved amongst all aligned organisms. Boxes indicate regions of high similarity.

Table 4.1. Growth behavior of *S. enterica* strains harboring plasmids encoding CobS variants							
Variant (plasmid)	Cbi (0.5nM)	Cbi (0.5nM) + DMB	Cbi (1nM)	Cbi (1nM) + DMB	Cbi (1.5nM)	Cbi (1.5nM) + DMB	Cbl (100 nM)
WT	0.3 ± 0.02 [7]	0.6 ± 0.01 [6]	0.8 ± 0.03 [6]	0.7 ± 0.01 [6]	0.8 ± 0.01 [6]	0.7 ± 0.01 [6]	0.8 ± 0.02 [6]
Vector (pBAD33)	NG	NG	NG	NG	NG	NG	0.8 ± 0.01[6]
Vector (pBAD24)	NG	NG	NG	NG	NG	NG	0.8 ± 0.03 [5]
CobS^{WT} (pCOBS69)	0.2 ± 0.03 [7]	0.6 ± 0.02 [6]	0.9 ± 0.05 [5]	0.7 ± 0.01 [5]	0.8 ± 0.01 [5]	0.7 ± 0.01 [5]	0.8 ± 0.03 [6]
CobS ^{WT} (pCOBS68)	0.2 ± 0.01 [7]	0.5 ± 0.03 [7]	0.8 ± 0.01 [7]	0.7 ± 0.01 [7]	0.8 ± 0.02 [7]	0.7 ± 0.01 [7]	0.8 ± 0.01 [7]
CobS^{H80A} (pCOBS71)	NG	0.6 ± 0.01 [6]	0.04 ± 0.01 [1]	0.7 ± 0.02 [6]	0.7 ± 0.2 [6]	0.8 ± 0.02 [7]	0.8 ± 0.02 [6]
CobS^{M104A} (pCOBS73)	NG	0.6 ± 0.01 [6]	NG	0.7 ± 0.02 [7]	0.8 ± 0.02 [6]	0.8 ± 0.01 [7]	0.7 ± 0.02 [6]
CobS^{D89A} (pCOBS78)	NG	NG	NG	NG	NG	NG	0.8 ± 0.03 [7]
CobS^{D86A} (pCOBS79)	NG	NG	NG	NG	NG	NG	0.8 ± 0.03 [7]
CobS^{G45E} (pCOBS82)	NG	NG	NG	NG	NG	NG	0.8 ± 0.02 [6]
CobS^{D229A} (pCOBS83)	NG	NG	NG	NG	NG	NG	0.8 ± 0.03 [7]
CobS^{G232A} (pCOBS84)	NG	0.5 ± 0.01 [8]	0.5 ± 0.2 [8]	0.7 ± 0.01 [8]	0.7 ± 0.05 [8]	0.7 ± 0.01 [8]	0.8 ± 0.03 [7]
CobS^{G225A} (pCOBS85)	0.1 ± 0.01 [9]	0.6 ± 0.02 [6]	0.7 ± 0.01 [7]	0.9 ± 0.01 [7]	0.7 ± 0.01 [6]	0.7 ± 0.01 [6]	0.8 ± 0.03 [7]
CobS^{D82A} (pCOBS89)	NG	NG	NG	NG	NG	NG	0.8 ± 0.03 [6]
CobS^{R159K} (pCOBS108)	0.2 ± 0.02 [6]	0.6 ± 0.01 [6]	1.0 ± 0.02 [6]	0.9 ± 0.03 [6]	1.0 ± 0.02 [5]	0.8 ± 0.01 [6]	0.8 ± 0.01 [6]
CobS^{R164K} (pCOBS106)	0.1 ± 0.01 [4]	0.7 ± 0.01 [6]	0.4 ± 0.03 [6]	0.8 ± 0.04 [6]	0.9 ± 0.03 [6]	0.8 ± 0.02 [6]	0.8 ± 0.04 [6]
CobS^{R108K} (pCOBS107)	0.1 ± 0.01 [4]	0.7 ± 0.01 [6]	0.7 ± 0.03 [6]	0.8 ± 0.03 [6]	0.9 ± 0.01 [6]	0.9 ± 0.02 [6]	0.9 ± 0.03 [6]
CobS^{R108E} (pCOBS109)	0.1 ± 0.01 [4]	0.7 ± 0.01 [6]	0.8 ± 0.04 [6]	0.8 ± 0.02 [6]	0.9 ± 0.01 [6]	0.8 ± 0.02 [6]	0.9 ± 0.03 [6]

CobS^{L168V} (pCOBS104)	0.1 ± 0.01 [1]	0.6 ± 0.01 [6]	0.7 ± 0.03 [7]	0.6 ± 0.01 [6]	0.7 ± 0.01 [6]	0.6 ± 0.02 [6]	0.7 ± 0.01 [6]
CobS^{R105K} (pCOBS105)	0.2 ± 0.01 [5]	0.6 ± 0.01 [6]	0.6 ± 0.04 [7]	0.5 ± 0.01 [7]	0.6 ± 0.01 [6]	0.5 ± 0.03 [7]	0.7 ± 0.02 [6]

All strains carried chromosomal *metE205* and *ara-9* mutations, which forced the cells to catalyze the last step of methionine synthesis (HCys-to-Met) via the cobamide-dependent methionine synthase (MetH) enzyme, and blocked arabinose catabolism, respectively. All strains were grown in NCE minimal medium supplemented with glycerol (22 mM) as the sole carbon and energy source. Growth rates (μ) are shown with the standard deviation of three replicates. The experiment was performed thrice. Lag times (h) are shown in brackets. Concentrations of added ring precursor or base are shown in parenthesis. NG, no growth; Cbi, dicyanocobinamide [$(CN)_2$Cbi]; DMB, 5,6-dimethylbenzimidazole; Cbl, cyanocobalamin (CNCbl, vitamin B_{12}). CobS variants encoded by *cobS* alleles cloned into pBAD33 are shown in blue font, and CobS variants encoded by *cobS* alleles cloned into pBAD24 are shown in red font.

SUPPLEMENTAL MATERIAL

MATERIALS AND METHODS

Bacterial strains, culture media, and chemicals. All chemicals were purchased from Sigma-Aldrich unless otherwise noted. Bacterial strains used in this study are listed in Table 4.2. All strains for growth analysis were derivatives of *Salmonella enterica enterica* sv Typhimurium LT2 (*S.* Typhimurium) or *Escherichia coli* C41 (λDE3). *S.* Typhimurium strains were grown at 37 °C on lysogeny broth (LB, Difco) (1, 2) or no-carbon essential (NCE) minimal medium (3) supplemented with glycerol (22 mM), $MgSO_4$ (1 mM), and Wolfe's trace minerals (4). When added to the medium, the precursor Cbi (added as $(CN)_2$Cbi), was at a concentration of 0.5, 1, and 1.5 nM, the DMB nucleobase was at a concentration of 150 μM, and Cbl (added as CNCbl) was at a concentration of 100 nM. *Escherichia coli* C41 (λDE3) (5) was used for protein overexpression and *E. coli* K12 strain DH5α (New England Biolabs) was used for plasmid construction. All *E. coli* strains were grown at 37°C in LB medium. Antibiotics for all media were used at the following concentrations: ampicillin, 100 μg mL^{-1}; chloramphenicol, 20 μg mL^{-1}.; isopropyl β-D-1-thiogalactopyranpside (IPTG, Gold BioTechnology), glycerol (Fisher), 4-(2-hydroxyethyl)-1-piperazineethanesulfonic acid buffer (HEPES, Gold BioTechnology) 3-[(3-Cholamidopropyl)dimethylammonio]-1-propanesulfonate detergent (CHAPS, Gold BioTechnology), 1-palmitoyl-2-oleoyl-glycero-3-phosphocholine (POPC, Avanti Polar Lipids), 1-palmitoyl-2-oleoyl-*sn*-glycero-3-phoshpo-L-serine (POPS, Avanti Polar Lipids), 1-palmitoyl-2-oleoyl-*sn*-glycero-3-phosphoethanolamine (POPE, Avanti Polar Lipids), Lissamine™ Rhodamine B 1,2-Dihexadecanoyl-*sn*-glycero-3-phosphoethanolamine (Rh-DHPE, Molecular Probes) (for chemical structures see Fig. 4.12), Oriole Fluorescent Gel Stain (Bio-Rad Laboratories).

Plasmid construction. Plasmids used in this study are listed in Table 4.2. Primers were synthesized by Integrated DNA Technologies, Inc. (IDT [Coralville, IA, United States]) and are listed in Table 4.3. Genes were amplified from *S. enterica* genomic DNA using Phusion DNA polymerase (ThermoFisher) as per manufacturer's instructions. Plasmids encoding CobS variants were amplified using PfuUltra II DNA (Agilent Technologies) polymerase as per manufacturer's instructions. Restriction enzymes were purchased from Fermentas.

General strategy used to construct plasmids encoding CobS variants of interest. Plasmid encoding CobS variants were constructed using primers shown in Table 4.3 and plasmid pCOBS68 DNA as the template. Briefly, the primers encoding a specific substitution change was used to amplify *cobS* on plasmid pCOBS68 or pCOBS69. Amplified products were digested with DpnI overnight at 37°C. The amplification product was then transformed in *E. coli* DH5α cells, and its nucleotide sequence was verified by Sanger sequencing. Using this strategy, we generated *cobS* alleles encoding variants $CobS^{G45E}$, $CobS^{H80A}$, $CobS^{D82A}$, $CobS^{D86A}$, $CobS^{D89A}$, $CobS^{M104A}$, $CobS^{G225A}$, $CobS^{D229A}$, $CobS^{G232A}$ from pCOBS68 and variants $CobS^{L168V}$, $CobS^{R105K}$, $CobS^{R108K}$, $CobS^{R108E}$, $CobSR^{159K}$, $CobS^{R164K}$ from pCOBS69. Plasmids encoding these variants are described in Table S1.

Strain construction and growth analysis. In-frame deletions of *S. enterica* genes were constructed using the phage lambda Red recombinase system as described (6). Plasmids were transformed into strains for complementation studies as described elsewhere (7). For growth analyses, 2-mL starter cultures in 13 x 100 mm borosilicate cultures tubes were

grown 16 h at 37 °C with shaking at 180 rpm in LB containing appropriate antibiotic. Growth experiments were performed in 96-well microtiter dishes (Falcon), with each well containing 198 μl of medium plus 2 μl of inoculum. In some cases, the inoculum size was varied. The growth behavior of three technical replicates of each strain was analyzed, and the experiment was performed thrice. Table 1 reports representative growth rates with standard deviations of technical triplicates. Growth was monitored using a computer-controlled plate reader (BioTek, Model Eon). The optical density at 630 nm was measured every 30 min for a total time of 24 h; the microtiter dish was shaken between measurements. Data were analyzed using GraphPad Prism version 8. Growth rate and lag were calculated using the Gompertz curve fitting model [Source code (https://github.com/scott-saunders/growth_curve_fitting/blob/master/growth_curve_fitting_ver0.2.Rmd)]. Figure legends indicate whether or not the inoculum used was greater than 1% (v/v). L-(+)-Arabinose was used as inducer when indicated.

Protein overproduction and purification. CobS overproduction and purification were based on methods described elsewhere (8) with modifications. $CobS^{WT}$ protein was overproduced from plasmid pCOBS5 in strain JE6663 [(*E. coli* C41 (λDE3)] in 2-L cultures of Terrific Broth (9). Protein synthesis was induced by the addition of IPTG at a final concentration of 500 μM in mid-log phase cultures (OD_{600} ~ 0.6) growing at 37 °C while shaking at 180 rpm in an Innova44 gyratory incubator (New Brunswick Scientific). After induction, cultures were grown for 3 h at 37 °C while shaking at 180 rpm. Cultures were harvested by centrifugation at 4 °C for 15 min at 6,000 x *g* in an Avanti J20-XPI refrigerated centrifuge equipped with a JLA-8.1000 rotor. Pelleted cells were stored at −20 °C until used. For protein purification, cell pellets were thawed and resuspended in 30 ml of Tris-

HCl buffer (100 mM, pH 7.9 @ 24°C). Cells were lysed with a cell press in a cell disruptor (Constant Systems) set at 1.72 × 10^5 kPa. A sample (0.5 mL) of a protease inhibitor cocktail (Sigma) was added to cell-free extracts (CFEs) to minimize CobS degradation during purification. CFEs were obtained after centrifugation at 4°C, at 5,000 x *g* for 15 min. Cell membranes were obtained from a high-speed centrifugation at 75,000 x *g* for 90 min in an Avanti J-25I Beckman/Coulter refrigerated centrifuge equipped with a JA-25.50 rotor. Membranes were resuspended in 10 ml of Tris-HCl buffer (0.1 M, pH 7.9 @ 24°C) with a glass homogenizer and were solubilized by the addition of CHAPS detergent to a final concentration of 20 mM. The detergent-containing CFE was incubated on ice for 1 h and centrifuged at 4°C at 75,000 x *g* for 30 min to remove solubilized contaminants. The insoluble fraction containing CobS was resuspended in 10 ml of Tris-HCl buffer (0.1 M, pH 7.9 @ 24°C) containing NaCl (0.5 M) and imidazole (20 mM) with a glass homogenizer and solubilized by the addition of 1,2- diheptanoyl-*sn*-glycero-3-phosphocholine (DHPC) to a final concentration of 15 mM. DHPC was added slowly to avoid denaturation of proteins. The CFE fraction containing detergent-solubilized CobS was incubated on ice for 1 h and centrifuged at 4°C at 75,000 x *g* for 30 min. A HisPur nickel-nitrilotriacetic acid (Ni-NTA) resin (2-mL bed volume, Thermo Scientific) was equilibrated with 10 bed volumes of water and 10 bed volumes of Tris-HCl buffer (100 mM, pH 7.9 @ 24°C) containing NaCl (0.5 M) and imidazole (20 mM). CFE containing solubilized CobS protein was incubated with the HisPur resin at 4 ºC with nutation for a minimum of 2 h before pouring the slurry into a column (Kontes FLEX-COLUMN 1.0 x 10cm). The column was washed with five bed volumes of Tris-HCl buffer (0.1 M, pH 7.9 @ 24°C) containing NaCl (0.5 M) and imidazole (20 mM) and DHPC (15 mM) then five bed volumes of Tris-HCl buffer (0.1 M, pH 7.9 @ 24°C) containing NaCl (0.5 M) and imidazole (60 mM) and DHPC (15 mM). Proteins were eluted with five bed volumes of Tris-HCl buffer (0.1 M, pH 7.9 @ 24°C) containing NaCl (0.5 M) and imidazole (0.5 M) and DHPC (15 mM). Proteins in

fractions of interest were resolved by sodium dodecyl sulfate polyacrylamide gel electrophoresis (SDS-PAGE) (10) and CobS-containing fractions were applied to a 5-mL Zeba Spin desalting column (ThermoFisher) to remove imidazole. Glycerol (10% [v/v], final concentration) was added to a desalted CobS sample, which was flash frozen in liquid N_2 prior to storage at -80 °C. The final buffer composition before storage was Tris-HCl buffer (0.1 M, pH 7.9 @ 24°C) containing NaCl (150 mM) and DHPC (15 mM). Protein concentration was determined using a Bradford Assay kit (Bio-Rad Laboratories). A typical CobS preparation yielded 0.5 mg of protein /g of cells.

Liposome preparation and protein reconstitution. The lipids used in the study were POPC, POPE, POPS and Rh-DHPE. Proteoliposomes were prepared using detergent-mediated reconstitution as described elsewhere (11). POPC:POPS:POPE:Rh-DHPE were combined at a molar ratio of 80:10:9.5:0.5 to yield 1 μmol lipid. Lipids were dried under a stream of N_2 gas and spun in an Eppendorf VacFuge at 30 ºC for 1 h. The dried lipid film was hydrated in 500 μl of HEPES buffer (20 mM, pH 7.4) containing NaCl (0.5 M), CHAPS (40 mM) and glycerol (10% [v/v]) to a final lipid concentration of 2 mM. Detergent-solubilized $CobS^{WT}$ was added at a lipid-to-protein molar ratio of 1000:1 and incubated with rotation on a Benchmark RotoBot at 4 °C for 1 h. Detergent removal and proteoliposome formation was achieved by four 20-h dialyses using Slide-A-Lyzer dialysis cassettes (20-kDa molecular mass cutoff) against HEPES buffer (20 mM, pH 7.4) containing NaCl (0.5 M) and glycerol (10% [v/v]). Dialysis was performed at a dialysate:sample volumetric ratio of 2000:1. After dialysis, the proteoliposome suspension was applied to a Histodenz (Sigma) gradient to perform a liposome flotation assay. The proteoliposome suspension was mixed with an equal volume with HEPES buffer (20 mM, pH 7.4) containing NaCl (0.15 M), Histodenz (80% [w/v]), glycerol (10% [v/v]) and

deposited in a Beckman Coulter Ultracentrifuge tube (polyallomer, 13 x 51 mm). A 4-mL overlay of HEPES (20 mM, pH 7.4) containing NaCl (0.15 M), Histodenz (30% [w/v]), glycerol (10% [v/v]) was applied followed by a 200-μL overlay of HEPES buffer (20 mM, pH 7.4) containing NaCl (0.15 M), glycerol (10% [v/v]). The gradient was subjected to centrifugation at 4 °C for 3 h at 268,000 x *g* in a refrigerated Beckman Coulter Optima™ MAX-XP Ultracentrifuge using an MLS-50 rotor. The size distribution of reconstituted liposomes was determined by dynamic light scattering in a 1.5-mL polystyrene cuvette using a Zetasizer Nano (Malvern Instruments). Lipid concentration of the reconstituted liposomes was determined by a standard curve generated from fluorescence of Rh-DHPE. Fluorescence measurements were read on a BioTek Gemini instrument set at an excitation wavelength of 540 nm and emission wavelength of 586 nm. Protein concentration in proteoliposomes was determined by generating a standard curve. Briefly, a range of known bovine γ-globulin (BGG) and lysozyme concentrations were separated by SDS-PAGE with unknown concentrations of CobS-containing proteoliposomes stained with Oriole Fluorescent stain and analyzed using TotalLab TL100 software. The presence of CobS in liposomes was confirmed by western blot and mass spectrometry analyses.

Mass spectrometry. Confirmation of protein identity was performed by the Proteomics and Mass Spectrometry (PAMS) core facility at the University of Georgia. Briefly, protein or liposome preparations were separated using SDS-PAGE. Bands of interest were excised and subjected to digest by trypsin and analyzed by MALDI-TOF mass spectrometry. Mass spectrometry results were compared to information in the MASCOT database (http://www.matrixscience.com/) to determine protein identity.

Proteolytic digest of CobS-containing proteoliposomes. To determine protein orientation in the lipid bilayer of the liposome, proteolytic digests were performed using proteinase K (Fisher), trypsin and chymotrypsin (Sigma). Reaction mixtures in HEPES buffer (20 mM, pH 7.4) containing NaCl (0.15 M), glycerol (10% [v/v]), 5 μL CobS-containing proteoliposomes and 1 μg protease were incubated for 1 h at 37 °C. Cobamide synthase reactions were stopped by the addition of Tris-HCl buffer (63 mM, pH 6.8) containing SDS (2% w/v), glycerol (10%, v/v), 2-mercaptoethanol (100 mM), and bromophenol blue (0.001%, w/v), followed by incubation at 90 °C for 5 min. Peptides were separated by SDS-PAGE electrophoresis and subsequently analyzed by western blot (12) with α-CobS rabbit polyclonal antibodies (Envigo, IN). Purified $CobS^{WT}$ protein was used as positive control.

Western blot analysis. To confirm the presence of CobS in liposomes and to analyze proteolytic digests, western blots were performed using rabbit polyclonal antibodies generated against a synthetic peptide of cytoplasmic loop 2 (hereafter α-CobS) (13). Liposomes harvested from the floatation assay previously described or proteolytic digests were resolved by SDS-PAGE and subsequently transferred to a polyvinylidene fluoride (PVDF) membrane (Millipore). The transfer was performed using a Trans-Blot Turbo system (Bio-Rad Laboratories) set to StandardSD mini gel (1.0 A, 25 V, 30 min) using Tris-HCl transfer buffer (25 mM, pH 8) containing glycine (192 mM) and methanol (10% v/v)]. Membranes were incubated for 30 min in blocking buffer of phosphate buffered saline containing Tween 20 (PBST) comprised of NaH_2PO_4 (10 mM, pH 7.2), NaCl (0.9% w/v), Tween 20 (0.1% v/v), and instant dry milk (5%, w/v). Membranes were probed with α-CobS antibodies (1:5,000 in blocking buffer) for 1 h, then washed thrice (30 min each) with PBST. Membranes were then probed for 1 h with horseradish peroxidase (HRP)-

conjugated goat α-rabbit secondary antibodies (Sigma) in PBST (1:10,000) before three, 30-min washes with PBST. Membranes were incubated in SuperSignal West Pico PLUS chemiluminescent substrate (ThermoFisher) for 2 min and imaged using a UVP ChemStudio imaging instrument (AnalytikJena). Purified $CobS^{WT}$ protein was used as positive control and SuperSignal Molecular Weight Protein Ladder (ThermoFisher) was used as reference for the electrophoretic behavior of molecules of known molecular masses.

Binding kinetics. Binding kinetics of α–RP to $CobS^{WT}$ was determined using the Differential Radial Capillary Action of Ligand Assay (DRaCALA) method described elsewhere (14). Briefly, 20-μL reaction mixtures containing varying concentrations of $CobS^{WT}$ protein or $CobS^{WT}$-containing liposomes were incubated with radiolabeled α–RP (4.2 μM and 420 nM respectively) in PBS. Two μL from each reaction mixture was spotted on a nitrocellulose membrane and allowed to dry for 2 h before exposing to a phosphor screen for 16-48 h. The distribution of radioactivity on the nitrocellulose membrane was visualized using an Amersham Typhoon 5 (GE Life Sciences) with ImageQuant TL 8.1. The pixel density was analyzed using one-dimensional array analysis in TotalLab TL100 (Nonlinear Dynamics), and the resulting data were analyzed using Prism version 8 (GraphPad). Each reaction was performed in triplicate. The dissociation constant (K_d) was determined using one-site-binding (hyperbola) nonlinear regression in Prism version 8 (GraphPad).

Limited trypsin proteolysis. An α-RP- induced conformational change of CobS was determined by limited trypsin proteolysis. The assay was performed based on the protocol outlined elsewhere (15) with modifications. Twenty-μL reactions were performed in Tris-

HCl buffer (0.1 M, pH 7.9 @ 24°C) containing NaCl (0.15 M) and DHPC (15 mM) using diphenylcarbamyl chloride-treated trypsin. When provided, substrates were at a final concentration of 50 μM and pre-incubated for 10 min prior to digestion by trypsin. Protein composition of the reaction mixture was analyzed by tricine-SDS PAGE using a 16% gel (16). Peptide fragments were excised from the gel and in-gel tryptic digest followed by MALDI-TOF mass spectrometry analysis was performed by the PAMS facility at the University of Georgia. The MASCOT database was used to analyze peptide fingerprint data.

AdoCbi-GDP and α-RP substrate preparation. The two substrates of CobS, namely AdoCbi-GDP and α-RP were not commercially available and were synthesized as described elsewhere (8, 17). Briefly, dicyanocobinamide [$(CN)_2$Cbi] was incubated with ATP and homogeneous ATP:Co(I)rrinoid adenosyltransferase CobA protein purified as described (18). The reaction mixture was incubated for 16 h at 37 °C under dark, anoxic conditions. The product of the reaction, adenosylcobinamide (AdoCbi) was separated from other reaction components using a Waters Sep-Pak C18 column. AdoCbi was eluted off the column with 100% methanol. Methanol was removed using an Eppendorf VacFuge for 16 h. Dried AdoCbi was resuspended in a reaction mixture containing GTP and homogeneous NTP:$(HO)_2$Cbi kinase, GTP:AdoCbi guanylyltransferase CobU enzyme purified as described elsewhere (19) and incubated at 37 °C for 16 h in the dark to yield AdoCbi-GDP. AdoCbi-GDP was separated from reaction components using a Waters Sep-Pak C18 column, and AdoCbi was eluted off the column with 100% methanol. Methanol was removed using an Eppendorf VacFuge for 16 h. AdoCbi-GDP was resuspended in water and its identity confirmed by its UV-visible spectrum. AdoCbi-GDP

was quantified by reading the absorbance at 367 nm after incubation with KCN at 90 °C for 10 min.

α–RP was synthesized as described elsewhere (7). Briefly, DMB was incubated with NaMN and homogeneous NaMN:DMB phosphoribosyltransferase CobT enzyme (20) 16 h at 37°C. α–RP was separated from reaction components by HPLC as described (21). Fractions containing α–RP were pooled, applied to a Waters Sep-Pak C18 column and eluted with 100 % methanol. Methanol was removed by 16h vacuum centrifugation using an Eppendorf VacFuge, and α–RP was quantified by reading absorbance at 280 nm.

Determination of the molar absorptivity of AdoCbi-GDP. The molar absorptivity of AdoCbi-GDP was determined by monitoring absorbance at 459 nm across a range of concentrations. A linear regression was generated from absorbance as a function of AdoCbi-GDP concentration using GraphPad Prism v8 software (Fig. S2). The molar absorptivity at 459 nm was determined to be 3352 M^{-1} cm^{-1}.

***In vitro* cobamide synthase assay**. A continuous *in vitro* activity assay of cobamide synthase activity was implemented by modifying conditions described elsewhere (8). To determine the specific activity of purified CobS protein and CobS-containing liposomes, the decrease in absorbance of AdoCbi-GDP was monitored at 459 nm for 5 min in a 96-well quartz microtiter plate using a SpectraMax Plus UV-visible spectrophotometer (Molecular Devices). CobS activity was calculated using the calculated AdoCbi-GDP molar absorptivity (ε_{459} = 3352 M^{-1} cm^{-1}) using Beer-Lambert's Law equation, $A = \varepsilon cl$. Data presented here represent technical triplicates of one experiment, which was repeated thrice.

HPLC analysis of reaction products. KCN was added to reaction mixtures to a final concentration of 2.4 μM, and the samples were incubated for 10 min at 90 ºC. Cyanated corrinoids were applied to a SpinX column (Costar, 0.45 μM cellulose acetate), eluted with methanol and diluted 10 fold in a 1:4 ratio of buffer B [KH_2PO_4 (0.1 M, pH 8) containing KCN (10 mM) and acetonitrile (50%, v/v)] to buffer C [KH_2PO_4 (0.1 M, pH 6.5) containing KCN (10 mM) in preparation for separation by HPLC. Cobamide 5'-P synthase reaction products were resolved by RP-HPLC using a Shimadzu Prominence UFLC SPD-M30A instrument equipped with a Phenomenex Synergi 4μ hydroRP80A 150 mm x 4.6 mm LC column as described (22, 23) with modifications as outlined elsewhere (24). Authentic CNCbl 5'-P was used HPLC as positive control. CNCbas were detected at 367 and 525 nm and eluted at 19 minutes

Table 4.2 Strains and plasmids used in this study		
***Salmonella*[1] Strains**	**Genotype**	**Reference or Source[2]**
TR6583	*metE205 ara-9*	K. Sanderson via J. Roth
Derivatives of strain TR6583		
JE22070	/ pCV1	Laboratory collection
JE15792	/ pBAD33	Laboratory collection
JE8248	Δ*cobS1313*	Laboratory collection
JE15888	Δ*cobS1313* / pCOBS69	
JE15762	Δ*cobS1313* / pCOBS68	
JE15800	Δ*cobS1313* / pCOBS71	
JE15802	Δ*cobS1313* / pCOBS73	
JE15937	Δ*cobS1313* / pCOBS79	
JE16281	Δ*cobS1313* / pCOBS82	
JE16282	Δ*cobS1313* / pCOBS83	
JE16283	Δ*cobS1313* / pCOBS84	
JE16284	Δ*cobS1313* / pCOBS85	
JE16523	Δ*cobS1313* / pCOBS89	
JE25590	Δ*cobS1313* / pCOBS104	
JE25591	Δ*cobS1313* / pCOBS105	
JE25592	Δ*cobS1313* / pCOBS106	
JE25593	Δ*cobS1313* / pCOBS107	
JE25594	Δ*cobS1313* / pCOBS108	
JE25595	Δ*cobS1313* / pCOBS109	
JE25839	Δ*cobS1313* / pCOBS78	

JE7088	Δ*metE2702 ara-9*	Laboratory collection
Derivatives of strain JE7088		
JE11685	/ pBAD24	Laboratory collection
JE22263	/ pCV1	Laboratory collection
Escherichia coli strains		
JE6663 C41(λDE3)	F – *ompT hsdSB (rB- mB-) gal dcm* (λDE3)	Avidis
Plasmid	**Genotype**	**Reference or Source**
pET-15b	*bla*$^+$ pBR322 origin of replication; cloning vector for the expression of protein with an *N*-terminal His-tag	Novagen
pTEV5	Overexpression vector that fuses the *N* terminus of the protein of interest to a H_6 tag, which can be removed by rTEV protease, *bla*$^+$	(25)
pBAD24	complementation vector, P_{araBAD}, *bla*$^+$	(26)
pBAD33	complementation vector, P_{araBAD}, *cat*$^+$	(26)
pCOBS68	*S.* Typhimurium *cobS*$^+$ pBAD33-SD1	
pCOBS69	*S.* Typhimurium *cobS*$^+$ pBAD24	
pCOBS71	*S.* Typhimurium *cobS1452* cloned into vector pBAD33-SD1; Encodes variant $CobS^{H80A}$	
pCOBS73	*S.* Typhimurium *cobS1459* cloned into vector pBAD33-SD1; Encodes variant $CobS^{M104A}$	
pCOBS78	*S.* Typhimurium *cobS1456* cloned into vector pBAD33-SD1; Encodes variant $CobS^{D89A}$	
pCOBS79	*S.* Typhimurium *cobS1455* cloned to vector pBAD33-SD1; Encodes variant $CobS^{D86A}$	
pCOBS82	*S.* Typhimurium *cobS1464* cloned into vector pBAD33-SD1; Encodes variant $CobS^{G45E}$	
pCOBS83	*S.* Typhimurium *cobS1461* cloned into vector pBAD33-SD1; Encodes variant $CobS^{D229A}$	

pCOBS84	*S.* Typhimurium *cobS1462* cloned into vector pBAD33-SD1; Encodes variant CobS^{G232A}	
pCOBS85	*S.* Typhimurium *cobS1460* cloned into vector pBAD33-SD1; Encodes variant CobS^{G225A}	
pCOBS89	*S.* Typhimurium *cobS1453* cloned into vector pBAD33-SD1; Encodes variant CobS^{D82A}	
pCOBS104	*S.* Typhimurium *cobS1472* cloned into vector pBAD24; Encodes variant CobS^{L168V}	
pCOBS105	*S.* Typhimurium *cobS1473* cloned into vector pBAD24; Encodes variant CobS^{R105K}	
pCOBS106	*S.* Typhimurium *cobS1474* cloned into vector pBAD24; Encodes variant CobS^{R164K}	
pCOBS107	*S.* Typhimurium *cobS1475* cloned into vector pBAD24; Encodes variant CobS^{R108K}	
pCOBS108	*S.* Typhimurium *cobS1476* cloned into vector pBAD24; Encodes variant CobS^{R159K}	
pCOBS109	*S.* Typhimurium *cobS1477* cloned into vector pBAD24; Encodes variant CobS^{R108E}	
pCOBS5	*S.* Typhimurium *cobS*$^{+}$ cloned into vector pET-15b	(17)

[1]All *Salmonella* strains were derivatives of *Salmonella enterica enterica* serovar Typhimurium LT2.

[2]Strains used were constructed during the course of this work, unless otherwise indicated.

Table 4.3 Primers[1] used in this work.	
Primer Name	**Primer Sequence (5'-3')**
cobS_G45E	GGGTTGATTCTGGAGGGCGTAAGCGGC
cobS_H80A	GCCCATCCAGGGCAAAACCACCGGTCAGCAGCG
cobS_D86A	GATGGGCTGGCCGCTACCTGCGATGGC
cobS_D89A	TGGCCGATACCTGCGCTGGCATTTTTTCCGC
cobS_M104A	GCCGTGAGCGAATGCTGGAGATTGCGCGTGATAGTCG
cobS_D82A	GTGGTTTTCACCTGGCTGGGCTGGCCGATAC
cobS_D229A	GTCAAACCGGCGCTACGCTGGGCGC
cobS_G232A	CGATACGCTGGCCGCGGCGATCG
cobS_G225A	CGTACGCTTGGCGCTCAAACCGGCGAT
cobS_L168V 1	CGCCCGTGAAGAGGGGGTCGGCAATGTATTTATC
cobS_L168V 2	GATAAATACATTGCCGACCCCCTCTTCACGGGCG
cobS_R159K 1	CCGTTTTATTGATGTACAAGCATCGCTACGCCCGTG
cobS_R159K 2	CACGGGCGTAGCGATGCTTGTACATCAATAAAACGG
cobS_R164K 1	CGTCATCGCTACGCCAAAGAAGAGGGGCTTGG
cobS_R164K 2	CCAAGCCCCTCTTCTTTGGCGTAGCGATGACG
cobS_R105K 1	CGAATGCTGGAGATTATGAAGGATAGTCGTCTGGGAAC
cobS_R105K 2	GTTCCCAGACGACTATCCTTCATAATCTCCAGCATTCG
cobS_R105E 1	GAATGCTGGAGATTATGGAGGATAGTCGTCTGGGAAC
cobS_R105E 2	GTTCCCAGACGACTATCCTCCATAATCTCCAGCATTC
cobS_R108K 1	CGAATGCTGGAGATTATGAAGGATAGTCGTCTGGGAAC
cobS_R108K 2	GTTCCCAGACGACTATCCTTCATAATCTCCAGCATTCG

[1]All primers were purchased from IDT, Coralville, IA.

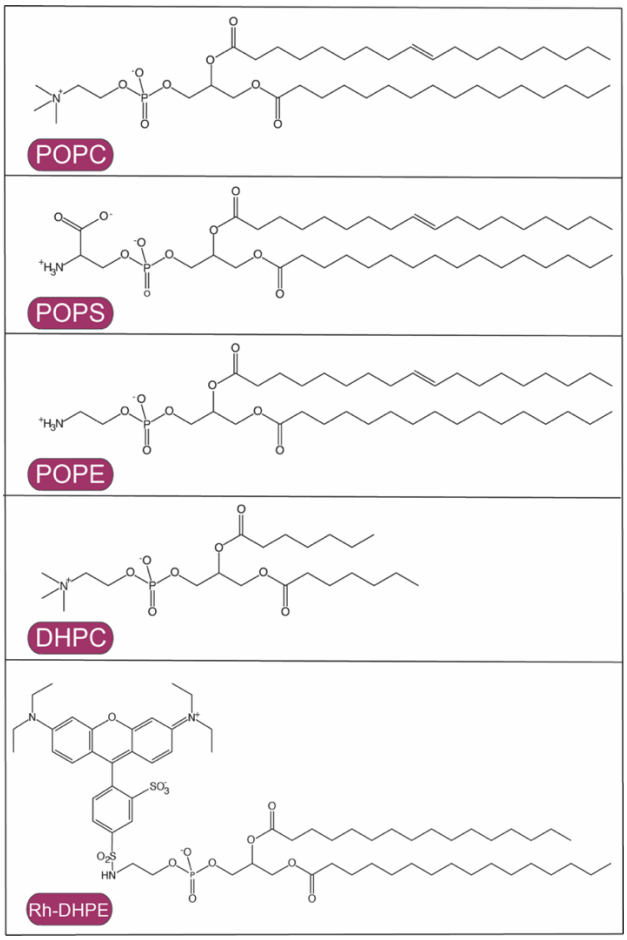

Fig. 4.12. Chemical structures of lipids used in this study. The structures of lipids used for liposome formation and CobS solubilization are shown. POPC (1-palmitoyl-2-oleoyl-glycero-3-phosphocholine), POPE (1-palmitoyl-2-oleoyl-*sn*-glycero-3-phosphoethanolamine), POPS (1-palmitoyl-2-oleoyl-*sn*-glycero-3-phoshpo-L-serine) and Rh-DHPE (Lissamine™ Rhodamine B 1,2-Dihexadecanoyl-*sn*-glycero-3-phosphoethanolamine) were used to generate liposomes. DHPC (1,2-diheptanoyl-*sn*-glycero-phosphocholine) was used to solubilize CobS during the purification process. Structures were generated using ChemDraw v19.0

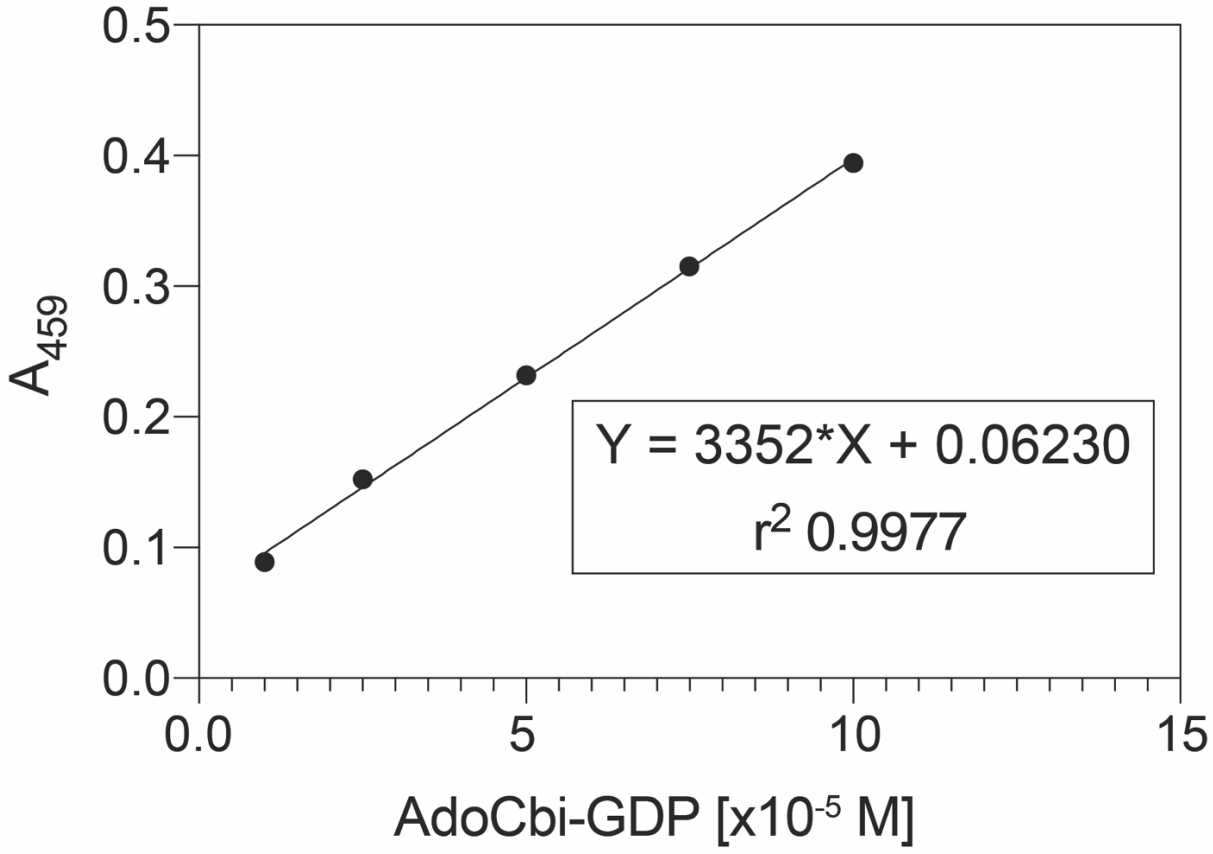

Fig. 4.13. Adenosylcobinamlde-GDP (AdoCbi-GDP) molar absorptivity. The figure shows the increase in the absorbance at 459 as a function of adenosylcobinamide-GDP (AdoCbi-GDP) concentration. Linear regression was performed using Prism v8 (GraphPad) to determine the molar absorptivity.

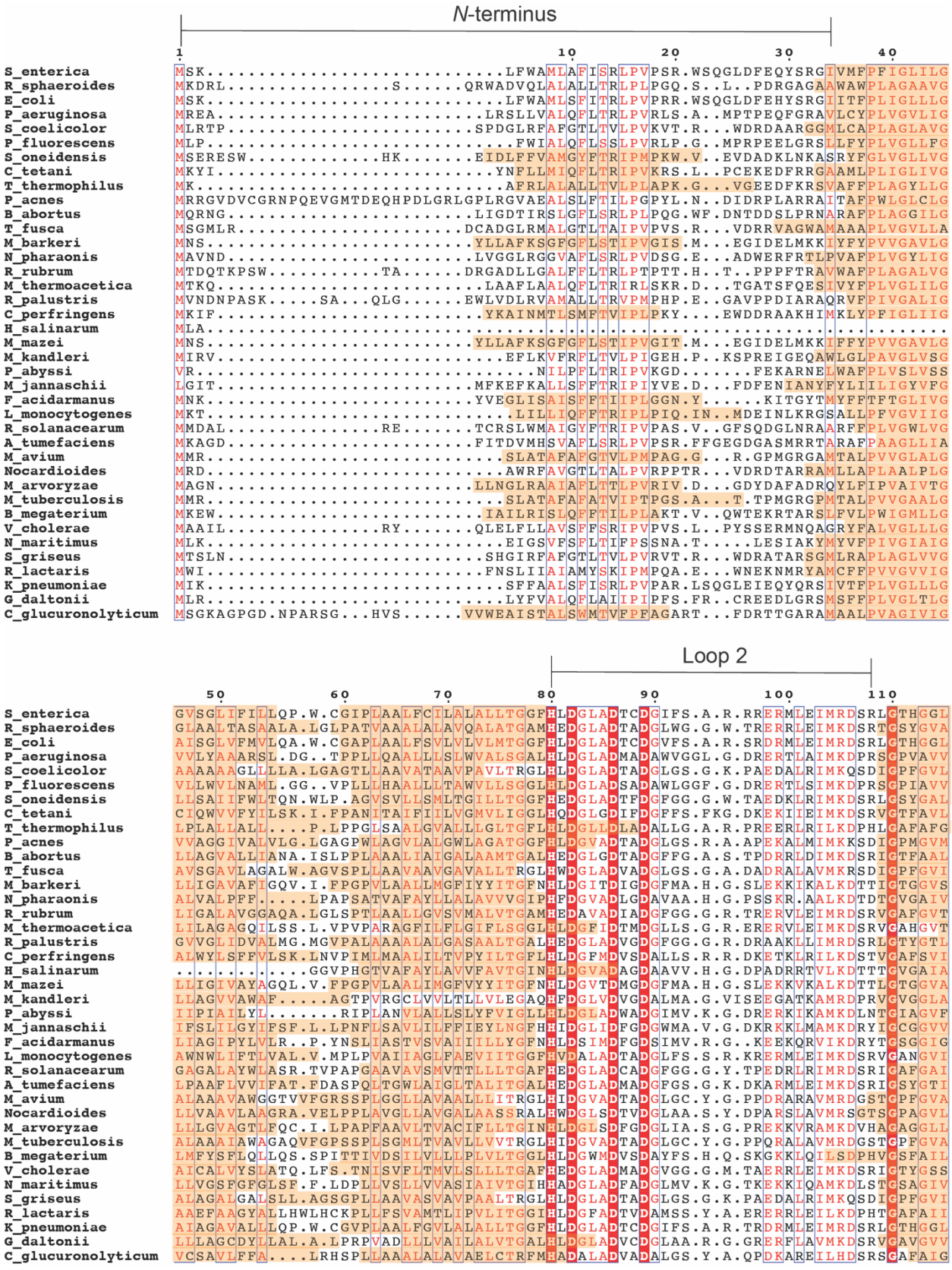
N-terminus
Loop 2
S_enterica
R_sphaeroides
E_coli
P_aeruginosa
S_coelicolor
P_fluorescens
S_oneidensis
C_tetani
T_thermophilus
P_acnes
B_abortus
T_fusca
M_barkeri
N_pharaonis
R_rubrum
M_thermoacetica
R_palustris
C_perfringens
H_salinarum
M_mazei
M_kandleri
P_abyssi
M_jannaschii
F_acidarmanus
L_monocytogenes
R_solanacearum
A_tumefaciens
M_avium
Nocardioides
M_arvoryzae
M_tuberculosis
B_megaterium
V_cholerae
N_maritimus
S_griseus
R_lactaris
K_pneumoniae
G_daltonii
C_glucuronolyticum

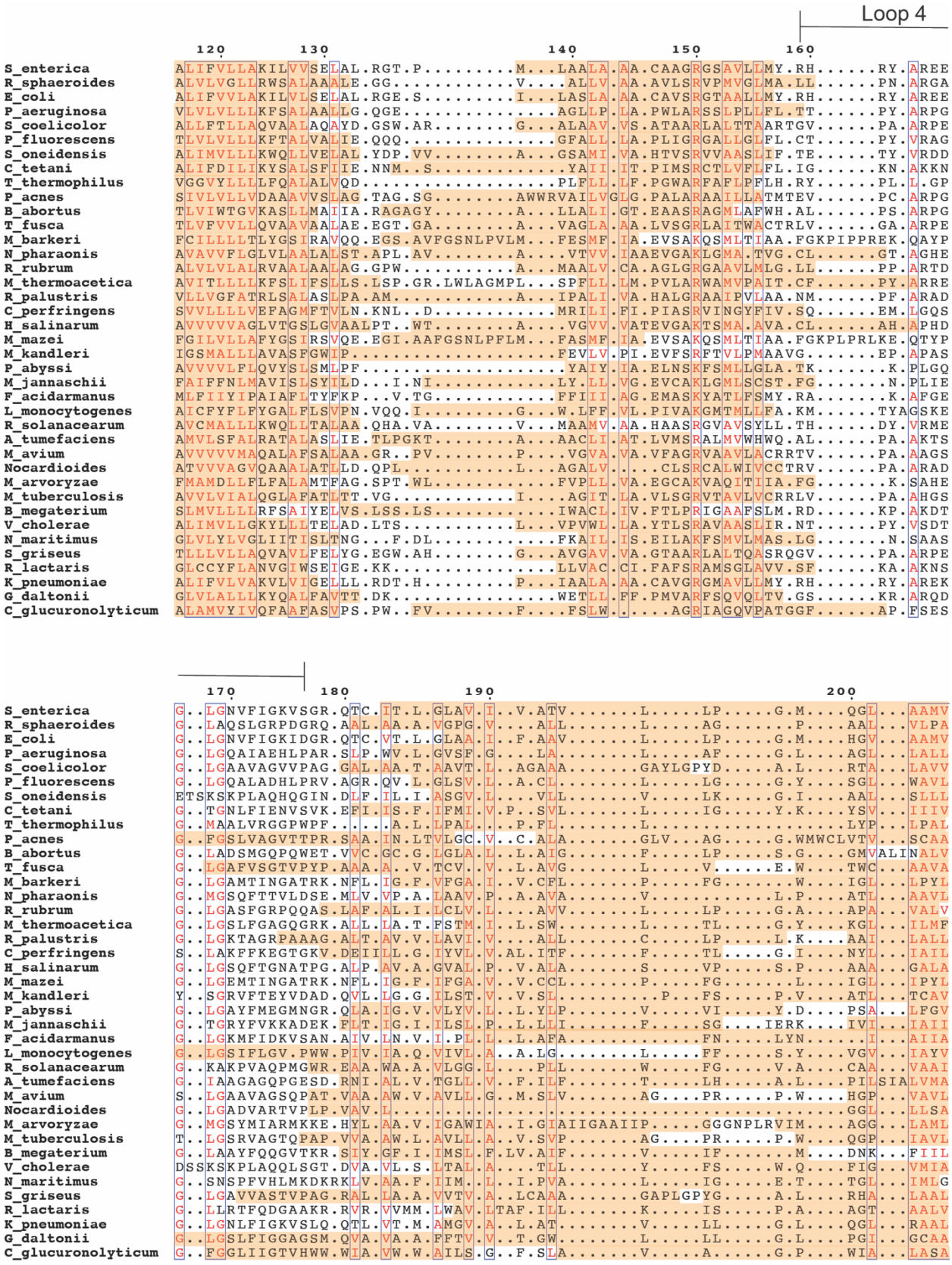
Loop 4
120
130
140
150
160
170
180
190
200
S_enterica
R_sphaeroides
E_coli
P_aeruginosa
S_coelicolor
P_fluorescens
S_oneidensis
C_tetani
T_thermophilus
P_acnes
B_abortus
T_fusca
M_barkeri
N_pharaonis
R_rubrum
M_thermoacetica
R_palustris
C_perfringens
H_salinarum
M_mazei
M_kandleri
P_abyssi
M_jannaschii
F_acidarmanus
L_monocytogenes
R_solanacearum
A_tumefaciens
M_avium
Nocardioides
M_arvoryzae
M_tuberculosis
B_megaterium
V_cholerae
N_maritimus
S_griseus
R_lactaris
K_pneumoniae
G_daltonii
C_glucuronolyticum

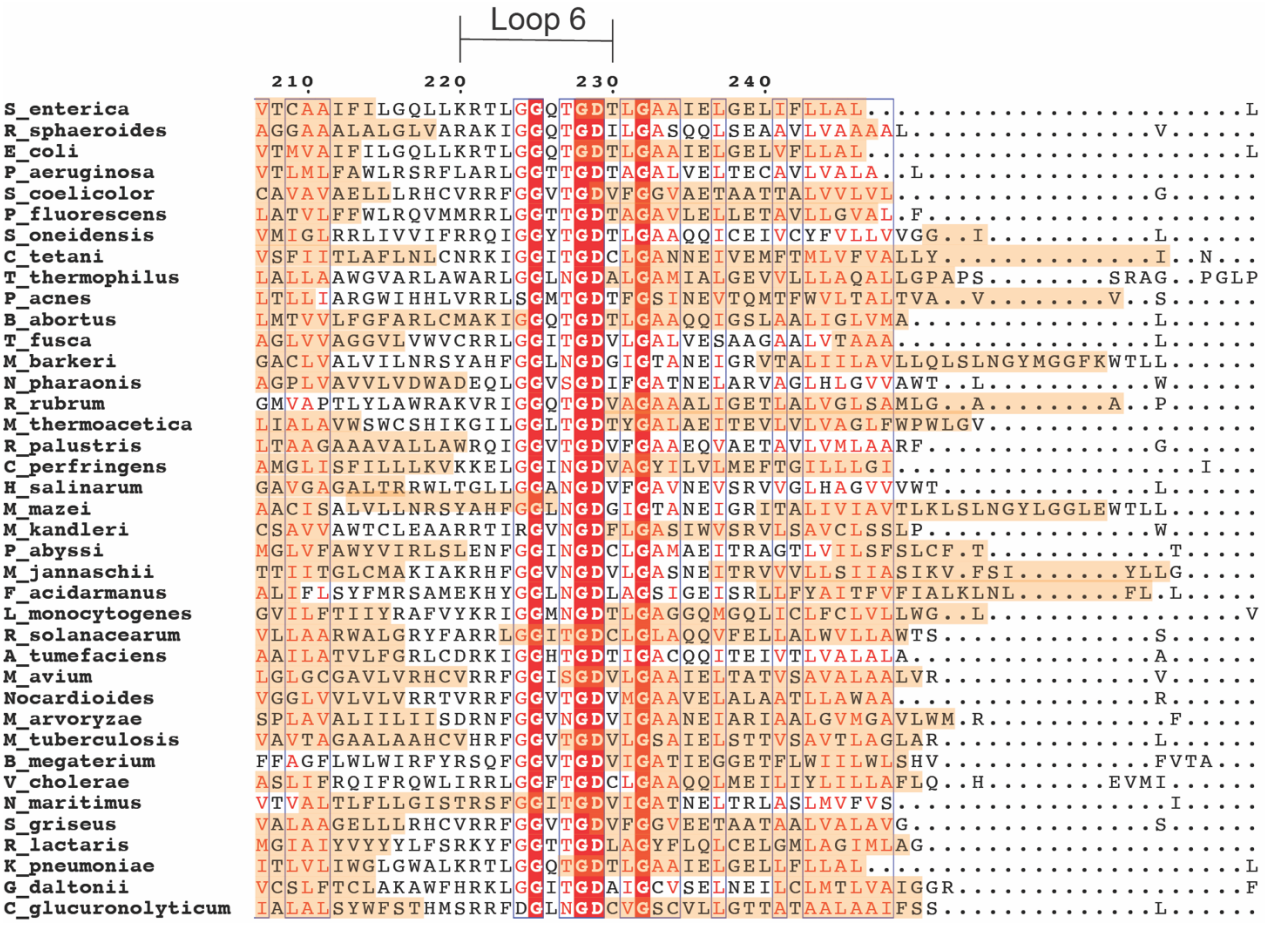

Fig. 4.14. Conservation of membrane association among bacterial and archaeal cobamide synthases. The alignment was generated using T-COFFEE multiple sequence alignment server (PSI/TM-Coffee) and visualized with ESPript 3.0 web-based application. Transmembrane domains predicted by PSI/TM-COFFEE are highlighted with orange. Cytoplasmic loops *of S. enterica* CobS are labelled. Red highlight indicates amino acid residues conserved amongst all aligned organisms. Boxes indicate regions of high similarity.

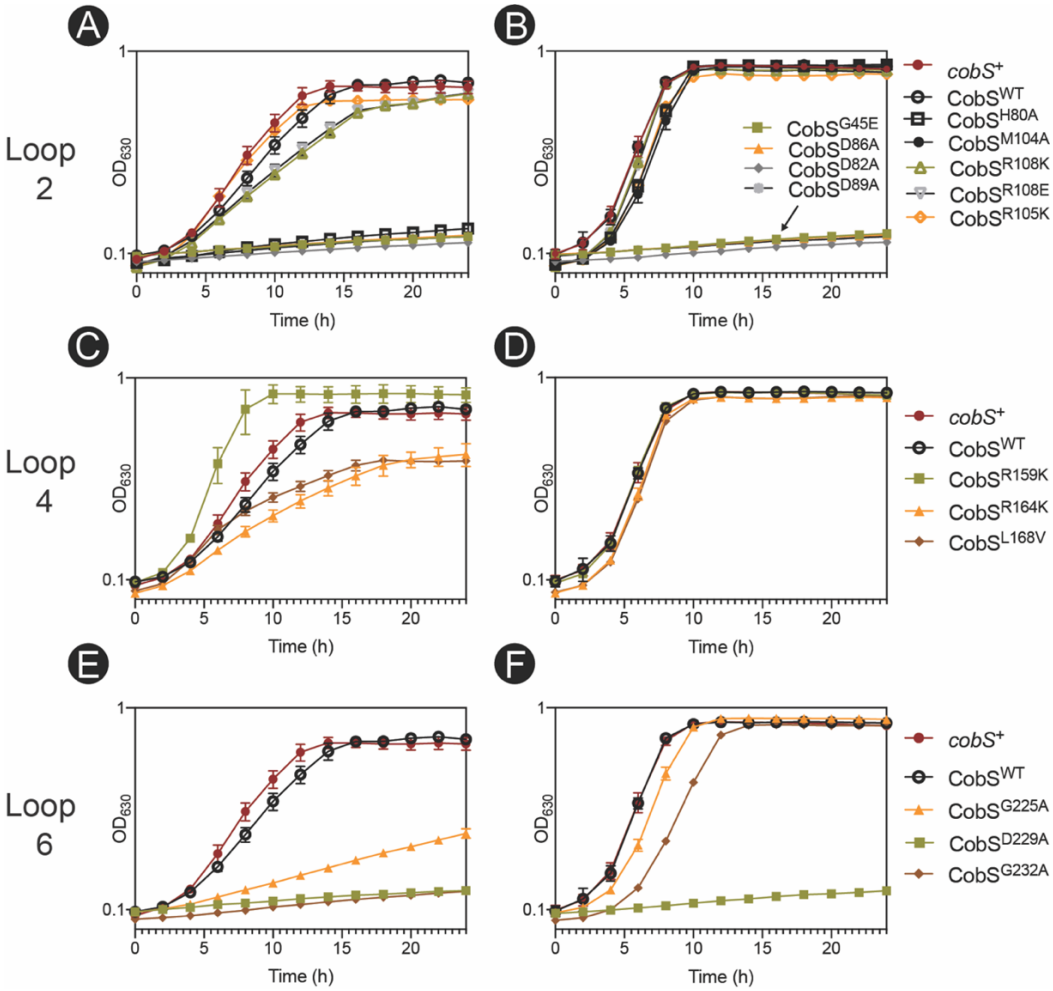

Fig. 4.15 Growth behavior of *cobS* strains synthesizing variant CobS proteins in minimal medium supplemented with 0.5 nM Cbi. Strains were grown in minimal NCE medium supplemented with $(CN)_2$Cbi (0.5nM) and glycerol (22mM) as a carbon and energy source. Panels B, D, and F were supplemented with DMB (150μM). Panels A and B include CobS variants in TM1 and cytoplasmic loop 2. Panels C and D include CobS variants in cytoplasmic loop 4. Panels E and F include CobS variants in cytoplasmic loop 6. A strain synthesizing wild-type CobS *in trans* is depicted with open, black circles. A *cobS*$^+$ strain is depicted with closed, red circles.

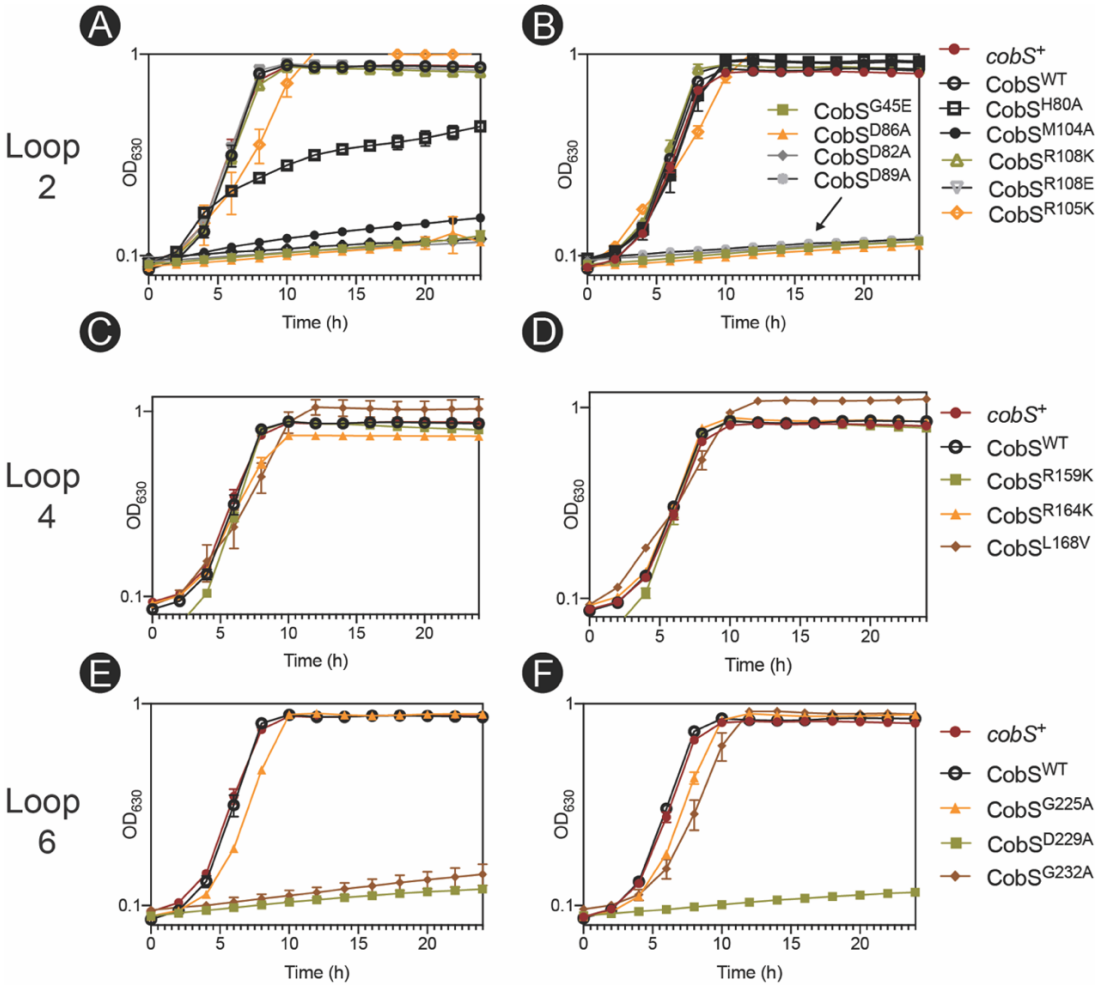

Fig. 4.16. Growth behavior of *cobS* strains synthesizing variant CobS proteins in minimal medium supplemented with 1 nM Cbi. Strains were grown in minimal NCE medium supplemented with $(CN)_2$Cbi (1nM) and glycerol (22mM) as a carbon and energy source. Panels B, D, and F were supplemented with DMB (150μM). Panels A and B include CobS variants in TM1 and cytoplasmic loop 2. Panels C and D include CobS variants in cytoplasmic loop 4. Panels E and F include CobS variants in cytoplasmic loop 6. A strain synthesizing wild-type CobS *in trans* is depicted with open, black circles. A *cobS*$^+$ strain is depicted with closed, red circles.

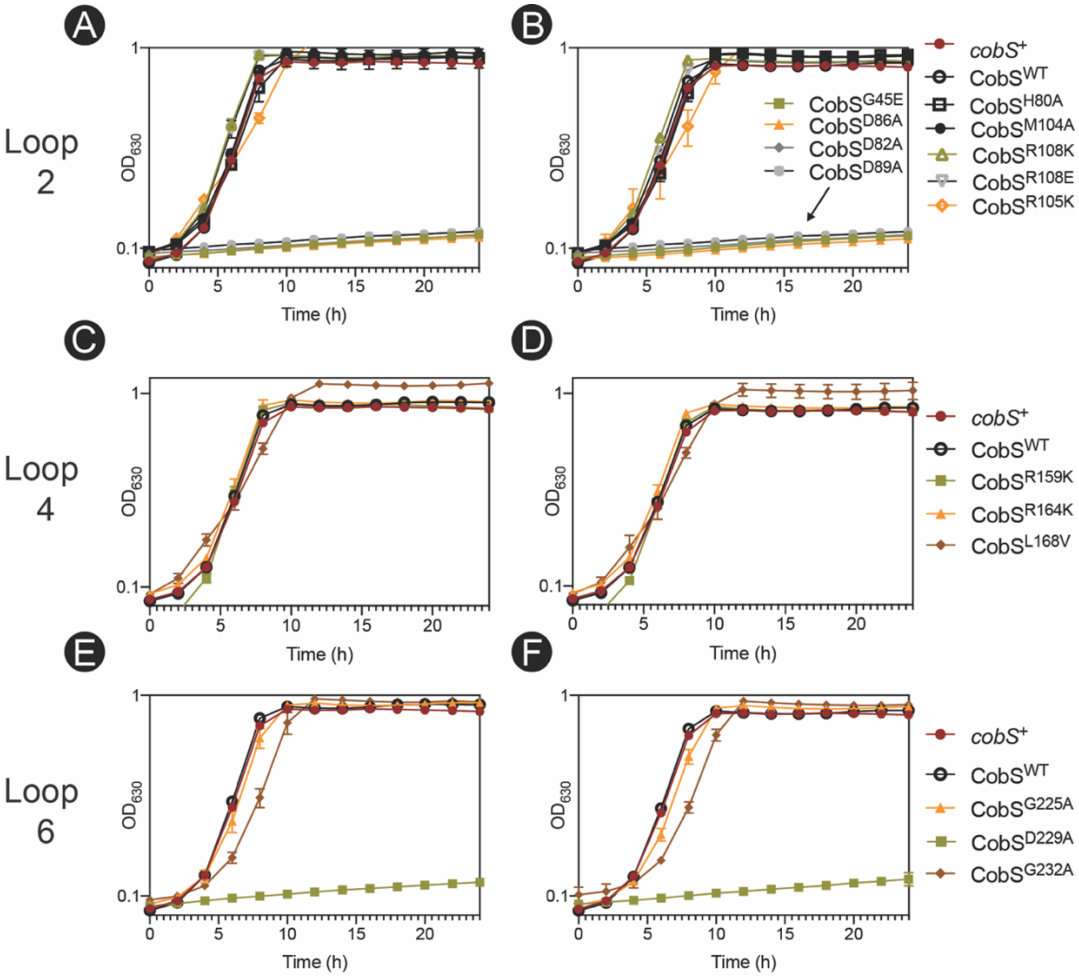

Fig. 4.17. Growth behavior of *cobS* strains synthesizing different CobS variants in minimal medium supplemented with 1.5 nM Cbi. Strains were grown in minimal NCE medium supplemented with $(CN)_2$Cbi (1.5nM) and glycerol (22mM) as a carbon and energy source. Panels B, D, and F were supplemented with DMB (150μM). Panels A and B include CobS variants in TM1 and cytoplasmic loop 2. Panels C and D include CobS variants in cytoplasmic loop 4. Panels E and F include CobS variants in cytoplasmic loop 6. A strain synthesizing wild-type CobS *in trans* is depicted with open, black circles. A *cobS*$^+$ strain is depicted with closed, red circles.

REFERENCES

1. Bertani G. 1951. Studies on lysogenesis. I. The mode of phage liberation by lysogenic *Escherichia coli*. J Bacteriol 62:293-300.
2. Bertani G. 2004. Lysogeny at mid-twentieth century: P1, P2, and other experimental systems. J Bacteriol 186:595-600.
3. Berkowitz D, Hushon JM, Whitfield HJ, Jr., Roth J, Ames BN. 1968. Procedure for identifying nonsense mutations. J Bacteriol 96:215-220.
4. Balch WE, Wolfe RS. 1976. New approach to the cultivation of methanogenic bacteria: 2-mercaptoethanesulfonic acid (HS-CoM)-dependent growth of *Methanobacterium ruminantium* in a pressurized atmosphere. Appl Environ Microbiol 32:781-791.
5. Miroux B, Walker JE. 1996. Over-production of proteins in *Escherichia coli*: mutant hosts that allow synthesis of some membrane proteins and globular proteins at high levels. J Mol Biol 260:289-298.
6. Datsenko KA, Wanner BL. 2000. One-step inactivation of chromosomal genes in *Escherichia coli* K-12 using PCR products. Proc Natl Acad Sci USA 97:6640-6645.
7. Jeter VL, Mattes TA, Beattie NR, Escalante-Semerena JC. 2019. A new class of phosphoribosyltransferases involved in cobamide biosynthesis is found in methanogenic archaea and cyanobacteria. Biochemistry 58:951-964.

8. Zayas CL, Escalante-Semerena JC. 2007. Reassessment of the late steps of coenzyme B_{12} synthesis in *Salmonella enterica*: Evidence that dephosphorylation of adenosylcobalamin-5'-phosphate by the CobC phosphatase is the last step of the pathway. J Bacteriol 189:2210-2218.

9. Sambrook J, Fritsch EF, Maniatis T. 1989. Molecular Cloning: A Laboratory Manual, Second ed. Cold Spring Harbor Laboratory, Cold Spring Harbor, N.Y.

10. Laemmli UK. 1970. Cleavage of structural proteins during the assembly of the head of bacteriophage T4. Nature 227:680-685.

11. Rigaud JL, Pitard B, Levy D. 1995. Reconstitution of membrane proteins into liposomes: application to energy-transducing membrane proteins. Biochim Biophys Acta 1231:223-246.

12. Winston SE, Fuller SA, Hurrell JGR. 1990. Western blotting, p 10.8.1-10.8.6. *In* Ausubel FA, Brent R, Kingston RE, Moore DD, Seidman JG, Smith JA, Struhl K (ed), Current Protocols in Molecular Biology, vol 1. Wiley Interscience, New York.

13. Maggio-Hall LA, Claas KR, Escalante-Semerena JC. 2004. The last step in coenzyme B(12) synthesis is localized to the cell membrane in bacteria and archaea. Microbiology 150:1385-1395.

14. Roelofs KG, Wang J, Sintim HO, Lee VT. 2011. Differential radial capillary action of ligand assay for high-throughput detection of protein-metabolite interactions. Proc Natl Acad Sci U S A 108:15528-15533.

15. Gupta S, Chakraborti PK, Sarkar D. 2005. Nucleotide-induced conformational change in the catalytic subunit of the phosphate-specific transporter from *M. tuberculosis*: implications for the ATPase structure. Biochim Biophys Acta 1750:112-121.

16. Schagger H. 2006. Tricine-SDS-PAGE. Nat Protoc 1:16-22.

17. Maggio-Hall LA, Escalante-Semerena JC. 1999. In vitro synthesis of the nucleotide loop of cobalamin by *Salmonella typhimurium* enzymes. Proc Natl Acad Sci U S A 96:11798-11803.

18. Suh S, Escalante-Semerena JC. 1995. Purification and initial characterization of the ATP:corrinoid adenosyltransferase encoded by the *cobA* gene of *Salmonella typhimurium*. J Bacteriol 177:921-925.

19. Thomas MG, Thompson TB, Rayment I, Escalante-Semerena JC. 2000. Analysis of the adenosylcobinamide kinase/adenosylcobinamide-phosphate guanylyltransferase (CobU) enzyme of Salmonella typhimurium LT2. Identification of residue His-46 as the site of guanylylation. J Biol Chem 275:27576-27586.

20. Trzebiatowski JR, Escalante-Semerena JC. 1997. Purification and characterization of CobT, the nicotinate-mononucleotide:5,6-dimethylbenzimidazole phosphoribosyltransferase enzyme from *Salmonella typhimurium* LT2. J Biol Chem 272:17662-17667.

21. Mattes TA, Escalante-Semerena JC. 2018. Facile isolation of alpha-ribazole from vitamin B12 hydrolysates using boronate affinity

chromatography. J Chromatogr B Analyt Technol Biomed Life Sci 1090:52-55.

22. Blanche F, Thibaut D, Couder M, Muller JC. 1990. Identification and quantitation of corrinoid precursors of cobalamin from *Pseudomonas denitrificans* by high-performance liquid chromatography. Anal Biochem 189:24-29.

23. Chan CH, Escalante-Semerena JC. 2011. ArsAB, a novel enzyme from *Sporomusa ovata* activates phenolic bases for adenosylcobamide biosynthesis. Mol Microbiol 81:952-967.

24. Mattes TA, Escalante-Semerena JC. 2017. *Salmonella enterica* synthesizes 5,6-dimethylbenzimidazolyl-(DMB)-alpha-riboside. Why some Firmicutes do not require the canonical DMB activation system to synthesize adenosylcobalamin. Mol Microbiol 103:269-281.

25. Rocco CJ, Dennison KL, Klenchin VA, Rayment I, Escalante-Semerena JC. 2008. Construction and use of new cloning vectors for the rapid isolation of recombinant proteins from *Escherichia coli*. Plasmid 59:231-237.

26. Guzman LM, Belin D, Carson MJ, Beckwith J. 1995. Tight regulation, modulation, and high-level expression by vectors containing the arabinose PBAD promoter. J Bacteriol 177:4121-30.

CHAPTER 5

THE LOCATION OF COBAMIDE BIOSYNTHETIC ENZYMES IN THE CELL MEMBRANE POSES PHYSIOLOGICAL CHALLENGES TO THE CELL[4]

[4]Jeter V.L., and Escalante-Semerena J.C. To be submitted to *Proceedings of the National Academy of the Sciences*.

SIGNIFICANCE

Salmonella is a human pathogen of global importance. Because this bacterium synthesizes cobamides *de novo* under anoxic conditions, it can respire ethanolamine in the gut facilitating the onset of disease. Here we show that cobamide biosynthesis is perilous, because high levels of the enzyme that catalyzes the penultimate step of the pathway, leads to dramatic changes in the cell membrane that ultimately dissipate the proton motive force, killing the cell. Significantly, the penultimate enzyme (*i.e.,* cobamide synthase) of the pathway is an integral membrane protein in all cobamide-producing bacteria and archaea whose genomes have been sequenced to date. Cobamide synthase anchors a multienzyme enzyme complex that assembles the nucleotide loop of cobamides.

ABSTRACT

Cobamides are complex, cobalt-containing cyclic tetrapyrroles utilized by organisms from all domains of life, but only produced *de novo* by some bacteria and archaea. The ‘late steps’ of the adenosylcobamide biosynthetic pathway are responsible for synthesis and attachment of the nucleotide loop and are required for both *de novo* synthesis and precursor salvaging. These steps are defined by activation of the corrin ring and lower ligand base, condensation of the activated precursors to adenosylcobamide-phosphate, and cleavage of the phosphate yielding a complete adenosylcobamide molecule. Condensation of the activated corrin ring and lower nucleotide base is performed by an integral membrane protein cobamide (5’-phosphate) synthase (CobS) and the final step is catalyzed

by adenosylcobalamin/α-ribazole phosphatase (CobC). CobS represents an important convergence of two pathways necessary for nucleotide loop assembly. Interestingly, membrane association of this penultimate step is conserved among all cobamide producers, yet the purpose of this association is not well understood. Here we investigate the consequences of CobS overproduction. We show that expression of this protein is corelated with dissipation of the proton motive force, membrane instability and decreased cell viability. Additionally, we report the expression of CobC alleviates the physiological stress of CobS expression through restoration of cell viability and provide the first evidence of protein-protein interactions in the late steps of cobamide biosynthesis.

INTRODUCTION

Cobamides (Cbas) represent an important family of metal-containing cofactors referred to as 'the pigments of life.' Other members of this family include hemes, chlorophylls and coenzyme F_{430} (1, 2). Cbas are cobalt-containing cyclic tetrapyyroles and are structurally unique from other cofactors. Cba requirement is found in cells across all domains of life, yet *de novo* synthesis is restricted to some bacteria and archaea (3). In addition to the prevalence of Cba-dependence, Cbas have also been shown to modulate community dynamics (4, 5). The complexity of Cbas allow it to participate in diverse reactions like intramolecular rearrangements, reductive dehalogenation, methyl-group transfers, elimination reactions and radical SAM-catalyzed carbon skeleton rearrangements (6). Additionally, Cba-

dependent regulation of carotenoid biosynthesis has been shown, utilizing the Cba molecule as a photoreceptor (7).

Cbas are defined by an equatorially coordinated cobalt and structurally unique from other cyclic tetrapyyroles through their upper axial (CoB) and lower axial (coA) ligands. A number of different naturally occurring upper and lower ligands form a diverse array of Cbas, however cobalamin (or B12) is characterized by a 5,6-dimethylbenzimidazole nucleobase (DMB). The coenzymic form of cobalamin contains a 5'-deoxyadenosine as the upper axial ligand and is referred to as adenosylcobalamin (AdoCbl) (Fig. 5.1) (8, 9).

Bioinformatics analysis estimate that 85% of bacteria have some form of Cba-dependence, however only 37% are capable of producing biologically active molecules (10, 11). In order to meet cellular requirements for Cbas, organisms lacking *de novo* synthetic pathways have enzymes for salvaging and remodeling exogenous incomplete Cbas. *Salmonella enterica* sv Typhimurium strain LT2 (henceforth *S.* Typhimurium) is capable of meeting Cba demand through *de novo* biosynthesis in anoxic conditions as well as scavenging exogenous corrinoids under normoxic conditions (12, 13)

The Nucleotide Loop Assembly (NLA) pathway comprises the late steps of *de novo* Cba biosynthesis, ultimately attaching the lower nucleobase ligand to the corrin ring. In *S.* Typhimurium, the NLA pathway is comprised of two branches: i) ring activation, and ii) base activation (Fig. 5.2). Ring activation occurs in two steps and begins with 1-amino-propanol phosphate (AP-P) attachment to adenosyl-Cby (AdoCby) forming adenosylcobinamide-phosphate (AdoCbi-P). AdoCbi-P

synthase (CbiB, EC 6.3.1.10) enzyme catalyzes this reaction (14). In the next step, AdoCbi-P is further activated by guanylylation generating AdoCbi-GDP, the activated form of the corrin ring. This reaction is catalyzed by the guanylyltransferase activity of the bifunctional enzyme CobU (NTP:AdoCbi kinase EC 2.7.7.62; GTP:AdoCbi-P guanylyltransferase, EC 2.7.1.156) (15-17) In *S.* Typhimurium*,* nucleobase activation is performed by the phosphorybosyltransferase (PRTase) CobT (EC 2.4.2.21). CobT activates DMB by transferring the phosphoribosyl moiety of nicotinate mononucleotide (NaMN) to yield the activated base α-ribazole-phosphate (α–RP) and releases nicotinic acid (18-22). The two active intermediates are the substrates of the cobamide 5'-P synthase (henceforth cobamide synthase) CobS (EC 2.7.8.26), which generate adenosylcobalamin 5'-phosphate (henceforth AdoCbl-P) by condensing AdoCbi-GDP and α-RP (23, 24). In the final step, AdoCbl-P is dephosphorylated by the CobC enzyme (EC 3.1.3.73) to yield AdoCbl (25, 26).

CobS is one of two polytopic, integral membrane proteins in the late steps of the AdoCba biosynthetic pathway (23). Membrane associated Cba biosynthesis is observed amongst all Cba producers, raising the question of localization of enzymes in this pathway. Here we report evidence that high levels of CobS result in dissipation of the proton motive force and decreased membrane stability that ultimately result in growth arrest. We also show that the detrimental effects of CobS can be counteracted by co-expression of NLA enzyme CobC. We expand on this finding by providing evidence of CobC-CobS interaction at the lipid bilayer.

MATERIALS AND METHODS

Bacterial strains, culture media, and chemicals. Bacterial strains used in this study are listed in Table 5.1. *Escherichia coli* C41 (λDE3) strains were grown at 37 °C on lysogeny broth (LB, Difco) (27, 28). *Escherichia coli* C41 (λDE3) (29) was used for protein overexpression, membrane assessments, and cell viability determinations. *E. coli* K12 strain DH5α (New England Biolabs) was used for plasmid construction. Antibiotics for all media were used at the following concentrations: ampicillin, 100 μg mL^{-1}; kanamycin, 50 μg mL^{-1}. All chemicals were purchased from Sigma-Aldrich unless otherwise noted; isopropyl β-D-1-thiogalactopyranpside (IPTG, Gold BioTechnology), glycerol (Fisher), 4-(2-hydroxyethyl)-1-piperazineethanesulfonic acid buffer (HEPES, Gold BioTechnology) 3-[(3-Cholamidopropyl)dimethylammonio]-1-propanesulfonate detergent (CHAPS, Gold BioTechnology), 1-palmitoyl-2-oleoyl-glycero-3-phosphocholine (POPC, Avanti Polar Lipids), 1-palmitoyl-2-oleoyl-*sn*-glycero-3-phosphoethanolamine (POPE, Avanti Polar Lipids), 1-palmitoyl-2-oleoyl-*sn*-glycero-3-phoshpo-L-serine (POPS, Avanti Polar Lipids), Lissamine™ Rhodamine B 1,2-Dihexadecanoyl-*sn*-glycero-3-phosphoethanolamine (Rh-DHPE, Molecular Probes) Oriole Fluorescent Gel Stain (Bio-Rad Laboratories).

Plasmid construction. Plasmids used in this study are listed in Table 5.1. Primers were synthesized by Integrated DNA Technologies, Inc. (IDT [Coralville, IA, United States]) and are listed in Table 5.2. Genes were amplified from *S.*

enterica genomic DNA using Phusion DNA polymerase (ThermoFisher) per manufacturer's instructions. Restriction enzymes were purchased from Fermentas. The BspQI restriction enzyme was purchased from New England BioLabs.

Plasmids pCOBS120 and pCOBS121. These plasmids were used for expression studies in *E. coli* C41 (λDE3). Plasmid pCOBS120 encoded $CobS^{WT}$, and plasmid pCOBS121 encoded variant $CobS^{D82A}$. Both plasmids provided resistance to ampicillin, and were constructed using the BspQI high-efficiency cloning method described elsewhere (30, 31) using primers cobS pCV1 F and cobS pCV1 R to amplify *cobS*$^{+}$, and primers cobS pCV1 F and cobS pCV1 R to amplify the *cobS* allele encoding $CobS^{D82A}$. Both *cobS* alleles were inserted between the pair of BspQI sites of pTEV16 (31).

Plasmid pCOBS122 and pCOBS123. This plasmid was constructed using traditional cloning methods with restriction enzyme digestion. The *cobS* allele was amplified from S. enterica using primers CobS NdeI F and CobS KpnI R. Amplified *cobS* and pRSFDUET-1 were digested with NdeI and KpnI as per manufacturer's directions. T4 DNA ligase was used according to manufacturer's instructions to insert *cobS* into MCS2 of pRSFDUET-1 yielding pCOBS122. pCOBS122 is 4,589 bp long and encodes resistance to kanamycin. Transcription of *cobS* was induced by the addition of IPTG, which triggered the synthesis of T7 polymerase. CobS expressed from pCOBS122 contains a *C*-terminal S-tag. The *cobC* allele was

amplified from *S. enterica* using primers CobC EcoRI F and CobC HindIII R. Amplified *cobC* and pCOBS122 were digested with EcoRI and HindIII according to manufacturer's instructions and ligated together using T4 DNA ligase as mentioned previously yielding pCOBS123. pCOBS123 is 5,208 bp long and encodes kanamysin resistance. Transcription of *cobC* was induced by the addition of IPTG, which triggered the synthesis of T7 polymerase. CobC produced using plasmid pCOBS123 contains a *N*-terminal 6x-hisitidine tag.

Plasmid pCOBC106. pTEV5 NheI and SacI This plasmid was constructed using traditional cloning methods with restriction enzyme digestion. The *cobC* allele was amplified from *S. enterica* using primers CobC NheI F and CobC SacI R. Amplified *cobC* and vector pTEV5 were digested according to manufacturer's directions using restriction enzymes NheI and SacI. The *cobC* allele was ligated into pTEV5 using T4 DNA ligase as per manufacturer's instructions. pCOBC106 was used for protein overproduction. The plasmid is 5,953 bp long and encodes resistance to ampicillin. Transcription of *cobC* was induced by the addition of IPTG, which triggered the synthesis of T7 polymerase. CobC synthesized from pCOBC106 yields *N*-terminal 6x-hisitidine tagged CobC.

CobS protein overproduction and purification. CobS overproduction and purification were based on methods described elsewhere (26) with modifications. $CobS^{WT}$ protein was overproduced from plasmid pCOBS5 in strain JE6663 [(*E. coli* C41 (λDE3)] in 2-L cultures of Terrific Broth (32). Protein synthesis was induced

by the addition of IPTG at a final concentration of 0.5 mM in mid-log phase cultures (OD_{600} ~ 0.6) growing at 37 °C while shaking at 180 rpm in an Innova44 gyratory incubator (New Brunswick Scientific). After induction, cultures were grown for 3 h at 37 °C while shaking at 180 rpm. Cultures were harvested by centrifugation at 4 °C for 15 min at 6,000 x *g* in an Avanti J20-XPI refrigerated centrifuge equipped with a JLA-8.1000 rotor. Pelleted cells were stored at −20 °C until used. For protein purification, cell pellets were thawed and resuspended in 30 ml of Tris-HCl buffer (100 mM, pH 7.9 at 24°C). Cells were lysed with a cell press in a cell disruptor (Constant Systems) set at 1.72×10^5 kPa. A sample (0.5 mL) of a protease inhibitor cocktail (Sigma) was added to cell-free extracts (CFEs) to minimize CobS degradation during purification. CFEs were obtained after centrifugation at 4°C, at 5,000 x *g* for 15 min. Cell membranes were obtained from a high-speed centrifugation at 75,000 x *g* for 90 min in an Avanti J-25I Beckman/Coulter refrigerated centrifuge equipped with a JA-25.50 rotor. Membranes were resuspended in 10 ml of Tris-HCl buffer (0.1 M, pH 7.9, 24°C) with a glass homogenizer and were solubilized by the addition of CHAPS detergent to a final concentration of 20 mM. The detergent-containing CFE was incubated on ice for 1 h and centrifuged at 4°C at 75,000 x *g* for 30 min to remove solubilized contaminants. The insoluble fraction containing CobS was resuspended in 10 ml of Tris-HCl buffer (100 mM, pH 7.9 at 24°C) containing NaCl (0.5 M) and imidazole (20 mM) with a glass homogenizer and solubilized by the addition of 1,2-diheptanoyl-*sn*-glycero-3-phosphocholine (DHPC) to a final concentration of 15 mM. DHPC was resuspended in 1mL Tris-HCl buffer (100 mM, pH 7.9 at 24°C)

containing NaCl (0.5 M) and imidazole (20 mM) and added to the insoluble fraction at a rate of 100μL/min to avoid denaturation of proteins. The CFE fraction containing detergent-solubilized CobS was incubated on ice for 1 h and centrifuged at 4°C at 75,000 x *g* for 30 min. A HisPur nickel-nitrilotriacetic acid (Ni-NTA) resin (2-mL bed volume, Thermo Scientific) was equilibrated with 10 bed volumes of water and 10 bed volumes of Tris-HCl buffer (0.1 M, pH 7.9 at 24°C) containing NaCl (0.5 M) and imidazole (20 mM). CFE containing solubilized CobS protein was incubated with the HisPur resin at 4 ºC with nutation for a minimum of 2 h before pouring the slurry into a column (Kontes FLEX-COLUMN 1.0 x 10 cm). The column was washed with five bed volumes of Tris-HCl buffer (0.1 M, pH 7.9 @ 24°C) containing NaCl (0.5 M) and imidazole (20 mM) and DHPC (15 mM) then five bed volumes of Tris-HCl buffer (0.1 M, pH 7.9 at 24°C) containing NaCl (0.5 M) and imidazole (60 mM) and DHPC (15 mM). Proteins were eluted with five bed volumes of Tris-HCl buffer (0.1 M, pH 7.9 at 24°C) containing NaCl (0.5 M) and imidazole (0.5 M) and DHPC (15 mM). Proteins in fractions of interest were resolved by sodium dodecyl sulfate polyacrylamide gel electrophoresis (SDS-PAGE) (33) and CobS-containing fractions were applied to a 5-mL Zeba Spin desalting column (ThermoFisher) to remove imidazole. Glycerol (10% [v/v], final concentration) was added to a desalted CobS sample, which was flash frozen in liquid N_2 prior to storage at -80 °C. The final buffer composition before storage was Tris-HCl buffer (0.1 M, pH 7.9 at 24°C) containing NaCl (0.15 M) and DHPC (15 mM). Protein concentration was determined using a Bradford Assay kit (Bio-Rad Laboratories). A typical CobS preparation yielded 0.5 mg of protein / g of cells.

CobC protein overproduction and purification. Wild-type CobC protein was overproduced from plasmid pCOBC106 in strain JE6663 (*E. coli* C41) in 1-L cultures of Terrific Broth (32). Protein synthesis was induced by the addition of IPTG at a final concentration of 1 mM in mid-log phase cultures (OD_{600} ~0.6) growing at 37°C with shaking at 180 rpm in an Innova44 (New Brunswick Scientific) gyratory incubator. After induction, cultures were grown for 17 h at 24°C with shaking at 180 rpm. Cultures were harvested by centrifugation at 4°C for 15 min at 6,000 x *g* in an Avanti J20-XPI refrigerated centrifuge equipped with JLA-8.1000 rotor. Pelleted cells were stored at -20°C until used. Frozen cells were thawed on ice and re-suspended in HEPES buffer (50 mM, pH 7.5) containing NaCl (0.5 M) and imidazole (20 mM) at a rate of 20% cell weight to buffer volume. Lysozyme (1 μg / mL) and DNaseI (25 μg / mL) were added to the cell suspension and incubated on ice for 10 min. Cells were lysed by sonication. phenylmethylsulfonyl fluoride (PMSF) was added to the cell lysate at a final concentration of 0.5 mM. Cellular debris was removed by centrifugation at 4°C for 30 min at 40,000 x *g* in an Avanti J-251 centrifuge (Beckman/Coulter) equipped with a JA 25.25 rotor. Clarified extract was filtered using a 0.45-μm syringe filter unit and applied to a 2-mL HisPur nickel-nitrilotriacetic acid (Ni-NTA) affinity column (ThermoFisher Scientific). The column was washed with 10 column volumes of HEPES buffer (25 mM, pH 7.5) containing NaCl [(0.5 M) and imidazole (20 mM) and six column volumes of HEPES buffer (25 mM, pH 7.5) containing NaCl (0.5 M)] and imidazole (40 mM). H_6-CobC was eluted with six column volumes of HEPES buffer (25 mM, pH 7.5)

containing NaCl (0.5 M) and imidazole (0.5 M). Fractions were collected throughout the wash and elution steps and H_6-CobC purification was monitored by SDS-PAGE compared to Precision Plus Protein Standards (BioRad). Fractions containing H_6-CobC were pooled and dialyzed against HEPES buffer (25 mM, pH 7.5) containing NaCl (0.5 M) to remove imidazole. H_6-CobC was then dialyzed against HEPES buffer (25 mM, pH 7.5) in three additional steps with decreasing concentrations of NaCl down to 0.15 M. Purified H_6-CobC was flash frozen in liquid nitrogen and stored at -80°C until used. Protein concentration was measured using a Bradford Assay Kit (Bio-Rad laboratories).

Liposome preparation and protein reconstitution. The lipids used in the study were POPC, POPE, POPS and Rh-DHPE. Proteoliposomes were prepared using detergent-mediated reconstitution as described elsewhere (34). POPC:POPS:POPE:Rh-DHPE were combined at a molar ratio of 80:10:9.5:0.5 to yield 1 μmol lipid. Lipids were dried under a stream of N_2 gas and spun in an Eppendorf VacFuge at 30 ºC for 1 h. The dried lipid film was hydrated in 500 μl of HEPES buffer (20 mM, pH 7.4) containing NaCl (0.5 M), CHAPS (40 mM) and glycerol (10% [v/v]) to a final lipid concentration of 2 mM. Detergent-solubilized $CobS^{WT}$ was added at a lipid-to-protein molar ratio of 1000:1 and incubated with rotation on a Benchmark RotoBot at 4 °C for 1 h. Detergent removal and proteoliposome formation was achieved by four 20-h dialyses using Slide-A-Lyzer

dialysis cassettes (20-kDa molecular mass cutoff) against HEPES buffer (20 mM, pH 7.4) containing NaCl (0.5 M) and glycerol (10% [v/v]). Dialysis was performed at a dialysate:sample volumetric ratio of 2000:1. After dialysis, the proteoliposome suspension was applied to a Histodenz (Sigma) gradient to perform a liposome flotation assay. The proteoliposome suspension was mixed with an equal volume with HEPES buffer (20 mM, pH 7.4) containing NaCl (0.15 M), Histodenz (80% [w/v]), glycerol (10% [v/v]) and deposited in a Beckman Coulter Ultracentrifuge tube (polyallomer, 13 x 51 mm). A 4-mL overlay of HEPES (20 mM, pH 7.4) containing NaCl (0.15 M), Histodenz (30% [w/v]), glycerol (10% [v/v]) was applied followed by a 200-μL overlay of HEPES buffer (20 mM, pH 7.4) containing NaCl (0.15 M), glycerol (10% [v/v]). The gradient was subjected to centrifugation at 4 °C for 3 h at 268,000 x *g* in a refrigerated Beckman Coulter Optima™ MAX-XP Ultracentrifuge using an MLS-50 rotor. The size distribution of reconstituted liposomes was determined by dynamic light scattering in a 1.5mL polystyrene cuvette using a Zetasizer Nano (Malvern Instruments). Lipid concentration of the reconstituted liposomes was determined by a standard curve generated from fluorescence of Rh-DHPE. Fluorescence measurements were read on a BioTek Gemini instrument set at an excitation wavelength of 540 nm and emission wavelength of 586 nm. Protein concentration in proteoliposomes was determined by generating a standard curve. Briefly, a range of known bovine γ-globulin (BGG) and lysozyme concentrations were separated by SDS-PAGE with unknown concentrations of CobS-containing proteoliposomes stained with Oriole

Fluorescent stain and analyzed using TotalLab TL100 software. The presence of CobS in liposomes was confirmed by western blot and mass spectrometry analyses.

Liposome Floatation Assay. To probe for interactions between CobC and CobS or CobC and the lipid bilayer, liposome floatation assays using CobS-containing proteoliposomes and empty liposomes were employed. Purified CobC protein (final concentration of 10 μM) was incubated with 100 μL of a 1.4 mM lipid solution of CobS proteoliposomes or empty liposomes for 1 h at 24°C on a Benchmark RotoBot. This mixture was mixed with an equal volume with HEPES buffer (20 mM, pH 7.4) containing NaCl (0.15 M), Histodenz (80% [w/v]), glycerol (10% [v/v]) and deposited in a Beckman Coulter Ultracentrifuge tube (polyallomer, 11 x 34 mm). A 2.5-mL overlay of HEPES (20 mM, pH 7.4) containing NaCl (0.15 M), Histodenz (30% [w/v]), glycerol (10% [v/v]) was applied followed by a 150-μL overlay of HEPES buffer (20 mM, pH 7.4) containing NaCl (150 mM), glycerol (10% [v/v]). The gradient was subjected to centrifugation at 4 °C for 3 h at 214,000 x *g* in a refrigerated Beckman Coulter Optima™ MAX-XP Ultracentrifuge using a TLS-55 rotor. The top layer was harvested and lipid concentration was determined by rhodamine fluorescence. A standard curve was generated by measuring the fluorescence of a series of rhodamine concentrations with a SpectraMax Gemini EM microplate reader (Molecular Devices) at excitation 540 nm and emission 586 nm.

Proteolytic digest of CobC-CobS proteoliposome complex. To determine if CobC embedded in the lipid bilayer upon interaction with CobS-containing proteoliposomes, proteolytic digests were performed using proteinase K (Fisher), trypsin (Sigma). Reaction mixtures in HEPES buffer (20 mM, pH 7.4) containing NaCl (0.15 M), glycerol (10% [v/v]), 10 μL CobC-CobS proteoliposome complex obtained from flotation assay and 1 μg protease were incubated for 1 h at 37 °C. Digestion reactions were stopped by the addition of Tris-HCl buffer (62.5 mM, pH 6.8) containing SDS (2% w/v), glycerol (10%, v/v), 2-mercaptoethanol (0.1 M), and bromophenol blue (0.001%, w/v), followed by incubation at 90 °C for 5 min. Peptides were separated by SDS-PAGE electrophoresis and subsequently analyzed by western blot (35) with α-CobC rabbit polyclonal antibodies. Purified CobC protein was used as positive control.

Western blot and dot blot analysis. To confirm the presence of CobC in liposome floatation mixtures and to analyze proteolytic digests, western blots and dot blots were performed using rabbit polyclonal antibodies generated against CobC (Envigo, IN). CobC-CobS proteoliposome complexes harvested from the floatation assay previously described or proteolytic digests were resolved by SDS-PAGE and subsequently transferred to a polyvinylidene fluoride (PVDF) membrane (Millipore) using a Trans-Blot Turbo system (Bio-Rad Laboratories) set to StandardSD mini gel (1.0 A, 25 V, 30 min) and Tris-HCl transfer buffer (25 mM, pH 8) containing glycine (192 mM) and methanol (10% v/v)]. For dot blot analysis, 3 μL of XuM

proteoliposome complexes obtained by liposome flotation and 100 ng of positive and nonspecific controls were spotted on a nitrocellulose membrane. Membranes were incubated for 30 min in blocking buffer of phosphate buffered saline containing Tween 20 (PBST) comprised of NaH_2PO_4 (10 mM, pH 7.2), NaCl (0.9% w/v), and Tween 20 (0.1% v/v), and instant dry milk (5%, w/v). Membranes were then probed with α-CobC antibodies (1:5,000 in blocking buffer) or α-CobS antibodies (1:5,000 in blocking buffer) for 1 h, then washed thrice (30 min each) with PBST. Membranes were then probed for 1 h with horseradish peroxidase (HRP)-conjugated goat α-rabbit secondary antibodies (Sigma) in PBST (1:10,000) before three, 30-min washes with PBST. Membranes were incubated in SuperSignal West Pico PLUS chemiluminescent substrate (ThermoFisher) for 5 min and imaged using a UVP ChemStudio imaging instrument (AnalytikJena). Purified CobC protein was used as positive control and SuperSignal Molecular Weight Protein Ladder (ThermoFisher) was used as reference for the electrophoretic behavior of molecules of known molecular masses.

Microscopy. The effect of CobS overproduction on the cell membrane was visualized by fluorescence microscopy. Starter cultures of *E. coli* C41 (λDE3) harboring empty cloning vector or plasmid encoding $CobS^{WT}$ protein were grown for 16 h in LB containing antibiotic at 37 °C shaking at 150 rpm. Starter cultures were used to inoculate (10% [v/v]) 5 mL of LB containing antibiotic. Cultures were incubated at 37 °C with shaking at 150 rpm. Expression of *cobS* was induced by

the addition of IPTG to a final concentration of 1 mM when cultures reached an OD_{600} of ~0.5. After the addition of IPTG, cultures were incubated for an additional 30 min. A 0.5-mL sample of culture was incubated for 5 min with the vital membrane stain FM 4-64FX (ThermoFisher) and 4',6'-diamidino-2-phenylindole (DAPI, ThermoFisher) at final concentrations of 5 μg mL^{-1} and 2 μg mL^{-1} respectively. Cells were subjected to centrifugation at 6,000 x g for 4 minutes, washed with 0.5 mL of phosphate buffered saline before resuspension in 0.1 mL of phosphate buffered saline. A 1.5-μL sample of stained cell suspension was applied to a 1% (w/v) agarose pad for imaging. Images were collected using a Nikon Eclipse Ni microscope equipped with a coolsnap MYO camera (photometrics) using filter sets for DAPI (exciter:ET395/25x emitter:ET460/50m, dichroic T425lpxr) and mCherry/TexasRed Longpass (for FM 4-64FX, exciter:ET560/40x emitter:ET590lp, dichroic T590lpxr).

Ethidium bromide accumulation assay. The effect of CobS overproduction and CobC and CobS co-expression on membrane permeability was examined by a modified ethidium bromide accumulation assay as outlined elsewhere (36). Briefly, starter cultures of *E. coli* C41 (λDE3) harboring empty cloning vector, or plasmids encoding $CobS^{WT}$, $CobS^{D82A}$, or CobC and $CobS^{WT}$ proteins were grown overnight in LB containing antibiotic at 37 °C with shaking at 150 rpm. Starter cultures were sub-cultured (1% v/v inoculum) into 198 μL of LB plus antibiotic in a 96-well microtiter plate (Falcon) and incubated in a plate reader (BioTek EON) at 37 °C

with orbital shaking. At an OD_{630} of ~0.4, IPTG was added to a final concentration 0, 0.5, or 1 mM to induce expression of *cobS,* or *cobS* and *cobC*. Cells were incubated for 30 min as described above. Cultures (150 μL) were transferred into the wells of a black, round-bottom 96-well microtiter plate and ethidium bromide was added to a final concentration of 6.25 μM. Relative fluorescence (excitation 530 nm, emission 600nm) was monitored immediately upon addition of ethidium bromide using a BioTek Gemini fluorescent plate reader for 180 s. The rate of relative fluorescence (RFU/s) was determined by linear regression. Significance was determined by unpaired student's *t*-test using Prism version 8 (GraphPad) software.

Flow cytometry. The effect of CobS overproduction on membrane potential and permeability were examined using the BacLight Membrane Potential Kit (Invitrogen) containing 3,3'-diethyloxacarbocyanine iodide [$DiOC_2(3)$] and TO-PRO-3 dyes (Molecular Probes). These experiments were modified from protocols described elsewhere (37, 38). Starter cultures of *E. coli* C41 (λDE3) harboring empty cloning vector, or plasmids encoding $CobS^{WT}$ or $CobS^{D82A}$ proteins were grown for 16 h in LB containing antibiotic at 37 °C shaking at 150 rpm. Starter cultures were used to inoculate (10% [v/v]) 5 mL of LB containing antibiotic. Cultures were incubated at 37 °C with shaking at 150 rpm. Expression of *cobS* alleles was induced by the addition of IPTG to a final concentration of 0.5 or 1 mM when cultures reached an OD_{600} of ~0.4. After the addition of IPTG, cultures were

incubated for an additional 15 min or 30 min. The final optical density at 600 nm was determined, 1 x 10^6 cells/mL were added to 1 mL of PBS, $DiOC_2(3)$ and TO-PRO-3 were added to a final concentration of 30 μM and 0.5 mM, respectively, and the cultures were incubated for 30 min at 24 °C before analyzing the fluorescence using a CyAn ADP instrument (Beckman Coulter). Cells and dyes were detected using forward scatter (FSC), side scatter (SSC), FL1 (488 nm / 530 nm), FL3 (488 nm / 613 nm), and FL9 (633 nm) channels. Data were analyzed as outlined by the BacLight Membrane Potential Kit. Significance was determined by one-way ANOVA with *post-hoc* Bonferroni multiple comparison. Cells subjected to carbonyl cyanide 3-chlorophenylhydrazone (CCCP, 5μM) and Polymyxin B (1 μg/mL) were used as controls for $DiOC_2(3)$ and TO-PRO-3, respectively.

Cell viability assay. The effect of CobS overproduction and CobC and CobS coexpression on cell viability was determined by counting colony forming units (CFUs). Cultures were grown and CobS or CobC and CobS expression was induced as outlined above for flow cytometry. Cells were serially diluted in sterile 0.85% (w/v) NaCl, plated on LB containing 1.5% (w/v) agar and ampicillin (100 μg mL^{-1}) or kanamycin (50 μg mL-1) and incubated for 16 h at 37 °C before colonies were counted. Cultures that were not induced were normalized to one and compared to cultures expressing CobS or CobC and CobS as a ratio of CFUs. The assay was performed in biological triplicate with three technical replicates each

time. Significance was determined by unpaired sudent's *t*-test using Prism (GraphPad) v8 software.

RESULTS & DISCUSSION

Excess CobS enzyme disrupts the proton motive force, cell membrane permeability, and cell viability. Previous work from our laboratory showed that attempts to overproduce CobS impaired cell growth and triggered the overproduction of the phase shock protein A (PspA) (23), a protein known to be produced under stressful conditions that dissipate the PMF (39-41). These intriguing results suggested that a physiologic excess of CobS might compromise cell membrane functionality, prompting us to investigate whether excess CobS negatively affected membrane function and if so, how. Among the many functions of the cell membrane is to house electron transport systems that separate protons from electrons generating of a chemical gradient of protons (a.k.a. the proton motive force, PMF) that fuels cell motility, nutrient transport, ATP synthesis, etc. We investigated the possibility that excess CobS could dissipate the PMF and negatively affect membrane permeability. We took three experimental approaches to test these ideas.

Excess CobS protein dissipates the proton motive force (PMF). The first approach we took was based on the fact that ethidium bromide (EtBr), a fluorescent dye routinely used to stain DNA, is efficiently kept outside the cell by a PMF-driven efflux pump (42). Others have shown that dissipation of the PMF leads to the accumulation of EtBr in the cytoplasm with the concomitant

intercalation of EtBr into DNA and increased cell fluorescence (43). We used this approach to probe the effect of CobS overproduction on the PMF. For this purpose, we measured EtBr accumulation in *E. coli* cells that synthesized $CobS^{WT}$ or $CobS^{D82A}$ proteins. Shown in figure 5.4A are the rates of EtBr accumulation in cells that expressed *cobS* alleles encoding $CobS^{WT}$ or $CobS^{D82A}$ proteins. We measured a significant increase in the rate of EtBr accumulation when the genes encoding $CobS^{WT}$ and $CobS^{D82A}$ were induced, a result that was consistent with PMF dissipation. The effect was not observed in cells harboring the empty cloning vector used to express the alluded *cobS* alleles. The fact that the enzymatically inactive variant $CobS^{D82A}$ also triggered EtBr accumulation suggested that the presence, not the activity of the CobS protein was necessary and sufficient to dissipate the PMF.

ii) CobS protein compromises cell membrane permeability. In addition to assessing the stability of the PMF, we also probed the integrity of the cell membrane by measuring the uptake of the membrane-impermeable dye TO-PRO-3, which is a fluorescent dye with strong affinity for DNA. The positive charge of this molecule is the chief reason for its inability to diffuse across the cell membrane (44). TO-PRO-3 has been shown to indicate membrane permeability in the absence of changes in membrane potential (45). Figure 5.4B shows the percentage of permeabilized cells in populations expressing $CobS^{WT}$ or $CobS^{D82A}$ 30 min after induction of the *cobS* alleles encoding these proteins. We observed a significant (*, $p<0.05$) increase in permeability as a result of $CobS^{WT}$

overproduction compared to an empty cloning vector control. Under these conditions, we did not see the same effect with excess inactive CobS.

In parallel to monitoring TO-PRO-3 uptake, we assessed the effect of CobS overproduction on membrane potential using the carbocyanine dye $DiOC_2(3)$ (Fig. 5.5). $DiOC_2(3)$ initially exhibits green fluorescence but shifts to red emission as the dye molecules self-associate in the cytoplasm of cells with larger membrane potentials (44). In Figure 5.5A, the mean fluorescence intensity (MFI) of red fluorescence (filled bars) and green fluorescence (open bars) is displayed for cells expressing $CobS^{WT}$ and inactive variant $CobS^{D82A}$. We observed an increase of green fluorescence in response to increases in $CobS^{WT}$ and $CobS^{D82A}$. In figure 5.5B, the ratio of red-to-green MFI is shown for the same cell populations analyzed in figure 5.5A. A significant decrease in red:green MFI was observed on cells expressing $CobS^{WT}$ and $CobS^{D82A}$ compared to the cells harboring empty cloning vector. The results from panel A and B strongly indicate membrane depolarization.

iii) Excess CobS protein reduces cell viability. In addition to monitoring the effects of excess CobS on the membrane, we assessed the consequences of membrane dysfunction on cell viability by conducting colony forming unit (CFU) counts (Fig. 6). We observed a significant decrease in CFUs as induction of $CobS^{WT}$ (p = 0.0003, 0.5mM IPTG; p = 0.0014, 1mM IPTG) and $CobS^{D82A}$ (p <0.0001, 0.5mM IPTG; p = 0.0003, 1mM IPTG) expression increased. Conversely, we saw an increase of CFUs in strains harboring a vector control. These results indicate a significant role of CobS expression on overall cell viability.

Increased CobS interrupts membrane architecture.

To visualize the effects of excess CobS on the membrane, we utilized fluorescence microscopy with the lipophilic stain FM4-64. FM4-64 is a membrane stain that exhibits uniform staining in wild-type cells. Membrane perturbations will disrupt the uniformity of staining, making FM4-64 an effective indicator of membrane abnormalities (46, 47). When stained with FM4-64, cells harboring an empty vector exhibited uniform staining of the membrane (Fig. 5.7A,C). As expected, based on the findings reported here, cells synthesizing CobS exhibited frequent non-uniform FM4-64 staining of the membrane (Fig. 5.7B,D). The significant membrane perturbations caused by excess CobS are visualized by three-dimensional fluorescence intensity spectrum (Fig. 5.7D). Compared to cells harboring empty vector (Fig. 5.7C), CobS synthesizing cells present a punctate staining around the membrane (Fig. 5.7D). This phenomenon is further exemplified by the ranges of fluorescent intensity across the cell perimeter depicted by the spectrum. The spectrum of cells harboring empty vector show uniform intensities around the perimeter of the cell, with a slight increase at the divisional septum (Fig. 5.7C).

A surprising finding exhibited by CobS synthesizing cells can be seen in Panel B (Fig. 5.7). Populations of these cells mostly lack any divisional septa and numerous elongated cells are seen, indicating potential effects of CobS on cell division and proliferation. Intact divisional septa are clearly visualized throughout the population in cells harboring empty vector (Fig. 5.7A). PMF is known to play an important role in proper localization of the division site (48, 49). The work

reported here indicates significant membrane depolarization as a result of increased levels of CobS, thus we posit that defective cell division may be ultimately a consequence of CobS overproduction.

Co-expression of the AdoCbl-P phosphatase (CobC) relieves membrane stress caused by excess CobS.

We sought to alleviate the membrane stress we observed as a consequence of excess CobS by co-expression with CobC**.** CobC catalyzes the final step of cobamide biosynthesis by cleaving the phosphate from cobamide-phosphate generated by CobS. CobC is predicted to have a single transmembrane domain, making it a potential candidate for interactions with the integral membrane protein CobS. To determine whether increased levels of CobC could counteract the negative effects of CobS overproduction, we utilized a vector (pRSFDUET-1) capable of co-expressing two proteins in tandem to generate both CobC and CobS in equal stoichiometry. Using this expression system, we repeated the ethidium bromide assay outlined previously. Figure 5.8A shows the rates of ethidium bromide accumulation of cells harboring the empty vector compared to cells synthesizing CobC and CobS across a range of inducer (IPTG) concentrations. We observed similar rates of accumulation between the CobC and CobS synthesizing cells and cells with the vector control, indicating the balance of CobC expression with CobS ameliorated the detrimental effects we observed with CobS alone.

Additionally, we sought to determine if overall cell viability was improved by co-expression of CobC with CobS. Figure 5.8B shows the ratio of CFUs compared to a no induction control. We observed no significant change in cell viability between induced and uninduced cells synthesizing both CobC and CobS. Previously, we showed a drastic decrease in cell viability as a function of CobS induction (Fig. 5.7). These results suggest CobC can inhibit the negative effects of excess CobS.

CobC interacts with CobS embedded in liposomes.

Given the restoration of cell viability and membrane stability observed when CobC was co-expressed with CobS, we sought to determine whether these proteins interacted. To probe for an interaction between CobC and CobS in a phospholipid bilayer, we employed a liposome floatation strategy. Purified CobC was first incubated with CobS-containing liposomes. The CobC-CobS proteoliposome suspension was then separated through a Histodenz gradient by ultracentrifugation. Any protein that interacted with CobS proteoliposomes would move through the density gradient and "float" in the top layer, while unbound or unincorporated proteins would not. We observed that CobC did associate with CobS-containing proteoliposomes, suggesting a strong interaction between CobS and CobC (Fig. 5.9A). Because CobC has a single predicted transmembrane domain, we sought to differentiate between an interaction between CobC and CobS-containing proteoliposomes and CobC and the liposomal phospholipid

bilayer. To probe for interaction with the lipid bilayer, the liposome floatation assay was performed with empty liposomes. Without CobS embedded in the liposome, we no longer observed floatation of CobC (Fig. 5.9A). The presence of CobS in the liposome suspension was confirmed by dot blot analysis after liposome flotation (Fig. 5.9B). These results strongly suggested that CobS recruited CobC when CobS was embedded CobS in the phospholipid bilayer.

CobC is predicted to have one transmembrane spanning domain with the *N*-terminus located in the periplasm and *C*-terminus in the cytoplasm (Fig. 5.10A). After confirming CobS-dependent recruitment of CobC, we asked whether the presence of CobS drove CobC insertion into the lipid bilayer. We used proteolysis by proteinase K and trypsin and subsequent western blot analysis to probe for membrane protection of CobC. The electrophoretic behavior of digests was compared to molecular mass standards (Fig. 5.10B, lane 1). The CobC/CobS proteoliposome complex obtained by liposome floatation was used as a control (Fig. 5.10B Lane 2). This solution was subjected to digestion by proteinase K (Fig. 5.10B Lane 3) and trypsin (Fig. 5.10B Lane 5). These digestions were repeated with the CobC/CobS proteoliposome complex after incubation with Triton-X (Fig. 5.10B, lanes 4 and 6). We used detergent to disrupt the liposomal bilayer, thus increasing the regions of protein accessible for proteolysis. Complete digestion of CobC was observed by proteinase K in the presence and absence of detergent (Fig. 5.10B, lanes 3 and 4). The level of undigested CobC remaining after incubation with trypsin remained the same regardless of whether or not detergent was added to the mixture. Collectively, these results suggested that CobC was not

inserted into the lipid bilayer, and that the interaction of CobC with the CobS proteoliposome was most likely due to protein-protein interactions independent of the lipid bilayer.

CONCLUDING REMARKS.

Collectively, work reported here provides insights into the challenges that cobamide-producing prokaryotes deal with when there is a need to scale up cobamide production. A clear obstacle is the amount of cobamide synthase embedded in the cell membrane. As supported by the evidence reported here, high levels of cobamide synthase protein generates two physiological stresses on the cell. First, it is clear that somehow excess CobS protein dissipates the PMF, and secondly, the membrane becomes more permeable to molecules that can alter the physiology of the cell in as-yet unknown ways. The consequences of excess CobS protein on the inner membrane lead to decreased cell viability. We speculate that these negative effects, elicited by both functional and enzymatically deficient CobS, are indicative of a pore-like structure of CobS. In sum, our working model proposes that cobamide synthase is one of several inner membrane proteins of the cobamide biosynthetic pathway that likely anchor a large multienzyme complex. We posit that, at a minimum, such a complex includes the AdoCbi-P synthase (CbiB) enzyme that catalyzes the last step of corrin ring biosynthesis, the CobC phosphatase that catalyzes the last step of the pathway. Evidence reported here support the recruitment of CobC by CobS in the inner membrane. In this working model, other enzymes involved in the synthesis of the nucleotide loop (*i.e.,*

CobU, CobT) are also postulated to associate with CobS to increase the efficiency of the synthesis of AdoCba.

It is remarkable that in all sequenced genomes of cobamide producers, CbiB and CobS are all likely to be integral membrane proteins, a fact that suggests, that an unknown, strong positive selection maintains cobamide synthesis in integral association with the cell membrane. It is noteworthy, that to date, not one CobS homologue found in genome databases has a sequence that would imply a cytosolic location. Clearly, cobamide biosynthesis poses chemical and physiological challenges to the cell, which apparently can only be met by involving the cell membrane and other enzymes in the nucleotide loop assembly pathway.

ACKNOWLEDGEMENTS

We thank Julie Nelson of the UGA Center for Tropical and Emerging Global Disease Cytometry Shared Resource Laboratory for assistance with the flow cytometry experiments and Vincent Starai for assistance with microscopy and liposome studies.

FUNDING

This work was supported by US PHS grant from the NIGMS R35-GM130399 to J.C.E.-S.

CONFLICT OF INTEREST

The authors have no conflict of interest to declare.

REFERENCES

1. Battersby, A.R., *Tetrapyrroles: the pigments of life.* Nat. Prod. Rep., 2000. **17**: p. 507-526.
2. Bryant, D.A., C.N. Hunter, and M.J. Warren, *Biosynthesis of the modified tetrapyrroles-the pigments of life.* J. Biol. Chem., 2020. **295**: p. 6888-6925.
3. Escalante-Semerena, J.C. and M.J. Warren, *Biosynthesis and use of cobalamin (B_{12})*, in *EcoSal - Escherichia coli and Salmonella: cellular and molecular biology*, A. Böck, et al., Editors. 2008, ASM Press: Washington, D. C.
4. Croft, M.T., et al., *Algae acquire vitamin B12 through a symbiotic relationship with bacteria.* Nature, 2005. **438**: p. 90-93.
5. Degnan, P.H., M.E. Taga, and A.L. Goodman, *Vitamin B12 as a modulator of gut microbial ecology.* Cell Metab., 2014. **20**: p. 769-778.
6. Bridwell-Rabb, J., et al., *A B12-dependent radical SAM enzyme involved in oxetanocin A biosynthesis.* Nature, 2017. **544**: p. 322-326.
7. Padmanabhan, S., et al., *A new facet of vitamin B12: Gene regulation by cobalamin-based photoreceptors.* Annu. Rev. Biochem., 2017. **86**: p. 485-514.
8. Chan, C.H. and J.C. Escalante-Semerena, *ArsAB, a novel enzyme from Sporomusa ovata activates phenolic bases for adenosylcobamide biosynthesis.* Mol. Microbiol., 2011. **81**: p. 952-967.

9. Keller, S., et al., *The SMUL_1544 gene product governs norcobamide biosynthesis in the tetrachloroethene-respiring bacterium Sulfurospirillum multivorans.* J. Bacteriol., 2016. **198**: p. 2236-2243.

10. Rodionov, D.A., et al., *Comparative genomics of the vitamin B_{12} metabolism and regulation in prokaryotes.* J. Biol. Chem., 2003. **278**: p. 41148-41159.

11. Shelton, A.N., et al., *Uneven distribution of cobamide biosynthesis and dependence in bacteria predicted by comparative genomics.* ISME J, 2019. **13**(3): p. 789-804.

12. Jeter, R.M., B.M. Olivera, and J.R. Roth, *Salmonella typhimurium synthesizes cobalamin (vitamin B12) de novo under anaerobic growth conditions.* J. Bacteriol., 1984. **159**: p. 206-213.

13. Woodson, J.D. and J.C. Escalante-Semerena, *CbiZ, an amidohydrolase enzyme required for salvaging the coenzyme B_{12} precursor cobinamide in archaea.* Proc. Natl. Acad. Sci. USA, 2004. **101**: p. 3591-3596.

14. Zayas, C.L., K. Claas, and J.C. Escalante-Semerena, *The CbiB protein of Salmonella enterica is an integral membrane protein involved in the last step of the de novo corrin ring biosynthetic pathway.* J. Bacteriol., 2007. **189**: p. 7697-7708.

15. O'Toole, G.A. and J.C. Escalante-Semerena, *Purification and characterization of the bifunctional CobU enzyme of Salmonella typhimurium LT2. Evidence for a CobU-GMP intermediate.* J. Biol. Chem., 1995. **270**: p. 23560-23569.

16. Thomas, M.G., et al., *Analysis of the adenosylcobinamide kinase/adenosylcobinamide-phosphate guanylyltransferase (CobU) enzyme of Salmonella typhimurium LT2. Identification of residue His-46 as the site of guanylylation.* J. Biol. Chem., 2000. **275**: p. 27576-27586.

17. Thompson, T.B., et al., *Three-dimensional structure of adenosylcobinamide kinase/adenosylcobinamide phosphate guanylyltransferase (CobU) complexed with GMP: evidence for a substrate-induced transferase active site.* Biochemistry, 1999. **38**: p. 12995-3005.

18. Trzebiatowski, J.R. and J.C. Escalante-Semerena, *Purification and characterization of CobT, the nicotinate-mononucleotide:5,6-dimethylbenzimidazole phosphoribosyltransferase enzyme from Salmonella typhimurium LT2.* J. Biol. Chem., 1997. **272**: p. 17662-17667.

19. Trzebiatowski, J.R., G.A. O'Toole, and J.C. Escalante-Semerena, *The cobT gene of Salmonella typhimurium encodes the NaMN: 5,6-dimethylbenzimidazole phosphoribosyltransferase responsible for the synthesis of N^1-(5-phospho-alpha-D-ribosyl)-5,6-dimethylbenzimidazole, an intermediate in the synthesis of the nucleotide loop of cobalamin.* J. Bacteriol., 1994. **176**: p. 3568-3575.

20. Cheong, C.G., J.C. Escalante-Semerena, and I. Rayment, *The three-dimensional structures of nicotinate mononucleotide:5,6-dimethylbenzimidazole phosphoribosyltransferase (CobT) from Salmonella typhimurium complexed with 5,6-dimethybenzimidazole and its*

reaction products determined to 1.9Å resolution. Biochemistry, 1999. **38**: p. 16125-16135.

21. Claas, K.R., et al., *Functional analysis of the nicotinate mononucleotide:5,6-dimethylbenzimidazole phosphoribosyltransferase (CobT) enzyme, involved in the late steps of coenzyme B_{12} biosynthesis in Salmonella enterica.* J. Bacteriol., 2010. **192**: p. 145-154.
22. Chan, C.H., et al., *Dissecting cobamide diversity through structural and functional analyses of the base-activating CobT enzyme of Salmonella enterica.* Biochim. Biophys. Acta, 2014. **1840**: p. 464-475.
23. Maggio-Hall, L.A., K.R. Claas, and J.C. Escalante-Semerena, *The last step in coenzyme B(12) synthesis is localized to the cell membrane in bacteria and archaea.* Microbiology, 2004. **150**: p. 1385-1395.
24. Maggio-Hall, L.A. and J.C. Escalante-Semerena, *In vitro synthesis of the nucleotide loop of cobalamin by Salmonella typhimurium enzymes.* Proc. Natl. Acad. Sci. U S A, 1999. **96**: p. 11798-11803.
25. O'Toole, G.A., J.R. Trzebiatowski, and J.C. Escalante-Semerena, *The cobC gene of Salmonella typhimurium codes for a novel phosphatase involved in the assembly of the nucleotide loop of cobalamin.* J. Biol. Chem., 1994. **269**: p. 26503-26511.
26. Zayas, C.L. and J.C. Escalante-Semerena, *Reassessment of the late steps of coenzyme B_{12} synthesis in Salmonella enterica: Evidence that dephosphorylation of adenosylcobalamin-5'-phosphate by the CobC*

phosphatase is the last step of the pathway. J. Bacteriol., 2007. **189**: p. 2210-2218.

27. Bertani, G., *Studies on lysogenesis. I. The mode of phage liberation by lysogenic Escherichia coli.* J. Bacteriol., 1951. **62**: p. 293-300.
28. Bertani, G., *Lysogeny at mid-twentieth century: P1, P2, and other experimental systems.* J. Bacteriol., 2004. **186**: p. 595-600.
29. Miroux, B. and J.E. Walker, *Over-production of proteins in Escherichia coli: mutant hosts that allow synthesis of some membrane proteins and globular proteins at high levels.* J. Mol. Biol., 1996. **260**: p. 289-298.
30. Galloway, N.R., et al., *Rapid cloning for protein crystallography using Type IIS restriction enzymes.* Crystal. Growth & Design, 2013. **13**(

): p. 2833-2839.

31. VanDrisse, C.M. and J.C. Escalante-Semerena, *New high-cloning-efficiency vectors for complementation studies and recombinant protein overproduction in Escherichia coli and Salmonella enterica.* Plasmid, 2016. **86**: p. 1-6.
32. Sambrook, J., E.F. Fritsch, and T. Maniatis, *Molecular Cloning: A Laboratory Manual*. Second ed. 1989, Cold Spring Harbor, N.Y.: Cold Spring Harbor Laboratory.
33. Laemmli, U.K., *Cleavage of structural proteins during the assembly of the head of bacteriophage T4.* Nature, 1970. **227**: p. 680-685.

34. Rigaud, J.L., B. Pitard, and D. Levy, *Reconstitution of membrane proteins into liposomes: application to energy-transducing membrane proteins.* Biochim. Biophys. Acta, 1995. **1231**: p. 223-246.

35. Winston, S.E., S.A. Fuller, and J.G.R. Hurrell, *Western blotting*, in *Current Protocols in Molecular Biology*, F.A. Ausubel, et al., Editors. 1990, Wiley Interscience: New York. p. 10.8.1-10.8.6.

36. Bulathsinghala, C.M., et al., *ExbB cytoplasmic loop deletions cause immediate, proton motive force-independent growth arrest.* J. Bacteriol., 2013. **195**: p. 4580-4591.

37. Maiden, M.M., M.P. Zachos, and C.M. Waters, *The ionophore oxyclozanide enhances tobramycin killing of Pseudomonas aeruginosa biofilms by permeabilizing cells and depolarizing the membrane potential.* J. Antimicrob. Chemother., 2019. **74**: p. 894-906.

38. Spindler, E.C., et al., *Deciphering the mode of action of the synthetic antimicrobial peptide Bac8c.* Antimicrob. Agents Chemother., 2011. **55**: p. 1706-1716.

39. Kleerebezem, M., W. Crielaard, and J. Tommassen, *Involvement of stress protein PspA (phage shock protein A) of Escherichia coli in maintenance of the protonmotive force under stress conditions.* Embo J., 1996. **15**: p. 162-171.

40. Kobayashi, R., T. Suzuki, and M. Yoshida, *Escherichia coli phage-shock protein A (PspA) binds to membrane phospholipids and repairs proton*

leakage of the damaged membranes. Mol. Microbiol., 2007. **66**: p. 100-109.

41. Darwin, A.J., *Stress relief during host infection: The phage shock protein response supports bacterial virulence in various ways.* PLoS Pathog, 2013. **9**(7): p. e1003388.
42. Zgurskaya, H.I. and H. Nikaido, *Bypassing the periplasm: reconstitution of the AcrAB multidrug efflux pump of Escherichia coli.* Proc. Natl. Acad. Sci. U S A, 1999. **96**: p. 7190-7195.
43. Takatsuka, Y. and H. Nikaido, *Covalently linked trimer of the AcrB multidrug efflux pump provides support for the functional rotating mechanism.* J. Bacteriol., 2009. **191**: p. 1729-1737.
44. Shapiro, H.M., *Flow cytometry of bacterial membrane potential and permeability.* Methods Mol. Med., 2008. **142**: p. 175-186.
45. Novo, D., et al., *Accurate flow cytometric membrane potential measurement in bacteria using diethyloxacarbocyanine and a ratiometric technique.* Cytometry, 1999. **35**: p. 55-63.
46. Fishov, I. and C.L. Woldringh, *Visualization of membrane domains in Escherichia coli.* Mol Microbiol, 1999. **32**(6): p. 1166-1172.
47. Pogliano, J., et al., *A vital stain for studying membrane dynamics in bacteria: a novel mechanism controlling septation during Bacillus subtilis sporulation.* Mol Microbiol, 1999. **31**(4): p. 1149-1159.

48. Chimerel, C., et al., *Indole prevents Escherichia coli cell division by modulating membrane potential.* Biochim Biophys Acta, 2012. **1818**(7): p. 1590-1594.

49. Strahl, H. and L.W. Hamoen, *Membrane potential is important for bacterial cell division.* Proc Natl Acad Sci U S A, 2010. **107**(27): p. 12281-12286.

50. Rocco, C.J., et al., *Construction and use of new cloning vectors for the rapid isolation of recombinant proteins from Escherichia coli.* Plasmid, 2008. **59**: p. 231-237.

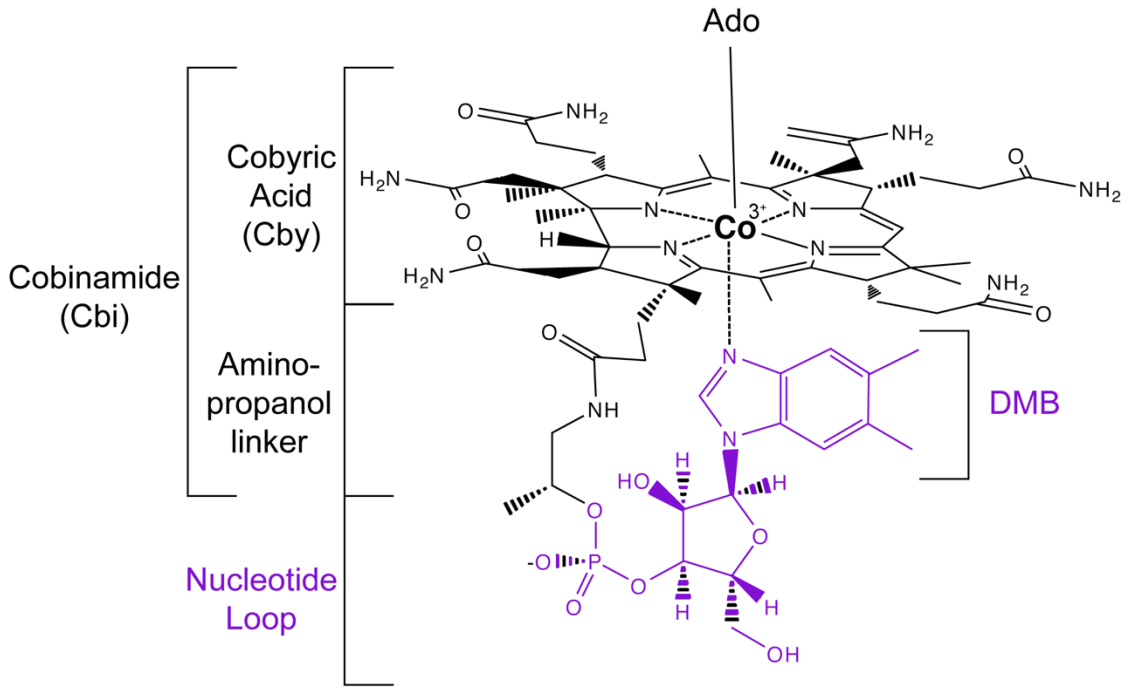

Figure 5.1. Adenosylcobalamin Structure. The chemical structure of cobalamin, a complete cobamide with 5'-deoxyadeonsine upper ligand and 5,6-dimethybenzimidazole lower ligand, is shown. The nucleotide loop is shown in purple.

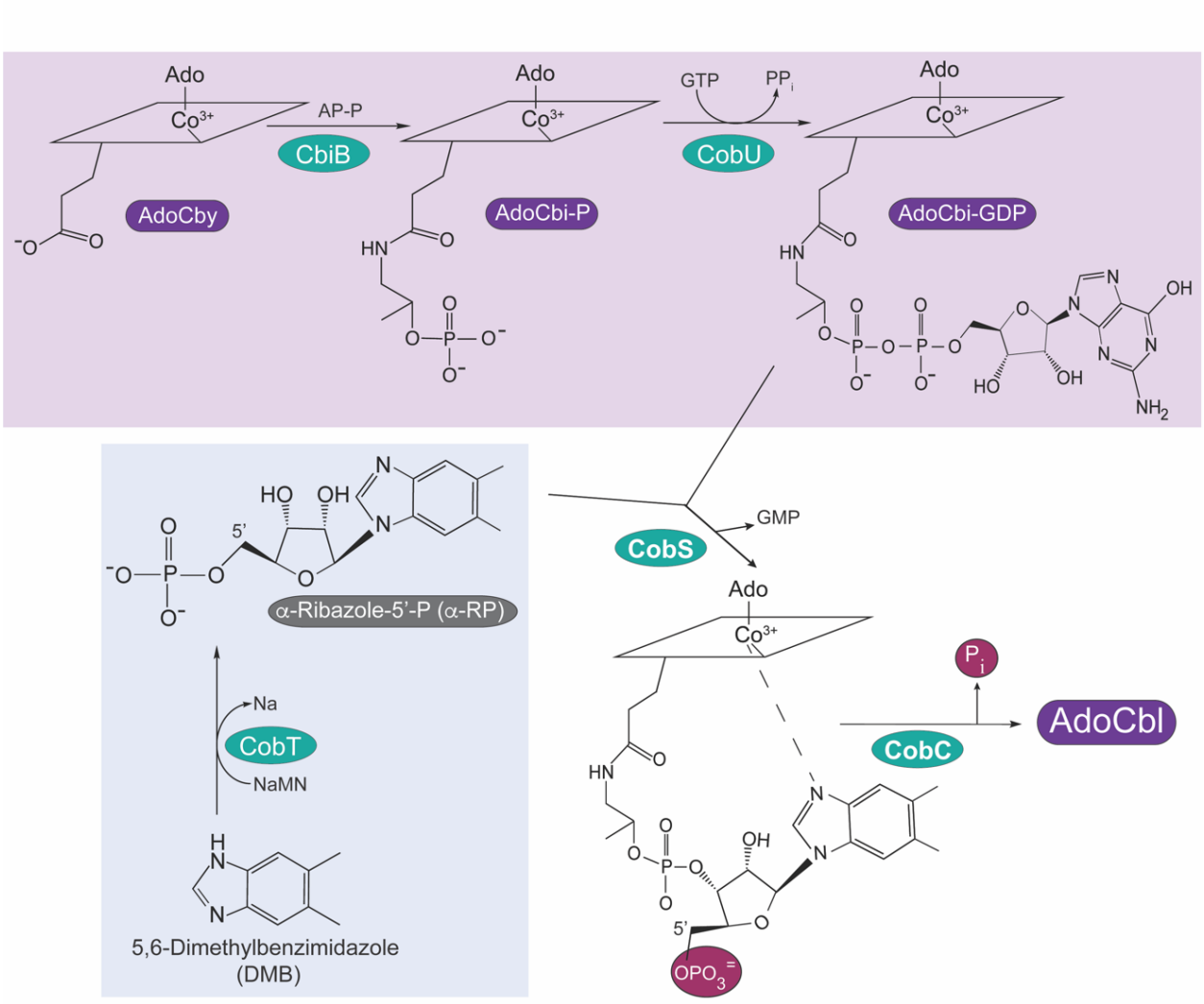

Legend on following page.

Figure 5.2. Nucleotide loop assembly pathway. The pathway for nucleotide loop assembly and attachment in *S.* Typhimurim is shown. Incomplete corrinoids enter the pathway from *de novo* synthesis or by uptake from the environment. Two pathways merge to generate a complete Cba: corrin ring activation highlighted in purple and base activation highlighted in blue. Corrin ring activation includes the attachment of an aminopropanol-phosphate (AP-P) moiety by CbiB and subsequent guanylylation by CobU. Base activation is performed by CobT to generate α-RP from DMB. CobS condenses the activated corrin ring and base substrates forming AdoCbl-P. In the final step, CobC dephosphorylates AdoCbl-P generating a complete AdoCbl.

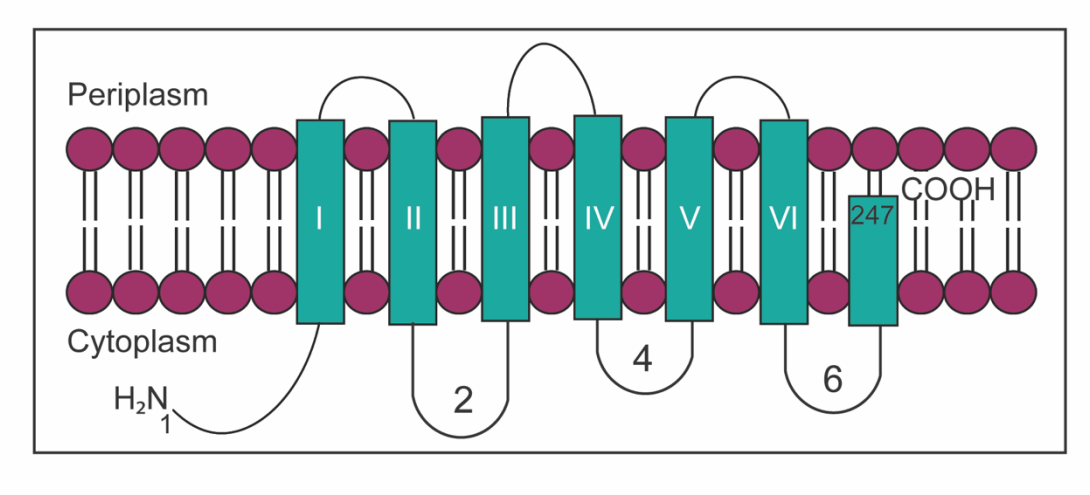

Figure 5.3. CobS is membrane associated. Polytopic integral membrane protein CobS topology is depicted. Transmembrane domains are indicated by roman numeral. Cytoplasmic loops are indicated in Arabic numerals.

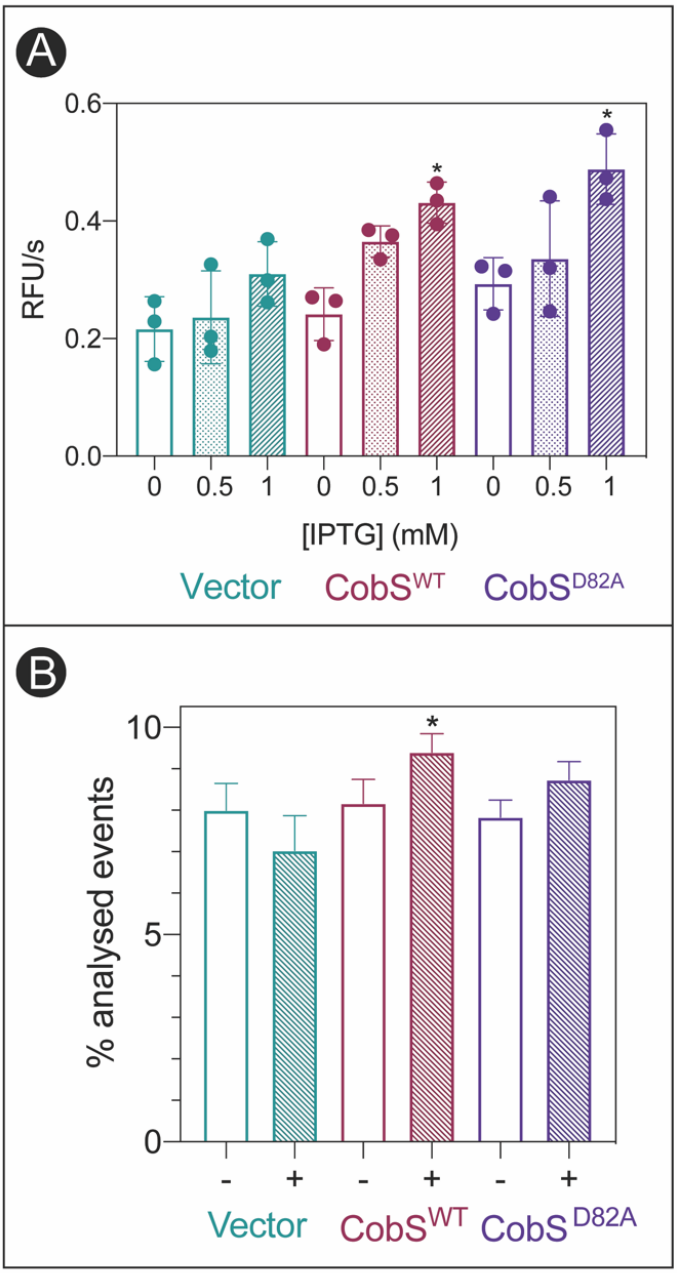

Legend on following page.

Figure 5.4. CobS expression compromises membrane stability. A. *E. coli* C41 cultures synthesizing CobS were grown in a microtiter dish to OD_{600} ~0.4, induced with ITPG (0.5 or 1 mM), and incubated for 30 min at 37 °C with shaking. Cells were stained with ethidium bromide and fluorescence at excitation = 530 nm/emission = 600 nm was monitored over 3 min. The rate of uptake is expressed as Relative Fluorescence Units per second as a function of increasing concentrations of IPTG for each condition. Experiments were conducted in biological triplicate with each experiment containing technical triplicates. Error bars represent standard error of the mean of technical triplicates. An unpaired student's t-test was performed compared to the vector control to determine statistical significance (*P<0.05). B. *E. coli* C41 (λDE3) cultures expressing *cobS* were grown to OD_{600} ~0.4, gene expression was induced with ITPG (1 mM), and incubated for 30 min at 37 °C with shaking at 180 rpm. Cells were stained with TO-PRO-3 and analyzed by flow cytometry to determine the number of cells that were permeabilized. Permeabilized cells are shown as percent averages plus the standard error of the mean for each condition tested. A paired *t*-test was performed to determine statistical significance compared to the empty vector (*p<0.05). Cells carrying the empty cloning vector or the *cobS* allele that encoded variant $CobS^{D82A}$ were analyzed as controls.

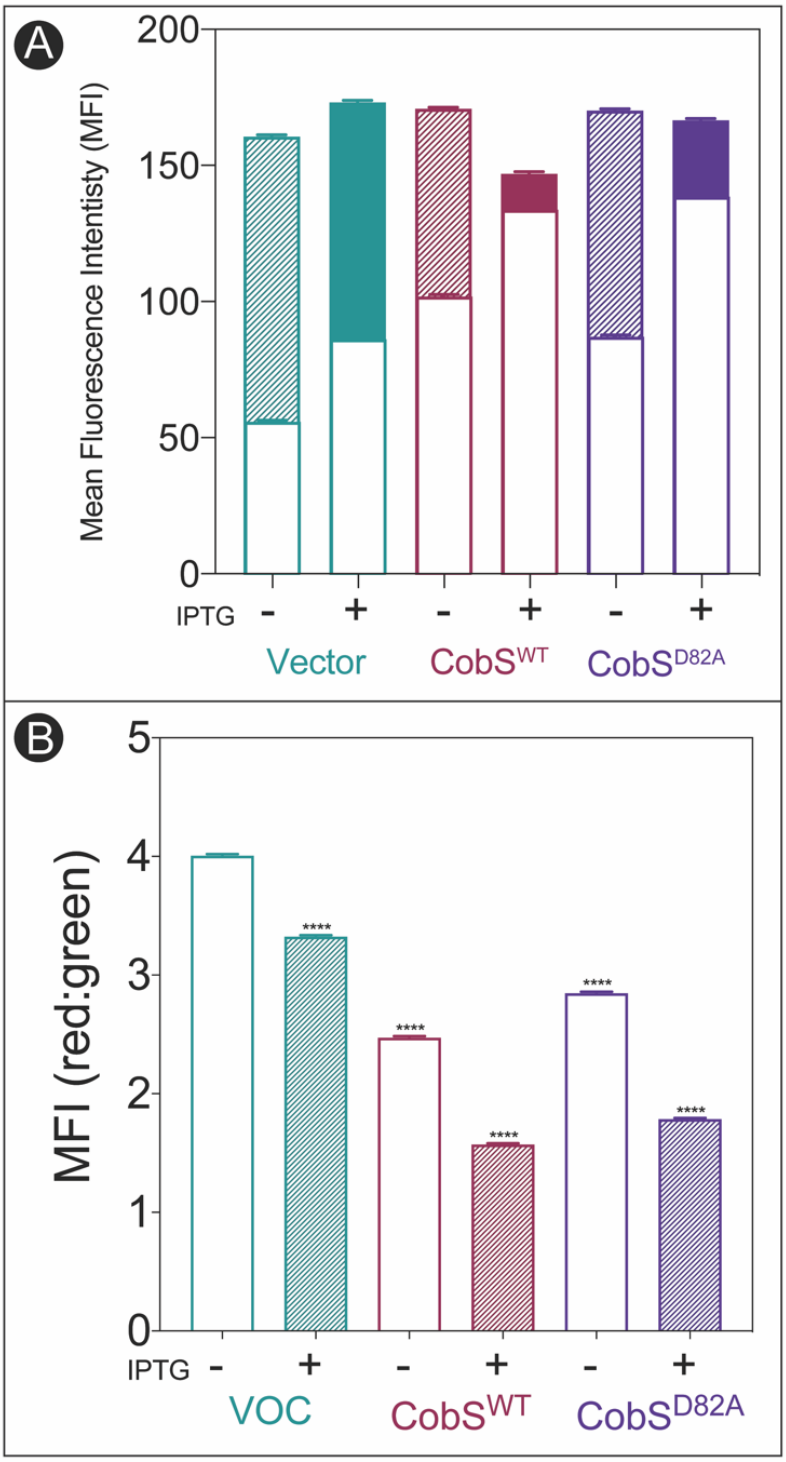

Legend on following page.

Figure 5.5. *In vivo* evidence that high CobS levels dissipate the PMF. *E. coli* C41 (λDE3) cultures synthesizing CobS were grown to OD_{600} ~0.4, gene expression was induced with ITPG (1 mM), followed by a 30-min incubation at 37°C with shaking at 180 rpm. Cells were stained with $DiOC_2(3)$ and analyzed by flow cytometry to determine membrane depolarization. Cells carrying the empty cloning vector and a vector carrying the *cobS* allele encoding $CobS^{D82A}$ were analyzed as controls. A. Mean Fluorescence Intensity (MFI) for both red (filled bars) and green (open bars) fluorescence is shown for each condition. B. The ratio of red to green fluorescence under each condition is shown. A one-way ANOVA followed by a *post hoc* Bonferroni's multiple comparison test was performed to determine the statistical significance between the empty vector control and CobS-synthesizing conditions (****p<0.0001).

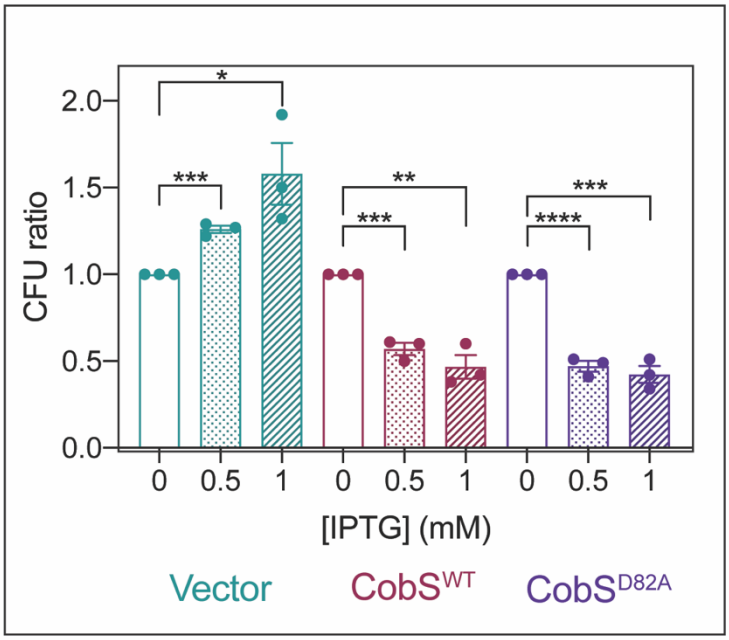

Figure 5.6. CobS expression decreases cell viability. *E. coli* C41 (λDE3) cultures synthesizing CobS were grown to OD_{600} ~0.4, gene expression was induced with ITPG (0.5mM and 1 mM), followed by a 30-min incubation at 37°C with shaking at 180 rpm. Cultures were diluted and colonies were counted after 16h growth at 37°C on LB 1.5% agar plates. Cells carrying the empty cloning vector and a vector carrying the *cobS* allele encoding $CobS^{D82A}$ were included as controls. The ratio of CFUs of cultures without induction compared to cultures with induction is shown. An unpaired student's *t*-test was performed to determine statistical significance between induced and non-induced conditions (*p 0.031, **p 0.0014, ***p 0.003, ****p<0.0001).

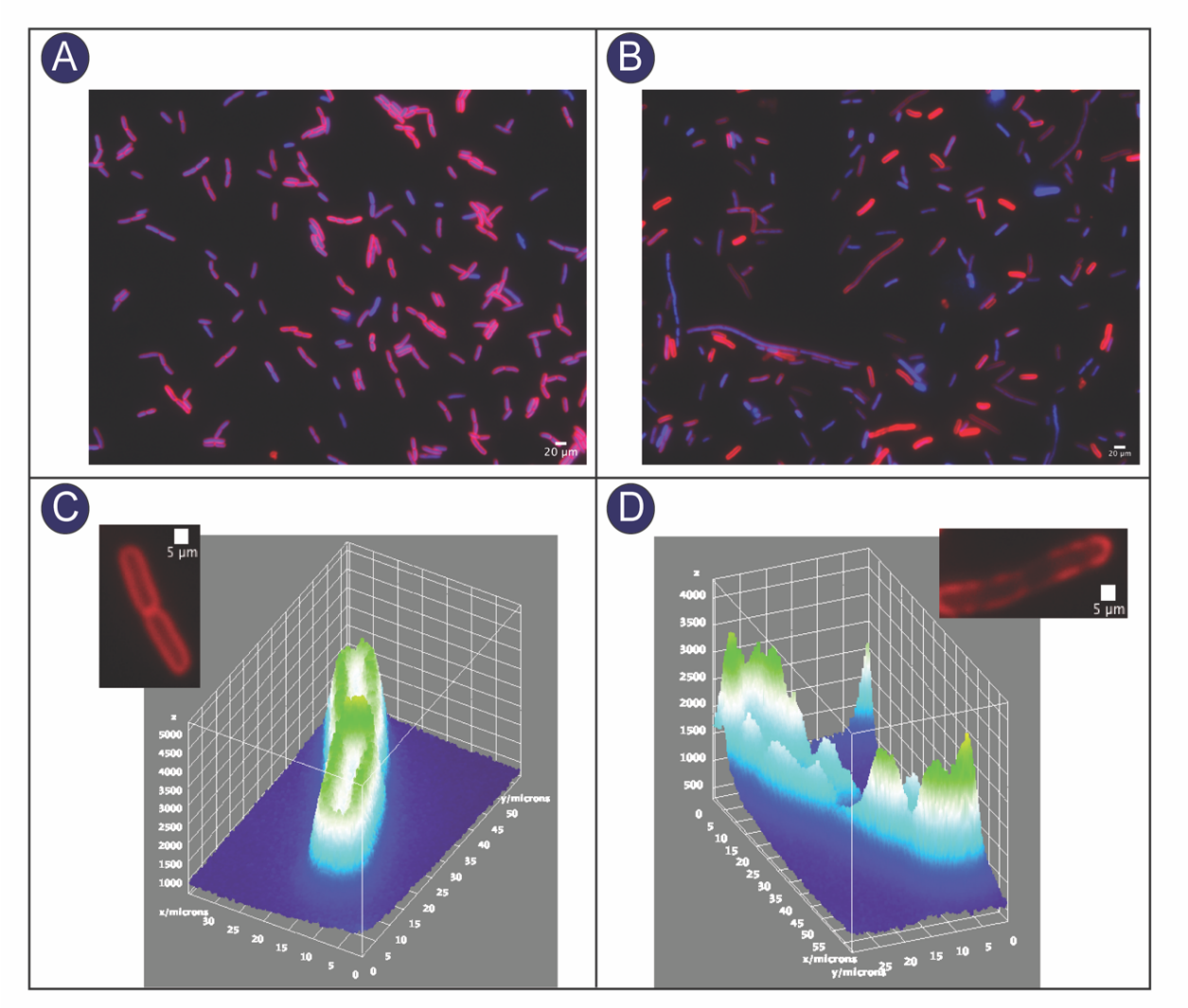

Legend on following page.

Figure 5.7. Microscopic evaluation of excess CobS on cell morphology. *E. coli* C41 (λDE3) cultures harboring an empty vector (A) or synthesizing CobS (B) were grown to OD_{600} ~0.4, gene expression was induced with ITPG (1 mM), followed by a 30-min incubation at 37°C with shaking at 180 rpm. Cells were stained with DAPI and FM4-64. C. Surface intensity plot of FM6-64 fluoresence from a cell carrying empty vector. Stained cell used to generate plot is shown. D. Surface intensity plot of FM6-64 fluoresence from a cell synthesizing CobS. Stained cell used to generate plot is shown. Scale in panels A and B is 20μm and panels C and D is 5μm. In panels C and D, the *z*-axis displays fluorescence intensity while the *x* and *y*-axes are plotted in microns.

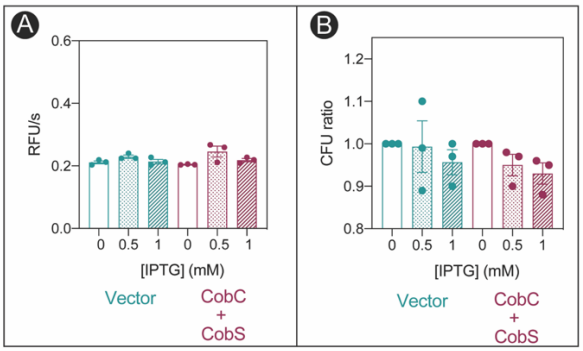

Figure 5.8. Coexpression of CobC ameliorates CobS induced membrane instability. A. *E. coli* C41 cultures synthesizing CobC and CobS were grown in a microtiter dish to OD_{600} ~0.4, induced with ITPG (0.5 or 1 mM), and incubated for 30 min at 37 °C with shaking. Cells were stained with ethidium bromide and fluorescence at excitation = 530 nm/emission = 600 nm was monitored over 3 min. The rate of uptake is expressed as Relative Fluorescence Units per second as a function of increasing concentrations of IPTG for each condition. Experiments were conducted in biological triplicate with each experiment containing technical triplicates. Error bars represent standard error of the mean of technical triplicates. No significant differences were observed across IPTG concentrations as determined by an unpaired student's t-test. B. *E. coli* C41 (λDE3) cultures synthesizing CobS and CobC were grown as previously described. Cultures were diluted and colonies were counted after 16h growth at 37°C on LB 1.5% agar plates. Cells carrying the empty cloning vector were included as a control. The ratio of CFUs of cultures without induction compared to cultures with induction is shown. An unpaired student's t-test determined there was no significant difference between strains and across IPTG concentrations.

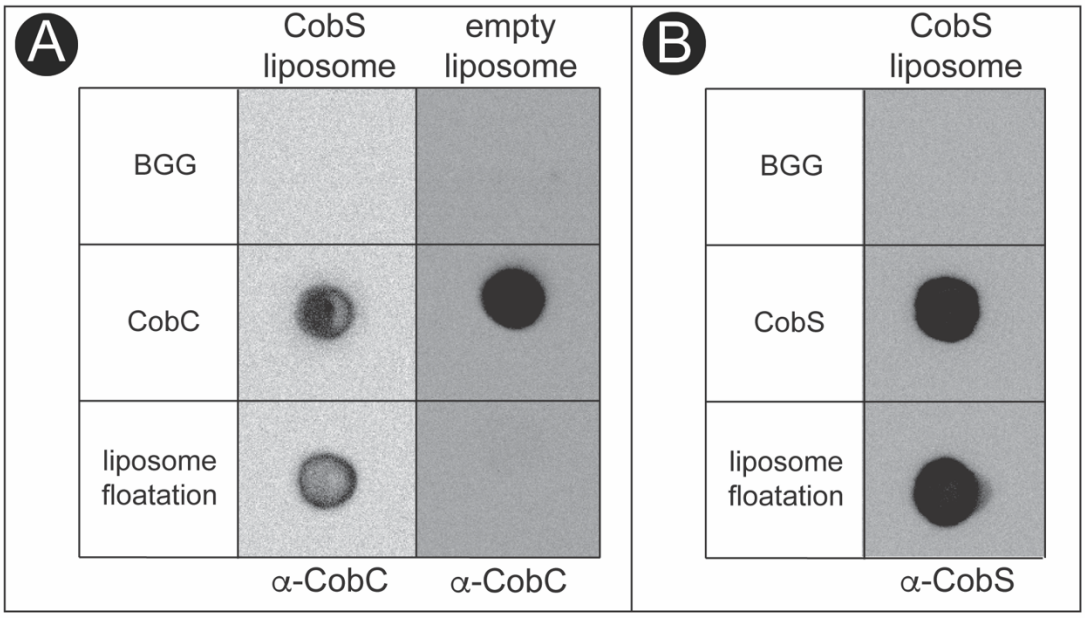

Figure 5.9. CobC interacts with CobS embedded in phospholipid bilayer. Dot Blot analysis of CobC-CobS proteoliposome complex. A. CobC was incubated with CobS-containing proteoliposomes or empty liposomes prior to floatation on Histodenz gradient. B. CobC-CobS proteoliposome complex probed Purified CobC and CobS were used as controls. BGG was used as a control for nonspecific binding.

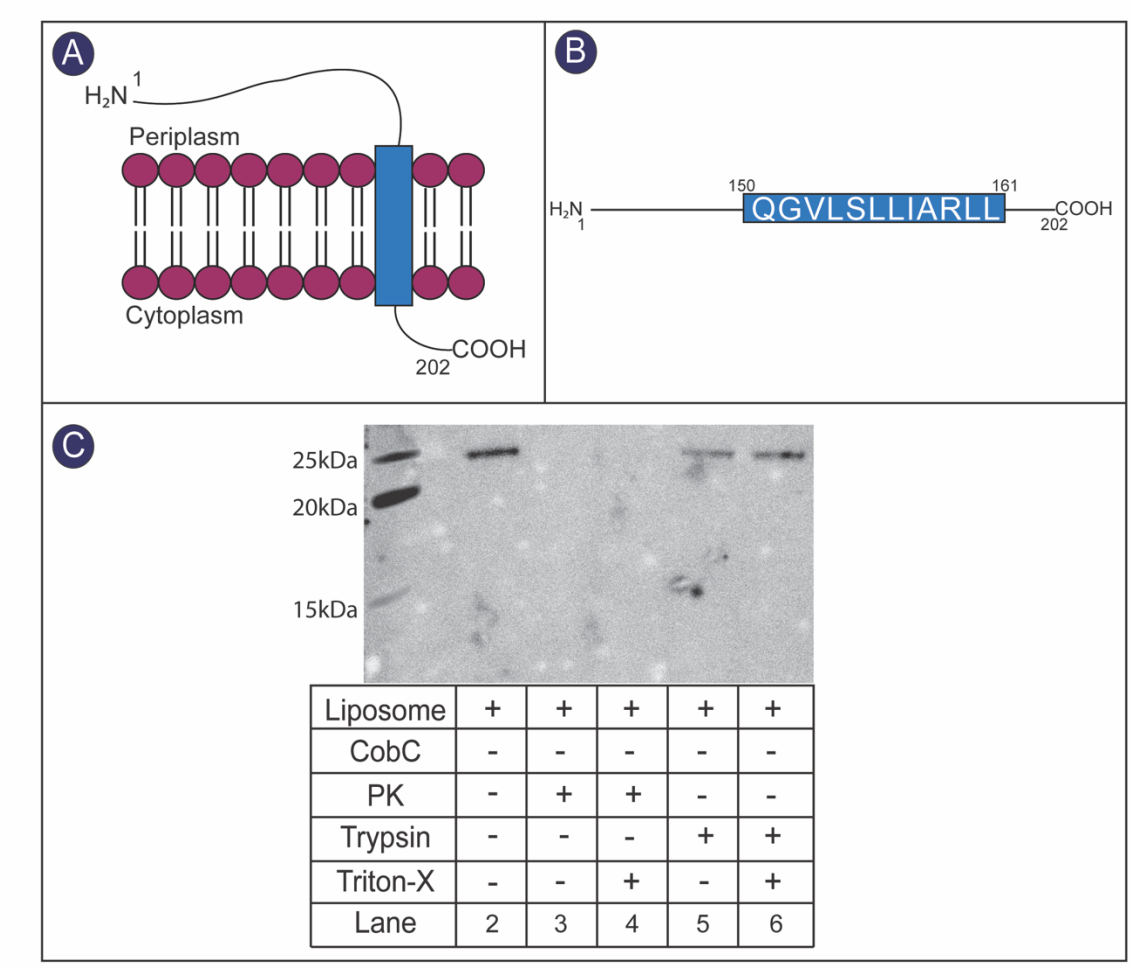

Figure 5.10. CobC does not insert into the phospholipid bilayer. B. Predicted CobC topology with *N*-terminus in the cytoplasm. B. Amino acid composition and location of predicted CobC transmembrane domain is shown. C**.** Western blot analysis of CobC-CobS containing proteoliposome complex proteolytic cleavage by proteinase K and trypsin using α-CobC antibodies. Detergent Triton-X 100 was added at 0.1% to disrupt the proteoliposome.

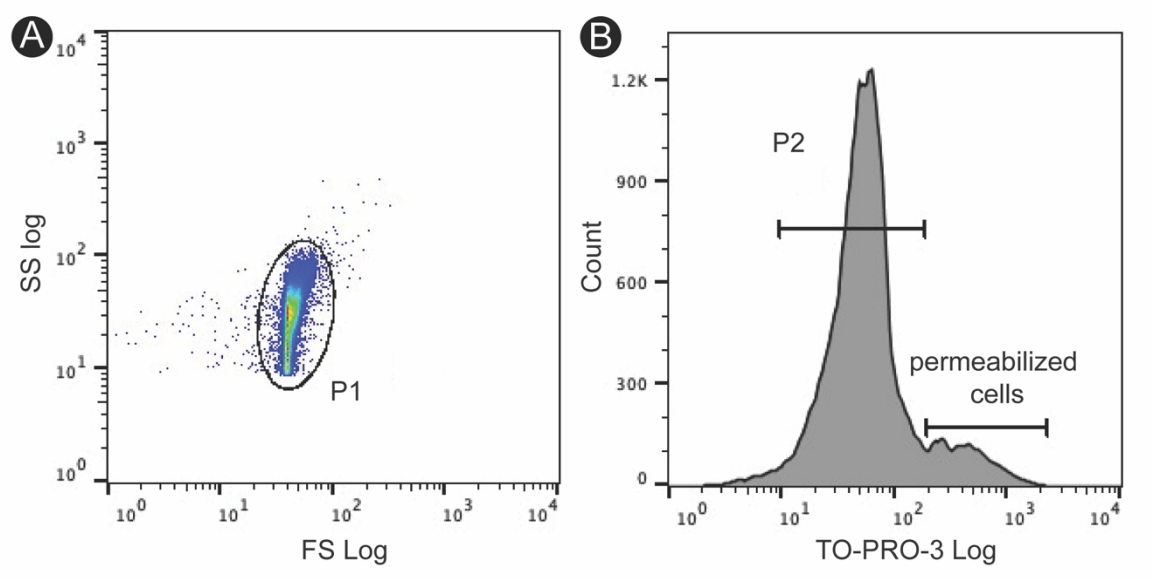

Figure 5.11. Flow cytometry analysis. A. Side scatter (SS log) and forward scatter (FS log) plots are gated to remove debris, yielding P1. B. TO-PRO-3 fluorescence is used to determine the percentage of the P1 population that is permeabilized. Intact cells are gated to yield P2. Cells treated with polymyxin B (1 μg/mL) were used to determine gating. Mean fluorescence intensity (MFI) of P2 is calculated for both red and green fluorescence of $DiOC_2(3)$. Cells treated with CCCP (5 μM) were used to determine gating of cells with compromised membrane potential ($\Delta\Psi$). The ratio of red:green MFI is used to compare the membrane polarization across populations.

Table 5.1. Strains and plasmids used in this work.

Strains	Genotype	Reference or Source
Escherichia coli strains		
JE6663 C41(λDE3)	F – *ompT hsdSB (rB- mB-) gal dcm* (λDE3)	Avidis
Plasmid	**Genotype**	**Source**
pTEV5	Overexpression vector that fuses the *N* terminus of the protein of interest to a H_6 tag, which can be removed by rTEV protease, *bla*$^+$	(50)
pTEV16	Overexpression vector that fuses the *N* terminus of the protein of interest to a H_6 tag, which can be removed by rTEV protease, *bla*$^+$	(31)
pRSFDUET-1	Overexpression vector that allows for co-expression of two ORFs, *kan*$^+$	Novagen
pCOBS5	*S.* Typhimurium *cobS*$^+$ cloned into vector pET-15b. The plasmid encodes a CobS protein with a histidine tag fused to its *N*-terminus	(24)
pCOBS120	*S.* Typhimurium *cobS*$^+$ cloned into vector pTEV16	
pCOBS121	*S.* Typhimurium *cobS1452.* This allele encodes variant CobS^{D82A}. The allele was cloned into vector pTEV16	
pCOBS122	*S.* Typhimurium *cobS*$^+$ MCS2 pRSFDUET-1	
pCOBS123	*S.* Typhimurium *cobC*$^+$ MCS1 *S.* Typhimurium *cobS*$^+$ MCS2 pRSFDUET-1	
pCOBS124	*E. coli pspA*$^+$ MCS1 *S.* Typhimurium *cobS*$^+$ MCS2 pRSFDUET-1	
pCOBC106	*S.* Typhimurium *cobC*$^+$ cloned into vector pTEV5	

Table 5.2. Primers used in this work.

Primer Name	Primer Sequence (5'-3')
cobS pCV1 F	NNGCTCTTCNTTCATGAGTAAGCTGTTTTGGGC
cobS pCV1 R	NNGCTCTTCNTTATAACAGAGCCAGCAGAA
CobS NdeI F	NNNNCATATGATGAGTAAGCTGTTTTGG
CobS KpnI R	NNNNGGTACCTAACAGAGCCAGCAG
CobC EcoRI F	NNNGAATTCGAGGAATACCATGCGA
CobC HindIII R	NNNAAGCTTTCACTCAGGCCGCCA
CobC NheI F	NNNGCTAGCGAGGAATACCATGCGA
CobC SacI R	NNNGAGCTCTCACTCAGGCCGCCA

CHAPTER 6

MEMBRANE ASSOCIATED COBAMIDE BIOSYNTHESIS: COBAMIDE SYNTHASE RECRUITS THE NUCLEOTIDE LOOP ASSEMBLY PATHWAY TO THE MEMBRANE[5]

[5]Jeter V.L., and Escalante-Semerena J.C. To be submitted to *mBio*.

ABSTRACT

Cobamides are complex cofactors utilized by organisms from all domains of life, but only produced *de novo* by some bacteria and archaea. *De novo* synthesis and precursor salvaging rely on the 'late steps' of the Cba biosynthetic pathway to assemble and attach the lower nucleotide ligand. The late steps are defined by activation of the corrin ring by bifunctional kinase/guanylyltransferase CobU, activation of the lower ligand base by phosphoribosyltransferase CobT, condensation of the activated precursors by cobamide synthase CobS to adenosylcobamide-phosphate, and cleavage of the phosphate by phosphatase CobC yielding a complete adenosylcobamide molecule. Condensation of the activated corrin ring and lower nucleotide base is catalyzed by integral membrane protein CobS. CobS catalyzes a critical step at the convergence of two branches of nucleotide loop assembly and membrane association of this step is found in all Cba producing organisms. Here we investigate the potential role of CobS as an anchor for localization of Cba biosynthesis to the inner membrane. We show that CobS recruits multiple enzymes involved in the assembly of the lower nucleotide loop when incorporated in a synthetic lipid bilayer. Additionally, we reconstitute the function of this multiprotein complex anchored by CobS *in vitro*.

INTRODUCTION

Cobamides are complex, cobalt-containing tetrapyrroles belonging to 'the pigments of life', a family of cofactors including hemes, chlorophylls and coenzyme F_{430} (1). *De novo* biosynthesis of Cbas is only found in some bacteria and archaea,

but Cbas are essential to cells from all three domains of life. Cbas are involved in myriad reactions including reductive dehalogenations, carbon skeleton rearrangements, methyl-group transfers, and elimination reactions (2). Cbas have also been shown to act as photoreceptors in certain biosynthetic pathways (3). Additionally, Cbas have been shown to be an important modulator in multi-organism communities (4, 5, 6).

Cbas are structurally unique compared to other cofactors by their upper (Coβ) and lower (Coα) coaxial ligands. All Cbas contain a central corrin ring, a cyclic tetrapyrrole with an equatorially coordinated cobalt. Cba diversity is represented by a broad range of lower ligand bases including purine and benzimidazole analogs as well as phenolics (7, 8). Cobalamin (Cbl) contains a 5,6-dimenthylbenzimidazole (DMB) lower ligand. An upper 5'deoxyadenosyl group is required for the coenzymic form, adenosylcobalamin (AdoCbl). The structure of adenosylcobalamin is shown in Figure 6.1.

The 'late steps' of Cba biosynthesis are responsible for the assembly and attachment of the nucleotide loop to the corrin ring (Fig. 6.2). These steps are referred to as Nucleotide Loop Assembly (NLA) and involves two distinct branches: 1.) activation of the corrin ring and 2.) activation of the nucleotide base. In *S.enterica*, NLA is required to complete *de novo* Cba synthesis and in salvaging corrin ring precursors from the environment. Before activation of the corrin ring, AdoCbi-P synthase (CbiB EC 6.3.1.10) attaches an aminopropanol-phosphate linker to the corrin ring to form AdoCbi-P (9). Activation of the corrin ring is catalyzed by bifunctional AdoCbi:NTP kinase/ GTP:AdoCbi-P guanylyltransferase

(CobU EC 2.7.7.62/ 2.7.1.156) forming AdoCbi-GDP (10, 11, 12). In the other branch of the pathway, DMB is activated to α-ribazole-phosphate (α-RP) by the nicotinate mononucleotide (NaMN):DMB phosphoribosyltransferase (CobT EC 2.4.2.21) (13, 14, 15, 16). The activated corrin ring AdoCbi-GDP and activated base a-RP are joined by cobamide (5' phosphate) synthase (CobS EC 2.7.8.26) forming adenosylcobalamin 5'-phosphate (AdoCbl-P) (17,18,19). In the final step, adenosylcobamide/α-ribazole phosphatase (CobC EC 3.1.3.73) dephosphorylates AdoCbl-P to generating AdoCbl (20).

Notably, two of the enzymes involved in synthesis and attachment of the nucleotide base are polytopic integral membrane proteins: CbiB and CobS (18,9). These enzymes are predicted to be membrane associated in all organisms that synthesize Cbas, prompting us to explore the role of membrane association in the late steps of Cba biosynthesis and the potential for localization of key enzymes to the membrane. Previously, we have reported on the characterization of CobS (Chapter 4) and the implications of excess CobS (Chapter 5). We identified a protein-protein interaction between CobC and CobS reconstituted in a lipid bilayer (Chapter 5). Here we expand our understanding of the multienzyme complex involving CobS by identifying additional interactions with both CobT and CobU. Additionally, we show CobS embedded in a lipid bilayer is sufficient to recruit CobUTC and NLA activity is reconstituted in the resulting multi-protein complex.

MATERIALS AND METHODS

Bacterial strains, culture media, and chemicals. All chemicals were purchased from Sigma-Aldrich unless otherwise noted. Bacterial strains used in this study are listed in Table 6.1. All strains for growth analysis were derivatives of *Salmonella enterica enterica* sv Typhimurium LT2 (*S.* Typhimurium) or *Escherichia coli* C41 (λDE3). *S.* Typhimurium strains were grown at 37 °C on lysogeny broth (LB, Difco) (21, 22) or no-carbon essential (NCE) minimal medium (23) supplemented with glycerol (22 mM), $MgSO_4$ (1 mM), and Wolfe's trace minerals (24). Cbl (added as CNCbl) was provided at a concentration of 100 nM. *Escherichia coli* C41 (λDE3) strains were grown at 37 °C on lysogeny broth (LB, Difco) 21, 22. *Escherichia coli* C41 (λDE3) 25 was used for protein overexpression. *E. coli* K12 strain DH5α (New England Biolabs) was used for plasmid construction. Antibiotics for all media were used at the following concentrations: ampicillin, 100 μg mL^{-1}. All chemicals were purchased from Sigma-Aldrich unless otherwise noted; isopropyl β-D-1-thiogalactopyranpside (IPTG, Gold BioTechnology), glycerol (Fisher), 4-(2-hydroxyethyl)-1-piperazineethanesulfonic acid buffer (HEPES, Gold BioTechnology) 3-[(3-Cholamidopropyl)dimethylammonio]-1-propanesulfonate detergent (CHAPS, Gold BioTechnology), 1-palmitoyl-2-oleoyl-glycero-3-phosphocholine (POPC, Avanti Polar Lipids), 1-palmitoyl-2-oleoyl-*sn*-glycero-3-phosphoethanolamine (POPE, Avanti Polar Lipids), 1-palmitoyl-2-oleoyl-*sn*-

glycero-3-phoshpo-L-serine (POPS, Avanti Polar Lipids), Lissamine^{TM} Rhodamine B 1,2-Dihexadecanoyl-*sn*-glycero-3-phosphoethanolamine (Rh-DHPE, Molecular Probes).

Strain construction and bioassay growth analysis. In-frame deletions of *S. enterica* genes were constructed using the phage lambda Red recombinase system as described 26. For growth analyses, 2-mL starter cultures in 13 x 100 mm borosilicate cultures tubes were grown 16 h at 37 °C with shaking at 180 rpm in LB containing appropriate antibiotic. Growth experiments were performed in 96-well microtiter dishes (Falcon), with each well containing 198 μl of medium plus 2 μl of inoculum. To test for Cba production in CobS proteoliposome complexes, 2μL of 0.22μM filtered reaction mixtures were added to the medium. The growth behavior of three technical replicates of each strain was analyzed, and the experiment was performed thrice. Growth was monitored using a computer-controlled plate reader (BioTek, Model Eon). The optical density at 630 nm was measured every 15 min for a total time of 24 h; the microtiter dish was shaken between measurements. Data were analyzed using GraphPad Prism version 8.

CobS protein overproduction and purification. CobS overproduction and purification were based on methods described elsewhere 19 with modifications. CobS^{WT} protein was overproduced from plasmid pCOBS5 in strain JE6663 [(*E. coli* C41 (λDE3)] in 2-L cultures of Terrific Broth 27. Protein synthesis was induced by

the addition of IPTG at a final concentration of 500 μM in mid-log phase cultures (OD_{600} ~ 0.6) growing at 37 °C while shaking at 180 rpm in an Innova44 gyratory incubator (New Brunswick Scientific). After induction, cultures were grown for 3 h at 37 °C while shaking at 180 rpm. Cultures were harvested by centrifugation at 4 °C for 15 min at 6,000 x *g* in an Avanti J20-XPI refrigerated centrifuge equipped with a JLA-8.1000 rotor. Pelleted cells were stored at −20 °C until used. For protein purification, cell pellets were thawed and resuspended in 30 ml of Tris-HCl buffer (100 mM, pH 7.9, 24°C). Cells were lysed with a cell press in a cell disruptor (Constant Systems) set at 1.72×10^5 kPa. A sample (0.5 mL) of a protease inhibitor cocktail (Sigma) was added to cell-free extracts (CFEs) to minimize CobS degradation during purification. CFEs were obtained after centrifugation at 4°C, at 5,000 x *g* for 15 min. Cell membranes were obtained from a high-speed centrifugation at 75,000 x *g* for 90 min in an Avanti J-25I Beckman/Coulter refrigerated centrifuge equipped with a JA-25.50 rotor. Membranes were resuspended in 10 ml of 0.1 M Tris-HCl buffer (pH 7.9, 24°C) with a glass homogenizer and were solubilized by the addition of CHAPS detergent to a final concentration of 20 mM. The detergent-containing CFE was incubated on ice for 1 h and centrifuged at 4°C at 75,000 x *g* for 30 min to remove solubilized contaminants. The insoluble fraction containing CobS was resuspended in 10 ml of Tris-HCl buffer (100 mM, pH 7.9 at 24°C) containing NaCl (500 mM) and imidazole (20 mM) with a glass homogenizer and solubilized by the addition of 1,2-diheptanoyl-*sn*-glycero-3-phosphocholine (DHPC) to a final concentration of 15 mM. DHPC was added slowly to avoid denaturation of proteins. The CFE fraction

containing detergent-solubilized CobS was incubated on ice for 1 h and centrifuged at 4°C at 75,000 x *g* for 30 min. A HisPur nickel-nitrilotriacetic acid (Ni-NTA) resin (2-mL bed volume, Thermo Scientific) was equilibrated with 10 bed volumes of water and 10 bed volumes of Tris-HCl buffer (100 mM, pH 7.9 at 24°C) containing NaCl (500 mM) and imidazole (20 mM). CFE containing solubilized CobS protein was incubated with the HisPur resin at 4 ºC with nutation for a minimum of 2 h before pouring the slurry into a column (Kontes FLEX-COLUMN 1.0 x 10cm). The column was washed with five bed volumes of Tris-HCl buffer (100 mM, pH 7.9 at 24°C) containing NaCl (500 mM) and imidazole (20 mM) and DHPC (15 mM) then five bed volumes of Tris-HCl buffer (100 mM, pH 7.9 at 24°C) containing NaCl (500 mM) and imidazole (60 mM) and DHPC (15 mM). Proteins were eluted with five bed volumes of Tris-HCl buffer (100 mM, pH 7.9 at 24°C) containing NaCl (500 mM) and imidazole (500 mM) and DHPC (15 mM). Proteins in fractions of interest were resolved by sodium dodecyl sulfate polyacrylamide gel electrophoresis (SDS-PAGE)(28) and CobS-containing fractions were applied to a 5-mL Zeba Spin desalting column (ThermoFisher) to remove imidazole. Glycerol (10% [v/v], final concentration) was added to a desalted CobS sample, which was flash frozen in liquid N_2 prior to storage at -80 °C. The final buffer composition before storage was Tris-HCl buffer (100 mM, pH 7.9 at 24°C) containing NaCl (150 mM) and DHPC (15 mM). Protein concentration was determined using a Bradford Assay kit (Bio-Rad Laboratories). A typical CobS preparation yielded 0.5mg/g of cells.

CobC protein overproduction and purification. Wild-type CobC protein was overproduced from plasmid pCOBC106 in strain JE6663 (*E. coli* C41) in 1L cultures of Terrific Broth (27). Protein synthesis was induced by the addition of IPTG at a final concentration of 1 mM in mid-log phase cultures (OD_{600} ~0.6) growing at 37°C with shaking at 180 rpm in an Innova44 (New Brunswick Scientific) gyratory incubator. After induction, cultures were grown for 17 h at 24°C with shaking at 180 rpm. Cultures were harvested by centrifugation at 4°C for 15 min at 6,000 x *g* in an Avanti J20-XPI refrigerated centrifuge equipped with JLA-8.1000 rotor. Pelleted cells were stored at -20°C until used. Frozen cells were thawed on ice and re-suspended in HEPES buffer (50 mM, pH 7.5) containing NaCl (0.5 M) and imidazole (20 mM) at a rate of 20% cell weight to buffer volume. Lysozyme (1μg/mL) and DNaseI (25μg/mL) were added to the cell suspension and incubated on ice for 10 min. Cells were lysed by sonication. Phenylmethylsulfonyl fluoride (PMSF) was added to the cell lysate at a final concentration of 0.5 mM. Cellular debris was removed by centrifugation at 4°C for 30 min at 40,000 x *g* in an Avanti J-251 centrifuge (Beckman/Coulter) equipped with a JA 25.25 rotor. Clarified extract was filtered using a 0.45-μm syringe filter unit and applied to a 2-mL HisPur nickel-nitrilotriacetic acid (Ni-NTA) affinity column (ThermoFisher Scientific). The column was washed with 10 column volumes of HEPES buffer (25 mM, pH 7.5) containing NaCl ((0.5 M) and imidazole (20 mM) and six column volumes of HEPES buffer (25 mM, pH 7.5) containing NaCl (0.5 M)) and imidazole (40 mM). H_6-CobC was eluted with six column volumes of HEPES buffer (25 mM, pH 7.5)

containing NaCl (0.5 M) and imidazole (0.5 M). Fractions were collected throughout the wash and elution steps and H_6-CobC purification was monitored by SDS-PAGE compared to Precision Plus Protein Standards (BioRad). Fractions containing H_6-CobC were pooled and dialyzed against HEPES buffer (25 mM, pH 7.5) containing NaCl (0.5 M) to remove imidazole. H_6-CobC was then dialyzed against HEPES buffer (25 mM, pH 7.5) in 3 additional steps with decreasing concentrations of NaCl down to 150 mM. Purified H_6-CobC was flash frozen in liquid nitrogen and stored at -80°C until used. Protein concentration was measured using a Bradford Assay Kit (Bio-Rad laboratories).

CobU protein overproduction and purification. CobU protein was purified as previously outlined (11).

CobT protein overproduction and purification. CobT protein was purified as previously outlined (15).

Liposome preparation and protein reconstitution. The lipids used in the study were POPC, POPE, POPS and Rh-DHPE. Proteoliposomes were prepared using detergent-mediated reconstitution as described elsewhere 29. POPC:POPS:POPE:Rh-DHPE were combined at a molar ratio of 80:10:9.5:0.5 to yield 1 μmol lipid. Lipids were dried under a stream of N_2 gas and spun in an Eppendorf VacFuge at 30 ºC for 1 h. The dried lipid film was hydrated in 500 μl of

HEPES buffer (20 mM, pH 7.4) containing NaCl (500 mM), CHAPS (40 mM) and glycerol (10% [v/v]) to a final lipid concentration of 2 mM. Detergent-solubilized $CobS^{WT}$ was added at a lipid-to-protein molar ratio of 1000:1 and incubated with rotation on a Benchmark RotoBot at 4 °C for 1 h. Detergent removal and proteoliposome formation was achieved by four 20-h dialyses using Slide-A-Lyzer dialysis cassettes (20 kDa molecular mass cutoff) against HEPES buffer (20 mM, pH 7.4) containing NaCl (500 mM) and glycerol (10% [v/v]). Dialysis was performed at a dialysate:sample volumetric ratio of 2000:1. After dialysis, the proteoliposome suspension was applied to a Histodenz (Sigma) gradient to perform a liposome flotation assay. The proteoliposome suspension was mixed with an equal volume with HEPES buffer (20 mM, pH 7.4) containing NaCl (150 mM), Histodenz (80% [w/v]), glycerol (10% [v/v]) and deposited in a Beckman Coulter Ultracentrifuge tube (polyallomer, 13 x 51 mm). A 4-mL overlay of HEPES (20 mM, pH 7.4) containing NaCl (150 mM), Histodenz (30% [w/v]), glycerol (10% [v/v]) was applied followed by a 200-μL overlay of HEPES buffer (20 mM, pH 7.4) containing NaCl (150 mM), glycerol (10% [v/v]). The gradient was subjected to centrifugation at 4 °C for 3 h at 268,000 x *g* in a refrigerated Beckman Coulter Optima™ MAX-XP Ultracentrifuge using an MLS-50 rotor. Lipid concentration of the reconstituted liposomes was determined by a standard curve generated from fluorescence of Rh-DHPE. Fluorescence measurements were read on a BioTek Gemini instrument set at an excitation wavelength of 540 nm and emission wavelength of 586 nm. Protein concentration in proteoliposomes was determined by generating a

standard curve. Briefly, a range of known bovine γ-globulin (BGG) and lysozyme concentrations were separated by SDS-PAGE with unknown concentrations of CobS-containing proteoliposomes stained with Oriole Fluorescent stain and analyzed using TotalLab TL100 software. The presence of CobS in liposomes was confirmed by western blot and mass spectrometry analyses.

Liposome Flotation Assay. To probe for interactions between CobC and CobS or CobC and the lipid bilayer, liposome flotation assays using CobS-containing proteoliposomes and empty liposomes were employed. Purified CobC, CobU, and/or CobT protein (final concentration of 10μM) was incubated with 100μL of a 2mM lipid solution of CobS proteoliposomes or empty liposomes for 1 hour at 24°C on a Benchmark RotoBot. For binding order experiments, reactions were similarly prepared with a 1 h incubation at 24°C on a Benchmark RotoBot after each enzyme was added. When added, GTP (2mM) and α-RP (50μM) were allowed to preincubate for 15 minutes at 37 ºC with CobU or CobS proteoliposomes respectively. This mixture was mixed with an equal volume with HEPES buffer (20 mM, pH 7.4) containing NaCl (150 mM), Histodenz (80% [w/v]), glycerol (10% [v/v]) and deposited in a Beckman Coulter Ultracentrifuge tube (polyallomer, 11 x 34 mm). A 2.5-mL overlay of HEPES (20 mM, pH 7.4) containing NaCl (150 mM), Histodenz (30% [w/v]), glycerol (10% [v/v]) was applied followed by a 150-μL overlay of HEPES buffer (20 mM, pH 7.4) containing NaCl (150 mM), glycerol (10% [v/v]). The gradient was subjected to centrifugation at 4 °C for 3 h at 214,000 x *g*

in a refrigerated Beckman Coulter Optima™ MAX-XP Ultracentrifuge using a TLS-55 rotor. The top layer was harvested and lipid concentration was determined by rhodamine fluorescence. A standard curve was generated by measuring the fluorescence of a series of rhodamine concentrations with a SpectraMax Gemini EM microplate reader (Molecular Devices) at excitation 540nm and emission 586nm.

Dot blot and far western analysis. To confirm the presence of CobC, CobU, CobT, and CobS in liposome flotation mixtures dot blots were performed using rabbit polyclonal antibodies generated against CobC, CobT, CobU and loop 2 of CobS. For dot blot analysis, 3μL of 1mM lipid proteoliposome complexes obtained by liposome flotation and 100ng of positive and nonspecific controls were spotted on a nitrocellulose membrane. Membranes were incubated for 30 min in blocking buffer of phosphate buffered saline containing Tween 20 (PBST) comprised of NaH_2PO_4 (10 mM, pH 7.2), NaCl (0.9% w/v), and Tween 20 (0.1% v/v), and instant dry milk (5%, w/v). Membranes were then probed with α-CobC, α-CobU, α-CobT or α-CobS antibodies (1:5,000 in blocking buffer) for 1 h, then washed thrice (30 min each) with PBST. Membranes were then probed for 1 h with horseradish peroxidase (HRP)-conjugated goat α-rabbit secondary antibodies (Sigma) in PBST (1:10,000) before three, 30-min washes with PBST. Membranes were incubated in SuperSignal West Pico PLUS chemiluminescent substrate (ThermoFisher) for 5 min and imaged using a UVP ChemStudio imaging

instrument (AnalytikJena). Purified CobU, CobT, CobC, or CobC protein was used as positive control and bovine gamma globulin (BGG) was used as a control for nonspecific binding.

For far western assays, CobU and CobT were deposited in 3μL spots on nitrocellulose membranes in varying amounts: 9μg, 4.5μg, 2.25μg, 1.13μg, and 0.6μg. Membranes were allowed to dry for an hour before a 30 min incubation in blocking buffer. Interactions were facilitated by incubating membranes in blocking buffer supplemented with 500nM CobS or CobS proteoliposomes for 1 h, then washed thrice (30 min each) with PBST. Membranes were then probed with monoclonal mouse anti-6xHis mouse antibodies conjugated to fluorophore CF680 in PBST (1:2,000) for 1 h before three, 30 min washes with PBST. All steps performed after addition of CF680 conjugated antibodies were kept in the dark. Membranes were imaged using red light and 700nm filter on a UVP ChemStudio imaging instrument (AnalytikJena). Bovine gamma globulin (BGG) was used as a control for nonspecific binding.

AdoCbi, AdoCbi-P, AdoCbi-GDP and α-RP substrate preparation. The substrates of CobS, CobU and CobC, namely AdoCbi, AdoCbi-P, AdoCbi-GDP and α-RP were not commercially available and were synthesized as described elsewhere 17, 19. Dicyanocobinamide [$(CN)_2$Cbi] was incubated with ATP and homogeneous ATP:Co(I)rrinoid adenosyltransferase CobA protein purified as described 30. The reaction mixture was incubated for 16 h at 37 °C under dark,

anoxic conditions. The product of the reaction, adenosylcobinamide (AdoCbi) was separated from other reaction components using a Waters Sep-Pak C18 column. AdoCbi was eluted off the column with 100% methanol. Methanol was removed using an Eppendorf VacFuge for 16 h. Dried AdoCbi was resuspended in a reaction mixture containing GTP or ATP and homogeneous NTP:$(HO)_2$Cbi kinase, GTP:AdoCbi guanylyltransferase CobU enzyme purified as described elsewhere 11 and incubated at 37 °C for 16 h in the dark to yield AdoCbi-P and AdoCbi-GDP. AdoCbi-P or AdoCbi-GDP were separated from reaction components using a Waters Sep-Pak C18 column, and subsequently eluted off the column with 100% methanol. Methanol was removed using an Eppendorf VacFuge for 16 h. AdoCbi-GDP was resuspended in water and its identity confirmed by its UV-visible spectrum. AdoCbi-P and AdoCbi-GDP were quantified by reading the absorbance at 367 nm after incubation with KCN at 90 °C for 10 min.

α–RP was synthesized as described elsewhere 31. DMB was incubated with NaMN and homogeneous NaMN:DMB phosphoribosyltransferase CobT enzyme 13 16 h at 37°C. α–RP was separated from reaction components by HPLC as described 32. Fractions containing α–RP were pooled, applied to a Waters Sep-Pak C18 column and eluted with 100 % methanol. Methanol was removed by 16h vacuum centrifugation using an Eppendorf VacFuge, and α–RP was quantified by reading absorbance at 280 nm.

Enzyme Assays. The activity of enzymes in complex with CobS proteoliposomes was tested and assayed via bioassay as described above. Reactions were performed in 100μL of HEPES buffer (20 mM, pH 7.4) containing NaCl (150 mM), glycerol (10% [v/v]) with 50μL of proteoliposome complex at 1mM lipid. For CobU-CobS protelipoosome assays, AdoCbi (500μM), GTP (2mM), $MgCl_2$ (2mM) and a-RP (200μM) were provided. For CobT-CobS proteoliposome reactions AdoCbi-GDP (500μM), DMB (1mM), $MgCl_2$ (2mM) and NaMN (1mM) were provided. For CobC-CobS proteoliposome reactions AdoCbi-GDP (500μM), $MgCl_2$ (2mM) and a-RP (200μM) were provided. For CobUTC-CobS proteoliposome reactions AdoCbi (500μM), GTP (2mM), $MgCl_2$ (2mM), DMB (1mM) and NaMN (1mM) were provided. A reaction mixture with all of the components listed here was assembled without proteoliposome complex to serve as a no enzyme control. Reactions were incubated for 1 hour at 37 ºC before the addition of KCN to a final concentration of 2.4 μM. Reactions were incubated for 10 min at 90 ºC to stop the reaction.

RESULTS AND DISCUSSION

CobT and CobU interact with CobS in solution.

In order to probe for interactions between NLA enzymes CobU and CobT and CobS we utilized far westerns. Briefly, varying concentrations of pure CobU or CobT were deposited on nitrocellulose membranes prior to incubation with either pure CobS protein or a CobS containing proteoliposome solution suspended in buffer. CobS binding to CobU or CobT on the membrane was probed using a 6x

histidine antibody. We observed a strong response for both CobS (Fig. 6.3A, top) and CobS containing proteoliposomes (Fig. 6.3A, bottom) when incubated with CobT on a membrane, indicating interaction between CobS and CobT. We were able to detect CobS binding across all concentrations of CobT tested. In contrast to the strong response we saw with CobT, we only observed CobS binding at the highest concentrations of CobU (Fig. 6.3B). Additionally, when CobS was embedded in a phospholipid bilayer, we no longer detected binding to CobU. These results suggest that CobS has a higher affinity for CobT than CobU. BGG was used as a control for nonspecific binding. We were unable to cleave the *N*-terminal 6x histidine tag from CobC or CobS, preventing us from analyzing interactions using this method. Other methods were used to probe for these interactions.

CobS embedded in the lipid bilayer recruits CobU, CobT and CobC individually and in complex together.

To probe for interactions between integral membrane protein CobS and the enzymes that catalyze the late steps of cobamide biosynthesis, we utilized a liposome flotation strategy. Briefly, CobU, CobT, and CobC were incubated with CobS reconstituted into liposomes prior to separation by density gradient and ultracentrifugation. This process suspends intact liposomes and any interacting partners in solution while unbound or unincorporated proteins are sedimented. Each of the NLA enzymes were incubated with CobS proteoliposomes individually and together in a multi-protein solution. In order to determine if this interaction was

CobS-dependent or if the lipid bilayer is sufficient to recruit these enzymes, these experiments were repeated with empty liposomes. CobU is more efficiently recruited when incubated with CobS proteoliposomes in the absence of CobT and CobC (Fig. 6.4A). Interestingly, CobT appears to be more efficiently recruited by CobS when providing CobC and CobU to the reaction mixture (Fig. 6.4B). Similar to the results obtained by far western, CobS seems to display a greater affinity for CobT than CobU. CobC is efficiently recruited by CobS embedded in the lipid bilayer (Fig. 6.4C). We still see recruitment of CobC when CobU and CobT are included in the reaction mixture with CobS proteoliposomes, however the capacity for binding appears to be diminished. This may be due to the presence of CobT which appears to maintain a strong interaction with CobS in the lipid bilayer. We did not observe recruitment of any enzymes when incubated with empty liposomes. The reconstitution of CobS in the lipid bilayer was necessary for recruitment for all enzymes tested (Fig. 6.4). suggesting CobS serves as an anchor for late step biosynthetic enzymes. Additionally, we observed binding of all enzymes tested when incubated with CobS proteoliposomes as a multi-protein complex solution. This may facilitate additional protein-protein interactions between binding partners.

Given the seemingly weak interaction between CobU and CobS, we sought to explore whether substrates influence the recruitment of CobU. CobU self-guanylylates forming a CobU-GMP intermediate with a significant change in overall structure. When providing GTP to our reactions containing CobU and CobS proteoliposomes, we were surprised to see complete inhibition of binding (Fig. 6.5).

In addition to GTP, we provided the a-ribotide substrate of CobS, a-RP. It was recently shown that binding of a-RP by CobS induces a significant conformational change, that may increase CobS affinity for the AdoCbi-GDP substrate (Chapter 4). Preincubation of a-RP with CobS proteoliposomes did not seem to increase the recruitment of CobU compared to the CobU only control (Fig. 6.5). We also tested the combination of GTP and a-RP to probe whether the structural changes of CobU and CobS increase their binding affinity for each other. As we saw with GTP alone, we no longer see recruitment of CobU, suggesting the structure of the CobU-GMP intermediate is not suitable for protein interaction with CobS (Fig. 6.5).

CobS binding to CobT inhibits further protein interactions with CobC and CobU.

To determine the potential binding order of CobU, CobT and CobC with CobS, we again used a liposome flotation strategy. Proteins were added sequentially to incubations with CobS proteoliposomes prior to separation on a density gradient. We were able to detect recruitment of CobT across all combinations, regardless of order of incubation (Fig. 6.6). These data suggest CobS binding to CobT is more efficient than CobS binding with either CobU or CobC. Additionally, when CobT is added first, we see complete inhibition of binding of CobC and CobU. In alignment with previous results, we observe minimal recruitment of CobU in the two combinations where CobU was provided first. We see less recruitment of CobU when CobT is added second compared to when CobC is provided second. This may suggest binding of CobT can displace CobU

that was previously bound or that the presence of CobC somehow facilitates the CobU-CobS interaction. We see the greatest level of recruitment when CobC is provided first, but we do still detect CobC when CobU is added before. We observe a decline in recruitment when CobT is provided after CobC incubation with CobS proteoliposomes, again suggesting CobT may interrupt previously formed interactions with CobS proteoliposomes.

Nucleotide loop assembly activity is reconstituted in multi-enzyme complex.

We sought to determine if any one or all of these enzymes retain activity when in complex with CobS embedded in the lipid bilayer. We employed a bioassay to test enzyme functionality of the harvested CobS proteoliposome protein complexes. Aliquots from reactions were added to S. enterica strain JE8248 (*metE205 ara-9* Δ*cobS1313*) and growth was assessed under Cba-dependent conditions (Fig. 6.7A). All strains used harbor a null allele of MetE, the Cba-independent methionine synthase, thus methionine synthesis is dependent upon the Cba-dependent methionine synthase MetH. The collected CobU-CobS proteoliposome complexes were incubated with AdoCbi, GTP and a-RP, requiring both kinase/guanylyltransferase activity from CobU and CobS activity to produce a complete Cba. When the growth medium was supplemented with this reaction, the *cobS* strain did not grow (Fig. 6.7A, gray triangles). Previous work has documented CobS function when reconstituted in liposomes (Chapter 4), suggesting CobU was not functional in this assay. When the growth medium was supplemented with the reaction obtained by incubating CobT-CobS

proteoliposome complexes with AdoCbi-GDP, DMB, and NaMN , growth was observed (Fig. 6.7A, maroon hexagons). Since AdoCbi-GDP was provided, complete Cba formation was dependent upon activation of DMB by PRTase CobT and subsequent condensation by CobS. When the growth medium was supplemented with the reaction obtained by incubating CobC-CobS proteoliposome complexes with AdoCbi-GDP and a-RP, growth was observed (Fig. 6.7A, purple diamonds). In this instance, the conditions for growth could be met by CobS function alone. We also tested the CobC-CobS proteoliposome complex for phosphatase activity using both *para*-nitrophenylphosphate (PNPP) and 4-methylumbelliferyl phosphate (MUP), two general phosphatase substrates. Under both conditions, no phosphatase activity was detected in the CobC-CobS proteoliposome suspension (data not shown). Given that the structures of these substrates are significantly different than AdoCba-P, the true substrate of CobC, we cannot definitively conclude CobC is active or inactive in complex with CobS proteoliposomes. Interestingly, when the growth medium was supplemented with the reaction obtained by incubating CobUTC-CobS proteoliposome complexes with AdoCbi, GTP, DMB, and NaMN , growth was observed (Fig. 6.7A, blue upside-down triangles). In this condition, growth is contingent upon the activity of CobU, CobT and CobS, indicating all three enzymes were functional in the proteoliposome complex suspension. Notably, the presence of CobT and/or CobC created a condition favorable for CobU function.

CONCLUDING REMARKS

The work reported here provides evidence of a multiprotein complex involving the late steps of Cba biosynthesis. We have shown that CobS serves as an anchor in the lipid bilayer to recruit nucleotide loop assembly enzymes. Given the conservation of membrane association of CobS across all Cba producers, we propose a model (Fig. 6.8) in which this enzyme forms the basis for localization of the late steps of Cba biosynthesis to the inner membrane. Our model incudes CobS interactions with CobU, CobT, and CobC the enzymes responsible for corrin ring activation, nucleotide base activation, and final dephosphorylation. CobC, the enzyme that catalyzes the final step of Cba biosynthesis, is predicted to contain one transmembrane domain with the *N*-terminus located in the periplasm, but membrane-association of this enzyme has not been shown. We have identified CobC interaction with CobS in the lipid bilayer, however additional work is needed to determine the localization of CobC. The potential for membrane insertion of CobC may expand the role of the inner membrane in Cba biosynthesis. Additionally, the orientation of CobC in the membrane poses the question of where the complete Cba molecule is finished: the periplasm or cytoplasm. Our model uses the predicted topology of CobC in the membrane.

Cba biosynthesis is an energetically demanding process, involving ~30 enzymes to complete a Cba molecule. It is possible that membrane localization of these enzymes is a way of protecting the investment made in synthesizing Cbas by facilitating flux of valuable intermediates through the pathway. Evidence of systems for Cba delivery to Cba-dependent enzymes has been shown in

eukaryotes, but have not been identified in prokaryotes (33). Membrane localization of the late steps of Cba synthesis may facilitate delivery to Cba-dependent enzymes in the cell, whether by direct interaction with Cba-dependent enzymes or interaction with delivery systems like those found in eukaryotes. Cba transporters used in salvaging corrinoid precursors are also membrane-bound. Localization of late step enzymes to the membrane may also facilitate corrinoid salvaging. Additional work is needed to investigate these possibilities.

REFERENCES

1. Battersby, A.R., *Tetrapyrroles: the pigments of life.* Nat. Prod. Rep., 2000. **17**: p. 507-526.
2. Bridwell-Rabb, J. and C.L. Drennan, *Vitamin B12 in the spotlight again.* Curr. Opin. Chem. Biol., 2017. **37**: p. 63-70.
3. Padmanabhan, S., et al., *A new facet of vitamin B12: Gene regulation by cobalamin-based photoreceptors.* Annu. Rev. Biochem., 2017. **86**: p. 485-514.
4. Croft, M.T., et al., *Algae acquire vitamin B12 through a symbiotic relationship with bacteria.* Nature, 2005. **438**: p. 90-93.
5. Degnan, P.H., M.E. Taga, and A.L. Goodman, *Vitamin B12 as a modulator of gut microbial ecology.* Cell Metab., 2014. **20**: p. 769-778.

6. Heal, K.R., et al., *Two distinct pools of B12 analogs reveal community interdependencies in the ocean.* Proc. Natl. Acad. Sci. U S A, 2017. **114**: p. 364-369.
7. Yan, J., et al., *Purinyl-cobamide is a native prosthetic group of reductive dehalogenases.* Nat. Chem. Biol., 2018. **14**: p. 8-14.
8. Chan, C.H. and J.C. Escalante-Semerena, *ArsAB, a novel enzyme from Sporomusa ovata activates phenolic bases for adenosylcobamide biosynthesis.* Mol. Microbiol., 2011. **81**: p. 952-967.
9. Zayas, C.L., K. Claas, and J.C. Escalante-Semerena, *The CbiB protein of Salmonella enterica is an integral membrane protein involved in the last step of the de novo corrin ring biosynthetic pathway.* J. Bacteriol., 2007. **189**: p. 7697-7708.
10. O'Toole, G.A. and J.C. Escalante-Semerena, *Purification and characterization of the bifunctional CobU enzyme of Salmonella typhimurium LT2. Evidence for a CobU-GMP intermediate.* J. Biol. Chem., 1995. **270**: p. 23560-23569.
11. Thomas, M.G., et al., *Analysis of the adenosylcobinamide kinase/adenosylcobinamide-phosphate guanylyltransferase (CobU) enzyme of Salmonella typhimurium LT2. Identification of residue His-46 as the site of guanylylation.* J. Biol. Chem., 2000. **275**: p. 27576-27586.
12. Thompson, T.B., et al., *Three-dimensional structure of adenosylcobinamide kinase/adenosylcobinamide phosphate guanylyltransferase (CobU) complexed with GMP: evidence for a*

substrate-induced transferase active site. Biochemistry, 1999. **38**: p. 12995-3005.

13. Trzebiatowski, J.R. and J.C. Escalante-Semerena, *Purification and characterization of CobT, the nicotinate-mononucleotide:5,6-dimethylbenzimidazole phosphoribosyltransferase enzyme from Salmonella typhimurium LT2.* J. Biol. Chem., 1997. **272**: p. 17662-17667.
14. Trzebiatowski, J.R., G.A. O'Toole, and J.C. Escalante-Semerena, *The cobT gene of Salmonella typhimurium encodes the NaMN: 5,6-dimethylbenzimidazole phosphoribosyltransferase responsible for the synthesis of N^1-(5-phospho-alpha-D-ribosyl)-5,6-dimethylbenzimidazole, an intermediate in the synthesis of the nucleotide loop of cobalamin.* J. Bacteriol., 1994. **176**: p. 3568-3575.
15. Claas, K.R., et al., *Functional analysis of the nicotinate mononucleotide:5,6-dimethylbenzimidazole phosphoribosyltransferase (CobT) enzyme, involved in the late steps of coenzyme B_{12} biosynthesis in Salmonella enterica.* J. Bacteriol., 2010. **192**: p. 145-154.
16. Chan, C.H., et al., *Dissecting cobamide diversity through structural and functional analyses of the base-activating CobT enzyme of Salmonella enterica.* Biochim. Biophys. Acta, 2014. **1840**: p. 464-475.
17. Maggio-Hall, L.A. and J.C. Escalante-Semerena, *In vitro synthesis of the nucleotide loop of cobalamin by Salmonella typhimurium enzymes.* Proc. Natl. Acad. Sci. U S A, 1999. **96**: p. 11798-11803.

18. Maggio-Hall, L.A., K.R. Claas, and J.C. Escalante-Semerena, *The last step in coenzyme B(12) synthesis is localized to the cell membrane in bacteria and archaea.* Microbiology, 2004. **150**: p. 1385-1395.

19. Zayas, C.L. and J.C. Escalante-Semerena, *Reassessment of the late steps of coenzyme B_{12} synthesis in Salmonella enterica: Evidence that dephosphorylation of adenosylcobalamin-5'-phosphate by the CobC phosphatase is the last step of the pathway.* J. Bacteriol., 2007. **189**: p. 2210-2218.

20. O'Toole, G.A., J.R. Trzebiatowski, and J.C. Escalante-Semerena, *The cobC gene of Salmonella typhimurium codes for a novel phosphatase involved in the assembly of the nucleotide loop of cobalamin.* J. Biol. Chem., 1994. **269**: p. 26503-26511.

21. Bertani, G., *Studies on lysogenesis. I. The mode of phage liberation by lysogenic Escherichia coli.* J. Bacteriol., 1951. **62**: p. 293-300.

22. Bertani, G., *Lysogeny at mid-twentieth century: P1, P2, and other experimental systems.* J. Bacteriol., 2004. **186**: p. 595-600.

23. Berkowitz, D., et al., *Procedure for identifying nonsense mutations.* J. Bacteriol., 1968. **96**: p. 215-220.

24. Balch, W.E. and R.S. Wolfe, *New approach to the cultivation of methanogenic bacteria: 2-mercaptoethanesulfonic acid (HS-CoM)-dependent growth of Methanobacterium ruminantium in a pressurized atmosphere.* Appl. Environ. Microbiol., 1976. **32**: p. 781-791.

25. Miroux, B. and J.E. Walker, *Over-production of proteins in Escherichia coli: mutant hosts that allow synthesis of some membrane proteins and globular proteins at high levels.* J. Mol. Biol., 1996. **260**: p. 289-298.

26. Datsenko, K.A. and B.L. Wanner, *One-step inactivation of chromosomal genes in Escherichia coli K-12 using PCR products.* Proc. Natl. Acad. Sci. USA, 2000. **97**: p. 6640-6645.

27. Sambrook, J., E.F. Fritsch, and T. Maniatis, *Molecular Cloning: A Laboratory Manual*. Second ed. 1989, Cold Spring Harbor, N.Y.: Cold Spring Harbor Laboratory.

28. Laemmli, U.K., *Cleavage of structural proteins during the assembly of the head of bacteriophage T4.* Nature, 1970. **227**: p. 680-685.

29. Rigaud, J.L., B. Pitard, and D. Levy, *Reconstitution of membrane proteins into liposomes: application to energy-transducing membrane proteins.* Biochim. Biophys. Acta, 1995. **1231**: p. 223-246.

30. Suh, S. and J.C. Escalante-Semerena, *Purification and initial characterization of the ATP:corrinoid adenosyltransferase encoded by the cobA gene of Salmonella typhimurium.* J. Bacteriol., 1995. **177**: p. 921-925.

31. Jeter, V.L., et al., *A new class of phosphoribosyltransferases involved in cobamide biosynthesis is found in methanogenic archaea and cyanobacteria.* Biochemistry, 2019. **58**: p. 951-964.

32. Mattes, T.A. and J.C. Escalante-Semerena, *Facile isolation of alpha-ribazole from vitamin B12 hydrolysates using boronate affinity*

chromatography. J. Chromatogr. B Analyt. Technol. Biomed. Life Sci., 2018. **1090**: p. 52-55.

33. Padovani, D., et al., *Adenosyltransferase tailors and delivers coenzyme B12.* Nat. Chem. Biol., 2008. **4**: p. 194-196.

34. Rocco, C.J., et al., *Construction and use of new cloning vectors for the rapid isolation of recombinant proteins from Escherichia coli.* Plasmid, 2008. **59**: p. 231-237.

Table 6.1. Strains and plasmids used in this study		
***Salmonella*[1] Strains**	**Genotype**	**Reference or Source[2]**
JE6583	*metE205 ara-9*	Laboratory collection
JE3207	*metE205 ara-9* Δ*299(hisG-cob)/*pGP1-2 pJO52	10
Derivatives of strain JE6583		
JE8248	Δ*cobS1313*	Laboratory collection
Escherichia coli strains		
JE6663 C41(λDE3)	F – *ompT hsdSB (rB- mB-) gal dcm* (λDE3)	Avidis
Plasmid	**Genotype**	**Source**
pET-15b	*bla*$^+$ pBR322 origin of replication; cloning vector for the expression of protein with an *N*-terminal His-tag	Novagen
pTEV5	Overexpression vector that fuses the *N* terminus of the protein of interest to a H_6 tag, which can be removed by rTEV protease, *bla*$^+$	34
pCOBS5	*S.* Typhimurium *cobS*$^+$ cloned into vector pET-15b	17
pCOBC106	*S.* Typhimurium *cobC*$^+$ cloned into vector pTEV5	
pJO52	*S.* Typhimurium *cobU*$^+$ cloned into vector pT7-7	10
pJO27	*S.* Typhimurium *cobT*$^+$ cloned into vector pT7-5	13

[1]All *Salmonella* strains were derivatives of *Salmonella enterica enterica* serovar Typhimurium LT2.

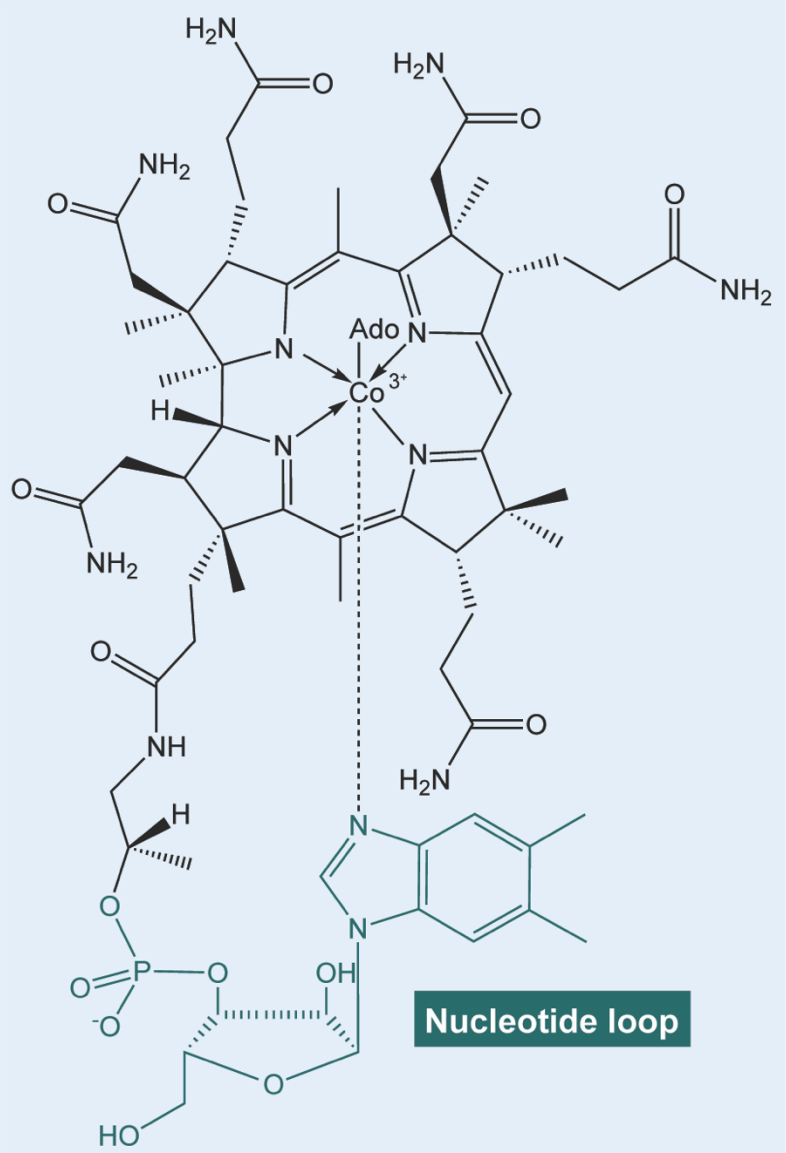

Figure 6.1. Chemical structure of adenosylcobalamin. The nucleotide loop or lower ligand is shown in teal.

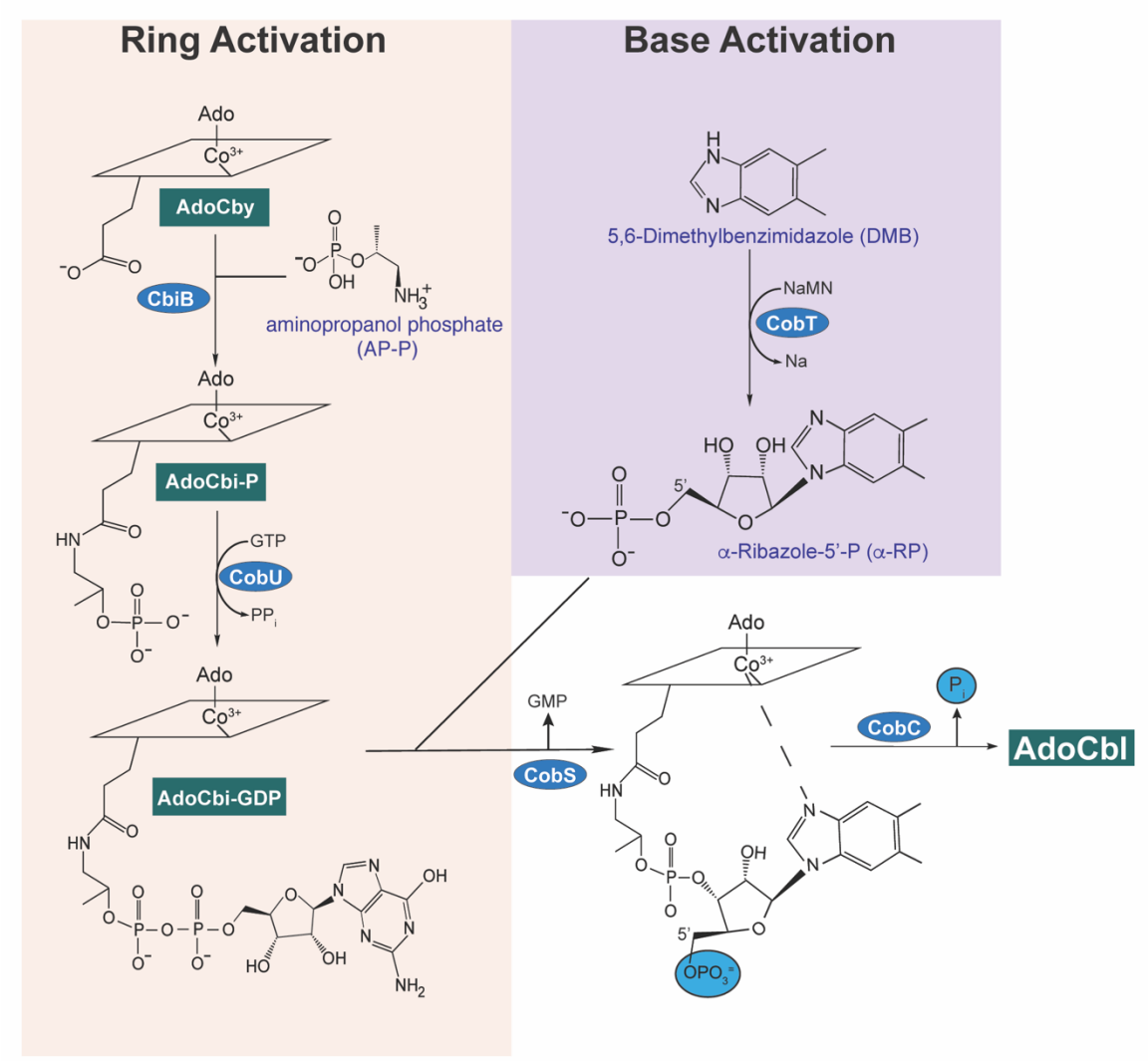

Figure 6.2. Late steps of Cba biosynthesis. Prior to activation of the corrin ring, CbiB attaches the aminopropanol-phosphate linker. Corrin ring AdoCbi is activated to AdoCbi-GDP by CobU (shown in beige) and nucleobase DMB is activated to α-RP by CobT (shown in purple). Cobamide synthase (CobS, in bold) catalyzes the penultimate step of cobamide biosynthesis by condensing AdoCbi-GDP and α-RP to form AdoCbl-P. CobC catalyzes the final step, removing the phosphate yielding AdoCbl. Intermediates are shown in teal.

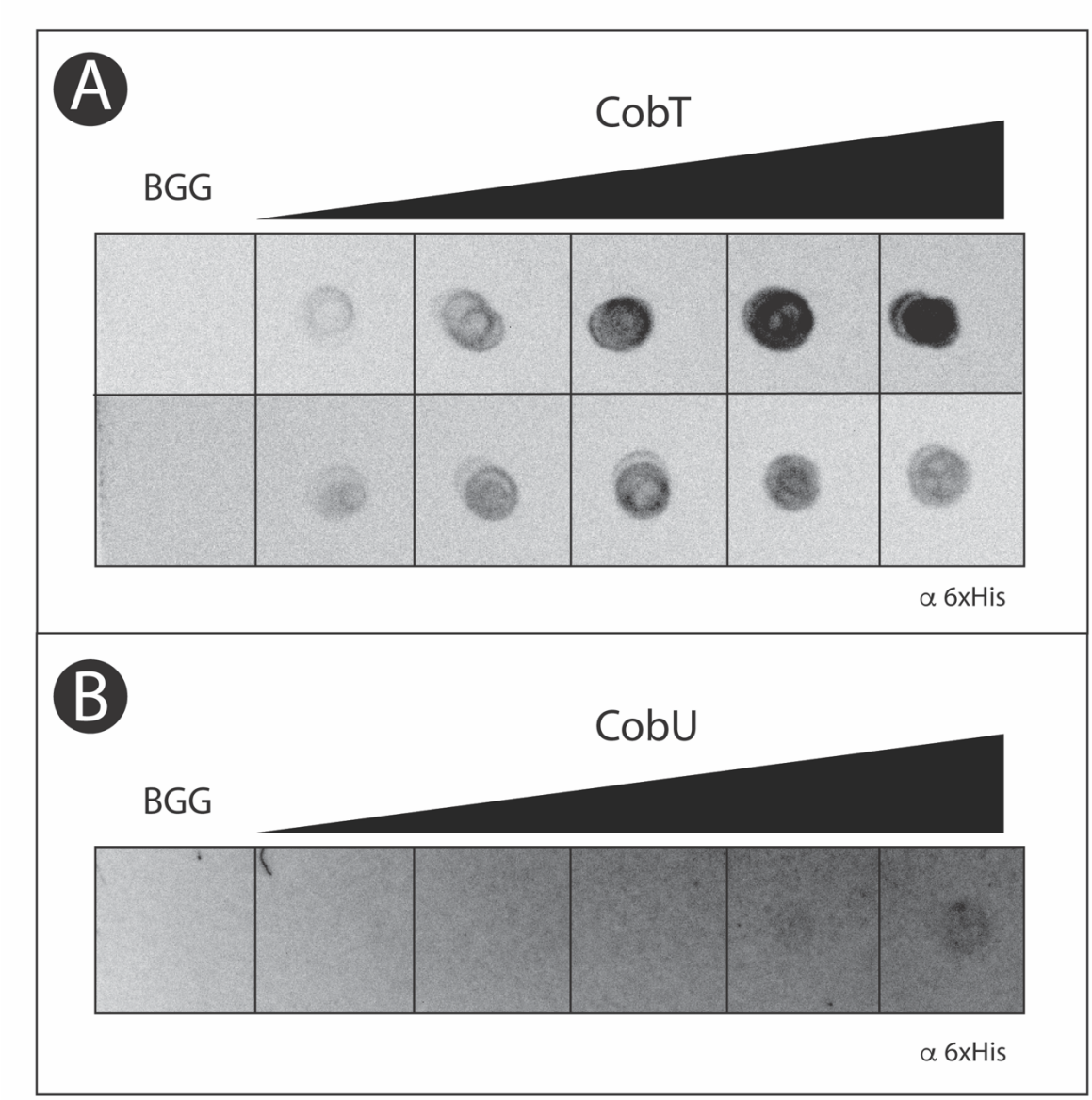

Figure 6.3. CobU and CobT interact with CobS in solution. A. Far western of CobT applied to a nitrocellulose membrane and incubated with a solution of CobS (top) or CobS containing proteoliposomes (bottom). B. Far western of CobU applied to a nitrocellulose membrane and incubated with a solution containing CobS. All blots were probed with α-6xHis monoclonal antibodies conjugated to CF680 fluorophore. BGG was included as a control for nonspecific binding.

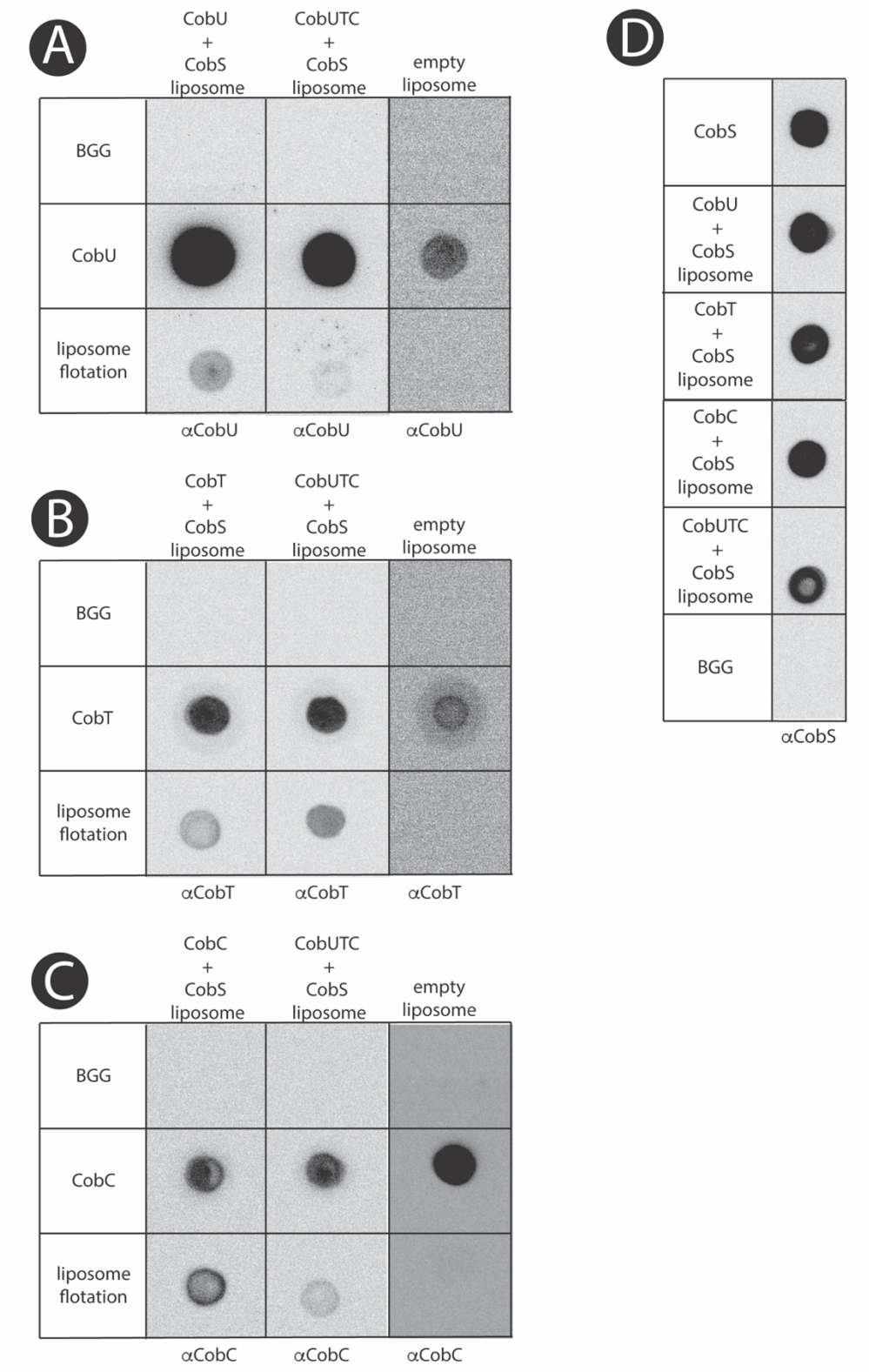

Legend on following page.

Figure 6.4. CobS in lipid bilayer recruits NLA enzymes CobU, CobT, and CobC. Dot blot analysis of liposome flotation assays are shown. A. CobU and a mixture of CobUTC were incubated with CobS-containing proteoliposomes before separation on a density gradient. Dot blots were probed with α-CobU antibodies and purified CobU was used a positive control. B. CobT and a mixture of CobUTC were incubated with CobS-containing proteoliposomes before separation on a density gradient. Dot blots were probed with α-CobT antibodies and purified CobT was used a positive control. C. CobC and a mixture of CobUTC were incubated with CobS-containing proteoliposomes before separation on a density gradient. Dot blots were probed with α-CobC antibodies and purified CobC was used a positive control. D. Confirmation of CobS in the harvested flotation mixtures. Dot blots were probed with α-CobS antibodies and purified CobS protein was used as a positive control. BGG was used to control for nonspecific interactions.

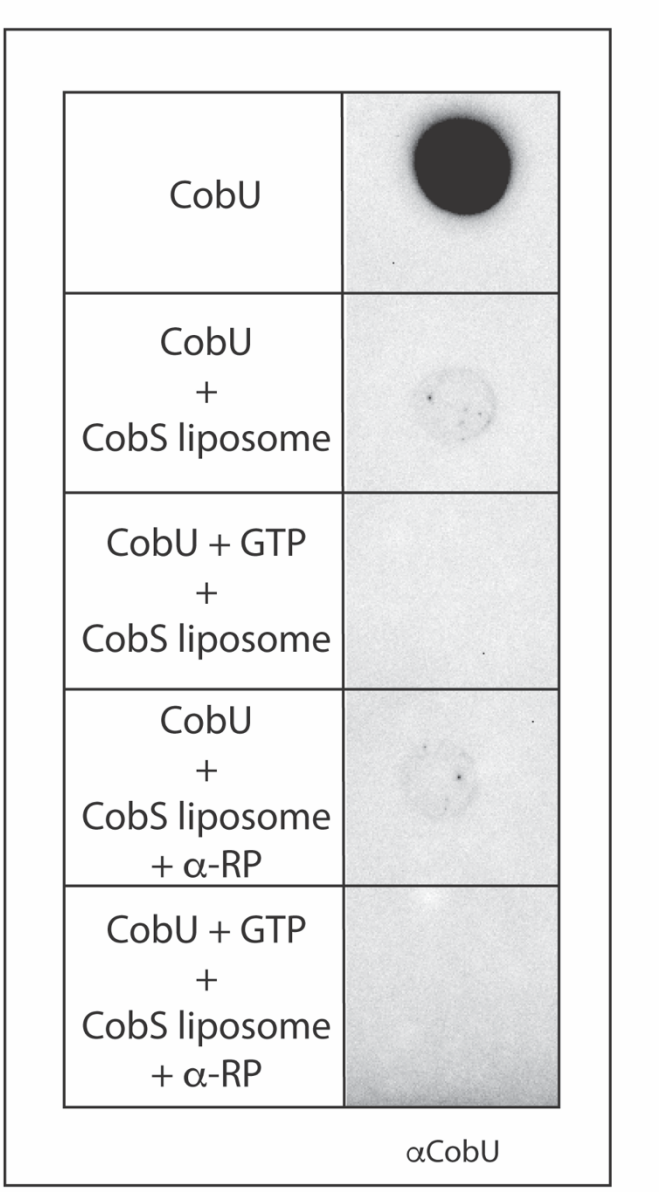

Figure 6.5. Preincubation with substrate does not increase CobS recruitment of CobU. Dot blot of liposome flotation is shown. CobU or CobS-containing proteoliposomes were preincubated with substrates prior to incubation together and subsequent separation by density gradient. Dot blots were probed with α-CobU antibodies. Purified CobU protein was used as a positive control.

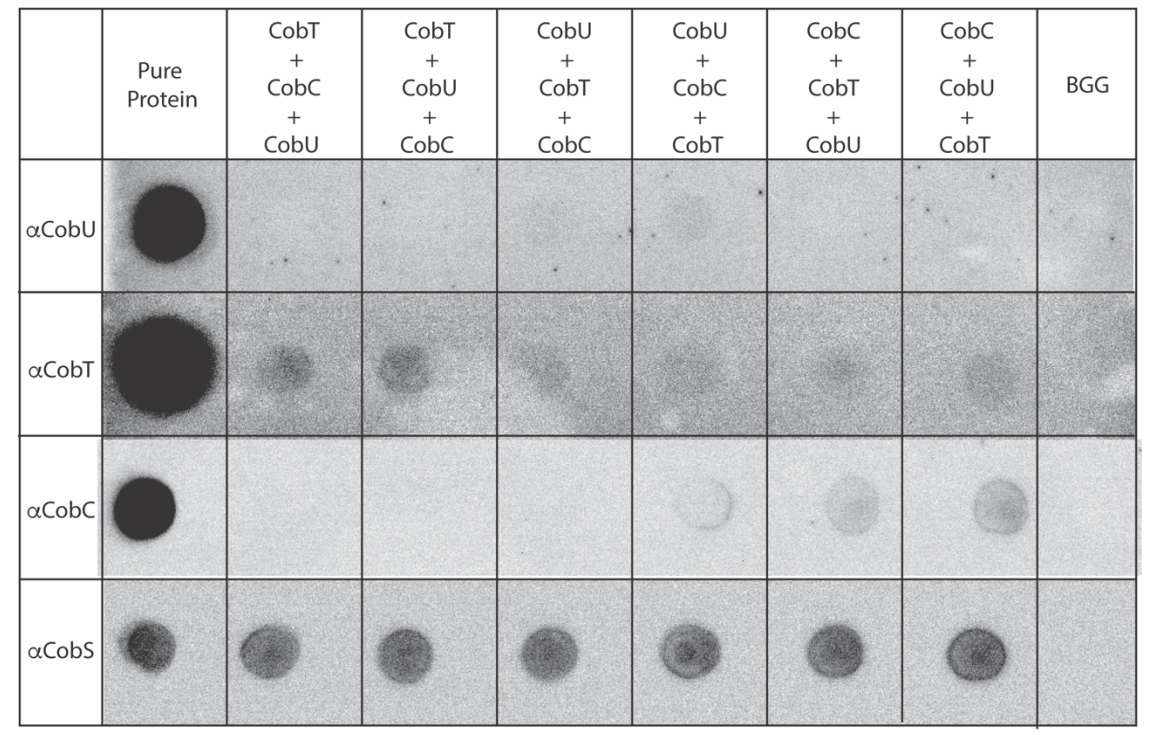

Figure 6.6. Binding order of NLA enzymes to CobS embedded in lipid bilayer. Dot blots of liposome flotation assays are shown. Blots were probed with antibodies as indicated in the left boxes. Order of enzyme addition to CobS-containing proteoliposomes is outlined across the top. Each enzyme was incubated with the CobS-containing proteoliposome suspension for 1h before the next enzyme was added. Purified CobU, CobT, CobS, and CobC proteins were used as positive controls. BGG was used as a control for nonspecific binding.

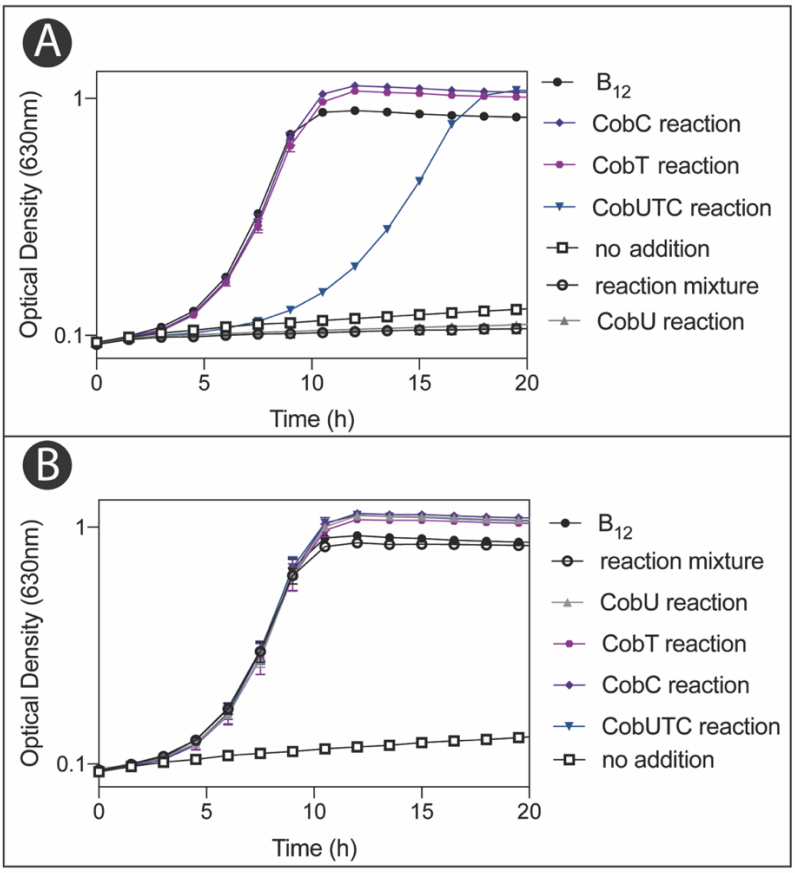

Figure 6.7. NLA activity is reconstituted in multi-enzyme complex. Bioassay of reactions using enzyme complexes collected from liposome flotation assay. A. *S. enterica* Δ*cobS* Δ*metE* strain (JE8248) was grown in minimal medium supplemented with 22mM glycerol as the sole carbon and energy source. The 0.22 μM filtered reactions from harvested liposome complexes were added and Cba-dependent growth was monitored. B. A *S. enterica* Δ*metE* (JE6583) strain was grown under the same conditions. Each strain was grown in triplicate and the experiment was performed thrice. Error bars represent the standard deviation of one representative experiment. Cyanocobalamin (or B_{12}) was provided to the medium as a positive control.

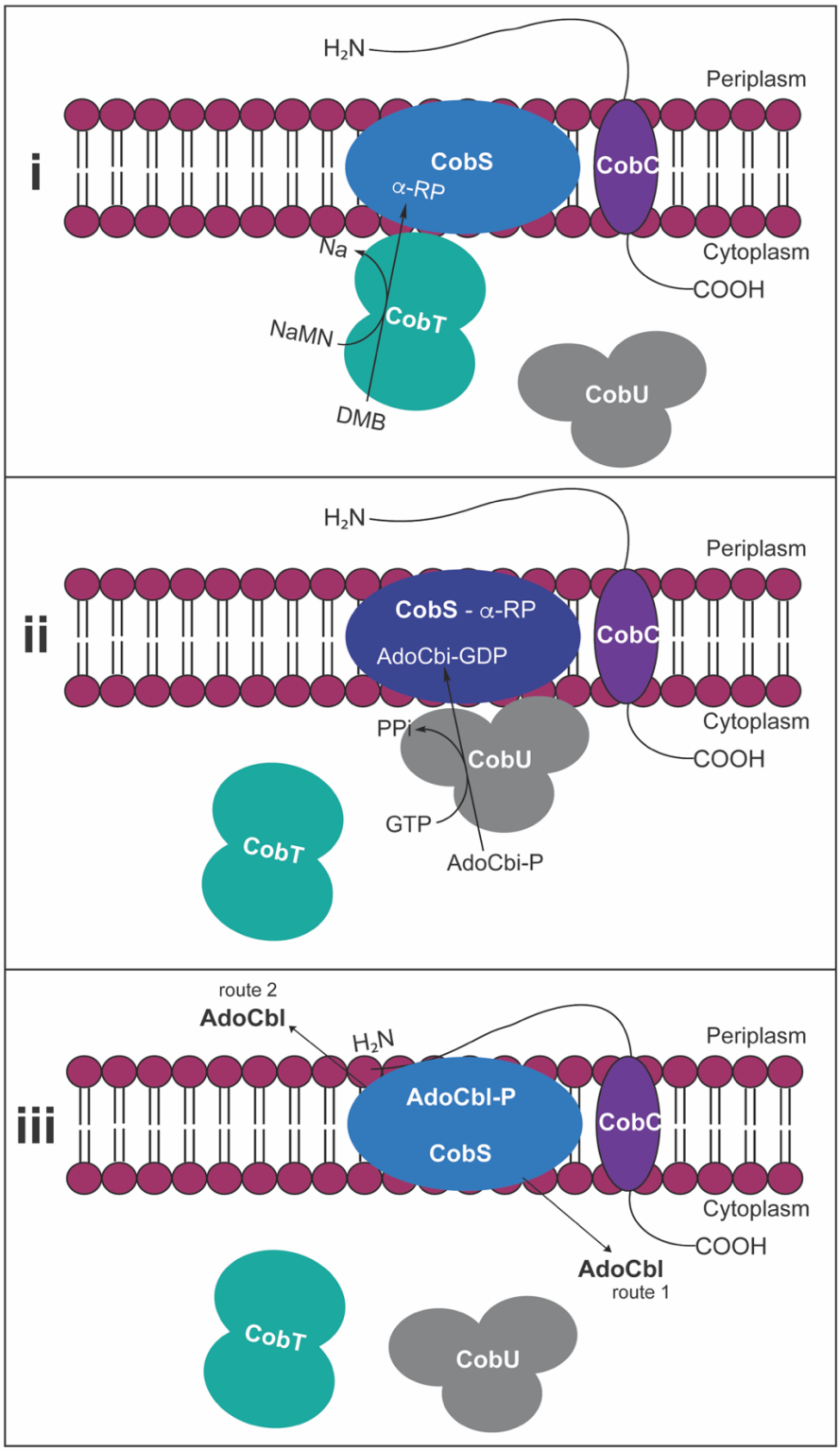

Legend on following page.

Figure 6.8. Model for membrane-associated nucleotide loop assembly. Our current working model of protein interactions within the nucleotide look assembly pathway of Cba biosynthesis in *S. enterica*. In step i, the nucleotide base is activated by CobT and delivered to CobS through an interaction with CobT. We have previously shown that CobS binding of α-RP induces a conformational change (indicated by color change here) and may increase the affinity for the corrin ring substrate, suggesting this step precedes CobS interaction with CobU. In step ii, the corrin ring is activated by CobU and delivered to CobS through an interaction with CobU. CobS then condenses the activated ring and base substrates to form AdoCbl-P. In step iii, CobC dephosphorylates the AdoCbl-P product of CobS to form AdoCbl. *In vivo* analysis of CobC variants suggests the *N*-terminus region to be the functional domain. Given that the functional domain of CobC is predicted to be periplasmic, we believe the complete cobamide can be released in the cytoplasm (route 1) or periplasm (route 2).

CHAPTER 7

CONCLUDING REMARKS

SUMMARY

The chapters in this dissertation focus on the late steps of nucleotide loop assembly and begin to address the physiological complexities that coincide with the synthesis of the complex compounds that are cobamides. Each chapter elaborates on the conclusions drawn from their respective studies. Chapters 2 and 3 characterized the structure and function of an archaeal homolog of the base activating enzymes CobT. While this work highlighted a number of differences between the archaeal homolog and its bacterial counterpart, there are enough similarities that allowed the archaeal CobT to function in a heterologous bacterial host. Organisms from drastically different environments utilizing similar strategies is a phenomenon often observed in the biosynthesis of cobamides. The selective pressure to maintain these systems is an area of particular interest and in chapters 4, 5, and 6 we explore the reason membrane association is observed in all cobamide producing organisms. The major findings of this dissertation follow.

***Mj*CobT represents a new class of base activating enzyme in Cba biosynthesis.**

In Chapter 2, we identified a new NaMN:DMB phosphoribosyltransferase from *Methanocaldococcus jannaschii*. This represents the first functional characterization of an archaeal CobT homolog. Previous work has suggested Cyanobacteria use an alternative route to activate the nucleobase in Cba biosynthesis. In finding this protein, we were able to identify CobT homologs in a number of cyanobacterial species. These newly identified CobT homologs represent a new class of NaMN:DMB phosphoribosyltransferases found in archaea and cyanobacteria.

In Chapter 3, we solved the crystal structure of the newly identified archaeal CobT from *Methanocaldococcus jannaschii*. We showed distinct differences in active site construction of *Mj*CobT compared to *Se*CobT. Active site architecture may explain the activity observed by *Mj*CobT at a physiological pH but absent from the *S. enterica* homolog. Despite the differences observed, the overall protein fold of these two CobT homologs is similar.

A protocol for CobS purification and liposome reconstitution.

In Chapter 4, we designed a protocol for the purification of CobS protein to 96% homogeneity. Given the polytopic nature of this inner membrane protein, previous attempts to isolate it were unsuccessful. A number of longstanding questions regarding the late steps of Cba biosynthesis focus on integral membrane proteins, so this protocol is a significant advancement in our efforts to

understand membrane associated Cba biosynthesis. Additionally, we show that this protein can be reconstituted into liposomes to further the *in vitro* characterization of this enzyme. These proteoliposomes proved to be a valuable tool in identifying protein interactions in the Cba biosynthetic pathway.

Highly conserved cytoplasmic loops of CobS contain regions critical for function *in vivo*.

In Chapter 4, we performed extensive *in vivo* mutational analysis to identify regions of importance for CobS function. We identified highly conserved motifs in loop 2 and loop 6 with a number of residues essential for in vivo functionality of CobS. These results suggest the cytoplasmic loops of CobS are necessary for function.

CobS function is improved in the lipid bilayer.

In Chapter 4, we show that CobS reconstitution in to liposomes drastically effects CobS function. We observed a 20-fold increase in specific activity of CobS in the lipid bilayer compared to purified CobS. Additionally, we observed a 3-fold increase in affinity for the nucleotide substrate α-RP upon reconstitution in the lipid bilayer. These results highlight the relationship between CobS and the inner membrane.

CobS binds α-RP first and undergoes a conformational change.

In Chapter 4, we observed a significant conformational change of CobS upon binding of the nucleotide substrate. Considering the both the in vivo mutational analysis and the work done on substrate binding, our work suggests that CobS binds the nucleotide substrate first. Our work also suggests that the conformational change induced by α-RP binding may increase affinity for the activated ring substrate AdoCbi-GDP. These results helped to inform the model for protein interactions presented in Chapter 6.

Increased levels of CobS result in detrimental effects on overall cell health.

In Chapter 5, we utilized a number of different strategies to identify the negative effects of CobS production. We observed a dissipation of the proton motive force, decreased membrane stability and a decrease in cell viability when we increased the synthesis of CobS. This was also observed when an inactive variant of CobS was produced suggesting the detrimental effects are attributed to the structure of CobS. Increased levels of CobS also result in a significant change in cell morphology. Membrane perturbations population-wide defects in cell shape and division were visualized using fluorescence microscopy. Importantly, we showed the detrimental effects of increased CobS production could be mitigated by co-expression of *cobC* or *pspA*. We were also able to show CobC interacts with CobS in the lipid bilayer. Overall, this work highlights the physiological burden on the cell from increased CobS production that may be

necessary to meet the high demand for Cba biosynthesis in certain environments.

CobS is an anchor responsible for recruiting a multiprotein complex of NLA enzymes to the membrane.

In Chapter 6, we showed that CobS functions as an anchor by recruiting enzymes of the late steps of Cba biosynthesis to the membrane. We utilized the tools generated in Chapter 4 to probe for protein interactions with CobS and observed multiple interactions. Both enzymes that generate the substrates for CobS, CobU and CobT, were shown to interact with CobS embedded in the lipid bilayer. This work built on the initial evidence of protein interaction between CobC and CobS outlined in Chapter 5. Using the collective results from this dissertation, we proposed a new model for the late steps of Cba biosynthesis informed by the protein interactions identified in Chapter 6.

RECOMMENDATIONS FOR FUTURE WORK

Expanded CobS variant analysis.

Previous work not included in this dissertation focused on generating a series of truncated CobS variants. Generally, *N*-terminal truncations will complement a *S.enterica* Δ*cobS* strain under Cba-dependent growth conditions, however there is a significant lag compared to strains synthesizing a wild-type CobS. Truncations at the *C*-terminus display a more drastic phenotype: removing the last 4 amino acids (LALL) completely abolishes growth in the conditions

described above. Previous work determined the *C*-terminus is embedded in the lipid bilayer. The phenotype observed by truncating this region of CobS suggests a more significant role on CobS function. *In vitro* activity assays could determine if this CobS variant is functional. If this variant is functional *in vitro*, additional work should focus on determining the cause of the observed phenotype. It is possible that a *C*-terminal truncation of CobS interrupts interactions with the cell membrane or other protein partners. A hunt for suppressor mutations that confer Cba-dependent growth of a Δ*cobS S. enterica* strain synthesizing a *C*-terminally truncated CobS variant could identify proteins of interest for further studies.

Some *in vitro* work has been done on the *N*-terminally truncated CobS variant, however further characterization is needed. *N*-terminally truncated CobS is active *in vitro* and can be reconstituted in liposomes similar to wild-type CobS. We have obtained suppressor mutants that decreased the lag observed when relying on Cba-biosynthesis using a *N*-terminal truncation CobS variant (phenotype described above). The suppressor mutations need to be mapped using whole genome sequencing. Once the mutations have been identified, further work on reconstructing mutations and assessing phenotypes can be explored.

CobS crystal structure.

Obtaining a crystal structure of CobS could provide further insight into the interactions with the membrane and other proteins. Further optimization of the purification protocol reported here could yield greater amounts of CobS protein.

Utilizing the mitigating effects of co-production of CobC or PspA with CobS may increase overall protein yields. In order to obtain the crystal structure, it would likely be beneficial to transition from reconstitution in liposomes to reconstitution in nanodiscs.

Determine the location of complete Cba formation.

A critical question of where the complete Cba molecule is formed remains. Previous unreported work in the lab has implicated a role of Cba transport machinery in Cba biosynthesis, suggesting that these processes may be coupled. Efforts to determine whether this molecule is released into the periplasm or the cytoplasm are necessary. Further characterization of CobC is needed to determine if it is membrane associated and if the active site region is periplasmic or cytoplasmic. Membrane association could be visualized by generating fluorescent protein fusions of CobC. Membrane topology could be explored by generating a series of PhoA and LacZ fusions. A focus on generating everted vesicles containing both CobC and CobS may isolate completed Cbas in the lumen of the vesicle, potentially providing evidence of periplasmic product formation and release. Synthetic fluorescent Cba compounds have been generated and may be useful in determining the location of product release of the Cba biosynthetic pathway. The fluorescent moieties are incorporated at the upper ligand of the Cba compound and may prevent interaction with CobS and CobC. Unraveling this critical question will likely prove to be a challenge.

Characterize the interactions between CobS and other NLA enzymes.

An in-depth investigation of the complex interactions identified here is necessary. We began to probe the effects of substrate/product binding of recruitment of NLA enzymes by CobS but this work could be expanded using the liposome flotation strategies outlined in this dissertation. In addition to liposome flotation assays, pursuing surface plasmon resonance analysis would provide information about the binding kinetics of this multiprotein complex. Visualizing the complex and co-localization of proteins to the membrane could be obtained by generating a series of fluorescent protein fusions with NLA enzymes and employing a variety of microscopy techniques. *In vitro* crosslinking and subsequent mass spectrometry analysis would provide detailed evidence of the regions of interaction between proteins.

In addition to the experiments outlined above, an *in vivo* confirmation of the *in vitro* interactions would strengthen the evidence of this multiprotein complex at the membrane. These *in vivo* confirmations could come from the previously discussed suppressor mutations generated using truncated CobS variants. A bacterial two-hybrid approach would also provide valuable evidence of these protein interactions in the cell.

Expand the search for CobS interaction partners.

It is possible that CobS interacts with additional proteins that were not covered in this dissertation. Employing the liposome flotation strategy outlined here, a number of potential interacting proteins could be screened for interactions

with CobS proteoliposomes. Investigating interactions with the Cba transport and cobalt transport machinery may provide further insight into the potential coupling of Cba biosynthesis with Cba transport.

CbiB, an integral membrane protein at the junction of the early and late steps of Cba biosynthesis, would be an ideal candidate for further investigation on the physiological role of membrane associated Cba biosynthesis. A number of the strategies used in the dissertation should be applied to CbiB to expand our understanding of this network of proteins.

Probe for Cba delivery systems.

Another potentially important aspect of membrane associated Cba biosynthesis could include Cba delivery systems to Cba-dependent enzymes. Thus far, no evidence of Cba delivery has been identified in prokaryotes, however it has been documented in eukaryotes. Maintaining membrane associated Cba biosynthesis may be a strategy to localize biosynthesis, transport, and delivery of Cbas in the cell. Probing for interacting proteins with Cba-dependent enzymes using co-immunoprecipitation or bacterial two-hybrid systems may elucidate Cba delivery systems in prokaryotes.

CONCLUSION

CobS is an integral membrane protein central to the nucleotide loop assembly pathway. This dissertation has made significant advances in our understanding of CobS function and has provided some insight into the structure.

Additionally, we have identified CobS as a site of interaction for the enzymes preceding (CobU and CobT) and following (CobC) it in the biosynthetic pathway, highlighting the centrality of CobS in the late steps of cobamide biosynthesis. The work presented here only begins to tease apart what is likely a vast network of interacting proteins involved in the synthesis, salvaging and delivery of cobamides in the cell. Hopefully the tools constructed here will prove to be useful for the next generation of graduate students who have the challenging, yet rewarding, task of unraveling cobamide biosynthesis. Thank you for reading.

APPENDIX A

SIRTUIN-DEPENDENT REVERSIBLE LYSINE ACETYLATION CONTROLS THE ACTIVITY OF ACETYL-COENZYME A SYNTHETASE IN CAMPYLOBACTER JEJUNI[6]

[6]Jeter V.L., and Escalante-Semerena J.C. To be submitted to *Molecular Microbiology.*

ABSTRACT

Posttranslational modifications are mechanisms for rapid control of protein function used by cells from all domains of life. Lysine acetylation of AMP-forming acetyl-CoA synthetase (Acs) is the paradigm for metabolic enzyme modulation by posttranslational modifications. In bacteria, an active site lysine of Acs can be modified by a number of different GCN5-type N-acetyltransferases (Type I,II, III and IV GNATs). Acs activity is inactivated as a result of acetylation, however this modification can be removed by a deacetylase, thus restoring Acs function. Here we show reversible lysine acetylation as a mechanism to modulate Acs function in *Campylobacter jejuni*, a prevalent cause of food-borne illness in humans. *In vivo* and *in vitro* data reported here confirm the acetate activating function of the annotated AMP-forming acetate:coA ligase CjAcs (*cj1537c*). Additionally, we identify that *cj1715* encodes a type IV GNAT (henceforth KatA) responsible for catalyzing the modification and inactivation of *Cj*Acs. We report *in vivo* confirmation of deacetylase activity of the annotated NAD^+-dependent (class III) protein deacetylase (sirtuin) *Cj*SrtN (*cj1050c,* previously NpdA). *In vitro* data show the restoration of modified *Cj*Acs activity by deacetylase *Cj*SrtN. This is the first documentation of metabolic enzyme control by acetylation in *C. jejuni*.

INTRODUCTION

Chemical modifications to control protein function is a strategy observed across all domains of life. Numerous modifications including hydroxylation, phosphorylation, glycosylation, methylation, prenylation, ubiquitination, ADP-ribosylation, and acylation have been identified (1). Acyltransferases have been

shown to most commonly use acetate as the organic acid; acetylating both small molecules and proteins (2-7). *N*ε-lysine acylation is important in regulating metabolic pathways and has been shown to allow cells to rapidly adapt and address cellular stresses (8). GCN5-type *N-a*cetyltransferases (GNATs) are a diverse superfamily (PR00583) of acyltransferases with little sequence homology outside of the core catalytic domain (9). Protein acetylation by GNATs can alter protein structure, stability and function (10). GNATs primarily transfer the acetyl moiety of acetyl-CoA to amino groups of small molecules or *N*-termini of proteins (*N*α) or the *N*ε of lysl residues (11, 12). Recent work has identified a GNAT capable of transferring the succinyl moiety of succinyl-CoA (7). In some cases, the acetyl group of modified proteins can be removed by deacetylases, restoring activity to the enzyme (13). This mechanism of metabolic regulation, referred to as reversible lysine acetylation (RLA), allows cells to rapidly respond to changing environments and cellular stress (Fig. A.1.).

Acetylation of the central metabolic enzyme acetyl-CoA synthetase is the most well understood model of RLA. AMP-forming Acs catalyzes the activation of acetate to acetyl-CoA through a two-step, ATP-dependent mechanism. Acs proteins from diverse organisms share a number of conserved regions, one of which is characterized by an active site lysine residue that is modified by GNATs in bacteria (13-16). Modification of this lysl residue inactivates Acs by blocking the adenylation reaction. Acs modification of this nature has been identified in a number of organisms including *Salmonella enterica*, *Streptomyces lividans*,

Staphylococcus aureus, *Bacillus subtilis*, *Rhodopseudomonas palustris*, and *Mycobacterium tuberculosis*, yet protein acetylation in *Campylobacter jejuni* has not been identified (6, 17-21;Burckhardt, 2019 #30755}).

Campylobacter jejuni jejuni NCTC 11168 (henceforth *C. jejuni*) is the leading cause of food-borne bacterial enteritis in humans around the world (22, 23). Despite the prevalence of *C. jejuni* as a pathogen, many questions regarding its physiology and pathogenesis remain (24). *C. jejuni* is a chemoheterotrophic bacterium with restricted capacity to catabolize carbohydrates (22, 25, 26). It has been shown that *C jejuni* catalyzes organic acids such as lactate, pyruvate, acetate and other TCA intermediates in addition to amino acids to fuel carbohydrate, lipid and protein biosynthesis (25, 27-30). *C. jejuni* lacks the pyruvate dehydrogenase found in other enteropathogenic bacteria and relies on a pyruvate:acceptor oxidoreductase (POR) to generate acetyl-CoA by oxidative decarboxylation of pyruvate (31). The TCA cycle and fatty acid biosynthesis are fueled by POR catalyzed formation of acetyl-CoA (26, 32, 33). *C jejuni* contains a phosphate acetyltransferase Pta (*cj0688*) and acetate kinase AckA (*cj0689*) responsible for converting acetyl-CoA to acetate by way of an acetyl-phosphate intermediate. Acetate generated through this process is excreted during logarithmic growth (30). Similar to what has been reported in other bacteria, exogenous acetate is predicted to be converted to acetyl-CoA by CjAcs (*cj1537c*) (34, 30).

Here we report *in vivo* and *in vitro* evidence that the annotated AMP-forming acetate:CoA ligase encoded by *cj*1537c is a *bona-fide* Acs and that biologically active *Cj*Acs is a trimer. Additionally, we confirm that *cj1715* encodes an acetyltransferase belonging to the GCN5-type *N*-acetyltransferase (GNAT) superfamily. Inactivation of *Cj*Acs via acetylation by *Cj*KatA is reported here. *In vivo* evidence reported here confirms deacetylase function of the annotated NAD^+-dependent (class III) protein deacetylase encoded by *cj1050c* (CjSrtN). We show that activity of *Cj*Acs can be restored by deacetylation by *Cj*SrtN, indicating the RLA paradigm controls the level of *Cj*Acs activity in *C. jejuni*.

MATERIALS AND METHODS

Bacterial strains, culture media, and chemicals. Bacterial strains used in this study are listed in Table A.1. All strains for growth analysis were derivatives of *Salmonella enterica* subsp. *enterica* sv Typhimurium LT2 (*S. enterica*) or *Escherichia coli* C41 (λDE3). *S. enterica* strains were grown at 37 °C on lysogeny broth (LB, Difco) (35, 36) or no-carbon essential (NCE) minimal medium (37) supplemented with acetate (10 mM), $MgSO_4$ (1 mM), and Wolfe's trace minerals (1x) 38. All *S. enterica* strains contain a null allele of methionine synthase MetE, requiring exogenous methionine or cobalamin for growth. Cobalamin was provided at a concentration of 100 nM. *Escherichia coli* C41 (λDE3) 39 was used for protein overexpression and *E. coli* K12 strain DH5α (New England Biolabs) was used for plasmid construction. All *E. coli* strains were grown at 37°C in LB medium.

Antibiotics for all media were used at the following concentrations: ampicillin, 100 μg mL^{-1}; chloramphenicol, 20 μg mL^{-1}; kanamycin, 50 μg mL^{-1} . All chemicals were purchased from Sigma-Aldrich unless otherwise noted; isopropyl β-D-1-thiogalactopyranpside (IPTG, Gold BioTechnology), glycerol (Fisher), tris(2-carboxyethyl)phosphine (TCEP, Gold Biotechnology), 4-(2-hydroxyethyl)-1-piperazineethanesulfonic acid buffer (HEPES, Gold BioTechnology).

Plasmid construction. Plasmids used in this study are listed in Table A.1. Primers were synthesized by Integrated DNA Technologies, Inc. (IDT [Coralville, IA, United States]) and are listed in Table A.2. Genes were amplified from *C. jejuni jejuni* NCTC 11168 genomic DNA using Phusion DNA polymerase (ThermoFisher) per manufacturer's instructions. Plasmids encoding *Cj*SrtN, and *Cj*KatA variants were amplified using PfuUltra II DNA (Agilent Technologies) polymerase per manufacturer's instructions. Restriction enzymes were purchased from Fermentas.

General strategy used to construct plasmids for overproduction and complementation studies . All plasmids used for complementation studies and protein overproduction were constructed using the BspQI high-efficiency cloning method described elsewhere (40, 41). The *cj1537c*, *cj1050c* and *cj1715* genes were amplified from *C. jejuni* NCTC 11168 genomic DNA. These genes were cloned into vectors under the control of L-(+)-arabinose inducible promoters in vectors pCV1 and pCV3 for use in complementation studies. These genes were

also cloned into vector pTEV18 under the control of the IPTG-inducible promoter for expression studies in *E. coli* C41 (λDE3). Resulting recombinant proteins synthesized from pTEV18 vectors contain a *N*-terminal H_6 tag.

General strategy used to construct plasmids encoding variants of interest. Plasmids encoding CjSrtN (*cj1050c*) and *Cj*KatA variants were constructed using primers shown in Table A.2 and plasmid pCJSRTN1, and pCJKATA2 DNA, respectively, as the template. Briefly, the primers encoding a specific substitution change were used to amplify *cj1050c* on plasmid pCJSRTN1 and *cj1715* on plasmid pCJKATA2 . Amplified products were cut with DpnI overnight at 37°C. The amplification product was then transformed in *E. coli* DH5α cells, and its nucleotide sequence was verified by Sanger sequencing. Using this strategy, we generated variants *Cj*SrtN^{H106A} resulting in plasmid pCJSRTN3 and *Cj*KatA^{E168Q} resulting in plasmid pCJKATA5. Plasmids encoding these variants are described in Table 1.

Strain construction and growth analysis. In-frame deletions of *S. enterica* genes were constructed using the phage lambda Red recombinase system as described (42). Plasmids were transformed into strains for complementation studies as described (43). For growth analyses, 2-mL starter cultures in 13 x 100 mm borosilicate cultures tubes were grown 16 h at 37 °C with shaking at 180 rpm in LB containing appropriate antibiotic. Growth experiments were performed in 96-well microtiter dishes (Falcon), with each well containing 198 μl of medium plus 2

μl of inoculum. The growth behavior of three technical replicates of each strain was analyzed, and the experiment was performed thrice. Growth was monitored using a computer-controlled plate reader (BioTek, Model Eon). The optical density at 630 nm was measured every 30 min for a total time of 24 h; the microtiter dish was shaken between measurements. Data were analyzed using GraphPad Prism version 8. L-(+)-arabinose was used as inducer when indicated.

In vitro acyl-CoA synthetase assays. *Cj*Acs activity was determined using an NADH-consuming couple assay (44). Reactions contained HEPES buffer (50mM pH 7.5), ATP (2.5mM), coenzyme A (CoASH, 0.5mM), phosphoenol pyruvate(3mM), NADH (0.1mM), pyruvate kinase (1U), lactate dehydrogenase (1.5U), myokinase (5U), TCEP (1mM), MgCl2 (5mM), and organic acid substrate (0.2mM). Acetate, propionate, malonate, butyrate, and succinate were screened as substrates. Reactions were started by adding 2μL of *Cj*Acs for a final concentration of 300nM. NADH consumption was monitored at 340nm using a SpectraMax Plus UV-visible spectrophotometer (Molecular Devices). Reactions were measured over 8 min in a 96-well plate. Enzyme activities were calculated as described and graphed in GraphPad Prismv8 (45). Experiments were performed in technical triplicate, three times. The data presented here represent technical triplicates from one biological replicate.

Determination of kinetic parameters. Pseudo first order kinetics of *Cj*Acs on acetate and propionate were determined using the spectrophotometric acyl-CoA synthetase assays outlined above. Acetate and propionate were provided across a range of concentrations from 5μM to 150μM and 0.5μM to 15μM respectively. Initial velocity was graphed as a function of substrate concentration using GraphPad Prism v8. Apparent K_m and V_{max} were determined using the onboard Michaelis-Menten nonlinear regression. Reactions were performed in technical triplicate, three times. Turnover constant (K_{cat}) was determined using the following formula where E is enzyme concentration:

$$k_{cat} = \frac{V_{max}}{E}$$

Catalytic efficiency was determined using the following formula: K_{cat}/K_m.

In vitro protein acetylation and deacetylation assays.

Acetylation assays. Acetylation of *Cj*Acs by *Cj*KatA was determined using *in vitro* acetylation assays with cell-free extracts. Cell-free lysates were generated using a *S. enterica* Δ*pat* (JE 11963) strain harboring plasmid pCJKATA2 or plasmid pCJKATA5. A 2mL culture was grown for 16h at 37°C with shaking at 180rpm. The 2mL culture was used to inoculate a 10mL culture at a rate of 1:100. The culture was grown at 37°C with shaking for 10h and cells were pelleted by centrifugation at 6,000 x *g* for 15 min at 4°C, before storing the pellet at -80°C. The cell pellet was thawed, resuspended in 1mL of HEPES buffer (50mM pH 7.0) containing SIGMAFAST protease inhibitor and cells were lysed by sonication

(thrice for 1 min total, 2s on/2s off, 60% amplitude) using a Model 550 sonic dismembrator (Fisher Scientific). Clarified lysates were obtained after centrifugation at 16,000 x *g* for 10 minutes at 4°C and quantified using a Bradford protein assay (BioRad). Acetylation reactions (100μL) contained HEPES buffer (50mM pH 7.0), TCEP (1mM), acetyl-CoA (100μM), *Cj*Acs (8μM), and cell-free lysate containing *Cj*KatA^{WT} or *Cj*KatA^{E168Q}(20μg). Reactions were incubated for 1 h at 37°C. Acetylated *Cj*Acs (incubated with *Cj*KatA^{WT}) activity was compared to the activity of unmodified *Cj*Acs (incubated with *Cj*KatA^{E168Q}) using the aforementioned continuous NADH-consuming spectrophotometric acyl-coA ligase assay.

Deacetylation assays. Deacetylation was determined by treating the acetylation reactions described above with *Cj*SrtN. Acetylation reactions were buffer exchanged using an Amicon ultra centrifugal filter unit (30,000 NMWL, Millipore) to remove free acetyl-coA. Deacetylase *Cj*SrtN (3μM) with co-substrate NAD^+ (1mM) was incubated with acetylated *Cj*Acs for 1h at 37°C. Nicotinamide (Nm, 1mM) was added in some reactions to inhibit *Cj*SrtN. *Cj*Acs activity was measured using the continuous NADH-consuming spectrophotometric assay.

Mass spectrometry. Identification of acetylated residues was determined by mass spectrometry analysis performed by the PAMS facility at the University of Georgia. Acetylation reactions prepared as described above were separated by SDS-PAGE. The *Cj*Acs band at ~74kDa was excised and subjected to in-gel trypsin digest prior to mass spectrometry analysis.

Purification of *C. jejuni* proteins. The same general protein purification scheme was used for *Cj*Acs, *Cj*SrtN, and *Cj*KatA. Wild-type *Cj*Acs protein was overproduced from plasmid pCJACS2, wild-type *Cj*SrtN protein was overproduced from plasmid pCJSRTN2, and wild-type *Cj*KatA protein was overproduced from plasmid pCJKATA1. All plasmids were expressed in strain JE6663 (*E. coli* C41) in 1-L cultures of Terrific Broth 46. Protein synthesis was induced by the addition of IPTG at a final concentration of 1mM in mid-log phase cultures (OD_{600} ~0.6) growing at 37°C with shaking at 180 rpm in an Innova44 (New Brunswick Scientific) gyratory incubator. After induction, cultures were grown for 17 h at 25°C with shaking at 180 rpm. Cells were harvested by centrifugation at 4°C for 15 min at 6,000 x *g* in an Avanti J20-XPI refrigerated centrifuge equipped with JLA-8.1000 rotor. Pelleted cells were stored at -80°C. Frozen cells were thawed on ice and re-suspended in HEPES buffer (50 mM, pH 7.5) containing NaCl (500mM) and imidazole (20 mM) at a rate of 20% cell weight to buffer volume. Lysozyme (1μg/mL), DNaseI (25μg/mL), and Phenylmethylsulfonyl fluoride (PMSF) (0.5mM) were added to the cell suspension and incubated on ice for 10 min. Cells were lysed by sonication using a Q500 sonicator (QSonica) (thrice, 1 min total, 2s on/

2s off at 60% amplitude). Cellular debris was removed by centrifugation at room temperature for 30 min at 40,000 x *g* in an Avanti J-251 centrifuge (Beckman/Coulter) equipped with a JA 25.25 rotor. Clarified extract was filtered using a 0.45-μm syringe filter unit and applied to a 2-mL HisPur nickel-nitrilotriacetic acid (Ni-NTA) affinity column (ThermoFisher Scientific). The column was washed with 10 column volumes (CV) of HEPES buffer (50 mM, pH 7.5) containing NaCl (0.5 M) and imidazole (20 mM) and six CV of HEPES buffer (50 mM, pH 7.5) containing NaCl (0.5 M) and imidazole (40 mM). Proteins were eluted with six CV of HEPES buffer (50 mM, pH 7.5) containing NaCl (0.5 M) and imidazole (0.5 M). Fractions were collected throughout the wash and elution steps and protein purification was monitored by SDS-PAGE gel compared to Precision Plus Protein Standards (BioRad). Protein containing fractions were combined and dialyzed against HEPES buffer (50 mM, pH 7.5) containing NaCl (0.5 M) to remove imidazole. At this point, all proteins contain a *N*-terminal 6x histidine tag. *N*-terminally tagged, recombinant tobacco etch virus protease (H_7-rTEV) was purified as described elsewhere 47 and mixed with the *N*-terminally H_6-tagged proteins at a ratio of 1:10 *C. jejuni* protein:H_7-rTEV. The mixture was incubated at 25°C for 3 h to remove the H_6 tag. Cleaved proteins were purified away from the tag and H_7-rTEV using the Ni-NTA affinity purification method outlined above and tag-less protein was dialyzed against HEPES buffer (50 mM, pH 7.5) in steps with decreasing concentrations of NaCl down to 150 mM. Purified proteins were flash frozen in liquid nitrogen and stored at -80°C until used. Protein concentration was measured using the Bradford protein assay kit (BioRad).

Gel filtration chromatography. Oligomeric state was determined using gel filtration chromatography. A Superose 12 10/300 column (GE Healthcare) connected to an AKTA pure fast protein liquid chromatography (FPLC) system was equilibrate with HEPES buffer (50mM, pH 7.5) containing NaCl (150mM). Purified *Cj*Acs and *Cj*KatA were applied to the column and molecular mass determined by linear regression generated by the gel filtration behavior of BioRad gel filtration standards in GraphPad Prism v8. Linear regression was determined by graphing the log of molecular mass as a function of retention time in min of the following compounds: vitamin B_{12} (1.35kDa), Myoglobin (17kDa), Ovalbumin (44kDa), γ-globulin (158kDa), and thyroglobulin (670kDa). Fractions were collected and Acetyl-CoA synthetase activity was confirmed from the peak used to determine *Cj*Acs molecular mass.

RESULTS AND DISCUSSION

In vivo evidence that *C. jejuni* Acs is a functional enzyme.

In the genome of *Campylobacter jejuni jejuni* NCTC 11168, *cj1537c* (*Cj*Acs) encodes a putative AMP-forming acetate:CoA ligase (or acetyl-CoA synthetase Acs). To date, no experimental evidence has confirmed this activity. We used an *in vivo* approach to determine whether *Cj*Acs had AMP-forming acetate:CoA ligase activity. For this purpose we introduced an arabinose-inducible plasmid encoding *C. jejuni acs*$^{+}$ into *S.enterica* Δ*acs* strain and

assessed growth on low (10mM) acetate (Fig. A.2). In *S.enterica* and *E.coli*, growth under these conditions is contingent upon a functional Acs (48, 16). The strain synthesizing *Cj*Acs grew on low acetate when the medium was supplemented with inducer at a final concentration of 250μM. The strain synthesizing *Se*Acs grew with inducer at a final concentration of 50μM. The strain harboring an empty vector failed to grow under these conditions. Growth of a *S. enterica acs*$^{+}$ strain was assessed as a control. These results indicate AMP-forming acetate:CoA ligase activity of *Cj*Acs *in vivo*.

Acetate is the preferred substrate for *Cj*Acs.

To gain insights into the substrate specificity of *Cj*Acs, we measured specific activity using a NADH-consuming coupled continuous spectrophotometric assay with various organic acid substrates. Acetate, propionate, malonate, butyrate, and succinate were screened as potential substrates. *Cj*Acs exhibited the highest specific activity on acetate and propionate (Fig. A.3). *Cj*Acs was able to activate butyrate, malonate, and succinate, however the specific activity was significantly lower compared to acetate and propionate as substrates (Fig. A.3). Given that *C. jejuni* preferentially catabolizes acetogenic amino acids as carbon and energy sources and lacks the enzymes necessary for propionate metabolism (49), it is likely that acetate is the biologically relevant substrate of *Cj*Acs.

Kinetic parameters for the reaction catalyzed by *Cj*Acs were obtained with acetate and propionate when ATP was provided at saturating levels (2.5mM). The rate of the reaction as a function of acetate concentration (Fig. A.4A) or propionate concentration (Fig. A.4B) is shown. The summaries of apparent kinetic parameters are shown in the insets (Fig. A.4). The K_m for acetate is similar to the values reported for *Se*Acs and *Sa*Acs (7). The low K_m for acetate is consistent with the idea that *Cj*Acs function is important when intracellular concentrations of acetate are low. Despite the differences in K_m and K_{cat} observed between acetate and propionate, the catalytic efficiencies are similar for these substrates which is consistent with previous reports (50, 51, 52).

Biologically active *Cj*Acs is a trimer.

The oligomeric state of *Cj*Acs was determined by gel filtration chromatography. The chromatographic behavior of pure *Cj*Acs protein was compared to that of standards with known molecular masses. *Cj*Acs is a 657 residue, 74 kDa protein. Under the conditions tested, *Cj*Acs eluted ~20 minutes after injection. Compared to the elution times of molecular mass standards, the retention time is consistent with that of a protein whose mass was approximately 234 kDa. Since the calculated molecular mass of *Cj*A*cs* was approximately 74 kDa, we concluded that *Cj*Acs was a trimer in solution (Fig. A.5). This is particularly interesting given that bacterial Acs homologs are typically monomers (53) or dimers (54, 55), but Acs functions as a trimer in yeast (56). Protein alignments comparing *Cj*Acs to bacterial Acs homologs (Fig. A.11) or a yeast

homolog (Fig. A.12) show similar levels of identity and similarity. The amino acid sequence of *Cj*Acs compared to *Se*Acs is 48% identical and 67% similar, while the comparison to *Saccharomyces cerevisiae* ACS is 43% identical and 61% similar. The *Cj*Acs amino acid sequence has low homology to yeast Acs in the regions responsible for forming the trimer interface. Additional structural studies on *Cj*Acs would provide insight into this unique organization.

C. jejuni cj1715 encodes a GCN5-related *N*-acetyltransferase KatA that acetylates *Cj*Acs

Blocking the adenylation activity of *Cj*Acs by acetylation of an active site lysine has been shown in other organisms (16, 18, 19, 20, 21, 6, 7). In these organisms, acetylation has been shown to be catalyzed by Pat homologs (Type I, II, and III GNATs) or AcuA homologs (Type IV GNATs). The genome of *C. jejuni* NCTC 11168 encodes a putative type IV GNAT at locus *cj1715*, however it does not show homology to Pat or AcuA acetyltransferases. To test the possibility of *Cj*Acs acetylation by *Cj*KatA, we used an *in vivo* approach. For this purpose we introduced two compatible, arabinose inducible plasmids encoding *cj1537c* and *cj1715* in a *S.enterica* Δ*acs* strain and assessed growth on low acetate. The strain synthesizing both *Cj*Acs and *Cj*KatA (Fig. A.6, open circles) exhibited a growth defect compared to a strain only synthesizing *Cj*Acs (Fig. A.6, black circles). The strain harboring empty vector failed to grow in these conditions (Fig. A.6, black squares). Growth of a *S.enterica acs*$^{+}$ strain was analyzed as a control (open triangles). These results suggested *Cj*KatA acetylates *Cj*Acs *in*

vivo, leading to a defect in growth on low acetate. In addition to these results, we assayed growth of a *S. enterica* Δ*pat* strain synthesizing *Cj*KatA^{WT} and *Cj*KatA^{E168Q} on low acetate. We observed a growth defect of the strain synthesizing *Cj*KatA^{WT} (Fig. A.13, open circles). This defect was no longer observed when a variant *Cj*KatA with a change glutamine substituted for a glutamate at residue 168 (Fig. A.13, open triangles). *S. enterica* Δ*pat* and *pat*$^{+}$ strains exhibit growth under these conditions (Fig. A.13). These results might suggest *Cj*KatA is capable of acetylating *Se*Acs *in vivo*, however this was not shown *in vitro*. Additionally, these results suggest the glutamine substitution at residue 168 inhibits the activity of *Cj*KatA *in vivo*.

In addition to the *in vivo* evidence, we sought to identify the site of acetylation of *Cj*Acs by *Cj*KatA. *Cj*Acs was incubated with cell free extracts from a *S. enterica* Δ*pat* strain expressing *Cj*KatA and acetyl-CoA, separated by SDS-PAGE, excised and digested before analysis by LC/MS/MS (Fig. A.7). Mass spectrometry identified lysine residue K617 as the site of acetylation in *Cj*Acs. We were unable to show acetylation of *Cj*Acs by pure *Cj*KatA, suggesting additional reactions components are necessary for *in vitro* function.

To expand our understanding of *Cj*KatA, we investigated the oligomeric state of pure protein in solution. *Cj*KatA is a 176 residue, 20.8 kDa protein. Under the conditions tested, *Cj*KatA eluted ~29 minutes after injection. Compared to the elution times of molecular mass standards, the retention time is consistent with that of a protein whose mass was approximately 19 kDa. Since

the calculated molecular mass of *Cj*KatA was approximately 20 kDa, we concluded that *Cj*KatA was a monomer in solution (Fig. A.14). This is consistent with reports for some other type IV GNATs like *Bs*AcuA, however multimerization varies amongst bacterial GNATs (57).

***In vivo* evidence that *C. jejuni* SrtN is a functional enzyme.**

The *C. jejuni* NCTC 1168 genome encodes a putative NAD^+-dependent (class III) protein deacetylase at locus *cj1050c* (*Cj*SrtN, previously NpdA), however there is no experimental evidence to support this annotation. We used an *in vivo* approach to determine whether *Cj*SrtN has deacetylase activity. For this purpose we introduced an arabinose-inducible plasmid encoding *C. jejuni srtN*$^+$ into *S.enterica* Δ*cobB* strain and assessed growth on low (10mM) acetate (Fig. A.8). Previous work has shown *S.enterica* strains lacking *cobB* exhibit poor growth on low acetate. (17). In the absence of the deacetylase, acetylated Acs cannot be reactivated and is unable to utilize acetate in the medium (13,58).The strain synthesizing *Cj*SrtN grew on low acetate when the medium was supplemented with inducer at a final concentration of 100μM (Fig. A.8, open hexagons). As expected, the strain harboring an empty vector did not grow in these conditions (Fig. A.8, black squares), however growth was restored by ectopic expression of *Se*CobB when inducer (100μM) was provided (Fig. A.8, black triangles). Growth of a *S. enterica cobB*$^+$ strain was assessed as a control (Fig. A.8, black circles). These results indicate *Cj*SrtN has *in vivo* deacetylase function.

Previous work has identified a histidine critical for function of NAD^+-dependent protein deacetylases. This active site histidine functions as a general base and is required for the nucleophilic attack on acetyllysine (59). We used an *in vivo* approach to determine if the conserved histidine residue (H106) is important for *Cj*SrtN function. As expected, a *S. enterica* Δ*cobB* strain synthesizing variant *Cj*SrtN^{H106A} was no longer able to grow on low acetate (Fig. A.15A, grey triangles). These results suggest H106 of *Cj*SrtN is necessary for deacetylase activity.

In multiple enterobacteria, CobB has two isoforms: long ($CobB_L$) and short ($CobB_S$). The long isoform is characterized by an extended cationic *N*-terminus (60). Recent work has shown this region to be targeted by *N*-terminal acetylation by GNAT YiaC in *S. enterica. N*-terminal acetylation of $CobB_L$ modulates deacetylase activity (61). We compared the sequence homology of *Cj*SrtN and *Se*CobB and show *Cj*SrtN lacks this extended *N*-terminus (Fig. A.15B). We were also unable to find YiaC homologs encoded in the *C. jejuni* genome. Collectively, these results suggest regulation of *Cj*SrtN deacetylase activity by *N*-terminal acetylation is not present in *C. jejuni*.

_Cj_SrtN restores _Cj_Acs activity via deacetylation.

To determine if *Cj*SrtN could deacetylate *Cj*Acs acetylated by *Cj*KatA, we assayed *Cj*Acs^{Ac} specific activity after incubation with purified *Cj*SrtN and NAD^+ using the continuous assay previously described. The specific activity of *Cj*Acs

was assayed after incubation with cell free extracts from *S. enterica* Δ*pat* strains expressing *Cj*KatA^{WT} (Fig. A.9; *Cj*Acs^{Ac}, dotted bar) or *Cj*KatA^{E168Q} (Fig. A.9; *Cj*Acs, white bar). Acetylated *Cj*Acs showed a significant decrease in specific activity compared to unmodified *Cj*Acs. The activity of acetylated *Cj*Acs was restored after incubation with *Cj*SrtN and NAD^+ (Fig. A.9, light grey bar). The specific activity of *Cj*Acs^{Ac} was not fully restored when Nicotinamide (Nm), a known inhibitor of protein deacetylases, was included during incubation with *Cj*SrtN (Fig. A.9, dark grey bar). Collectively, these results suggest *Cj*SrtN is responsible for reactivating acetylated *Cj*Acs by deacetylation.

CONCLUDING REMARKS

Here we show that *C. jejuni* uses reversible-lysine acetylation to modulate Acs activity. Our findings have informed the model shown in Figure A.10. The physiology of this prominent food-borne pathogen is an area of active investigation. Acs has been implicated in infection when tested in a rabbit model. An Δ*acs* strain of *C. jejuni* displayed a defect in colonization. Additionally, an increase in *acs* gene expression was observed *in vivo* compared to cells grown *in vitro* (62). This study A recent study has shown that *acs* is significantly downregulated when cells are transitioned from high to low oxygen. Additionally, Acs abundance was measure to be 63 fold higher in cultures at 150% aerobiosis compared to 40% aerobiosis. Collectively these results indicate a positive correlation between Acs abundance and increasing aerobiosis (63). *C. jejuni*

adaptation in environments with varying oxygen levels is important for the survival of this organism. Modulation of Acs activity by reversible lysine acetylation may be implicated in the survival and pathogenicity of *C. jejuni*. Additional work is needed to elucidate the roles of protein acetylation and deacetylation in *C. jejuni*.

ACKNOWLEDGEMENTS

We thank Jessica Irons for the *Campylobacter jejuni jejuni* NCTC 11168 strain. We thank Christofer Zepeda-Guisa for technical assistance.

FUNDING

This work was supported by US PHS grant from the NIGMS R35-GM130399 to J.C.E.-S.

CONFLICT OF INTEREST

The authors have no conflict of interest to declare.

REFERENCES

1. Walsh, C.T., *Posttranslational Modification of Proteins: Expanding Nature's Inventory*. 2006, Greenwood Village, CO: Roberts and Company Publishers.
2. VanDrisse, C.M., A.R. Parks, and J.C. Escalante-Semerena, *A toxin involved in Salmonella persistence regulates its activity by acetylating its*

cognate antitoxin, a modification reversed by CobB sirtuin deacetylase. MBio, 2017. **8**(3): p. e00708-17.

3. Rycroft, J.A., et al., *Activity of acetyltransferase toxins involved in Salmonella persister formation during macrophage infection.* Nat. Commun., 2018. **9**: p. 1-11.
4. VanDrisse, C.M. and J.C. Escalante-Semerena, *Small-molecule acetylation controls the degradation of benzoate and photosynthesis in Rhodopseudomonas palustris.* MBio, 2018. **9**: p. e01895-18.
5. VanDrisse, C.M. and J.C. Escalante-Semerena, *In Salmonella enterica, OatA (Formerly YjgM) Uses O-Acetyl-Serine and Acetyl-CoA to Synthesize N,O-Diacetylserine, Which Upregulates Cysteine Biosynthesis.* Front Microbiol, 2018. **9**: p. 2838.
6. VanDrisse, C.M. and J.C. Escalante-Semerena, *In Streptomyces lividans, acetyl-CoA synthetase activity is controlled by O-serine and N(varepsilon)-lysine acetylation.* Mol. Microbiol., 2018. **107**: p. 577-594.
7. Burckhardt, R.M., B.A. Buckner, and J.C. Escalante-Semerena, *Staphylococcus aureus modulates the activity of acetyl-Coenzyme A synthetase (Acs) by sirtuin-dependent reversible lysine acetylation.* Mol. Microbiol., 2019. **112**: p. 588-604.
8. Hentchel, K.L. and J.C. Escalante-Semerena, *Acylation of biomolecules in prokaryotes: a widespread strategy for the control of biological function and metabolic stress.* Microbiol. Mol. Biol. Rev., 2015. **79**: p. 321-346.

9. Vetting, M.W., et al., *Structure and functions of the GNAT superfamily of acetyltransferases.* Arch. Biochem. Biophys., 2005. **433**: p. 212-226.

10. Walsh, C.T., S. Garneau-Tsodikova, and G.J. Gatto, Jr., *Protein posttranslational modifications: the chemistry of proteome diversifications.* Angew. Chem. Int. Ed. Engl., 2005. **44**: p. 7342-7372.

11. Tucker, A.C. and J.C. Escalante-Semerena, *Acetoacetyl-CoA synthetase activity is controlled by a protein acetyltransferase with unique domain organization in Streptomyces lividans.* Mol. Microbiol., 2013. **87**: p. 152-167.

12. Burckhardt, R.M. and J.C. Escalante-Semerena, *In Bacillus subtilis, the SatA (formerly YyaR) acetyltransferase detoxifies streptothricin via lysine acetylation.* Appl. Environ. Microbiol., 2017.

13. Starai, V.J., et al., *Sir2-dependent activation of acetyl-CoA synthetase by deacetylation of active lysine.* Science, 2002. **298**: p. 2390-2392.

14. Gulick, A.M., *Conformational dynamics in the acyl-CoA synthetases, adenylation domains of non-ribosomal peptide synthetases, and firefly luciferase.* ACS Chem. Biol., 2009. **4**: p. 811-827.

15. Starai, V.J. and J.C. Escalante-Semerena, *Acetyl-coenzyme A synthetase (AMP forming).* Cell. Mol. Life Sci., 2004. **61**: p. 2020-2030.

16. Starai, V.J. and J.C. Escalante-Semerena, *Identification of the protein acetyltransferase (Pat) enzyme that acetylates acetyl-CoA synthetase in Salmonella enterica.* J. Mol. Biol., 2004. **340**(5): p. 1005-1012.

17. Starai, V.J., et al., *A link between transcription and intermediary metabolism: a role for Sir2 in the control of acetyl-coenzyme A synthetase.* Curr. Opin. Microbiol., 2004. **7**: p. 115-119.

18. Gardner, J.G., et al., *Control of acetyl-coenzyme A synthetase (AcsA) activity by acetylation/deacetylation without NAD$^+$ involvement in Bacillus subtilis.* J. Bacteriol., 2006. **188**: p. 5460-5468.

19. Crosby, H.A., et al., *Reversible N(epsilon)-lysine acetylation regulates the activity of acyl-CoA synthetases involved in anaerobic benzoate catabolism in Rhodopseudomonas palustris.* Mol. Microbiol., 2010. **76**: p. 874-888.

20. Xu, H., S.S. Hegde, and J.S. Blanchard, *Reversible acetylation and inactivation of Mycobacterium tuberculosis acetyl-CoA synthetase is dependent on cAMP.* Biochemistry, 2011. **50**: p. 5883-5892.

21. You, D., et al., *Acetyl-CoA synthetase is acetylated on multiple lysine residues by a protein acetyltransferase with single GNAT domain in Saccharopolyspora erythraea.* J. Bacteriol., 2014. **196**: p. 3169-3178.

22. Parkhill, J., et al., *The genome sequence of the food-borne pathogen Campylobacter jejuni reveals hypervariable sequences.* Nature, 2000. **403**(6770): p. 665-668.

23. Kramer, J.M., et al., *Campylobacter contamination of raw meat and poultry at retail sale: identification of multiple types and comparison with isolates from human infection.* J Food Prot, 2000. **63**(12): p. 1654-1659.

24. Young, K.T., L.M. Davis, and V.J. Dirita, *Campylobacter jejuni: molecular biology and pathogenesis.* Nat Rev Microbiol, 2007. **5**(9): p. 665-679.

25. Velayudhan, J. and D.J. Kelly, *Analysis of gluconeogenic and anaplerotic enzymes in Campylobacter jejuni: an essential role for phosphoenolpyruvate carboxykinase.* Microbiology (Reading), 2002. **148**(Pt 3): p. 685-694.

26. Gundogdu, O., et al., *Re-annotation and re-analysis of the Campylobacter jejuni NCTC11168 genome sequence.* BMC Genomics, 2007. **8**: p. 162.

27. Westfall, H.N., D.M. Rollins, and E. Weiss, *Substrate utilization by Campylobacter jejuni and Campylobacter coli.* Appl Environ Microbiol, 1986. **52**(4): p. 700-705.

28. Hinton, A., Jr., *Growth of Campylobacter in media supplemented with organic acids.* J Food Prot, 2006. **69**(1): p. 34-38.

29. Guccione, E., et al., *Amino acid-dependent growth of Campylobacter jejuni: key roles for aspartase (AspA) under microaerobic and oxygen-limited conditions and identification of AspB (Cj0762), essential for growth on glutamate.* Mol Microbiol, 2008. **69**(1): p. 77-93.

30. Wright, J.A., et al., *Metabolite and transcriptome analysis of Campylobacter jejuni in vitro growth reveals a stationary-phase physiological switch.* Microbiology (Reading), 2009. **155**(Pt 1): p. 80-94.

31. St Maurice, M., et al., *Flavodoxin:quinone reductase (FqrB): a redox partner of pyruvate:ferredoxin oxidoreductase that reversibly couples*

pyruvate oxidation to NADPH production in Helicobacter pylori and Campylobacter jejuni. J Bacteriol, 2007. **189**(13): p. 4764-4773.

32. Leach, S., P. Harvey, and R. Wali, *Changes with growth rate in the membrane lipid composition of and amino acid utilization by continuous cultures of Campylobacter jejuni.* J Appl Microbiol, 1997. **82**(5): p. 631-640.
33. Kirkpatrick, A.S., et al., *Campylobacter jejuni fatty acid synthase II: structural and functional analysis of beta-hydroxyacyl-ACP dehydratase (FabZ).* Biochem Biophys Res Commun, 2009. **380**(2): p. 407-412.
34. Wolfe, A.J., *The acetate switch.* Microbiol. Mol. Biol. Rev., 2005. **69**: p. 12-50.
35. Bertani, G., *Studies on lysogenesis. I. The mode of phage liberation by lysogenic Escherichia coli.* J. Bacteriol., 1951. **62**: p. 293-300.
36. Bertani, G., *Lysogeny at mid-twentieth century: P1, P2, and other experimental systems.* J. Bacteriol., 2004. **186**: p. 595-600.
37. Berkowitz, D., et al., *Procedure for identifying nonsense mutations.* J. Bacteriol., 1968. **96**: p. 215-220.
38. Balch, W.E. and R.S. Wolfe, *New approach to the cultivation of methanogenic bacteria: 2-mercaptoethanesulfonic acid (HS-CoM)-dependent growth of Methanobacterium ruminantium in a pressurized atmosphere.* Appl. Environ. Microbiol., 1976. **32**: p. 781-791.

39. Miroux, B. and J.E. Walker, *Over-production of proteins in Escherichia coli: mutant hosts that allow synthesis of some membrane proteins and globular proteins at high levels.* J. Mol. Biol., 1996. **260**: p. 289-298.

40. Galloway, N.R., et al., *Rapid cloning for protein crystallography using Type IIS restriction enzymes.* Crystal. Growth & Design, 2013. **13**(

): p. 2833-2839.

41. VanDrisse, C.M. and J.C. Escalante-Semerena, *New high-cloning-efficiency vectors for complementation studies and recombinant protein overproduction in Escherichia coli and Salmonella enterica.* Plasmid, 2016. **86**: p. 1-6.

42. Datsenko, K.A. and B.L. Wanner, *One-step inactivation of chromosomal genes in Escherichia coli K-12 using PCR products.* Proc. Natl. Acad. Sci. USA, 2000. **97**: p. 6640-6645.

43. Jeter, V.L., et al., *A new class of phosphoribosyltransferases involved in cobamide biosynthesis is found in methanogenic archaea and cyanobacteria.* Biochemistry, 2019. **58**: p. 951-964.

44. Reger, A.S., J.M. Carney, and A.M. Gulick, *Biochemical and crystallographic analysis of substrate binding and conformational changes in acetyl-CoA synthetase.* Biochemistry, 2007. **46**: p. 6536-6546.

45. Garrity, J., et al., *N-lysine propionylation controls the activity of propionyl-CoA synthetase.* J. Biol. Chem., 2007. **282**: p. 30239-30245.

46. Sambrook, J., E.F. Fritsch, and T. Maniatis, *Molecular Cloning: A Laboratory Manual*. Second ed. 1989, Cold Spring Harbor, N.Y.: Cold Spring Harbor Laboratory.

47. Blommel, P.G. and B.G. Fox, *A combined approach to improving large-scale production of tobacco etch virus protease.* Protein Expr. Purif., 2007. **55**: p. 53-68.

48. Kumari, S., et al., *Cloning, characterization, and functional expression of acs, the gene which encodes acetyl coenzyme A synthetase in Escherichia coli.* J. Bacteriol., 1995. **177**: p. 2878-2886.

49. Wagley, S., et al., *Differences in carbon source utilisation distinguish Campylobacter jejuni from Campylobacter coli.* BMC Microbiol, 2014. **14**: p. 262.

50. Maruyama, K., *Short-chain acyl-coenzyme A synthetases in Rhodopseudomonas sphaeroides.* J. Biochem. (Tokyo), 1982. **91**: p. 725-730.

51. Preston, G.G., J.D. Wall, and D.W. Emerich, *Purification and properties of acetyl-CoA synthetase from Bradyrhizobium japonicum bacteroids.* Biochem. J., 1990. **267**: p. 179-183.

52. Priefert, H. and A. Steinbüchel, *Identification and molecular characterization of the acetyl- coenzyme A synthetase gene (acoE) of Alcaligenes eutrophus.* J. Bacteriol., 1992. **174**: p. 6590-6599.

53. Gulick, A.M., et al., *The 1.75Å crystal structure of acetyl-CoA synthetase bound to adenosine-5'-propylphosphate and coenzyme A.* Biochemistry, 2003. **42**: p. 2866-2873.

54. Jetten, M.S., A.J. Stams, and A.J. Zehnder, *Isolation and characterization of acetyl-coenzyme A synthetase from Methanothrix soehngenii.* J Bacteriol, 1989. **171**: p. 5430-5435.

55. Martinez-Blanco, H., et al., *Isolation and characterization of the acetyl-CoA synthetase from Penicillium chrysogenum. Involvement of this enzyme in the biosynthesis of penicillins.* J Biol Chem, 1992. **267**: p. 5474-5481.

56. Jogl, G. and L. Tong, *Crystal structure of yeast acetyl-coenzyme A synthetase in complex with AMP.* Biochemistry, 2004. **43**(6): p. 1425-1431.

57. Gardner, J.G. and J.C. Escalante-Semerena, *In Bacillus subtilis, the sirtuin protein deacetylase encoded by the srtN gene (formerly yhdZ), and functions encoded by the acuABC genes control the activity of acetyl-CoA synthetase.* J. Bacteriol., 2009. **191**: p. 1749-1755.

58. Starai, V.J., et al., *Short-chain fatty acid activation by acyl-coenzyme A synthetases requires SIR2 protein function in Salmonella enterica and Saccharomyces cerevisiae.* Genetics, 2003. **163**: p. 545-55.

59. Smith, B.C. and J.M. Denu, *Sir2 protein deacetylases: evidence for chemical intermediates and functions of a conserved histidine.* Biochemistry, 2006. **45**: p. 272-282.

60. Tucker, A.C. and J.C. Escalante-Semerena, *Biologically active isoforms of CobB sirtuin deacetylase in Salmonella enterica and Erwinia amylovora.* J. Bacteriol., 2010. **192**: p. 6200-6208.

61. Parks, A.R. and J.C. Escalante-Semerena, *Modulation of the bacterial CobB sirtuin deacylase activity by N-terminal acetylation.* Proc.Natl. Acad. Sci. U S A, 2020. **117**(27): p. 15895-15901.

62. Shang, Y., et al., *Insights into Campylobacter jejuni colonization and enteritis using a novel infant rabbit model.* Sci Rep, 2016. **6**: p. 28737.

63. Guccione, E.J., et al., *Transcriptome and proteome dynamics in chemostat culture reveal how Campylobacter jejuni modulates metabolism, stress responses and virulence factors upon changes in oxygen availability.* Environ Microbiol, 2017. **19**(10): p. 4326-4348.

64. Robert, X. and P. Gouet, *Deciphering key features in protein structures with the new ENDscript server.* Nucleic Acids Res., 2014. **42**(Web Server issue): p. W320-4.

Table A.1. Strains and plasmids used in this work. All strains were derivatives of

Strains	Genotype	Reference or Source
JE6583	*metE205 ara-9*	Laboratory collection
Derivatives of strain JE6583		
JE22070	/ pCV1	Laboratory collection
JE22072	/pCV3	Laboratory collection
JE23686	Δ*acs2* / pCV1	41
JE22085	Δ*acs2* / pACS62	41
JE24207	Δ*cobB1375* / pCV1	7
JE24209	Δ*cobB1375* / pCOBB141	7
JE25624	Δ*acs2* / pCJACS1	
JE25625	Δ*cobB1375* / pCJSRTN1	
JE25749	Δ*cobB1375* / pCJSRTN3	
JE25866	Δ*acs2* / pCJACS1 pCV3	
JE25867	Δ*acs2* / pCJACS1 pCJKATA3	
JE25868	*pat2::kan* / pCJKATA2	
JE25869	*pat2::kan* / pCJKATA5	
Escherichia coli strains		
JE6663 C41(λDE3)	F – *ompT hsdSB (rB- mB-) gal dcm* (λDE3)	Avidis
Plasmid	**Genotype**	**Source**
pTEV18	Overexpression vector that fuses the *N* terminus of the protein of interest to a H_6 tag, which can be removed by rTEV protease, *bla*$^+$	41
pCV1	complementation vector, P_{araBAD}, *bla*$^+$	41
pCV3	complementation vector, P_{araBAD}, *cat*$^+$	41
pACS62	S. enterica acs+ in pCV1	41

pCOBB141	S. enterica cobB+ in pCV1	41
pCJACS1	*C.jejuni 1537c*$^{+}$ in pCV1 bla+	
pCJACS2	*C. jejuni 1537c*$^{+}$ in pTEV18 bla+	
pCJSRTN1	*C. jejuni 1050c*$^{+}$ in pCV1 bla+	
pCJSRTN2	*C. jejuni 1050c*$^{+}$ in pTEV18 bla+	
pCJSRTN3	*C. jejuni 1050c*$^{+}$ *Cj*SrtN^{H106A} in pCV1 bla+	
pCJKATA1	*C. jejuni 1715*$^{+}$ in pTEV18 bla+	
pCJKATA2	*C. jejuni 1715*$^{+}$ in pCV1 bla+	
pCJKATA3	*C. jejuni 1715*$^{+}$ in pCV3 cat+	
pCJKATA5	*C. jejuni 1715*$^{+}$ *Cj*KatA^{E168Q} in pCV1 bla+	

Table A.2. Primers used in this work.

Primer Name	Primer Sequence (5'-3')
CjAcs pCV F	NGCTCTTCNTTCATGCTTAATCAAAATA
CjAcs pCV R	NNGCTCTTCNTTATTATTCAAACTCTGCCT
Cj1050c pCV F	NNGCTCTTCNTTCATGAAAAACA TTATGATA
Cj1050c pCV R	NNGCTCTTCNTTATCAAACATTACC ATCTTT
Cj1715 pCV F	NNGCTCTTCNTTCATGCAAAACACTATCATA
Cj1715 pCV R	NNGCTCTTCNTTATCAAAAAGCTTTTTGGTT
Cj1050c H106A 1	GTAGTACATTTGGCTGGCTTTTTGC
Cj1050c H106A 2	GCAAAAAGCCAGCCAAATGTACTAC
Cj1715 E168Q 1	CAAGATCCTTTTTTAGCTTATCAGAAAATTCTAAACCAAAAAGC
Cj1715 E168Q 2	TTCTAGGAAAAAATCGAATAGTCTTTTAAGATTTGGTTTTTCGA

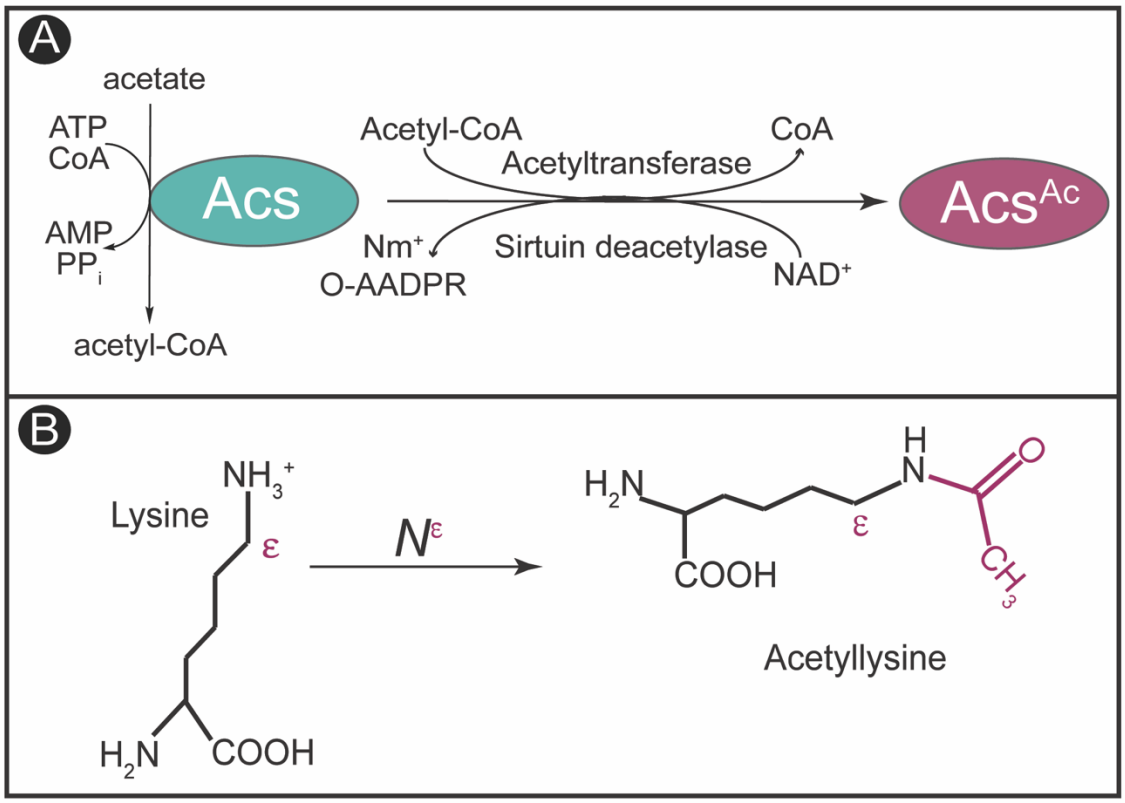

Figure A.1. Reversible lysine acetylation model. A. A general scheme for sirtuin-dependent reversible lysine acetylation of enzymes is shown. B. *N*ε lysine acetylation.

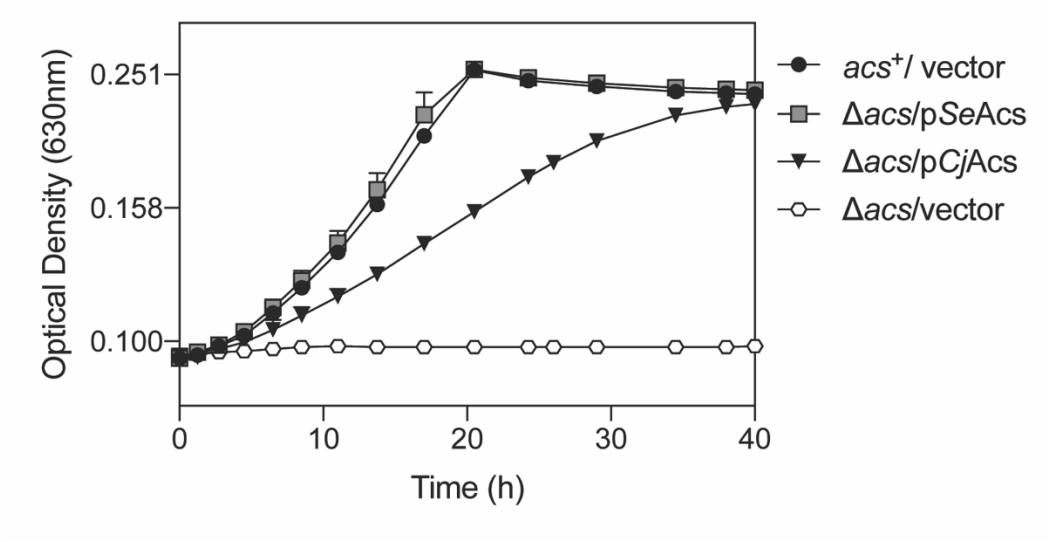

Figure A.2. *Cj*Acs compensates for the absence of Acs in a *S. enterica* Δ*acs* strain on low acetate. *S. enterica* Δ*acs* strains synthesizing *Cj*Acs (black triangles), *Se*Acs (grey squares), or harboring empty vector (pCV1, open hexagons) were grown in minimal medium supplemented with acetate (10 mM) as the sole carbon and energy source. A *S. enterica acs*$^+$ strain harboring empty vector was included in the growth analysis (black circles). Gene expression was induced by L-(+)-arabinose to a final concentration of 50μM. Growth of the *S.enterica* Δ*acs* strain synthesizing *Cj*Acs required 250μM inducer. Each strain was grown in technical triplicate, three times. Error bars represent the standard error of the mean of one experiment.

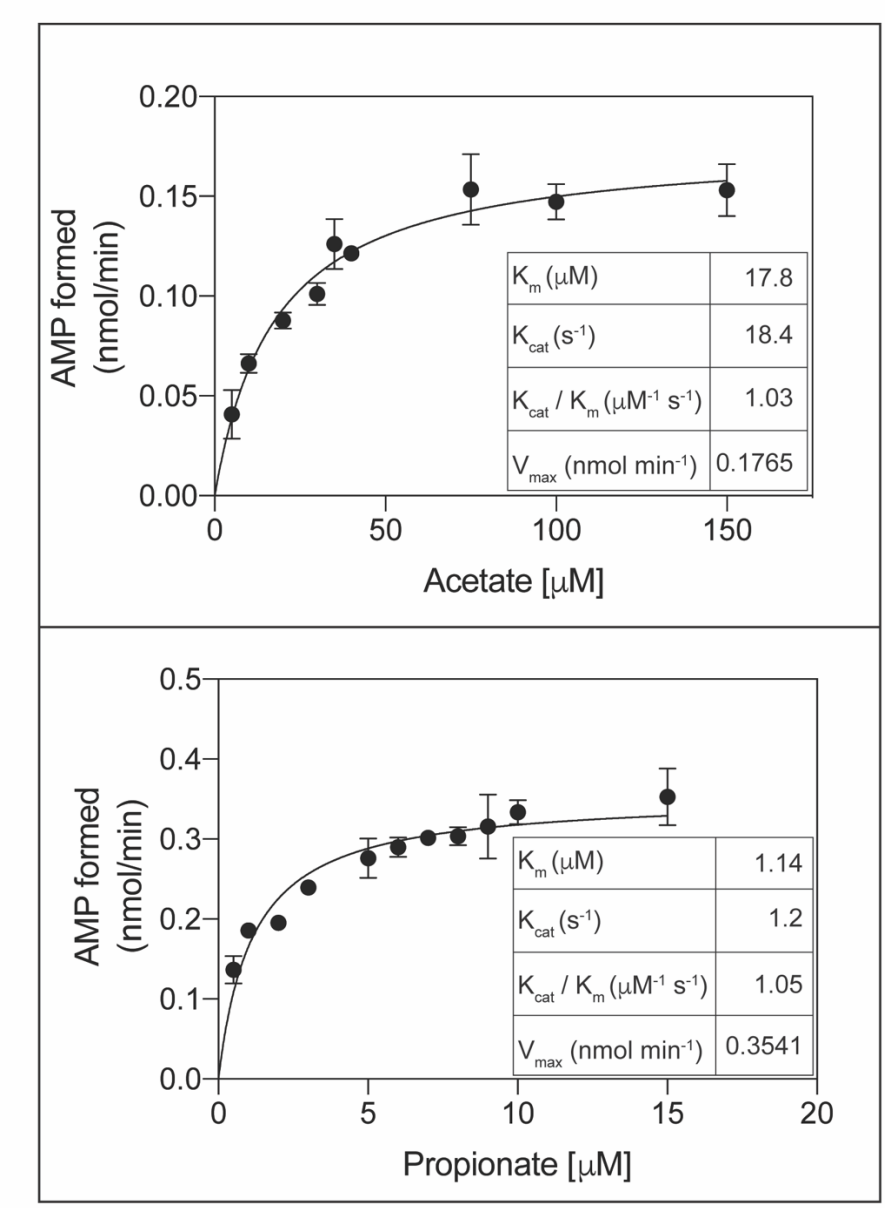

Figure A.3. Kinetic parameters of *Cj*Acs for acetate and propionate. In all reaction conditions ATP was present at saturating levels (2.5mM). Apparent kinetic parameters for acetate (A) and propionate (B) are shown in the insets. Protocol details are described in materials and methods.

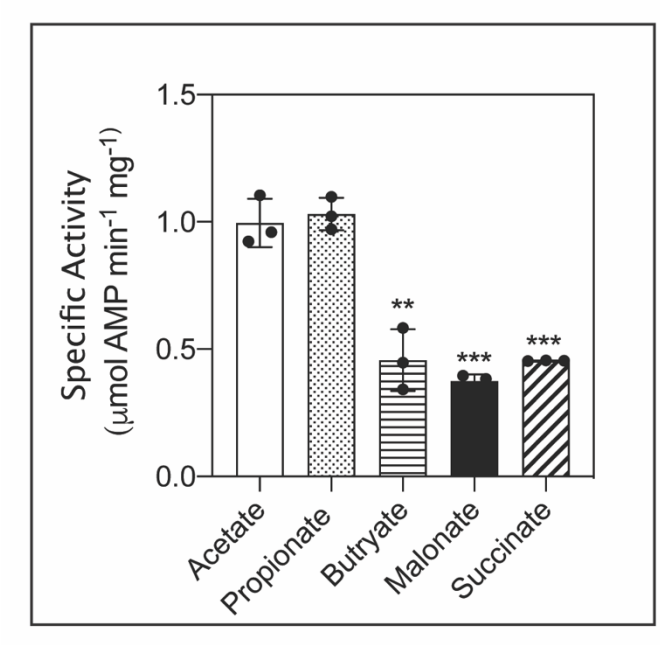

Figure A.4. *Cj*Acs preferentially activates acetate and propionate. The specific activity of *Cj*Acs using different organic acids is shown. Organic acids were provided at a final concentration of 200μM. Assays were performed in technical triplicate, twice. Error bars present the standard error of the mean. An unpaired student's t-test was performed against acetate (** p = 0.0038, *** p = 0.0006).

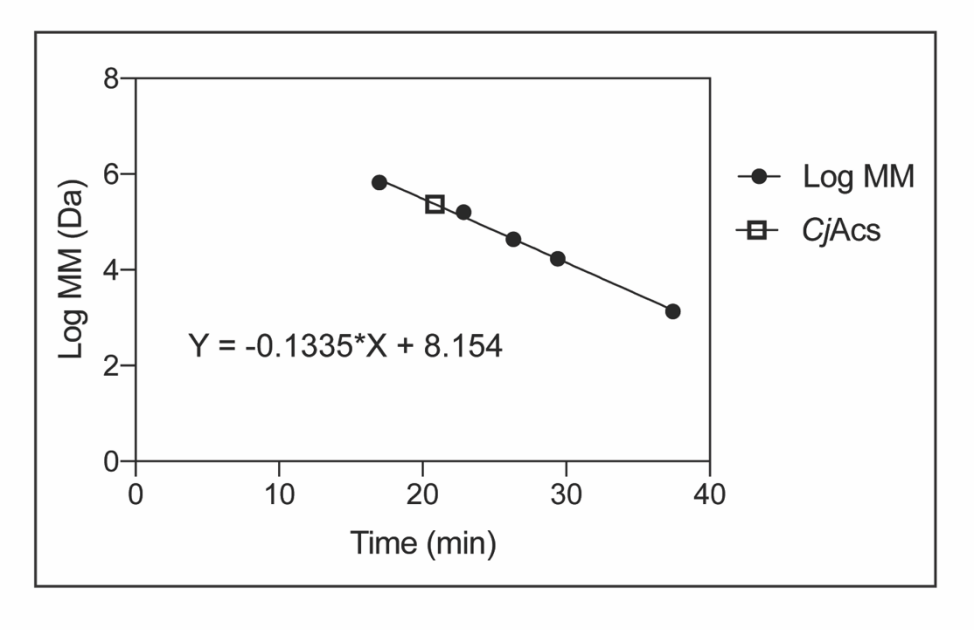

Figure A.5. *Cj*Acs is a trimer in solution. Gel filtration behavior of *Cj*Acs (open square) was analyzed by linear regression compared to molecular mass standards (black circles) as outlined in materials and methods.

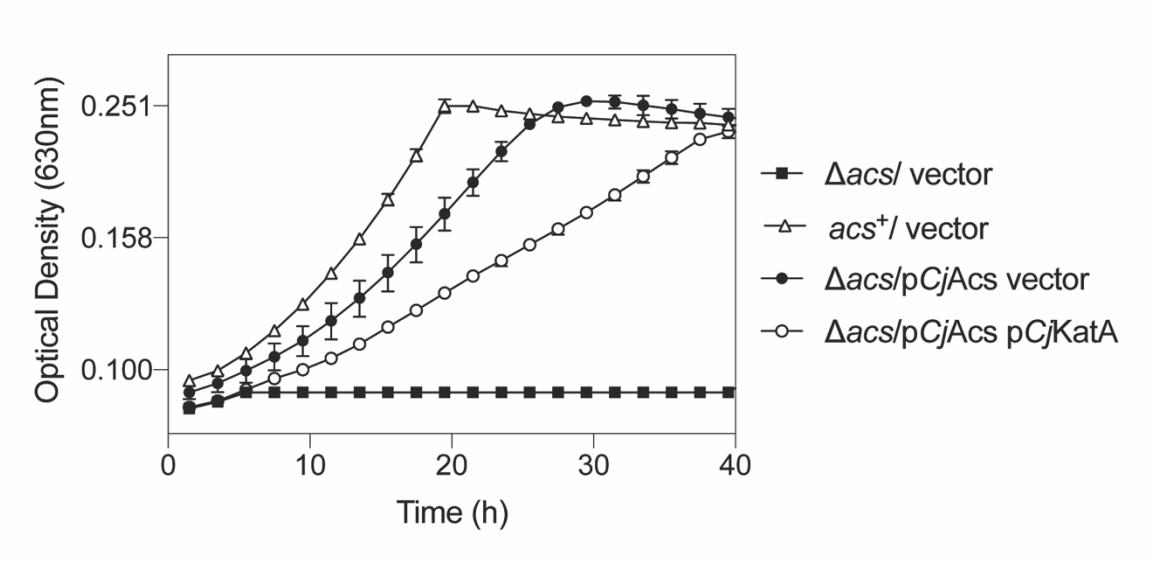

Figure A.6. *Cj*KatA expression confers a growth defect in *S.enterica* Δ*acs* strain synthesizing *Cj*Acs. *S. enterica* acs strains synthesizing *Cj*Acs and harboring a plasmid encoding *Cj*KatA (open hexagons) or empty vector (pCV3, black circles) were grown in minimal medium supplemented with acetate (10 mM) as the sole carbon and energy source. *S. enterica acs*$^+$ (open triangles) and Δ*acs* (black squares) strains harboring empty vector was included in the growth analysis. Gene expression was induced by L-(+)-arabinose to a final concentration of 250μM. Each strain was grown in technical triplicate, three times. Error bars represent the standard error of the mean of one experiment.

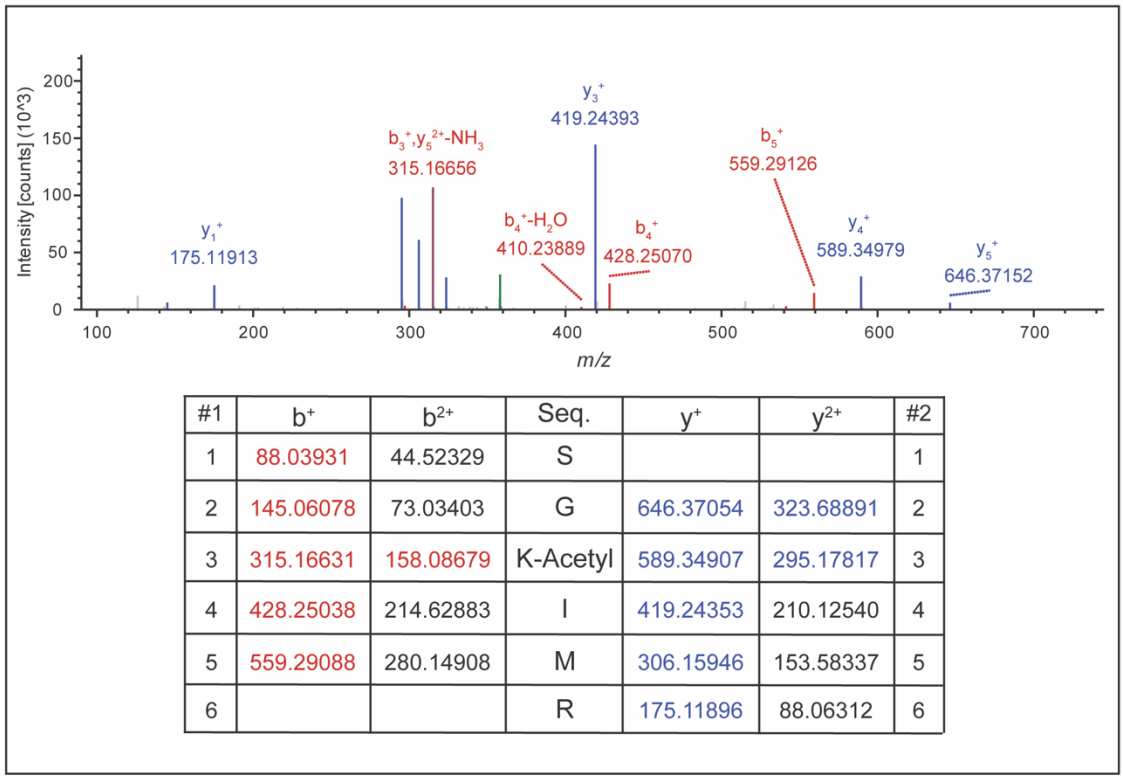

#1	b+	b2+	Seq.	y+	y2+	#2
1	88.03931	44.52329	S			1
2	145.06078	73.03403	G	646.37054	323.68891	2
3	315.16631	158.08679	K-Acetyl	589.34907	295.17817	3
4	428.25038	214.62883	I	419.24353	210.12540	4
5	559.29088	280.14908	M	306.15946	153.58337	5
6			R	175.11896	88.06312	6

Figure A.7. *Cj*KatA acetylates lysine 617 of *Cj*Acs. *Cj*Acs peptide SGK^{Ac}IMR was identified by LC/MS/MS analysis of *in vitro* acetylation reaction as described in materials and methods. Series of fragments extending from the *N*-terminus are *b* ions; series of fragments extending from the *C*-terminus are *y* ions. Peptides were identified using MASCOT software.

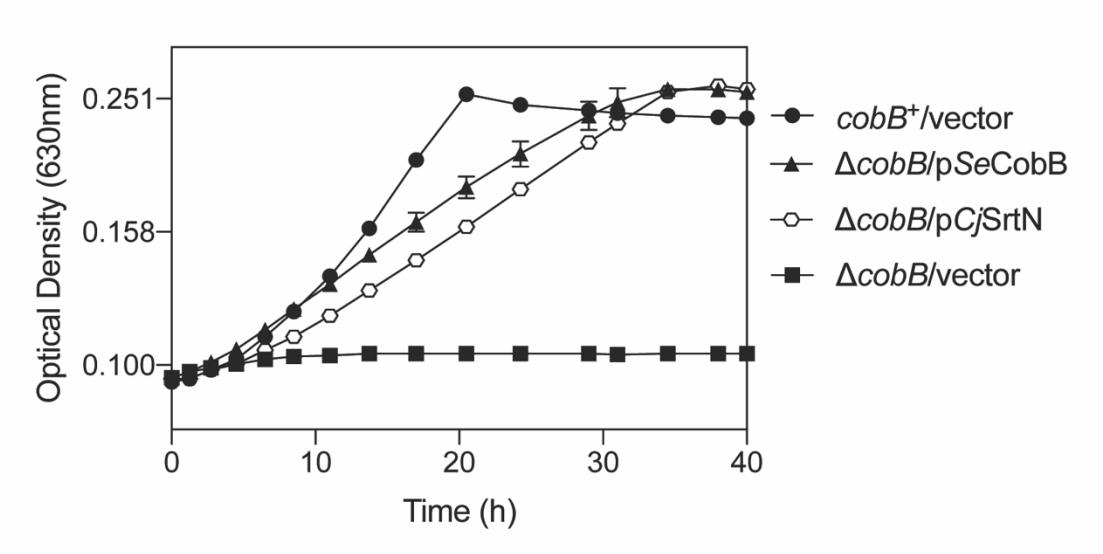

Figure A.8. *Cj*SrtN restores growth of a *S. enterica* Δ*cobB* strain on low acetate. *S. enterica* Δ*cobB* strains synthesizing *Se*CobB (black triangles), *Cj*SrtN (open hexagons), or harboring empty vector (black squares) were grown on minimal medium supplemented with acetate (10mM) as the carbon and energy source. Growth of a *S. enterica cobB*$^{+}$ strain was also monitored (black circles). Gene expression was induced by L-(+)-arabinose to a final concentration of 100μM. Each strain was grown in technical triplicate, three times. Error bars represent the standard error of the mean of one experiment.

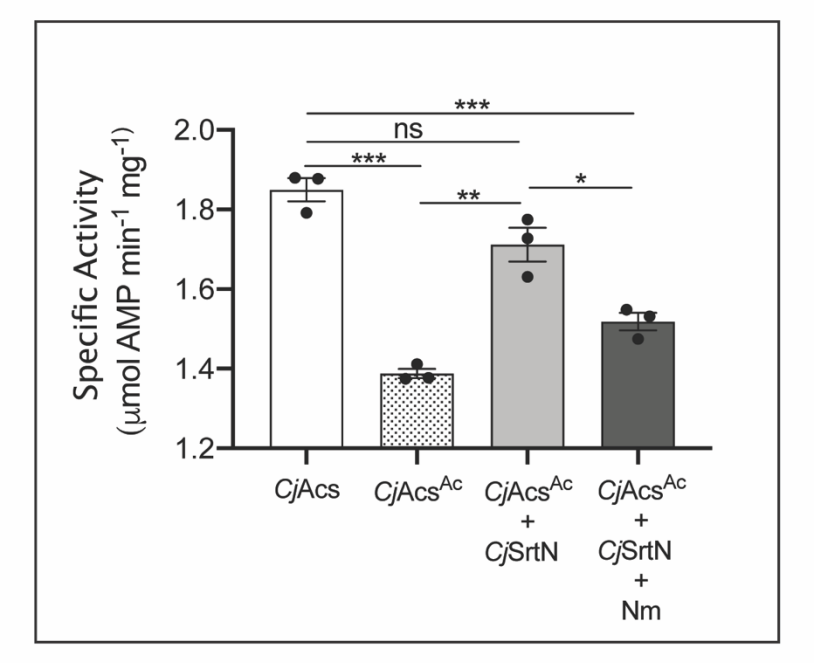

Figure A.9. *Cj*Acs^{Ac} activity is restored by deacetylation by *Cj*SrtN. Specific activity of *Cj*Acs after incubation with cell free extracts containing *Cj*KatA^{WT} (CjAcs^{Ac}, dotted bar) or *Cj*KatA^{E168Q} (*Cj*Acs, open bar) was determined. *Cj*Acs^{Ac} was incubated with *Cj*SrtN and NAD^+ and specific activity was analyzed (light grey bar). Nicotinamide (Nm) was added as to the aforementioned reaction to inhibit deacetylase activity (dark grey bar). Measurements were made in technical triplicate, twice. Error bars represent the standard error of the mean. Significance was determined by unpaired student's t-test (* p = .0157, ** p=.0.0018, *** p<0.0008).

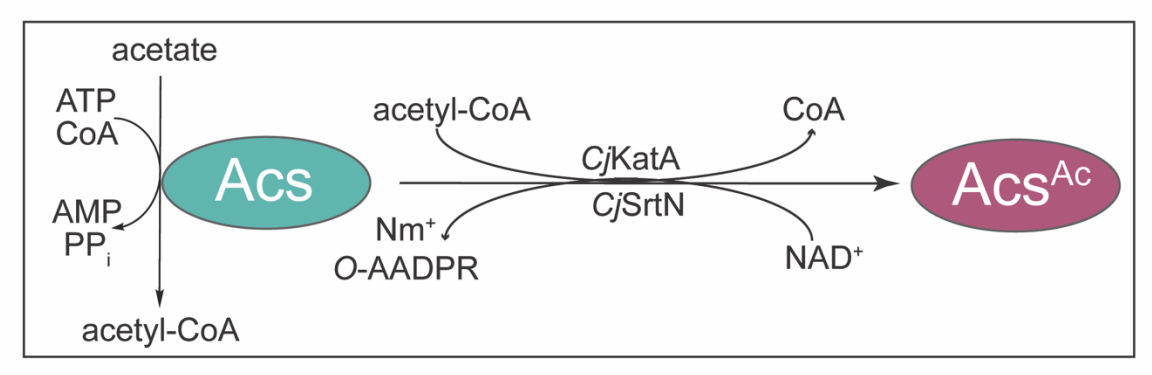

Figure A.10. Reversible lysine acetylation in *C. jejuni*. Acetylation of *Cj*Acs by *Cj*KatA inactivates the enzyme. Inactivation of *Cj*Acs is restored through deacetylation by NAD-dependent protein deacetylase *Cj*SrtN. Acetate is likely the substrate for *Cj*Acs in *C. jejuni.*

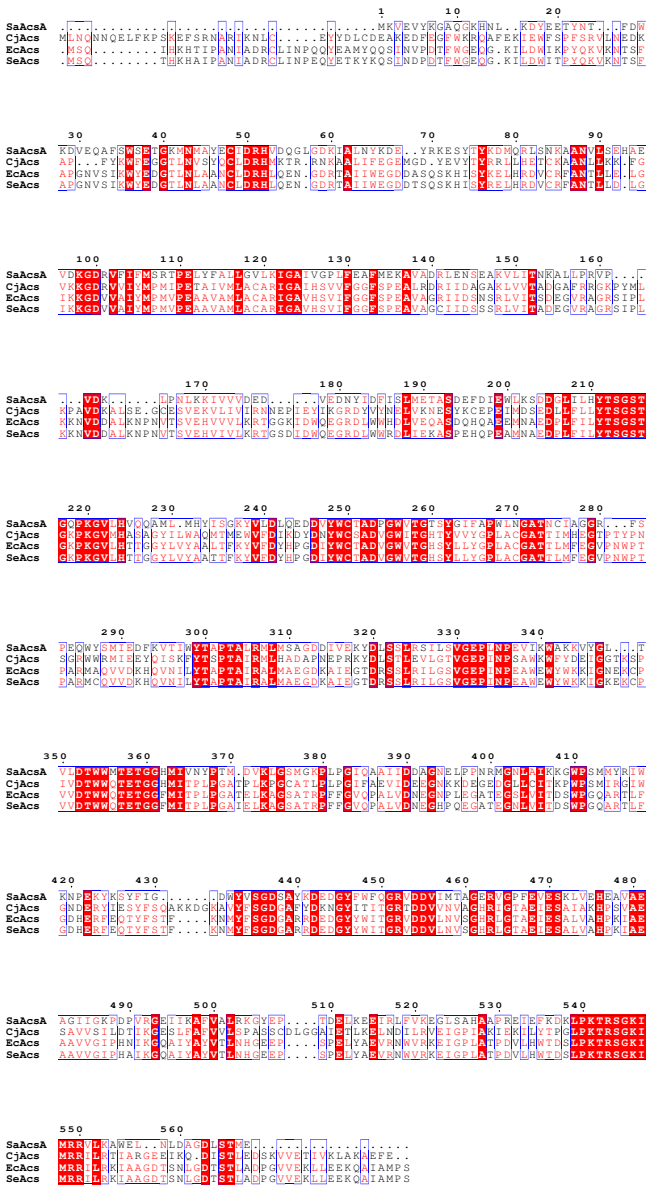

Figure A.11. Alignment of bacterial Acs homologs. Protein alignment comparing *Cj*Acs to several bacterial Acs homologs was generated using clustal omega and visualized by ESPript 3.0 (64).

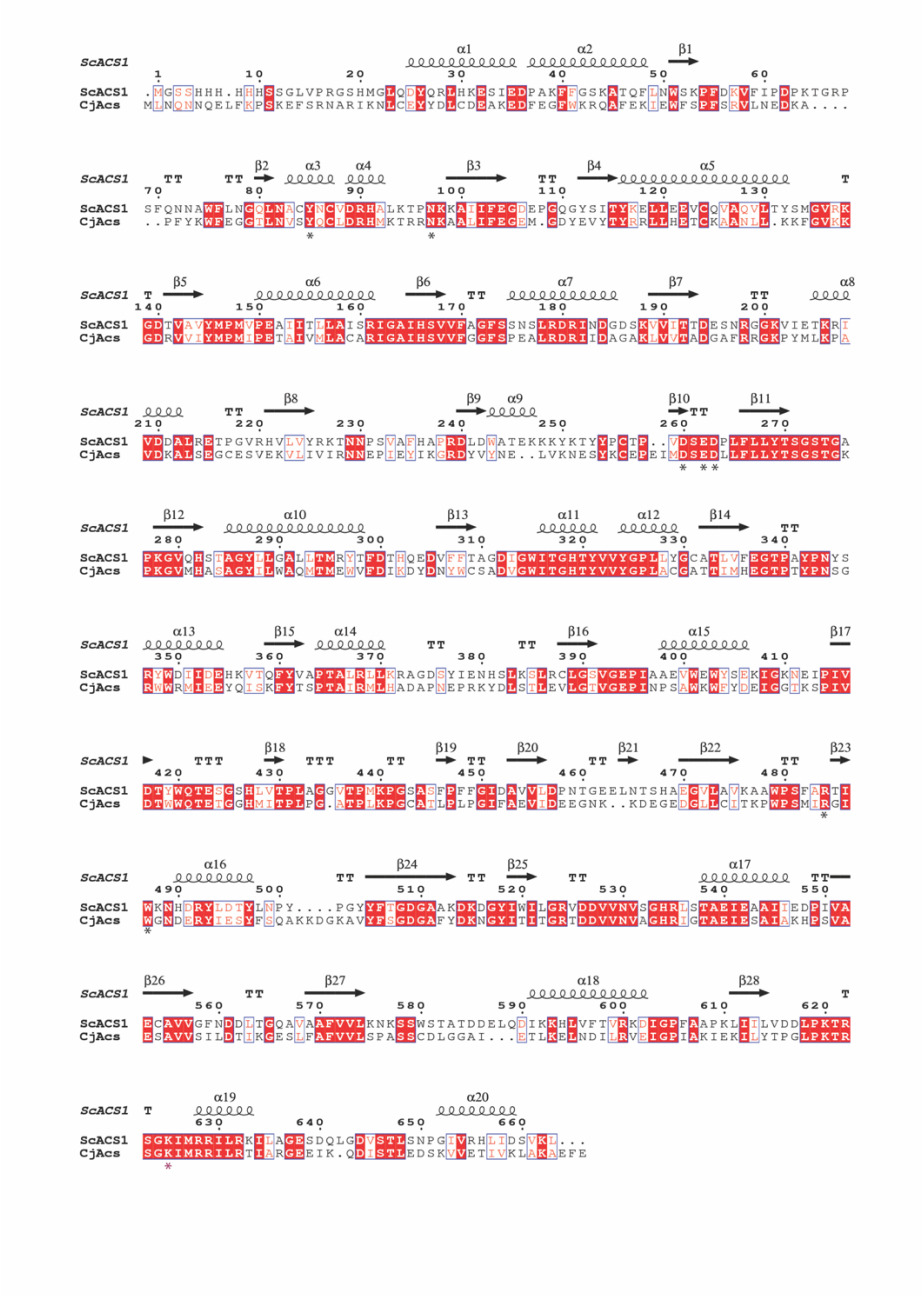

Figure A.12. Alignment of *Cj*Acs and *Saccharomyces cerevisiae* ACS. Protein alignment comparing CjAcs to *Saccharomyces cerevisiae* Acs homologs was generated using clustal omega and visualized by ESPript 3.0 (64). Black asterisks identify conserved residues that form the trimer interface in *Sc*ACS. Secondary protein structure of ScACS is shown above the alignment based off the crystal structure (PDG 1RY2).

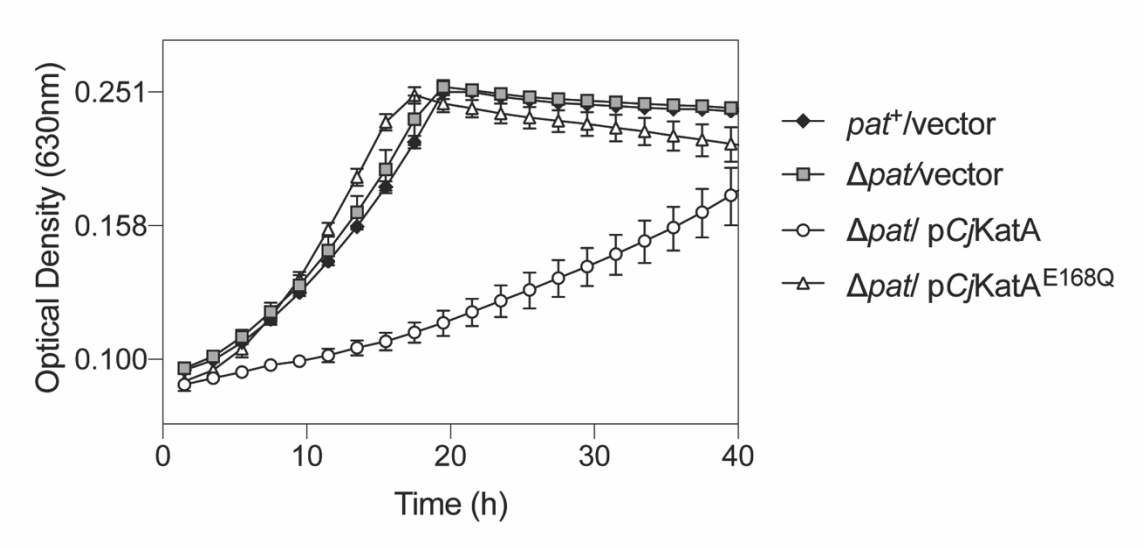

Figure A.13. Variant *Cj*KatA^{E168Q} expression does not display growth inhibition observed in *S. enterica* Δ*pat* strain synthesizing *Cj*KatA^{WT} on low acetate. *S. enterica* Δpat strains synthesizing *Cj*KatA^{WT} (open circles), *Cj*KatA^{E168Q} (open triangles), or harboring empty vector (pCV1, grey squares) were grown in minimal medium supplemented with acetate (10 mM) as the sole carbon and energy source. A *S. enterica* *pat*$^{+}$ strain harboring empty vector was included in the growth analysis (black diamonds). Gene expression was induced by L-(+)-arabinose to a final concentration of 250μM. Each strain was grown in technical triplicate, three times. Error bars represent the standard error of the mean of one experiment.

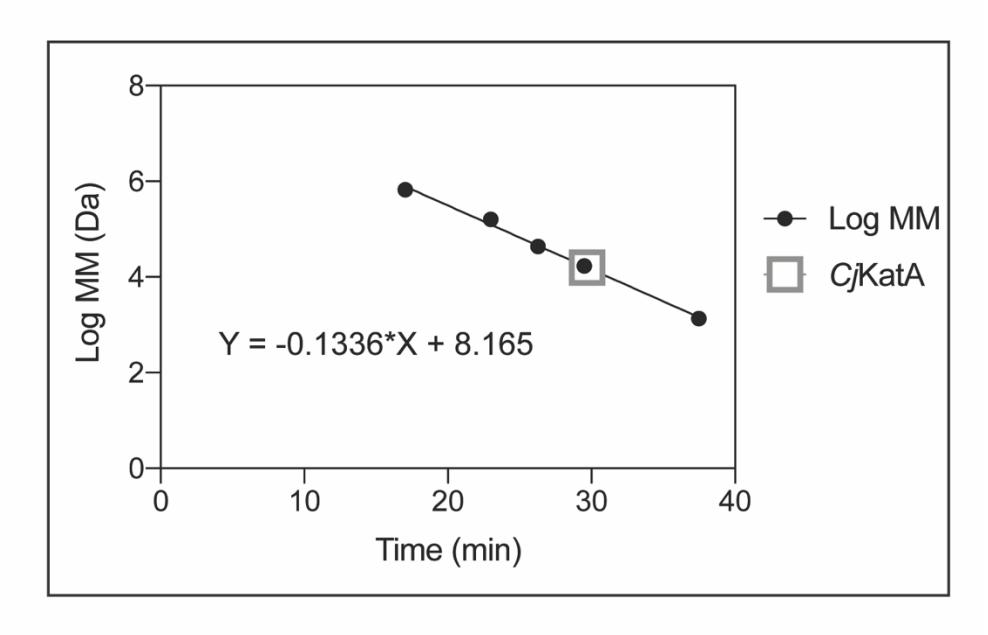

Figure A.14. *Cj*KatA is a monomer in solution. Gel filtration behavior of *Cj*KatA (open square) was analyzed by linear regression compared to molecular mass standards (black circles) as outlined in materials and methods.

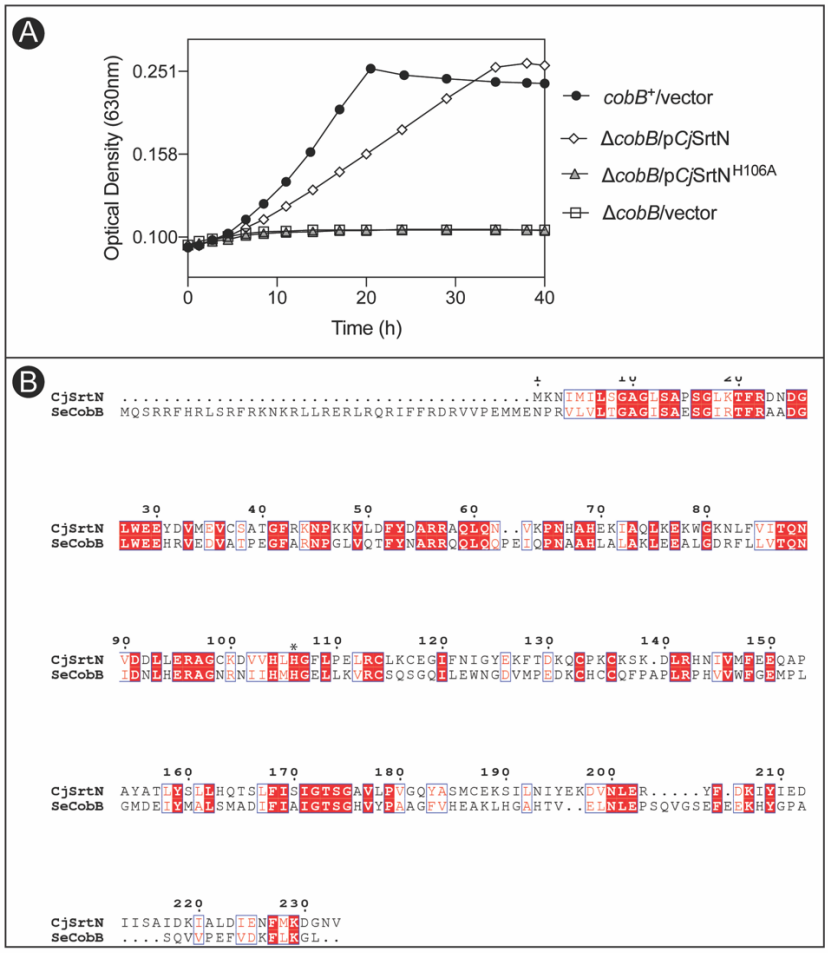

Figure A.15. Histidine 106 is necessary for *in vivo* function of *Cj*SrtN. A. *S. enterica* Δ*cobB* strains synthesizing *Cj*SrtN^{WT}(open diamonds), *Cj*SrtN^{H106A}(grey triangles), or harboring empty vector (open squares) were grown on minimal medium supplemented with acetate (10mM) as the carbon and energy source. Growth of a *S. enterica cobB*$^{+}$ strain was also monitored (black circles). Gene expression was induced by L-(+)-arabinose to a final concentration of 100μM. Each strain was grown in technical triplicate, three times. Error bars represent the standard error of the mean of one experiment. B. Protein alignment comparing *Cj*SrtN to *Se*CobB was generated using clustal omega and visualized by ESPript 3.0 (64). Black asterisks identify conserved histidine residue targeted for alanine substitution.